Fault Diagnosis for Transmission Lines Using Chromatic Processing

A Thesis submitted to the University of Liverpool
for the degree of Doctor of Philosophy
in the Faculty of Engineering

By
Ziyad S. D. Almajali
Department of Electrical Engineering & Electronics

2015

Abstract

Diagnosing the type of fault and its location in a transmission lines is performed by a variety of techniques and mainly relies on monitoring currents and voltages in the transmission line. Accurate fault diagnosis plays an important role in improving the overall system reliability, has a significant effect on the quality of service provided, improves the protection system efficiency, reduces power outage time and limits the risks and the economic losses.

Transmission lines extend over wide areas and are exposed to vulnerable situation, to the harsh and uncontrolled environment random events (e.g. lightning), this can lead to loss of lines due to various faults. This fact has an attraction for researchers to focus on utilising possible methods to improve protection system and supporting fault diagnosis solutions to overcome many of the transient fault conditions. This thesis explores an alternative method of fault diagnosis and location.

The approach uses chromatic methodology to extract information from current and voltage waveforms from a simulated transmission line with different fault conditions. These waveforms are processed chromatically. The process involves two steps, filtering which is performed on a cycle by cycle basis of the three symmetrical components for each waveform, and then using the chromatic transformations to represent the outputs in an information space. Various chro-

matic models are available but the hue, lightness and saturation (HLS) model is employed in this study and the relation between changes in the waveforms and changes in the chromatic parameters forms the foundation for building the proposed diagnosis algorithms.

A fault type classifier algorithm for the asymmetrical faults has been proposed for both, double and single line transmission systems. It employs the chromatic H parameter variation with the fault type for the negative sequence component. The processed waveforms are either the voltage or the current at a single terminal of the transmission line. L chromatic parameter values of the zero sequence component are incorporated in the algorithm to add the ground fault distinguishing element and the L parameter values of the rectified negative sequence component were used to support the classification decision even with high fault resistance.

Another algorithm for fault location estimation for all types of faults has been used for the double transmission line system. It employs the L chromatic parameter values of the rectified positive sequence component. The processed waveforms are the current collected from both terminals of the transmission line.

Finally, the proposed algorithms have been tested by variation of possible conditions of the faults, such as changing the fault location, the fault resistance, the line configurations and parameters, etc. In addition to robustness testing with different fault scenarios. Experimental results taken from a lumped parameter laboratory system have been also used to verify the outputs of the chromatic processing. The performance of the chromatic approach and other reported methods have been compared. The error of the chromatic method compares favourably with others. As such overall performance can be described as being good, this is encouraging and future work through proposing diagnostic tools for other power system components is needed.

Contents

List of Figures

List of Tables

List of Abbreviations and Symbols

a	The conductor cross sectional area.
α	Phasor operator equal to a unit vector at an angle of 120 degrees.
AI	Artificial Intelligence.
ANN	Artificial Neural Network.
C0	Zero sequence capacitance.
C1	Positive sequence capacitance.
CIE	The International Commission on Illumination.
CIELab	The International Commission on Illumination colour model.
CIMS	The Centre for Intelligent Monitoring Systems.
d	The distance between bundle conductors.
D	The distance between the centres of the conductors.
DLG	Double line to ground fault.
ε	The permittivity.
$\varepsilon_{\mathbf{r}}$	The relative permittivity for air.
$\varepsilon_{\mathbf{0}}$	The permittivity of free space.

γ	The propagation constant.
GMD	The geometrical mean distance.
GMR	Geometric mean radius.
$GMR_{\mathbf{Bundle}}$	The geometric mean radius For bundled lines.
GPS	The Global Positioning System.
GUI	Graphical user interface.
HLS	Hue, Lightness and Saturation colour model.
HSV	Hue, Saturation and Value colour model.
$\mathbf{I_a}$, $\mathbf{I_b}$, $\mathbf{I_c}$	Three phase currents.
$\mathbf{I_{a_1}}$, $\mathbf{I_{a_2}}$, $\mathbf{I_{a_0}}$	The positive, negative and zero sequence components for phase 'A' current.
$I_{\mathbf{F}}$	The fault current.
$I''_{\mathbf{FR}}$, $I''_{\mathbf{FS}}$	The fault current components generated from the receiver and the source terminals respectively.
$\mathbf{I_R}$	The residual current.
k	The combined skin and proximity correction factor.
$K_{\mathbf{0}}$	The ground compensation factor.
l	The conductor length .
L0	Zero sequence inductance.
L1	Positive sequence inductance.
$L_{\mathbf{External}}$	The external inductance per unit length.
$L_{\mathbf{Internal}}$	The internal inductance per unit length.
r	The radius of the conductor.

LL	Double line to line fault.
LLL	Three lines fault.
LLLG	Three lines to ground fault.
μ_0	The magnetic constant.
ρ	The resistivity of the conductor material.
$\mathbf{R_0}$,$\mathbf{G_0}$,$\mathbf{B_0}$	Outputs of Red, Green and Blue filters.
R, L and C	Resistance, inductance and capacitance.
R0	Zero sequence resistance.
R1	Positive sequence resistance.
$R_{\mathbf{AC}}$, $R_{\mathbf{DC}}$	The resistance with AC and DC current.
$R_{\mathbf{F}}$	The fault resistance.
RGB	Red, Green and Blue filters.
RMS	The root mean square.
SLG	Single line to ground fault.
T	The temperature coefficient of resistivity.
v	The speed of light.
$\mathbf{V_a}$, $\mathbf{V_b}$, $\mathbf{V_c}$	Three phase voltages.
$\mathbf{V_{a_1}}$, $\mathbf{V_{a_2}}$, $\mathbf{V_{a_0}}$	The positive, negative and zero sequence components of phase 'A' voltage.
$\mathbf{V_r}$, $\mathbf{I_r}$	The receiving end voltage and current respectively.
$\mathbf{V_s}$, $\mathbf{I_s}$	The sending end voltage and current respectively.
$V_{\mathbf{S}}^{"}$, $I_{\mathbf{S}}^{"}$	The pure fault voltage and current.
WFNN	A wavelet-fuzzy-neuro network.

$\boldsymbol{x}$	The distance to the fault.
y	The shunt admittance per unit length.
$\mathbf{Y}$	The equivalent shunt admittance of the transmission line.
z	The series impedance per unit length.
Z	The equivalent series impedance of the transmission line.
$Z_{\mathbf{0L}}$	The zero-sequence line impedance.
$Z_{\mathbf{c}}$	Transmission line characteristic impedance.
$Z_{\mathbf{L}}$	The positive-sequence line impedance.
$Z_{\mathbf{m}}$	The mutual impedance.

Acknowledgement

I thank **God Almighty** for his grace and mercy. Asking him the support by his power to grant me an entry with truthful intentions and an exit with truthful intentions, and allow me a power that gives me success.

"*He has not thanked God, who has not thanked people.*"

Prophet Mohammed

I have been very privileged to work under **Professor Joseph Spencer** supervision and receiving **Professor Gordon Jones** continuous advice. I am grateful for their encouragement, motivation, support and inspiration.

I wish to dedicate this thesis to my mother and to the memory of my father. Without their lifelong continuous support, understanding, love and encouragement I never would have been able to achieve my goals. I would also like to express my gratitude to my wife **Sana** and my parents-in-law for standing beside me to accomplish my education with care, love and quiet patience.

My sincerest thanks are extended to my sisters, brothers, friends and my big family, for their love and encouragement. And finally, thanks to my children: **Nooreddin**, **Baida** and **Shaima**, they always make me smile.

My acknowledgement is given to Mutah University and Jordanian Ministry of Higher Education and Scientific Research for the financial support I have received.

Chapter 1

General introduction

Transmission line is the vital component of any power system and 80% to 90% of the faults occurs in the transmission line system. Only the 10% to 20% of the faults occur in the rest of the power system components [1]. When a fault occurs, fast action and repair are key priorities. In the meantime, the transmission line's comprehensive protection system ensures satisfactory service for the rest of the system whilst protecting the faulty section of line.

In addition to fault detection, transmission line protection systems should include fault isolation and identification. In the early stages of power system development, the focus was on service continuity, for instance, adding redundant transmission line circuits help in both, reducing losses and providing continuity in case of fault occurrence. The challenge then was the way to detect the fault, isolate it and fix the problem in the minimum time. The detection function was tackled through using relays such as differential protection and distance relay. The isolation challenge was successfully implemented by reliant competent circuit breakers whose opening is initiated by the fault detection system operating appropriate relays.

Fault identification and diagnosis were not given much attention initially. Fault detection using distance relays could be classified as the earliest employed fault diagnosis tool, its first usage was in Germany in 1921 followed by the United States shortly thereafter. The impedance estimation in this tool was mainly for supporting the decision to trip based on the fault estimated location and if it fell within the relay zone of protection a trip command was issued to the circuit breaker. That is, the target was focusing on fault detection rather pinpointing its location.

The power system size transition from a simple source-load systems into complex-interconnected networks aiming to provide an integrated service over larger areas increased the need for efficient and reliable fault detection systems. At the same time, researchers continue their work on improving existent protection system functions. The main function of power system protection continues to be the fast fault detection and limiting the effects of the fault through isolating it. In addition to working towards increasing the sensitivity and reliability of protection systems and protocols, improvement also includes working on providing additional comprehensive fault diagnostic tools such as fault location estimation and fault type determination, such tools could help eventually in enhancing the overall system reliability and service quality.

The foremost requirement of diagnostic tools is to provide more information about the fault. In protection relays, time is a critical factor, as the delay could lead to catastrophic network damage and major asset losses. For the maintenance crews, accurate fault location is required, with good accuracy preferred over fast information but with a high margin of error in location. Accurate location information helps in saving time and reducing searching expenses, especially in harsh weather when most faults tend to occur.

After depending for a while on the visual inspection of the faulty line, several alternative approaches were then proposed by the field researchers. These methods in general fall into three broad categories. The first category includes the traditional methods, such as the impedance based calculation method and the travelling wave based method. The second category methods are based on recent modern technologies using the artificial intelligence (AI) techniques, such as artificial neural networks, fuzzy logic and genetic algorithm, while the last category includes hybrid methods which could be either based on the traditional method combined with modern methods, or methods combining two or more new intelligent approaches.

The motivation for developing alternative solutions was due to limitations encountered with traditional methods, but new challenges have slowed their introduction based on their reliability and dependability. The time consuming training for some methods and the high computation complexity for others make most of the commercially adopted methods belong to the first category [2] [3].

The chromatic monitoring approach, developed by Jones et al. in the Centre for Intelligent Monitoring Systems (CIMS) at Liverpool University, has been applied successfully in monitoring complex systems. Diagnostic provided information shows good performance for a variety of complex problems in various fields [4]. Therefore, in this work, the chromatic approach is proposed as a possible candidate for providing alternative, accurate, fast and low-cost solutions for transmission line fault diagnostic problem.

1.1 Research methodology

The aim of this thesis is to explore the possibility of developing novel and accurate diagnostic tools for transmission line faults based on chromatic monitoring approach.

A literature review of traditional and recent methods is performed; the study aims to compare different methods requirements, their advantages, disadvantages and the achieved performance of their diverse approaches. A further aim is to consider combining strengths and avoiding limitations in the design of a new tools.

A few simple power systems configurations are simulated under Matlab® simulation environment using its SimPowerSystems™ component libraries and analysis tools. This package that was developed in collaboration with Hydro-Québec of Montreal, for modelling and simulating electrical power systems. In addition, a hardware-based model is built with educational based module components of power system.

The collected data for different conditions and various possible scenarios simulating with different faults include a sampled three-phase waveforms from transmission line at both terminals. For the sake of simplicity, cycle by cycle time domain based monitoring is selected for this study. The collected data are then used as inputs to several proposed algorithms for the new tools. The research aims to establish direct relationships between the fault characteristics and the chromatic parameters. Extra transformation and processing might be required for providing useful and additional information. The different tools are tested for a wide range of possible conditions variations such as the fault resistance, inception angle, different sampling rates, different locations and multiple fault scenarios.

1.2 Thesis overview

This chapter starts by presenting thesis aims and objectives in addition to the proposed research methodology for tackling the diagnosis of faults encountered in transmission lines by chromaticity approach. This section present brief thesis overview.

A general background is included in Chapter 2, starting with an introduction to the transmission line specifications, parameter calculations and the different models for the transmission line. Faults types and causes in transmission lines are then discussed, followed by a literature review of research work in this area, with description of methods used for locating and classifying faults and the advantages and disadvantages of different methods are assessed. Chapter 2 is concluded by a description of the chromatic methodology and its transformation algorithms

Description of the power system networks used for generating data is included in Chapter 3 where samples of raw current and voltage waveforms are included. Implementations of chromatic method filtering and transformations outcomes are presented in Chapter 4. The analyses of the different parameters are concluded by proposing of fault diagnosis algorithms.

Discussion of the results is presented in Chapter 5 where a final and enhanced algorithm for fault location and fault analysis on overhead transmission lines are proposed. Chapter 6 present the work completed summary and conclusions. In addition to suggestions for work need to be carried out in the future, which include enhancement of the proposed tools and based on the work reported results in this thesis. Numerous issues are also suggested as potential future research area.

Appendix A present two conference papers based on the work of this thesis. The fault diagnosis algorithms are implemented by two methods, first implementation using Matlab® software technical computing language, the second

implementation was by combining all of the tools under one package with the user-friendly GUI of LabView®. Samples of Matlab® codes and screen shots of LabView® windows are included in Appendices B and C respectively.

Chapter 2

Background

2.1 Introduction

The main purpose of a power system cannot be achieved without an efficient, well-designed transmission system. Being the backbone of the power system; the principal aim of the transmission system is to deliver the electrical energy to consumers with minimal losses and disruption. For the power networks the length of transmission line between the generation units and the customers was initially limited to around half a mile and this was the maximum economic distance to minimise power loss.

To cover the industrial development needs, a massive increase in the electrical energy demand needed to be satisfied, together with the increased demand from the general population adopting a modern lifestyle. These two principal factors impacted the development strategies of modern power system networks. The increase in the population caused a spread in the residential areas which require delivering power to points far from the generation centres. As a result, medium and long transmission line were developed and these became part of the system

network. While the industrial development requires an increase in electrical energy and its increasing remoteness from the point of generation, the transmission voltage needs to be increased to reduce the ($I^2 \times R$) losses in the lines.

The use of high voltages in a network requires additional specifications to be implemented using towers that support the lines. Their dimensions are designed to provide safe line clearance between conductors and the ground and between the conductors themselves. The materials used in these lines and their arrangements also are selected carefully. The first part of this chapter will give a description of those requirements with examples of tower configurations and lines arrangements.

To study, understand and analyse the behaviour of a system, it is essential to model its different components accurately. As a part of the power system, the transmission line length, its lines arrangement, construction materials and the configurations of the towers and dimensions are used in the modelling of the transmission network. A description of the line modelling for different length lines is discussed in detail in Section 2.4

In an ideal world, the overhead lines should not affect or be affected by the surrounding environment. But in reality, these lines are susceptible to different fault events with random causes (e.g., lightning, insulation failure, etc.). Section 2.5 describes those faults and possible sequences caused by them. There is a large number of research publications in the fault diagnosis area, Sections 2.6 and 2.7 will give a literature review of conventional and modern methods and techniques used for monitoring the line by fault's location and the fault type classification, a few examples of typical research publications are included. The last part of the chapter introduces the chromatic method for processing data which is applied to fault location and fault type for the first time in this thesis.

2.2 Transmission lines

Overhead transmission lines consist of two main components, the conductors (including their construction materials) and the towers holding them. Both components specifications depend mainly on the system voltage. At the generation stage of the power system, the voltage is usually in the range of 15 to 25 kV. Step up transformers are utilised to raise the voltage to levels that reach 500 kV or 750 kV, transmitting power at these voltages will reduce the current in the lines leading to reduced losses. For the distribution network, the voltage is reduced to 133 kV and below before delivering to industrial and domestic customers at 415 V or 230 V.

Underground cables are used for the low voltage distribution near and within cities despite their high cost mainly due to environmental concerns. In contrast, overhead transmission lines are preferable for the high and extra high voltages and are mainly used in the open areas between cities, for their low-cost advantage and are easier to maintain. In terms of conductor number, the transmission line is either single circuit or double circuit configuration, for typical three phase AC systems. For a single circuit this means three cables are used, and in double circuits there are six.

The double circuit is preferable over single circuit transmission lines for its ability to carry more power. Also, double circuits introduce a level of redundancy, where in case of failure in one of the circuits, the other circuit should be able to maintain the supply. Figure 2.1(a) shows different towers designs for carrying single while Figure 2.1(b) shows tower designs for double circuits [5]. Figure 2.1 also shows that as the voltage level for transmission increased so do the tower size.

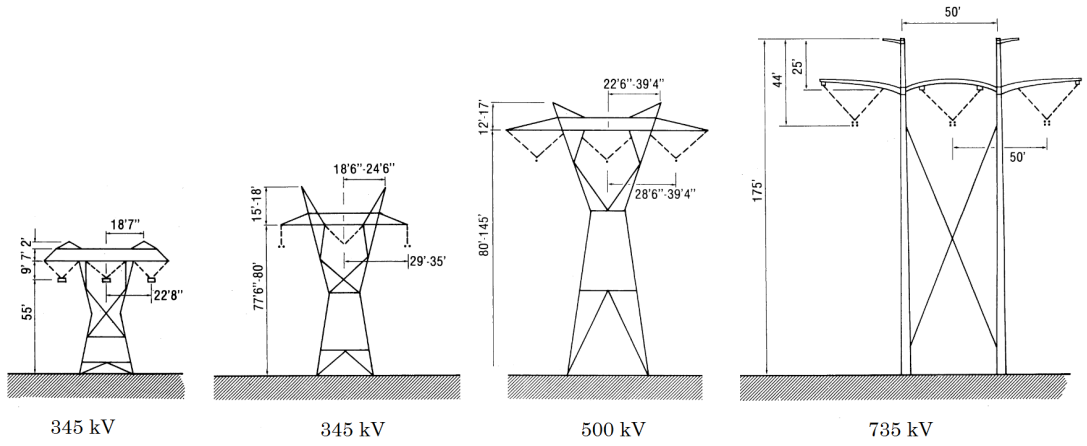

(a) Single circuit towers

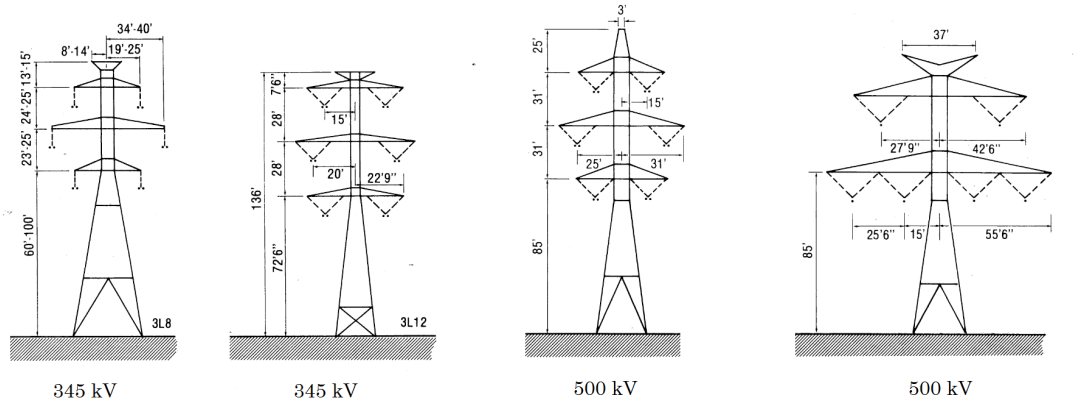

(b) Double circuit towers

Figure 2.1: Power Transmission Towers

Although the design of the tower could be considered only as a civil engineering issue, the engineer must also consider electrical issues such as conductor spacing, sag and the span of the conductors between the towers. These latter characteristics depend on electrical design considerations such as dielectric insulation and other properties. The mechanical characteristics are also important such as the ability of the tower to withstand the different tension forces due to the heavy weight of the conductors and also environmental factors like the wind and ice for instance.

Figure 2.2 shows a physical arrangement of a typical double circuit transmission line. The top of the tower carries the earth conductor for lightning protection. The arms of the tower hold the insulators. To specify the length of the insulator, the clearance between the conductors and the body of the tower together with the clearance specification between the conductors themselves are considered. The lower part of the tower is the foundations and it contains grounding electrodes.

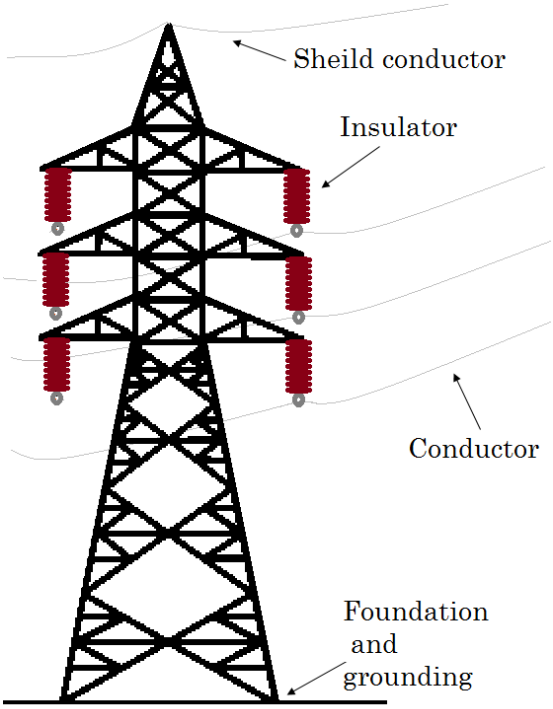

Figure 2.2: Typical double circuit transmission tower

The towers in the transmission line system support the conductors and keep a fixed distance between them over its length. Different towers are used for transposing the lines at respective intervals. This transposition is shown in Figure 2.3 and it is the process of swapping the conductors positions periodically. The benefit gained from doing this transposition is explained in the transmission modelling and parameter calculation Section 2.4.

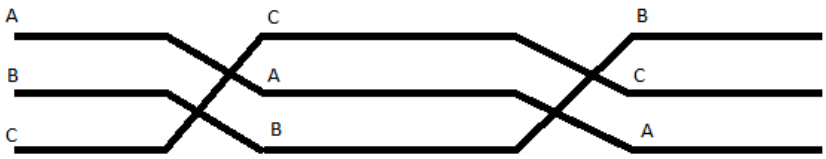

Figure 2.3: Transposition of three phases

The conductors are the major part of the transmission line system. Their material characteristics and specification are such to meet electrical and mechanical requirement of service. In terms of weight, aluminium material is chosen, but they are reinforced with steel to provide additional strength. The steel reinforcement strands are surrounded by the aluminium strands. This arrangement has minimal effect on the resistance, the steel located in the centre of the cable does not affect the overall resistance of the cable. An important aspect in cable design is the possible loading of the power system and the designer need also to study the feasible growth in the load demand over time.

To maximise power transmission in the towers groups of three or four conductors are usually bundled together. Figure 2.4 shows an example of four bundles of stranded conductor for each phase. Standard bundles are usually found in two, three or four conductors.

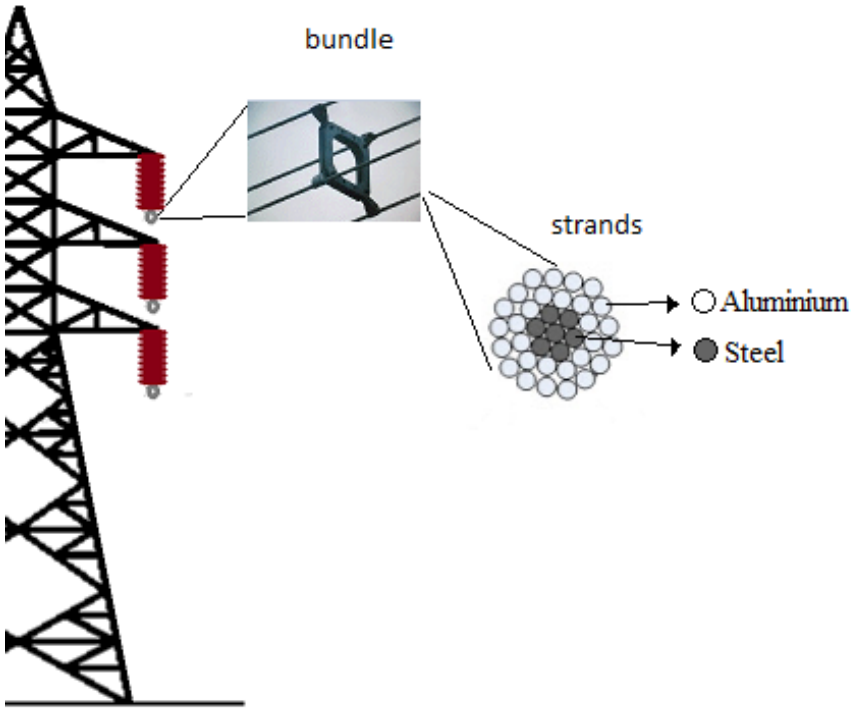

Figure 2.4: Four bundle stranded conductor

2.3 Transmission line parameters calculation

To simulate and analyse a power system, it is important to design an equivalent model for the different component which constructs that system. To model the transmission line system, we need to determine its parameters by studying the line conductors material, the length of the line and the geometry and dimension of the supporting towers. In this section, the calculation formulae of different parameters of the transmission line, the resistance, the inductance and the capacitance are presented. The different line length usually has different models and this will be discussed in Section 2.4.

2.3.1 Resistance

The resistance of the line depends basically on the physical composition of the used conductor. Assuming direct current (DC) flowing uniformly on a given conductor, the resistance R_{DC} of the conductor is calculated by Equation 2.1:

$$R_{\mathrm{DC}} = \rho \times \frac{l}{a} \tag{2.1}$$

Where ρ is the resistivity of the conductor material which is a constant, 'l' is the length of the conductor and 'a' is its cross sectional area.

For an (AC) system, some factors usually cause an increase in the apparent resistance. For instance, a phenomenon known as skin effect where a portion of the current tends to flow near the outer surface of the conductor than the centre, this cause a reduction in the effective cross section, an increase in the apparent resistance then occur due to the irregularity of the current distribution. The proximity effect is another phenomenon that causes a further increase in the resistance of the lines. This phenomenon appears on parallel wires, where due to the effect of the magnetic fields from current in each conductor on the other, the current will not be distributed uniformly around them.

If R_{AC} is the resistance with AC current, it can be calculated by the equation:-

$$R_{\mathrm{AC}} = R_{\mathrm{DC}} \times k \tag{2.2}$$

In Equation 2.2, 'k' is the combined skin and proximity correction factor, depending on the conductor material, dimension, system frequency and the space between parallel conductors, which are all parameters that are considered in the calculation of total equivalent resistance, 'k' could reach a value of up to 1.82 [6].

The length of spirally twisted strands conductors is actually longer than the line length by approximately 2%. Although twisted strands of conductor gives flexibility to the line, this contributes to an increase in resistance. The strands in each layer and the number of layers are also considered in the calculation of total equivalent resistance.

Temperature is also another factor that should not be forgotten in this area. Although the increase in temperature causes an increase in the line length, its major effect in resistance value. The resistance of metals varies linearly with temperature given by the equation:

$$R_{\text{new}} = R_{\text{initial}}[1 + T(t_2 - t_1)] \tag{2.3}$$

Where 'R_{new}' is the newly calculated resistance value at 't_2' which is the new temperature. 'R_{initial}' is the initial resistance value at 't_1' which is the initial temperature, 'T' is the temperature coefficient which depends on the conductor material, its unit is $[1/C^{\text{o}}]$.

2.3.2 Inductance

The sinusoidal variation of the current in a conductor will cause a sinusoidal variation on the associated magnetic field, and this induce voltage that oppose the current flow. This inductance parameter depends on the configuration and dimension between the conductors. It is composed of two components resulting from the generated internal and external magnetic field.

$$L_{\text{Total}} = L_{\text{Internal}} + L_{\text{External}} \qquad [H/m] \tag{2.4}$$

The internal inductance component per unit length due to the internal flux linkage (L_{Internal}) is given by Equation 2.5. And Equation 2.6 is used for the calculation of the external inductance parameter component for each phase conductor (L_{External}) [6] [7].

$$L_{\text{Internal}} = \frac{\mu_0}{8\pi} \qquad [H/m] \tag{2.5}$$

$$L_{\text{External}} = \frac{\mu_0}{2\pi} \times ln\frac{D}{GMR} \qquad [H/m] \tag{2.6}$$

Where μ_0 is the magnetic constant which is equal to $4\pi\times$ 10^{-7} $[H/m]$

The terms D and GMR depend on the conductors configurations, for a two wires, single phase line shown in Figure 2.5 [6], D is the distance between the centres of the conductors, GMR (geometric mean radius) = $0.7788\times r$ where 'r' is the radius of the conductor.

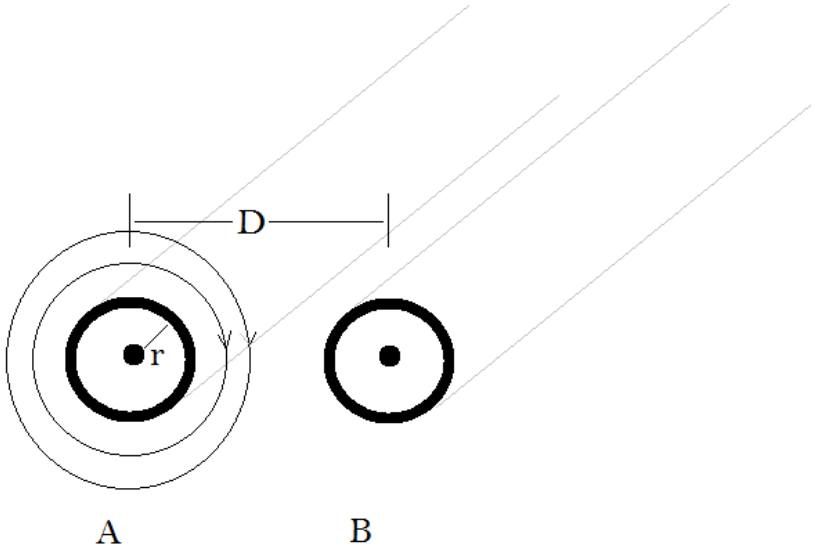

Figure 2.5: Two wire, single phase line

For a three phase circuit as shown in Figure 2.6 [6], and assuming fully transposed line. D term is replaced by the geometrical mean distance(GMD) and it is evaluated by

$$GMD = \sqrt[3]{D_{\mathrm{AB}} \times D_{\mathrm{BC}} \times D_{\mathrm{AC}}} \tag{2.7}$$

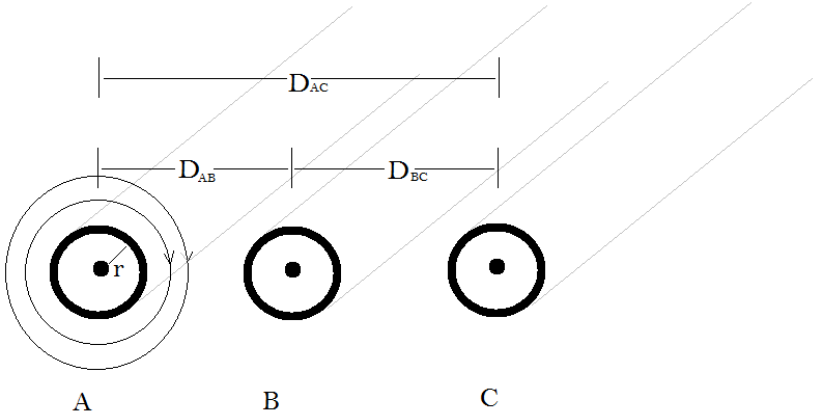

Figure 2.6: Three wires, three phase line

In both cases, GMR is calculated assuming solid conductor with radius equal to 'r'. For actual lines with strands, the GMR is calculated considering all the strands and the layers and this is usually available from the standard information tables for each conductor type.

For bundled lines, GMR term is replaced by GMR_{Bundle}, and this is evaluated by:

$$GMR_{\mathrm{Bundle}} = (d^{\mathrm{n\text{-}1}} \times GMR_{\mathrm{stranded}})^{1/\mathrm{n}} \tag{2.8}$$

Where 'd' is the distance between bundle conductors and 'n' is the number of conductors per bundle.

The calculated inductance for each phase is the total of both the internal inductance and the external inductance, and it is clear from Equations 2.5 and 2.6

how the inductance value is effectively influenced by the tower dimensions and the distances between the wires and also the conductor material.

If line transposing is not used, the middle line while have higher inductance, and this will lead to different voltage drops, so it is important to apply the technique of phase conductors transposing in order to maintain symmetry in the calculated parameter and thus symmetry of the system. where each conductor occupies the location of the other two phases for one-third of the total line length.

2.3.3 Capacitance

Similar to the inductance, the capacitance parameter also depends on the configuration and dimension between the conductors. The following general equation is used for the calculation of the capacitance parameter for each phase conductor [7].

$$C = \frac{2\pi\varepsilon}{ln\frac{D}{r}} \qquad [F/m] \tag{2.9}$$

ε is the permittivity and it is equal to $\varepsilon_{\mathrm{r}} \times \varepsilon_0$. Where ε_{r} is the relative permittivity and for air it is equal to 1, ε_0 is the permittivity of free space and it is equal to 8.85×10^{-12} $[F/m]$. Generally, permittivity will vary with environmental conditions such as the humidity, and thus it should be considered in the calculations [8].

Both terms 'D' and 'r' depend on the conductors configurations. For two wires, single phase line shown in Figure 2.5, D is the distance between the centres of the conductors, r is the radius of the conductor.

For three phase circuit as shown in Figure 2.6, and assuming fully transposed line, D term is replaced by the geometrical mean distance(GMD) and it is evaluated by

$$GMD = \sqrt[3]{D_{\mathrm{AB}} \times D_{\mathrm{BC}} \times D_{\mathrm{AC}}} \tag{2.10}$$

For bundled lines r is replaced by r_{Bundle} which is evaluated by:

$$r_{\mathrm{Bundle}} = (d^{\mathrm{n\text{-}1}} \times r)^{1/\mathrm{n}} \tag{2.11}$$

Where 'd' is the distance between bundle conductors and 'n' is the number of conductors per bundle.

2.4 Transmission line modelling

Models are employed in the design calculation and power system simulations. The arrangement of the R, L and C parameters depends on the length of the line. The following subsections show the different models used for different lengths.

2.4.1 Short line

Any line less than 80 km is considered short line. For short transmission lines, the capacitance parameter usually has a negligible value; therefore, its value does not appear in the model. The line can be modelled as R and L.

Figure 2.7 shows the equivalent circuit for a short transmission line. The line is represented by lumped elements of resistance R and inductance L connected in series. $\mathrm{V_s}$, $\mathrm{V_r}$ are the voltage at the sending end and at the receiving end respectively and I is the line current.

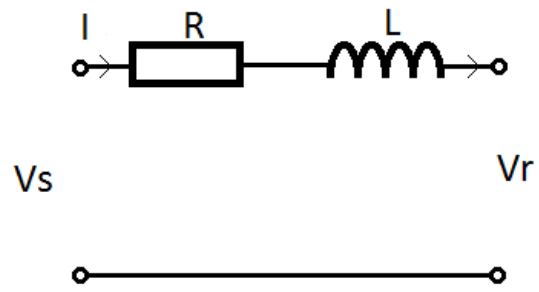

Figure 2.7: Short transmission line model

2.4.2 Medium line

If the line is more than 80 km but less than 240 km, then it is considered medium length line. For medium transmission lines, and unlike the short line, the capacitance parameter becomes more significant; therefore, its value is included in the model and cannot be ignored.

Figure 2.8 shows two equivalent circuit configurations for the medium length transmission line. V_s, I_s are the sending end voltage and current respectively. V_r, I_r are the voltage and current respectively obtained from the receiving end. The π model is shown in Figure 2.8(a), the line is represented by lumped elements of resistance R and inductance L connected in series, the capacitance parameter is divided into two halves, connected as shunt components, one at the sender and one at the receiver.

Figure 2.8(b) shows the T model; a series branch of half the resistance and half of inductance parameter is used at the sender terminal and similar branch is used at the receiver terminal, the capacitance is connected in shunt at the centre of the two branches.

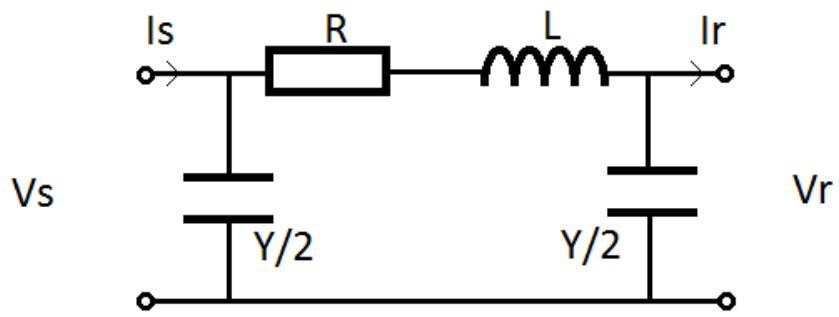

(a) π model

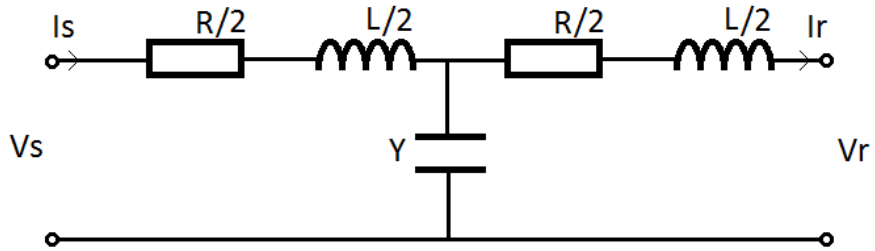

(b) T model

Figure 2.8: Medium transmission line models

2.4.3 Long line

The approximated lumped parameters based model is adequate in modelling short and medium lines, but for lines more than 240 km, the distributed element model is more accurate, and this is due to the fact that the actual line parameters are not lumped together, they are uniformly distributed along the length of the line.

Figure 2.9 show the model for a long transmission line. V_s, I_s are the sending end voltage and current respectively. V_r, I_r are the voltage and current respectively obtained from the receiving end. Z is the impedance of (R+jwL).

For small length element Δl; Z=zl is the total equivalent impedance of the line and Y= yl is the total shunt admittance, z is the series impedance per unit length(Ω/m) and y is the shunt admittance per unit length (S/m).

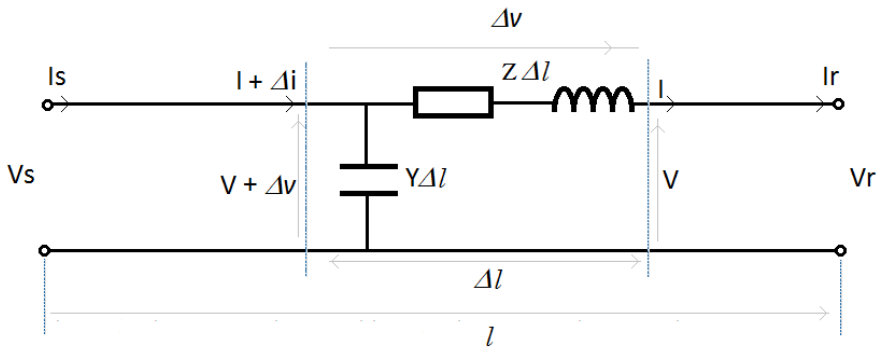

Figure 2.9: Long transmission line model

The propagation constant is defined by $\gamma = \sqrt{zy}$, and the characteristic impedance $Z_c = \sqrt{z/y}$ (Ω). The voltages and currents are described as function of the propagation constant and the characteristic impedance of the line, given by [9]:

$$V_s = V_r cosh(\gamma l) + Z_c I_r sinh(\gamma l) \tag{2.12}$$

$$I_s = \frac{V_r sinh(\gamma l)}{Z_c} + I_r cosh(\gamma l) \tag{2.13}$$

2.5 Faults in transmission line

In the design stage of the transmission line, the equipment is carefully specified in order to prevent the possibility of fault occurrence. Starting with the tower; the type of material, the dimension suitable for the system voltage and its structural strength to handle the weight of conductors and insulators are factors to consider. Strong foundations are essential to prevent tower collapsing as well as the addition of grounding wires to provide a lightning shield.

For the conductors, the construction is important to deal with and withstand the tension forces, and its electrical specifications should be able to withstand the maximum possible currents including faults without damage. Insulators material and length also are selected carefully for keeping an adequate isolation distance between the conductors and the tower body.

Despite all these measures and specifications, faults on the transmission system cannot be avoided due to the fact that the system is located in an open environment and therefore it is exposed to random events and abnormal conditions. Also, failure in the materials used for insulation, the development of high resistance at joints due to corrosion can lead to development of faults.

Faults can be classified by their duration. Some faults are transient, taking few cycles to clear, for example, a lightning strike that do not cause any damage to equipment, or leakage over a dirty insulator or sometimes could be caused by treeing.

Some faults are permanent, and this occurs due to some severe damage that cannot be cleared by itself, e.g., failed joints, or tower collapse, etc. In this case, the protection system needs to operate to isolate the faulty part of the network and at the same time activate an alarm to alert the maintenance crew.

In either case, i.e. the permanent and the transient faults situations, there is a need to locate the fault quickly. In case of permanent fault, the speed in locating the fault will save time in fixing the fault, and although the faulty part of the system could be isolated successfully, the remaining network configuration may not be designed to deliver the same power to the consumers for long periods of time, especially during peak demand.

Also, transient faults are required to be located, as this action will help the maintenance engineer to identify potential future faults. Although these faults are transient, they could develop into serious permanent faults leading to major power cuts or even total blackout if not rectified.

Faults can be classified as symmetrical and asymmetrical faults, the asymmetrical faults include several conditions such as a single line to ground faults, a double line fault with no ground and a double line to ground faults. While the symmetrical are faults that involved all of the three phases lines, either together with or without ground involvement.

The two categories summarizing those faults are:-

- Asymmetrical, faults. Figure 2.10(a) [10] and this includes:-
    1. Single line to ground (SLG) faults: - AG, BG, and CG.
    2. Double line to ground (DLG) faults: - ABG, BCG, and ACG.
    3. Double line to line (LL) faults: - AB, BC, and AC.
- Symmetrical faults. Figure 2.10(b) [10] and this include:-
    1. Three lines to ground (LLLG) faults: - ABCG.
    2. Three lines (LLL) faults : - ABC.

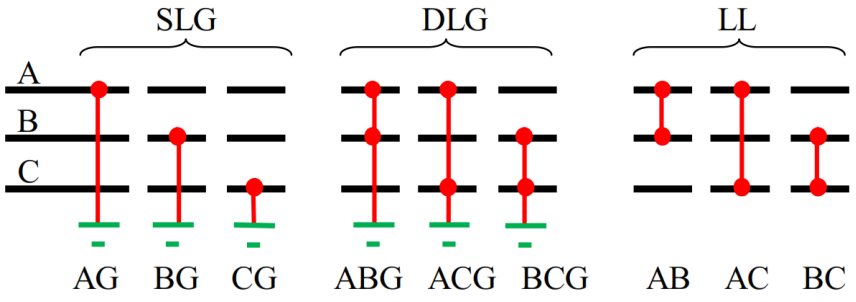

(a) Asymmetrical Faults

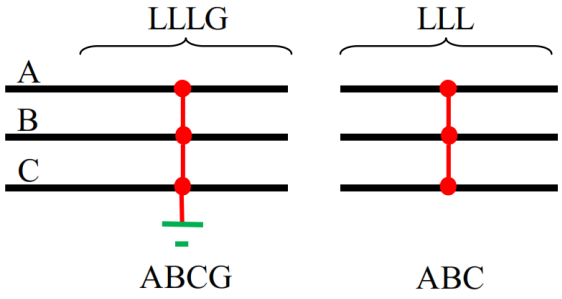

(b) Symmetrical Faults

Figure 2.10: Simulated faults.

2.6 Methods used for fault location

To enhance the reliability and efficiency of a protection system, information about fault should be available immediately after it has been detected; this will help to reduce outage times and restore service quickly. Hence, researchers are developing numerous tools for efficient algorithms for fault diagnosis.

The visual inspection of the line was the first method used for determining fault location [11], and it is still in use especially in the distribution systems. However, considering the time and effort taken, new methods for fault location was and still is an active research area. Different approaches have been used for developing different methods for estimating the location of faults. This section will present examples of the most popular and common methods in the field.

Methods in general fall into three broad categories. The first category (Section 2.6.1) includes two traditional methods; the first type is based on impedance calculation using line parameters, voltage and/or current data to calculate the distance while the second type is based on the travelling wave theory which uses the surge impedance of the line and calculates the distance to a fault by timing the fault transient wave reaching the terminals.

The second category (Section 2.6.2.1) includes the modern knowledge-based methods while the third category (Section 2.6.2.2) includes hybrid methods which could be either based on traditional methods combined with modern methods or methods combining two or more new intelligent approaches. A general summary and comparison between different methods is included in Section 2.8.

To evaluate the accuracy of the different method's estimations, Equation 2.14 is usually used to calculate the estimated error percentage.

$$Estimated\,error\,percentage = \frac{Actual\,location - Estimated\,location}{line\,length} \times 100\% \tag{2.14}$$

2.6.1 Traditional methods

The methods in this category can be divided into two basic groups, impedance measurement based and travelling wave-based schemes ones. The impedance based methods are classified according to how many data collection terminals are involved in the calculations, whether single or double terminal method. Travelling wave methods can be classified according to the source of the travelling wave, some of them use injected waves while some of them depend on analysing the transients generated by the fault occurrence.

2.6.1.1 Impedance calculation methods

Methods based on impedance calculation approach rely on calculating the impedance apparent from the source to the point of the fault using circuit analysis techniques. Thus, knowledge of the impedance parameters of the network is a common requirement for these approaches, and the accuracy of this type of fault locator depends on the accuracy of the calculated transmission impedance [12].

2.6.1.1.1 Single-ended impedance based fault location techniques

The earliest proposed versions of impedance-based fault location depended on estimating the location with the calculation of the impedance using voltage and current readings collected from a single end of a transmission line.

Practically, this approach is easier to carry out than the other methods presented in the coming sections. And also for economic factors, the single-ended impedance based fault location techniques became a common standard feature in relays. Its major advantage is that the communication channels are not required and no need for data from the far end terminals. [10]

Based on the assumptions that the impedance is homogeneously and symmetrically distributed throughout the line length, the ratio of the impedance between the measuring line to the fault point to the total impedance will be proportionate to the distance to the fault.

Figure 2.11 [13] shows a simple power system, where the transmission line is experiencing a fault at point F with R_{F} as the fault resistance. And for illustration, an example of the basic logic behind the performed calculations is based on this simple representation.

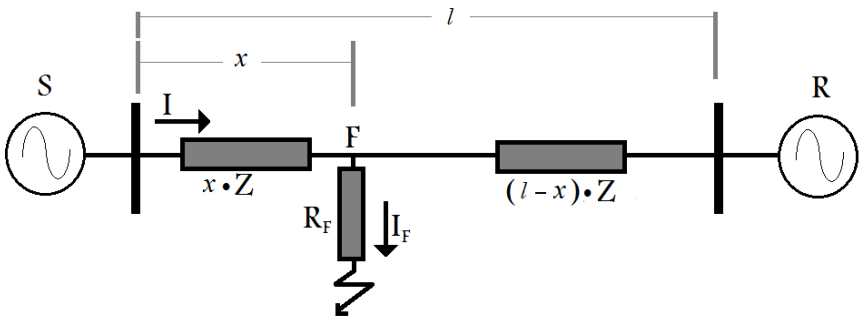

Figure 2.11: Power system fault

Assuming a three phase fault at distance (x) from the source terminal through R_{F} resistance, the voltage equation at one terminal (S) can be expressed in terms of the fault current (I_{F}), line impedance (Z) and the distance (x) of the fault as in Equation 2.15. This can be rewritten as Equation 2.16 [13]

$$V_{\mathrm{S}} = (x \times Z \times I) + (R_{\mathrm{F}} \times I_{\mathrm{F}}) \tag{2.15}$$

$$x = \left[\frac{V_{\mathrm{S}}}{Z \times I}\right] - \left[\frac{R_{\mathrm{F}} \times I_{\mathrm{F}}}{Z \times I}\right] \tag{2.16}$$

High fault resistances cause inaccuracy in the estimation because its value cannot be predicted. In the simple reactance method, which is an example of the single-ended impedance based fault location technique, the effect of R_{F} is eliminated by ignoring the second term of Equation 2.16 and performing the calculations using the imaginary part of the line impedance, to yield Equation 2.17.

$$x = \frac{Im(\frac{V_{\mathrm{S}}}{I})}{Im(Z)} \tag{2.17}$$

For line to line faults, the distance calculation require the availability of voltages and currents for both faulty lines. Equation 2.18 describe the case for phase B to phase C fault condition. Assuming zero fault resistance, the distance therefore can be evaluated by Equation 2.19 for this particular fault.

$$V_{\mathrm{B}} - V_{\mathrm{C}} = xZ(I_{\mathrm{B}} - I_{\mathrm{C}}) \tag{2.18}$$

$$x = \frac{V_{\mathrm{B}} - V_{\mathrm{C}}}{I_{\mathrm{B}} - I_{\mathrm{C}}} \times \frac{1}{Z} \tag{2.19}$$

For single line to ground fault cases, the calculation require the availability of voltage and current for the faulty line. Assuming zero fault resistance, Equation 2.20 describe the AG fault example. using the relationship between the mutual impedance (Z_{m}) with the positive (Z_{L}) and zero sequence impedance ($Z_{0\mathrm{L}}$) given by Equation 2.21 [10], the voltage equation is simplified as in Equation 2.22, and the distance can then be evaluated using Equation 2.23

$$V_{\mathrm{A}} = x((Z - Z_{\mathrm{m}})I_{\mathrm{A}} + Z_{\mathrm{m}}(I_{\mathrm{A}} + I_{\mathrm{B}} + I_{\mathrm{C}})) \tag{2.20}$$

$$Z_{\mathrm{m}} = \frac{(Z_{0\mathrm{L}} - Z_{\mathrm{L}})}{3} \tag{2.21}$$

$$V_{\mathrm{A}} = xZ_{\mathrm{L}}(I_{\mathrm{A}} + K_0 I_{\mathrm{R}}) \tag{2.22}$$

$$x = \frac{V_{\mathrm{A}}}{I_{\mathrm{A}} + K_0 I_{\mathrm{R}}} \times \frac{1}{Z_{\mathrm{L}}} \tag{2.23}$$

The K_0 is the ground compensation factor evaluated by Equation 2.24 while the I_{R} is the residual current.

$$K_0 = \frac{(Z_{0\mathrm{L}} - Z_{\mathrm{L}})}{3Z_{\mathrm{L}}} \tag{2.24}$$

Table 2.1 summarizes the Positive-Sequence Impedance equations for the different faults [12] [13]. Inspecting Equations 2.17, 2.19 and 2.23 and their summary in Table 2.1 shows how the availability of line parameter impedance characteristic information is a must in performing such calculations. Moreover, the zero sequence characteristics information is also required for the single line to ground fault cases [12] [13] [14]. The inclusion of the K_0 term in cases of single phase to ground faults, also indicates the need to know the type of fault [14]. Incorrectly identified fault type will lead to incorrect fault location estimation [13].

Table 2.1: Positive-Sequence Impedance Equations

Fault Type	Positive-Sequence Impedance Equation
A-Ground	$\mathrm{V_A}/(\mathrm{I_A}+K_0 I_{\mathrm{R}})$
B-Ground	$\mathrm{V_B}/(\mathrm{I_B}+K_0 I_{\mathrm{R}})$
C-Ground	$\mathrm{V_C}/(\mathrm{I_C}+K_0 I_{\mathrm{R}})$
A-B or A-B-G	$\mathrm{V_{AB}}/\mathrm{I_{AB}}$
B-C or B-C-G	$\mathrm{V_{BC}}/\mathrm{I_{BC}}$
C-A or C-A-G	$\mathrm{V_{CA}}/\mathrm{I_{CA}}$
A-B-C	Either ($\mathrm{V_{AB}}/\mathrm{I_{AB}}$), ($\mathrm{V_{BC}}/\mathrm{I_{BC}}$) or ($\mathrm{V_{CA}}/\mathrm{I_{CA}}$)

Another assumption which is also made is about the phase shift between the line current during a fault at the terminal and the fault current through the fault resistor R_{F}. This phase shift is assumed to be zero. In addition to this, there is a need with this type of fault to assume no load prior to the fault.

All the above assumptions to simplify the methodology actually generate errors in the final estimation of the fault. Further research is, therefore, focused on improving the method by eliminating these errors arising from the assumptions.

For example, to reduce the effect of both terminals on the fault current, a method proposed by [15] was one of the earliest reported to tackle these errors. It considers two components which form the fault current generated from each of the terminals of the transmission line. Figure 2.12 [13] shows the I''_{FS}, which is the fault current component generated from the source terminal, and I''_{FR} is the fault current component generated from the receiver terminal; Equation 2.25 describes the voltage drop at the fault point.

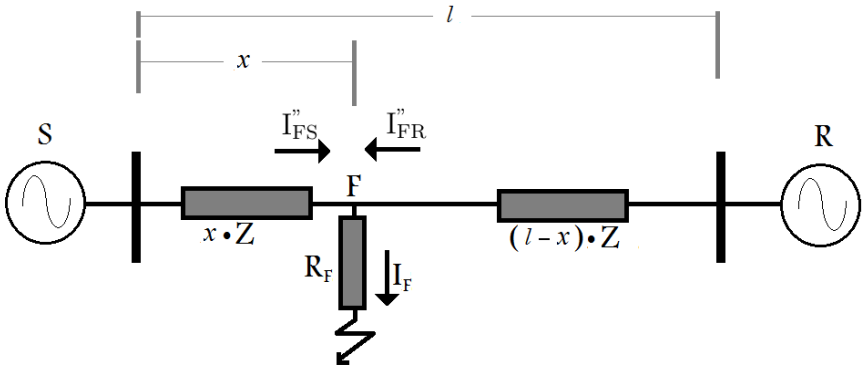

Figure 2.12: Fault current components

$$V_{\mathrm{F}} = I_{\mathrm{F}} R_{\mathrm{F}} = (I''_{\mathrm{FS}} + I''_{\mathrm{FR}}) R_{\mathrm{F}} \tag{2.25}$$

Using the long transmission line equations in hyperbolic form, the voltage at the fault point and the fault current component generated from the source terminal can be expressed by Equations 2.26 and 2.27. Where V''_{S} and I''_{S} are the pure fault values and computed as the difference between the pre-fault and the after fault values.

$$V_{\mathrm{F}} = V_{\mathrm{S}} cosh(\gamma x) - Z_{\mathrm{c}} I_{\mathrm{S}} sinh(\gamma x) \tag{2.26}$$

$$I^{"}_{\mathrm{FS}} = \frac{V^{"}_{\mathrm{S}}}{Z_{\mathrm{c}}} sinh(\gamma x) - I^{"}_{\mathrm{S}} cosh(\gamma x) \tag{2.27}$$

Assuming a purely resistive fault impedance, solving for the imaginary part of impedance will yield Equation 2.28:

$$Im \left\{ \frac{V_{\mathrm{S}} cosh(\gamma x) - Z_{\mathrm{c}} I_{\mathrm{S}} sinh(\gamma x)}{V^{"}_{\mathrm{S}} \frac{sinh(\gamma x)}{Z_{\mathrm{c}}} - I^{"}_{\mathrm{S}} cosh(\gamma x)} \right\} = 0 \tag{2.28}$$

This is a non-linear function where the fault distance x is gained by solving the equation numerically using the Newton-Raphson method [15].

The author in [16], introduces one of the earliest reported algorithms which exploit voltage and current data from a single end of the transmission line. The algorithm calculations are performed using a microprocessor and considering automatic correction of the potential error sources. Reported errors (Equation 2.14) from field tests in estimations range from 0.7% to 2.7% for SLG faults and from 0.6% to 1.3% for DLG faults. The author considered the result satisfactory.

Comparison between different approaches was presented in [17]. The single end method evaluation shows that the results accuracy is highly affected by the high fault resistance. It also shows that the error in the estimation was affected by the location of the fault.

There are several other attempts aiming to improve this approach. An example of further enhancement was reported in [18]. The paper focus is on testing the algorithm with the SLG faults only, and it considers the effect of the mu-

tual inductance between parallel transmission lines. The reported error in the simulation results was less than 1% under varying conditions.

2.6.1.1.2 Double-ended impedance based fault location techniques

This method benefits from the advancement and availability of communications technology. The double-ended impedance method is based on voltage and current measurement at both ends of the transmission line. Most of the single terminal method disadvantages do not exist in this type as most of the simplifying assumptions which were causing the errors are no longer present.

In Figure 2.12, the voltage at the fault point can be expressed as shown in Equations 2.29 and 2.30.

$$V_{\mathrm{F}} = V_{\mathrm{S}} - ZxI^{"}_{\mathrm{FS}} \tag{2.29}$$

$$V_{\mathrm{F}} = V_{\mathrm{R}} - Z(l-x)I^{"}_{\mathrm{FR}} \tag{2.30}$$

x is then can be determined by Equation 2.31

$$x = \frac{\left(\frac{V_{\mathrm{S}} - V_{\mathrm{R}}}{Z}\right) + I^{"}_{\mathrm{FR}}}{I^{"}_{\mathrm{FS}} + I^{"}_{\mathrm{FR}}} \tag{2.31}$$

Equations 2.29, 2.30 and 2.31 use lumped elements for the transmission line. For long transmission lines, these equations are in hyperbolic form. The voltage at the fault point can be expressed by Equations 2.32 and 2.33

$$V_{\mathrm{F}} = V_{\mathrm{S}} cosh(\gamma x) - Z_{\mathrm{c}} I^{"}_{\mathrm{FS}} sinh(\gamma x) \tag{2.32}$$

$$V_{\mathrm{F}} = V_{\mathrm{R}} cosh\gamma(l\text{-}x) - Z_{\mathrm{c}} I''_{\mathrm{FR}} sinh\gamma(l\text{-}x) \tag{2.33}$$

And x is then can be calculated by Equation 2.34. [19]

$$x = \frac{tanh^{\text{-}1}\left[\dfrac{V_{\mathrm{S}} + Z_{\mathrm{c}} I''_{\mathrm{FR}} sin(\gamma l) - V_{\mathrm{R}} cosh(\gamma l)}{Z_{\mathrm{c}} I''_{\mathrm{FS}} + Z_{\mathrm{c}} I''_{\mathrm{FR}} cosh(\gamma l) - V_{\mathrm{R}} sin(\gamma l)}\right]}{\gamma} \tag{2.34}$$

Since the fault resistance R_{F} value is not required in calculation of Equation 2.34,this give the method an advantage of in-dependability on the fault resistance unpredicted value. It depends mainly on available measurements with no approximations. However, similar to the single end approaches, the line parameter need to be known before the algorithm is used. On the other hand, only positive-sequence components are used in the calculation for all fault types eliminating the need to classify fault type.

Unlike relays, the time is not a critical factor in the work of the fault locators. However, to compare, it is worth noting that the data required for the single-ended methods are collected from one terminal, and this provides an advantage requiring less time than the double terminals methods.

Synchronisation between reading the data from both ends is another challenge that adds complexity to the algorithms. As there are two types of categories for the algorithm which depend on this requirement, the synchronised data based category has higher accuracy, but has greater communication requirements. The recent advancement in communications technology such as The Global Positioning System (GPS) services provides a solution for the communication requirement challenge.

This category of algorithms has advantages of being unaffected by changes in loads or the fault resistance, but the loss of synchronisation threatens its accuracy. An example of using synchronized data of both terminals in a differential protection approach is given by [20]. The performance of this approach was evaluated on a simulated protection system and found to be fast and accurate.

Numerous variations of the approach of double terminal fault location synchronized algorithms are found in the literature. An example of using the approach in a fault locator is given by [21]. No fault classification was required as the proposed technique was independent of the fault type. It was found to be insensitive to fault resistance, and the errors (Equation 2.14) were less than 0.05%. The same approach was utilised in [22], and [23], and a good level of accuracy was achieved. The results indicate a small error for all cases which never exceeds 0.75% and the average value was in the range of 0.5%.

The unsynchronised based category was also an active research area. With the aim of improving its accuracy, some algorithms depending on signal processing for providing synchronization which added an element of complexity to the algorithms design. As an example of this approach, [24] provide a comparison between a single-ended and a double-ended impedance based fault locator. The estimation in the latter uses data from both ends, which does not require the data to be synchronized. The location estimation was found accurate irrespective of the fault type or fault resistance.

Another example of a double terminal fault location unsynchronized algorithm is given in [25], the proposed algorithm was designed for asymmetrical faults, and the evaluation was reported by both simulated and field data. The author claims satisfactory accuracy. The error in the results ranges between 1.43% and 2.79% which was due to missing the shunt capacitance modelling in the algorithm.

A further example of this approach is given in [26]. In this paper, excellent average error (Equation 2.14) was reported for the asymmetrical faults (maximum 0.17%) while relatively higher error was recorded for the symmetrical one (2.8%). The method starts by defining a synchronization index to obtain a synchronization angle and perform unsynchronized measurements corrections. The fault location can then be estimated by the impedance calculations.

2.6.1.2 Travelling wave based methods

Travelling wave based methods requirements are much more than impedance based methods. Despite this, travelling wave based methods were adopted widely as an alternative method for fault locating especially after improvements in communications systems and advancement in data acquisition tools and methods. The technique depends mainly on measuring the time required for travelling waves from fault incidence points to reach the terminals [10].

Fault occurrence appears as a surge in both the voltage and the current and are related to each other by the surge impedance of the line. These waves propagate away from the disturbance point towards both terminals of the transmission line, the wave shapes and magnitudes depend on several factors like the type of the fault, fault inception angle and the fault resistance, but governed mainly by the characteristic impedance of the line.

Measuring the exact time taken for the wave to travel between the fault point and the measurement point is key to estimating the distance accurately [12]. The general requirement of the algorithm is a fault detecting element and the central data processing unit which does the calculations in addition to synchronising time reference at both line terminals. This synchronization may be provided by the Global Positioning System (GPS).

The line in which this method may be implemented should not be composed of different segments, i.e., using the method for overhead lines only or underground cables only, but not a combination of both. This is due to different surge impedance which will produce multiple reflections leading to reduced accuracy. Another factor that is necessary for the system's overall accuracy is the detector element sensitivity as the error in detection travelling waves may cause inaccuracy.

Bewley's lattice diagram [27] is a graphical visualisation method that is used for providing illustrations in this type of method. Figure 2.13 [27] shows an example of a lattice diagram scenario for the fault already shown by Figure 2.11 in Section 2.6.1.1.

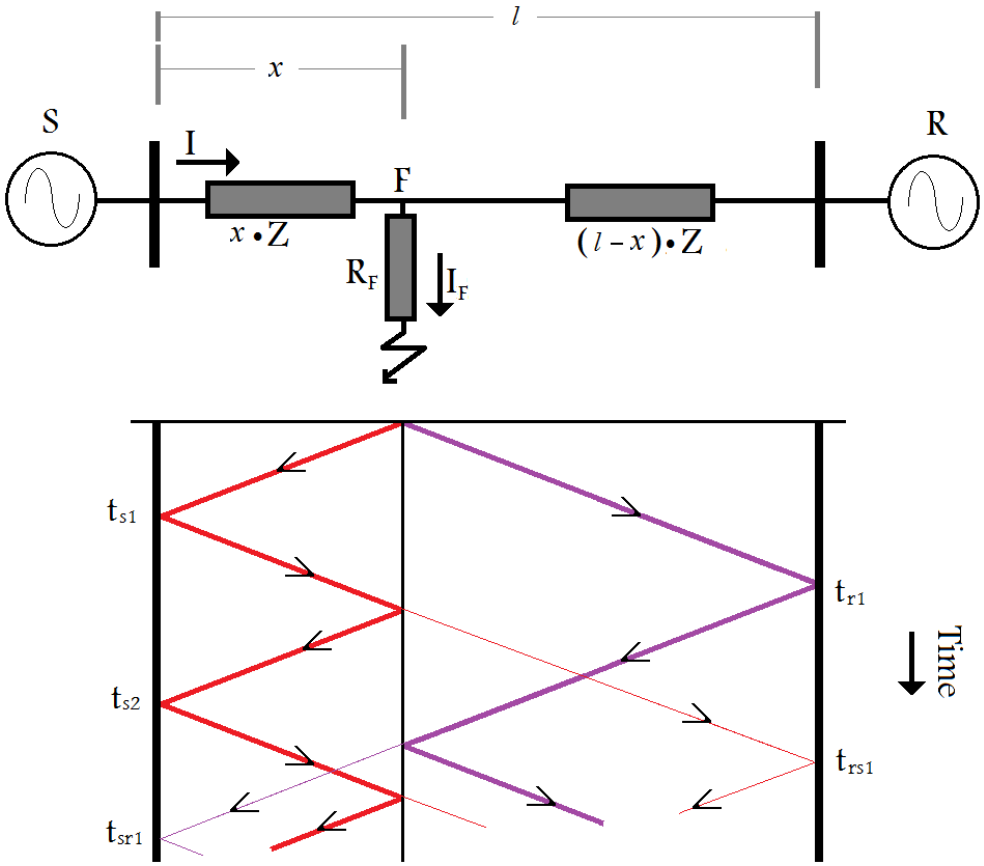

Figure 2.13: Bewley's lattice diagram

The two transient waves start their journey travelling from the fault point towards their respective terminals as illustrated by the arrows in Figure 2.13. Attenuation in wave magnitude is expected, and it is determined by the line characteristics, and this depends on the line construction material and the tower physical dimension if it is an overhead transmission line.

Upon reaching the terminal of the transmission line, a proportion of the wave will be reflected depending on the impedance of the line and to what it is connected. This reflected wave will travel back to the fault point. The magnitude of the reflected part experiences further attenuation depending on the line characteristics.

These waves continue to be reflected at discontinuities in impedance as illustrated in Figure 2.13 until they are totally attenuated. If those waves are monitored, a series of subsequent travelling waves will be captured which will hold adequate information about the location and the type of the fault.

For instance, the distance x in Figure 2.13 can be estimated using t_{s1} which is the time of the first travelling wave to reach the source terminal, and t_{s2} which is the time of the reflected part of the first travelling wave to reach the source terminal again as shown in Equation 2.35 where v is the speed of light ($3x10^8$ m/s) [28].

$$x = \frac{t_{s2} - t_{s1}}{2} \times v \tag{2.35}$$

With the same aim, there are different approaches found in the literature using the same techniques. They are categorised into five distinct types depending on the data source, and the processing performed as shown summarized in Table 2.2 [29]. For instance, the last calculation is categorized as Type A [30] [10], it

is the single end based travelling wave calculation type, where information from only one terminal is analysed to determine the fault position. It represents the simplest type with the lowest cost and highest reliability. The detector elements are only necessary at one line terminal, and no communication link is required.

Table 2.2: Travelling wave method types

Type	The measuring method used	Measurement terminals
A	Measuring the time for wave generated by fault when reaching the fault locator and the time for the wave reflected from the fault location reaches the fault locator.	One end of the line.
B	Analysing pulses injected in the line.	Both ends of the line.
C	Analysing pulses injected in the line.	One end of the line.
D	Use of two synchronized devices installed at both ends of the line.	Both ends of the line.
E	Use wave which is generated by closing circuit breaker on transmission line.	One end of the line.

Among the different types which are based on a travelling wave method, and involving the number of terminals, both Types E and C are single-ended method similar to Type A while both Types B and D are double-ended [10].

Differences in the processing can be found in the source of the travelling wave. For example, Type D is like Type A, categorised as a passive method since they are analysing the waves which are generated by the fault incident, while Types B and C are active methods since they depend on analysing pulses

injected into the line by additional circuitry. Type E can also be considered as an active method, as it uses the transients generated when a circuit breaker re-energises a line [10].

The two passive methods have their own differences. For example, when Type A systems analyse the wave and its reflections at one end, Type D analyses the two waves generated from the fault and reaching the two terminals and this gives the additional requirement of needing an effective communication tool providing an accurate GPS synchronisation service so that the difference in the times of first arrival of the two waves are determined accurately. Although this is an additional requirement that adds cost and decreases system reliability, it avoids problems associated with multiple reflections between the terminal and the fault point.

A typical advantage found in the travelling wave methods and worth mentioning is that there is no need to consider most of the simplifying assumptions already considered for the impedance based methods as they are not required in this method calculations. In addition, and in terms of accuracy, satisfactory results are reported which found fault location estimations to be within ± 300 m irrespective of line length [12]. On the other hand, its main disadvantage appears in poor performance with high fault resistance cases, faults with zero inception angle and faults occurring close to the measurement terminal [31]. Another disadvantage related is the accuracy proportionality to the sampling rate [27].

2.6.2 Recent technology based methods

The era of microprocessors with greater processing power enabled rapid developments opened the doors wide for researchers to suggest new more sophisticated methods for determining fault location based on artificial intelligence (AI) techniques. In terms of accuracy in estimating the fault location, various AI-based techniques have reported as giving an advantage over conventional techniques [10]. Section 2.6.2.1 introduces a few examples of methods which are based solely on the application of new artificial intelligence techniques approaches such as artificial neural networks and fuzzy logic, while Section 2.6.2.2 includes a few examples of methods that combine one or more of recent technologies with conventional methods in hybrid approaches.

The Fourier transform was the basic transformation tool that was applied to extract the fundamental frequency component for fault analysis [32] [33] [34], but this method was found not suitable in the transient periods and it was giving relatively big errors [10]. The wavelet transform was then proposed as a new analysis tool for its ability to overcome limitations of the Fourier transform, it is characterised by its fast and very effective means of analysing transient waveforms, the wavelet transform mathematical tool was widely adopted and employed as a preprocessing stage in transmission line fault diagnosis research and examples will be shown later [32] [35] [33].

2.6.2.1 Knowledge based methods

In this category, among several types, the artificial neural networks (ANNs) have the largest number of researchers using its various architectures [36]. ANNs have been also applied successfully in tackling many power systems related aspects, such as load forecasting [37] [38], unit scheduling [39], power quality [40] and transformer protection [41] [42] and many other related issues [43].

Artificial neural network construction is based on interconnected neurons cells, each connection between neuron cells has an initial weight and the different neurons are arranged in multiple layers, the number of neurons of the first layer(input layer) depends on the complexity of the problem specified by the number of inputs selected by the researcher. Figure 2.14 shows an example of the multilayer feed forward type of ANN which is adopted in the majority of the research work, the middle layers are called the hidden layers which could consist of one or more layers, the output layer in the example contain one neuron, but it may contain more [44].

The learning algorithms and pattern recognition are gained by modifying the connection weight between neural cells by performing training on cases simulating many possible conditions. Neural networks learning ability is gained from its adaptive nature to the training cases. At the end of training, the network is required to recognise conditions, even if they are not included in the training session cases. The outputs of a poorly trained network are unpredictable, and this explains the need for a large training set to cover a wide range of possible conditions [45] [44].

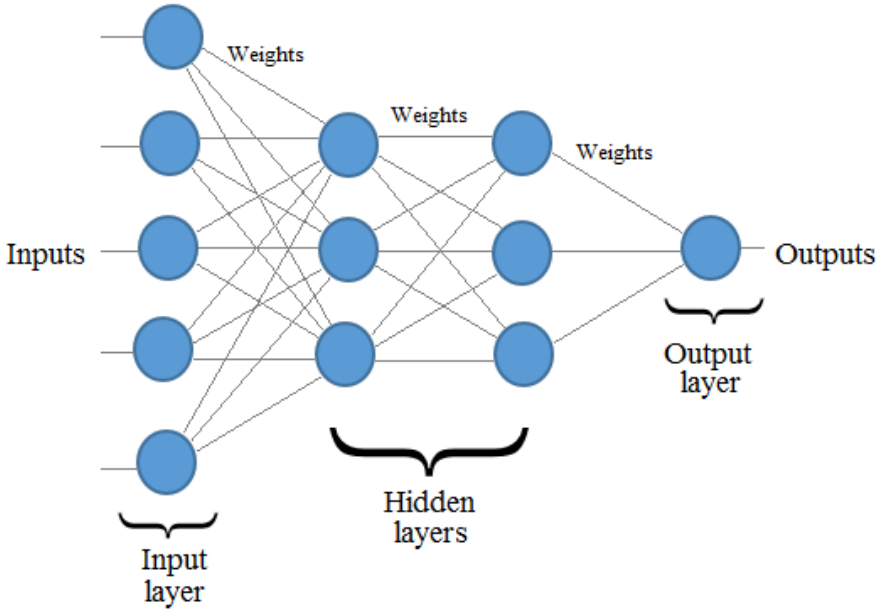

Figure 2.14: Artificial neural network: feed forward

Generally, one major limitation of neural networks is the possibility of unpredictable behaviour and giving unexpected outputs without indications that it is doing so. Also, due to the final trained network black box nature, errors are difficult to target.

The method has been applied to solve different problems and carry out tasks in various research disciplines, and the power system fault location research area has been an active subject of interest.

In protection, many successful applications focus on protection of power system components such as transformers [46] [41] [47], generator protection [48] [49], in addition to distribution system diagnosis [50].

As part of the protection field, the fault diagnosis in transmission line was covered by several works. As an example, in [51] the ANN method was used in the implementation of three single terminal fault locators. Similar to the single terminal impedance methods, the voltages and currents were collected from one terminal and fed to the input layer. In this paper, all proposed locators operations

are triggered by fault detection, and the average error (Equation 2.14) in the estimations did not exceed 0.15%.

In another example [52], a combination of the self-organizing neural network and the multilayer feed forward network was suggested as a fault recognition system. The processing was conducted on the voltage measurements, and good results are reported as the maximum error does not exceed 0.5%.

Some work using wavelet transform as the preprocessing tool for the ANN has been reported, [53], this approach applies the Discrete Wavelet Transform processing on voltage and current signals at the end of the transmission line. The algorithm serves in type classification in addition to location estimation by utilising a neural network. A low average error (Equation 2.14) was reported, and its maximum error percentage did not exceed 0.30%.

In [54] as further examples of Wavelet Transform processing with the utilisation of a neural network. The current signals of both ends are used to classify the faults, the estimation of fault location was then carried out by an Artificial Neural Networks. Even with high maximum percentage error reaching 1.89% in some cases, but the average error did not exceed 0.16% for all types of fault.

Although well trained ANNs have general advantages, that it could overcome the traditional methods in terms of accuracy. However, ANN-based fault locators have the general disadvantage that they require a comprehensive set of training data and a considerable amount of training effort [45]. Paper [55] gives an example of an accurate neural network that was trained on single-phase-earth fault cases. The author shows how poor the performance became when subjected to data for other types of fault. In addition, ANN has a slow learning rate [56] and there is a need for retraining in case of network structure is modified.

Fuzzy logic is another popular artificial intelligence method that was adopted successfully in many fields [57]. When processing a specific condition by a fuzzy logic based system, the purpose is to assign a degree of membership for this condition to one or more members of a fuzzy set of solutions. Unlike the Boolean logic, the membership degree is not restricted to a 'zero' or a 'one' sharp value, but could range to any value between them. In electrical engineering, fuzzy logic main application is in control systems [58]. In fault diagnosis it can, in successful implementations, provide both classification and location of faults even under complicated conditions and this is due to its ability to deal with imprecise or vague data and making decisions despite complex situations [59].

A broad range of research work was undertaken using fuzzy logic with the wavelet transform used as the waveform preprocessing tool. As an example, in [60], the author proposes a fault locator for a double transmission line. The technique employed discrete wavelet transform for extracting high-frequency component from positive sequence current signals. The variations of the high-frequency component were the input for the Fuzzy Logic based decision algorithm. The simulated line was 200 km long and the reported average error was 0.84 km. So using Equation 2.14, the estimated error percentage was 0.42%.

Another example of wavelet-Fuzzy combined approach was published in [61]. The wavelet transform is employed in capturing the dynamic characteristics of fault signals, and the fuzzy logic is employed to estimate location. The reported error (Equation 2.14) reaches a maximum of 6.5%.

The genetic algorithm was applied in estimating fault location based on its ability to deal with optimisation problems. In addition, it was also employed successfully in providing further information such as the fault resistance. For an example, [62] presents a new fault location method using a genetic algorithm.

The line parameters of a compensated line were the initial data for the problem. Voltage and current samples at both terminals are then acquired for processing, no need for fault type information and the reported results show high accuracy. The error in the estimation (Equation 2.14) did not exceed 0.41% in its worst case. The author reports the method achieves same high accuracy degree regardless of the fault type and fault resistance.

2.6.2.2 Hybrid methods

Recent approaches tend to combine several methods in one tool. The aim is to benefit from the various advantages available in the different methods and to reduce errors. For example, the ANN method may be combined with conventional travelling wave theory. Based on the ANNs capability of pattern recognition, it can be trained to recognise the travelling waves different shapes generated by a fault and thus can estimate their location.

Another combined approach was published in [63]; a wavelet-neuro-fuzzy combined approach for fault location is presented. The wavelet transform is used for analysing the captured waveforms and the adaptive-neuro-fuzzy inference system is used to estimate the location using the extracted features. In another example, paper [55] give an artificial neural network and genetic algorithm possible combination into location estimation tool using current signals only.

In general, the reported performance of recent non-conventional methods is found promising and, in particular, the hybrid methods. But due to concerns about the reliability and other challenges related to factors such as the time consuming training or the high computation complexity, all of these factors play role in slowing their introduction and commercial adopting [2] [3].

2.7 Methods used for fault classification

For early developed impedance based fault location systems, in particular the single end type [12], the availability of fault type information was an essential. There was an attempt to remove this requirement by researchers, and this was successfully achieved in the two terminals based algorithms [19].

As a major part of power quality monitoring, researchers on fault type classification put effort into developing tools for providing helpful diagnostics. The wavelet transform was one of the foremost methods which were adopted successfully in many classification algorithms. For example, in [64], the wavelet transform is used to detect and classify different faults in transmission lines. The algorithm is based mainly on analysing the wavelet coefficients RMS values of current signals at both the ends of the transmission line. Another fault classification which is based on wavelet transform was also published in [65]. The algorithm identifies and classifies the fault based on analysing the three phase line currents.

With adequate training, the neural network's ability of pattern recognition was found useful in identifying fault types. Many artificial neural networks (ANNs) have been successfully applied to power systems and have been found to give good levels of accuracy in fault diagnosis [50]. They have also been used for fault classification in transformer [46], [47] and also for faults in synchronous generator [49]. For transmission lines faults classification, an example of the neural network method implementation of a fault classifier is reported in [66].

The wavelet transform has served as the signals preprocessing tool for artificial intelligence methods. For an example of ANN classifier, in [67], the classification method for extra high voltage transmission line faults using wavelet transform is presented. The wavelet transform is used to analyse short circuit transient signals. The ANN is then used to identify the fault. Another example [68],

investigates a classifier system which combines the wavelet transform and neural network techniques using single-ended voltage and current signals measurement. The wavelet transform has been used for signal analysis, and the neural network is used as the classification tool. In [54] the author proposes a neural network for accomplishing the locator algorithm, but the classifier part of the paper depends only on analysing the wavelet transform outcomes of the current signal analyses. Another example of Wavelet Transform classifier with ANN is reported in [53].

The fuzzy logic ability on solving uncertainty problem can be used in building fuzzy based classification tools. An example of a fuzzy based classifier is presented in [69], where a fuzzy-set logic was used in proposing fault classifier on a transmission line.

The wavelet transform has also been used as a tool for signals preprocessing stage before the fuzzy logic based classifier. For example, in [70] the author proposes a new asymmetrical fault classification method using fuzzy-logic-based approach. Only currents are handled through Wavelet Transform. The fault type decision is taken through fuzzy rule sets. As another example of the wavelet-fuzzy combined fault classification approach, the method in [61] employs wavelet transform for preprocessing the waveforms, and the fuzzifier stage performs the classification of the fault type. Another example of Wavelet Transform classifier with fuzzy logic is reported in [71]. The wavelet analyses of current signals from a series compensated transmission line are given as input for the fuzzy logic classifier.

A wavelet-fuzzy-neuro network (WFNN) combined approach was published in [63]; the proposed algorithm is utilised to function as a classifier, in support of the location estimation function algorithm already mentioned in Section 2.6.2.2. The system is using WFNN combined approach to analyse extracted features of

wavelet transform outcomes. Paper [72] provides another example of this approach utilization for extracting useful information about SLG faults, the characteristics are revealed by analysing the transient feature and the high frequency components of the waveform and the authors claim obtaining a highly accurate information which is not affected by the fault resistance.

Fault classifier approaches which adopt Hybrid neuro-fuzzy methodology were presented in some papers such as [73], [74] and [75]. While [76] propose a fuzzy based classifier combined with a travelling wave method. An example of a classifier that combine fuzzy with neural can be found in [77].

2.8 Methods summary

In Tables 2.3 and 2.4, a general summary and comparison between conventional and recent diagnostic tools already discussed in Sections 2.6 and 2.7 is presented.

The tables include methods general basic principles, main advantages, different parameters required for operation, limitations sources that influence the accuracy and the achieved accuracy.

Limitations encountered in some methods encourage researchers for proposing new improved and enhanced methods, and some disadvantages of the newly proposed methods put restrictions on their commercial application and implementations. The study of the advantages and disadvantages of the various methods helps researchers in proposing diagnostic tool replacement candidate with enhanced features. Main limitations that should be avoided are represented in the time-consuming preprocessing, high cost and high data requirements.

Table 2.3: Conventional methods

Method	Features and requirements	Performance
Impedance based	Features - popular - estimating distance by calculating apparent impedance from the measuring point to the fault location - two types: The double end and single-ended Requirements - the line parameter - voltage and current - fault type	The double end is better than single -ended in terms of accuracy, but the double end methods take extra cost for synchronization and communication requirements. Accuracy limitations in both types are caused by approximation assumptions Need filtering process to eliminate high frequency component and the DC transients effects Depend on line parameter information so accuracy depend on transmission line parameter calculation accuracy
Travelling wave-based	Features - popular - determining the time for the wave to travel between the fault position and the measuring point - two types: Active wave generated by the fault - and passive wave injected in the line - need high sampling rate Requirements - the line parameter - voltage or current - accurate timing	Remarkable performance compared to Impedance based as no need for simplifying assumptions Disadvantages:- the reliability, maintenance problems the economical factor : need extra hardware, and need communication and synchronization tools. factors affecting accuracy: attenuation of the waves, fault inception angles, faults near measurement point. error in detection waves cause inaccurate estimation and accuracy proportionality to the sampling rate

Table 2.4: Recent methods

Method	Features and requirements	Performance
Wavelet transform	Effective tool, its main usage was as the preprocessing tool for the other artificial intelligence methods. Requirements - High sampling rate. - Voltage and/or current	- Fast and very effective means of analysing transient waveforms. - Remarkable performance.
Artificial neural network	Popular utilisation as classifier owing to being Powerful in pattern recognition. Advanced networks with preprocessing tools and hybrid methods are utilised as a locator. Requirements - Voltage and/or current	- Remarkable performance especially as classifier. - Enhanced locator accuracy when combined in hybrid method with other methods. - Efficiency depends on sufficient and comprehensive training. - Retraining is needed in case of network change.
Genetic algorithm	Requirements - Voltage and/or current - Line parameter	- Remarkable performance - Depend on line parameter information so accuracy depend on transmission line parameter calculation accuracy.
Fuzzy	Popular utilisation as classifier owing to being Powerful in making decisions despite imprecise or vague data. Requirements - Voltage and/or current	- Acceptable performance As classifier. - Enhanced locator accuracy when combined in hybrid method with other methods.
Hybrid methods Example: (WFNN)	Combined advantages Requirements - Voltage and/or current	- Remarkable performance. Disadvantages - Time consuming training - High computation complexity.

2.9 Chromatic methodology

Methods used for monitoring and diagnosis of faults in complex power systems have been evolved from mathematical impedance calculations into modern advanced methods using tools based on intelligent techniques. And the search is continuous to find more accurate, reliable tools.

Chromatic processing techniques have been applied to complex systems with very good effect [4], [78]. The modern Power system and its faults with their accompanied interactions is a case of a complex system. Applying chromaticity to this might lead to a design of a reliable and high-speed protection scheme or may improve existent protection functions.

The chromatic methodology technique provides a means of signal recognition in terms of parameters which are analogous to those encountered in colour science but which have been extended to complex data. This chromaticity research is not the typical colour monitoring methodology which is normally used as an experimental method for extracting information from colour or light changes in the complex system. However, an understanding of its signal transformation is needed as the basic principles are derived from this technique. Therefore, this section explains the eye colour vision principles in order to provide the background to the methodology, [79] as well as examples of the mathematical model of chromatic filtering and transformation. [4]

It is worth noting that although the techniques utilised in this work are derived from the field of chromatic processing, almost every aspect of the developed tools here for the power system use are different from those found in the applications of the technique to date.

2.9.1 Colour vision

Before focusing on the application of chromaticity, it is necessary to understand some basic principles of the approach.

Vision is the dominant sense in human. The visual system is a highly complicated network of neural and genetic connections, and to discuss its full detail is beyond the scope of this work. This introduction is focusing on eye vision technique in recognising colour which forms the basis of modern colour science.

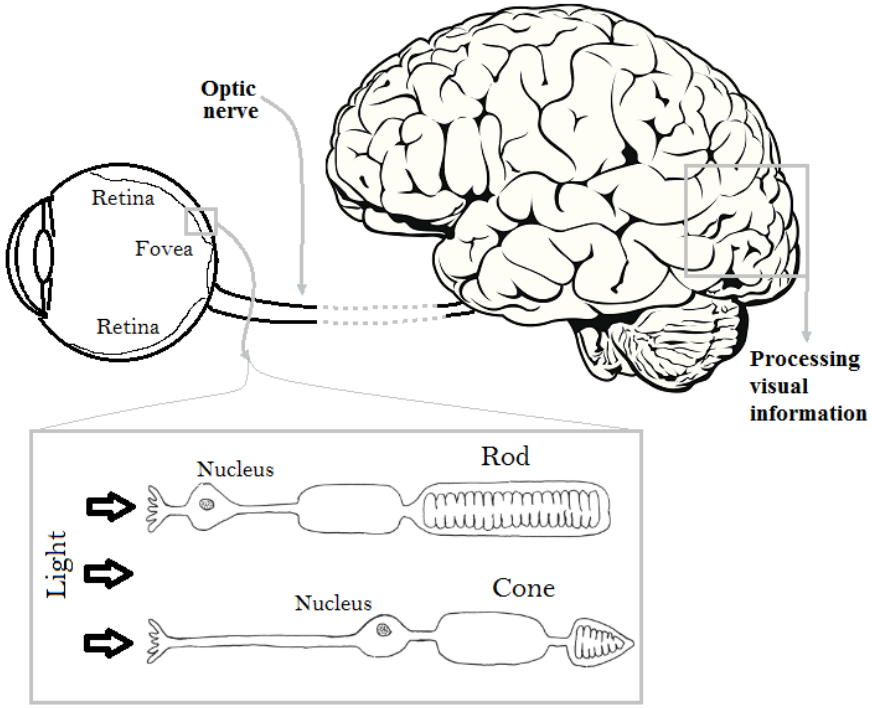

Figure 2.15: Human visual system

Figure 2.15 shows the human visual system, the eye is the front-line of this system. Light from outside is focused by the lens onto the retina. Which is absorbed by pigments in light-sensitive cells, those light receptors are called rods and cones and they got their names from their shapes. Rods are about 125 million cells distributed evenly over the whole surface of the retina. While cones are

roughly 6 million cells in the eye and their distribution is highly concentrated in the fovea, near the centre of the retina. Both receptors transfer their output to the Visual cortex which is the visual processing region of the brain, the information is transferred through the optic nerve. [79]

The cones respond to a different range of colour and they are sensitive to a wide range of brightness. Humans have three different types of cones and they are sensitive to short, medium and long wavelengths, respectively. Rods are more sensitive than the cones and they have the capability of responding to lower light level.

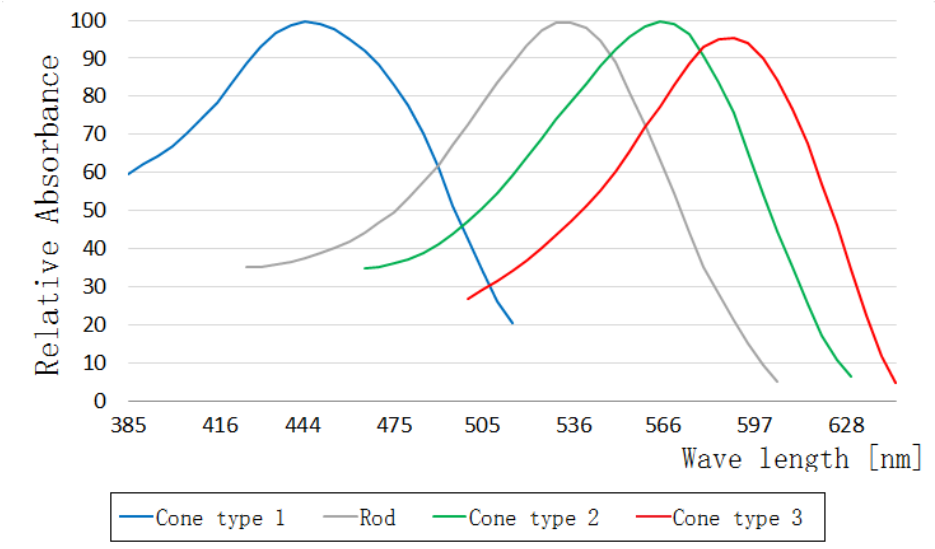

Figure 2.16: Rods and Cones filtering

Figure 2.16 shows the sensitivity of the different cones to varying wavelengths. The response varies with wavelength for each kind of receptor. Type 1 of cones got a maximum sensitivity to the 440 nm wavelength. Type 2 of cones, maximum sensitivity found to be located at the 550 nm while the last type maximum sensitivity is located at 600 nm wavelength. Thus, three parameters, corresponding to levels of the stimulus of the three types of cone cells, can in principle describe any colour sensation. There is an overlap between their response which means that

some wavelengths will not stimulate only one type of cone cell, and this overlap is important in the application of chromaticity processing. [4]

The described process handled by the cones and rods cells is the filtering stage. Receptors are covering the complete wavelength range from about 380 to 750nm. Non-orthogonality feature of the receptors profiles gives them comprehensive coverage regardless the complexity degree of the monitored scene. The next stage is transforming the outputs information to a form that the brain can recognise and use.

The entire process has been adopted in colour science. Both stages have been modelled and applied successfully, and different models are available in the field. The following subsections contain examples and description of filtering and transformations models used in colour science.

2.9.2 Chromatic modulation (Filtering)

Inspired by the cone cells function, implementation of chromatic processing is performed by the utilisation of non-orthogonal filters covering the intended range of the signal domain [4]. As an example, Figure 2.17 [80] is illustrating the filtering process for two signal P1 and P2, three overlapping filters labelled: R for red, G for green and B for blue, are covering the signals domain.

The output value of each filter depends mainly on the filter shape, and monitored signal distribution at the filter. Different profile shapes could be used for filtering. The one shown in Figure 2.17 is the Gaussian. Another shape is triangular which is adopted in this work for its easy implementation in simulation packages.

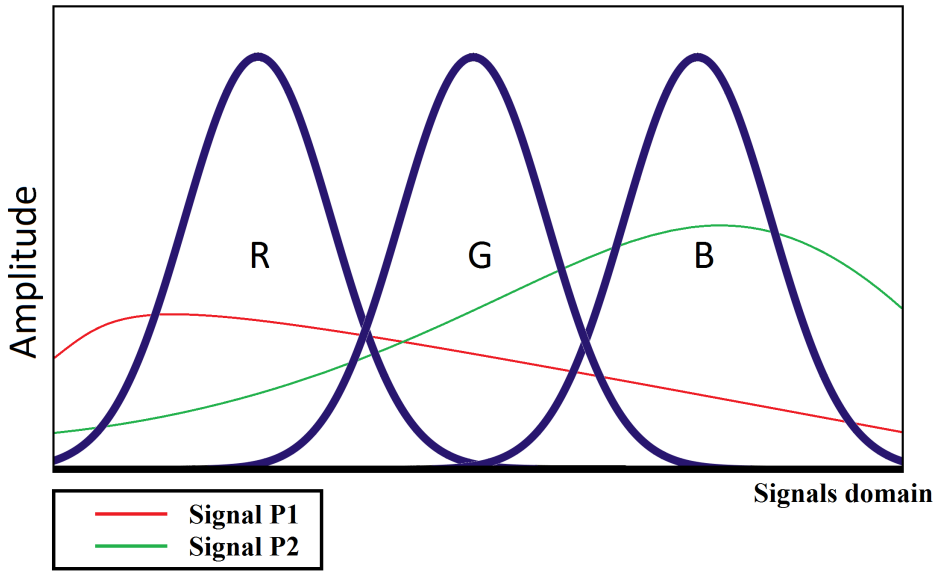

Figure 2.17: RGB filters

The Gaussian was used originally for similarity with cone filter profiles, and mathematically adopted from Gabor transform theory, while the triangular shape is preferred for simple calculations. Regardless the filter shape, the three filters outcomes are given by:

$$R_0 = \int R(\varphi)P(\varphi)d\varphi \tag{2.36a}$$

$$G_0 = \int G(\varphi)P(\varphi)d\varphi \tag{2.36b}$$

$$B_0 = \int B(\varphi)P(\varphi)d\varphi \tag{2.36c}$$

P(φ) is the monitored signal and R(φ), G(φ) and B(φ) are the filters profiles, φ is the monitored signals domain.

2.9.3 Transformations based on colour models

The colour model is simply the way of describing the colour. This is achieved by mathematical relationships which define a tool for mapping the monitored wavelengths and their related colour which result in a specific organisation of colours called the colour space.

The filtering process outputs (R_0, G_0 and B_0) for the monitored wavelengths will form the input for the colour model. Models are used for simulating the vision system response to light and transformation aims to produce useful information about colour attributes such as hue, lightness and saturation.

Through their contribution to the colour science field, researchers work on developing several algorithms for producing tools for chromatic mapping into colour space. One of the earliest defined colour models is the CIE xyz model which was created in 1931 by the International Commission on Illumination (CIE).

Numerous models have also been developed such as the Hue, Lightness and Saturation (HLS) colour model, the Hue, Saturation and Value (HSV) colour model and the International Commission on Illumination (CIELab) colour model in addition to many more [81] [82]. Most models were adopted commercially for applications in image processing, presentation, video applications, printers, etc.

In some art materials and digitized images, some models are sometimes preferable for its ability to emulate how humans perceive colour and for the easy implementation such as the (HLS) model. Work presented in this thesis is based mainly on the this model and the transformation performed using its equations. Next subsection defines the mathematical relationships. Work using other colour models are left as part of future work suggestions which will be discussed later in Chapter 6.

2.9.3.1 HLS colour model

HLS (hue-lightness-saturation) colour model was developed in the 1970s for computer graphics applications. It is one of the most common colour representation models [82] and it is mainly used in image editing software. [81]

The (HLS) colour model parameters are Hue, Lightness, and Saturation. The Hue parameter values are given in the form of an angle between 0° and 360°, starting with the blue colour at 0° and followed by magenta, red, yellow, green and cyan with 60° between them. Equations 2.37a, b and c are used for evaluating the Hue for this colour model.

$$H = 240 - \frac{120 \times g}{g + b} \qquad r = 0 \tag{2.37a}$$

$$= 360 - \frac{120 \times b}{b + r} \qquad g = 0 \tag{2.37b}$$

$$= 120 - \frac{120 \times r}{r + g} \qquad b = 0 \tag{2.37c}$$

Where

$$r = R_0 - Minimum(R_0, G_0, B_0) \tag{2.38a}$$

$$g = G_0 - Minimum(R_0, G_0, B_0) \tag{2.38b}$$

$$b = B_0 - Minimum(R_0, G_0, B_0) \tag{2.38c}$$

Lightness of the colour can be evaluated by calculating the average of the three filters outputs. The lightness ranges from black to white with the grey

scale in between. The lightness indicate the darkness of the colour, where the values of 0 and 1 belong to the white and black respectively and the pure hues lie at L = 0.5 . Lightness value can be determined using Equation 2.39

$$L = \frac{R_0 + G_0 + B_0}{3} \tag{2.39}$$

The saturation S, determine how much the intensity is distributed across the spectrum, its value ranges from 0 to 1, and the pure colour have a saturation value S = 1. Equation 2.40 is used to evaluate saturation in the HLS colour model.

$$S = \frac{[Maximum(R_0, G_0, B_0) - Minimum(R_0, G_0, B_0)]}{[Maximum(R_0, G_0, B_0) + Minimum(R_0, G_0, B_0)]} \tag{2.40}$$

As an example, when the three RGB filters are applied on the two signals P1 and P2 illustrated in Figure 2.17, the R_0,G_0 and B_0 outputs are equal to 0.42, 0.29 and 0.2 respectively for signal P1 and equal to 0.17, 0.4 and 0.7 respectively for signal P2.

For signal P1, calculating the r,g and b values using Equations 2.38a, b and c will yield 0.22, 0.09, and 0 respectively, so Equation 2.37c will be used to evaluate the H value for this signal since b=0, and its value will be equal to:

$$H = 120 - \frac{120 \times r}{r + g} = 120 - \frac{120 \times 0.22}{0.22 + 0.09} = 34.9$$

While for signal P2, the r,g and b values are 0, 0.23, and 0.53 respectively. Equation 2.37a is then used to evaluate the H value for this signal since r=0, and H value will be equal to:

$$H = 240 - \frac{120 \times g}{g + b} = 240 - \frac{120 \times 0.23}{0.23 + 0.53} = 203.7$$

Equations 2.39 and 2.40 are used for the L and S calculations. For signal P1 the results are:

$$L = \frac{R_0 + G_0 + B_0}{3} = \frac{0.42 + 0.29 + 0.2}{3} = 0.3$$

$$S = \frac{[Maximum(0.42, 0.29, 0.2) - Minimum(0.42, 0.29, 0.2)]}{[Maximum(0.42, 0.29, 0.2) + Minimum(0.42, 0.29, 0.2)]}$$
$$= \frac{0.42 - 0.2}{0.42 + 0.2} = 0.35$$

The same equations are used for signal P2 and the results are:

$$L = \frac{R_0 + G_0 + B_0}{3} = \frac{0.17 + 0.4 + 0.7}{3} = 0.42$$

$$S = \frac{[Maximum(0.17, 0.4, 0.7) - Minimum(0.17, 0.4, 0.7)]}{[Maximum(0.17, 0.4, 0.7) + Minimum(0.17, 0.4, 0.7)]}$$
$$= \frac{0.7 - 0.17}{0.7 + 0.17} = 0.61$$

After evaluating the parameters of the colour, different representation might be used to visualise the relationship between them, Figure 2.18 gives a 2-D representation of the parameters on chromatic maps in the form of H-S and H-L polar diagrams, with H as the angle and S and L as the radius. As examples, points correspond to the signals P1 and P2 chromatic parameters are shown in the polar plots.

The key factor in choosing suitable parameters depends on the nature of the problem under study and the feature to be extracted. In this work, in addition to the useful polar diagrams, an alternative representation of parameters change versus time will be used.

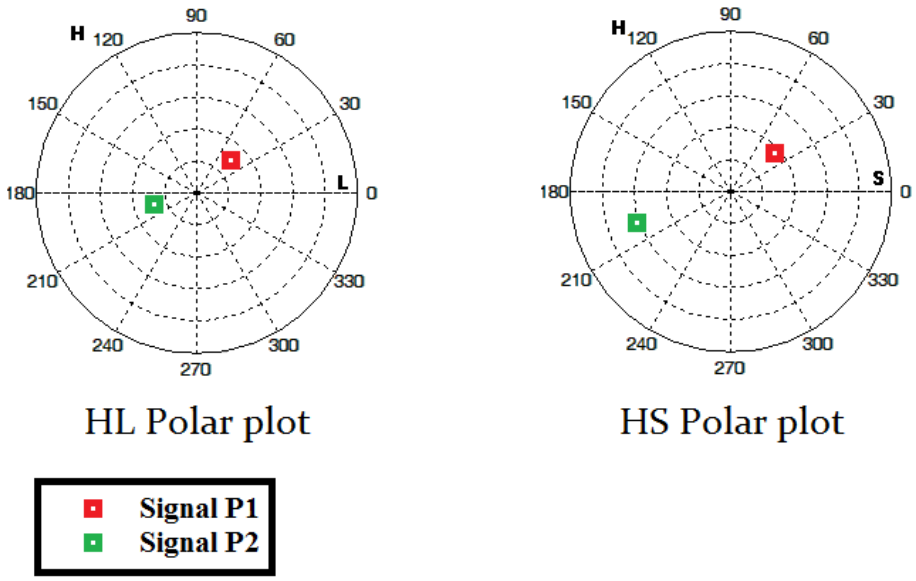

Figure 2.18: HS and HL polar plots, chromatic diagram

2.9.4 Chromatic monitoring applications

The chromatic processing methodology has been used in applications involving sensing and analysing signals from different sources, types, etc. Although diverse fields are studied, chromaticity development led to a generic type of monitoring systems for quantifying light in the wavelength domain.

As examples of the applications, emission spectra monitoring of material processing plasmas was presented in [83] and a reliable performance was reported. Monitoring can address the behaviour of light if it passes through a specimen of material or an object under study, thereby providing useful applications [84] such as monitoring urine samples for predicting urinary tract infection. Another example in [85] monitored the light passing of transformer oil sample for condition assessment.

Chromatic methodology has been extended to other application domains including temporal, spatial, frequency, etc. For example [86], analyse the acoustic signals collected for a transformer under operation. The approach in [87] employ monitoring performed in the time domain; the monitoring covers partial discharges occurring in the first quarter of a single cycle.

In the power system research, few applications were focusing on monitoring vital elements such as the transformer. As example [88] monitored the radio frequency signals from a transformer in an attempt to provide a classification of the partial discharges sources and types. Another transformer related application was described in [86], [89]. The approaches are based on tracking acoustic events by continuous acoustic condition monitoring of transformers chromatically. A further example in [85], propose a system for optical monitoring of transformers oils, aiming to provide oil degradation information by chromatic analyses of light transmitted through the oil samples.

The paper [87] includes successful attempts to extract information about dielectric from signals emitted by partial discharge, the approach is based on chromaticity methodology. A review of chromatic approaches for monitoring power transformer partial discharge signals is published in [90]. In high voltage applications, [80] present a study of high voltage interrupters characteristics under various operating conditions, the system can provide critical operational conditions for such units.

Based on the chromaticity distinguished ability to extract useful information from monitoring complex systems signals, the research methodology in this work will be an attempt to explore the possibility of using chromaticity as a diagnostic tool for transmission line faults, and this attempt will be the first to employ such tool in this field.

2.10 Summary

The transmission line is a vital element of a complex power system; operational measures are taken to ensure it is reliable with minimum losses and to avoid any possible failures. However, the overhead transmission lines are in an open environment and subject to random events, making it impossible to avoid accidents that could lead to transient and sometimes permanent faults that threaten the integrity and the reliability of the power systems and, in particular, the transmission line.

Providing accurate fault classification and location estimation has been an active research area, and researchers have used many schemes. Conventional methods depend mainly on impedance calculations or travelling waves while nowadays approaches use modern intelligent methods like fuzzy systems, neural networks or wavelet transform approaches. Good results have been achieved, but a literature review has shown no known approach that is based on the methodology of chromatic monitoring.

Chromatic monitoring methodology has been used in monitoring complex systems and proven to be effective in providing a diagnosis of their conditions. Chromaticity is presented as a potential method for monitoring power system signals and providing accurate fault classification and location estimation.

Chapter 3

Computer simulations, experimental apparatus and setup

3.1 Introduction

To test the possible algorithms and to validate the results, an experimental test facility is required to replace testing on a real power system with the potential risks that cause its reliability and service availability. Also waiting for a natural occurrence of various events could take an unrealistic amount of time and is therefore probably not feasible.

This chapter describes selected system configurations that have been simulated by computer and their experimental setup. These systems are designed to be a long double circuit transmission line connecting two networks and simple power supplying basic resistive load through a single circuit short transmission line.

A set of fault conditions are set up in the software and hardware on a model network system. Current and voltage readings are recorded during the simulation and from the model system from various case studies are presented with their calculated symmetrical component values. They also include non-fault conditions. The symmetrical components calculations are based on the symmetrical components method presented in Appendix D.

In part of this study, a double circuit three phase transmission line is experimentally investigated under different faults. The SimPowerSystems™ package from Matlab® is used for building typical system simulations. The circuit components are provided from a built-in component library. Also, components are used to build the hardware models of a simplified single circuit three phase transmission line delivering power to a resistive load. The details of the two cases are described in Sections 3.3 and 3.4.

3.2 Simulated faults

Various faults can occur during the process of power transmission, the majority of which are asymmetrical faults (97%) [91] [92], 80% of which are single line to ground and 17% are double line to ground faults. Symmetrical faults account for 3%of the faults [91] [92]. For the purpose of testing algorithm, various types of faults described in Section 2.5 are simulated, for these following conditions.

Fault location: 10%, 50%, and 90% of the distance.

Fault resistance: 0.001, 10 and 100 Ohm.

3.3 Case study 1 : Double transmission line

Parallel transmission lines are commonly used at higher voltages. This configuration minimises power losses and, therefore, maximises delivered power. The transmission lines play a major role in an AC power system, and it is this part of the network which is investigated in the following sections.

3.3.1 Case 1. System description

The power system schematic diagram shown in Figure 3.1 is simulated using the Simulink® SimPowerSystems™ package. The system is an example of a typical 735 kV system, served by a 200 km double circuit transmission line. The diagram shows a fault (F) located on the transmission line, the data collection points are at M1 and M2.

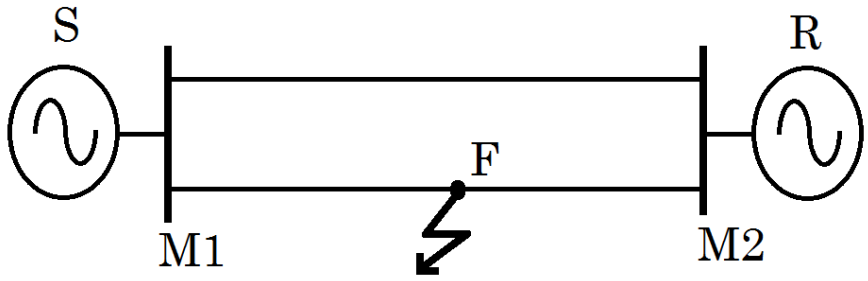

Figure 3.1: Simulated double transmission line (S: Source, R: Receiver)

Different line models are available in the SimPowerSystems™ package. The distributed parameter line model is selected in this study. The values of the power line parameters used in the simulation are given in Table 3.1. Simulink® provides a user-friendly interface through which the user can choose the transmission line parameters, length and frequency that suit the application configuration. Length is used for the purpose of specifying the values of R, L and C calculations.

Table 3.1: Line Parameters

Positive sequence resistance R1	0.01165 Ω/km
Zero sequence resistance R0	0.2676 Ω/km
Positive sequence inductance L1	0.8679×10^{-3} H/km
Zero sequence inductance L0	3.008×10^{-3} H/km
Positive sequence capacitance C1	13.41×10^{-9} F/km
Zero sequence capacitance C0	8.57×10^{-9} F/km

Each branch of the parallel transmission line is constructed from two transmission line model block units connected in series. The location of the fault is simulated by setting the length of the first transmission line unit and subsequently modifying the second unit length. The total length of the two parts will give the full length of the transmission line.

Various types of short circuit faults illustrated in Section 2.5 can be performed using a three phase fault block. This block is connected between the two transmission line blocks. The interface dialogue box that is associated with this element gives the user the ability to choose the fault type, start time and the duration of the event. The user can also add the resistance to ground that the fault presents. A number of cases have been considered by varying the fault resistance and the faults locations.

The system under consideration is tested repeatedly by selected fault conditions. The signals are captured in a discrete form covering time before and during the fault. The data are taken from the three phases of the transmission line under different types of asymmetrical and symmetrical faults. The discrete sample time is specified by the setting 'SampleTime' parameter and this is selected as 5×10^{-6} sample time step (3333 samples per cycle).

Matlab's Simulink® scopes are used for voltages and currents recording. Upon completing the simulation, the data are moved to the Matlab workspace. From there they are subsequently exported to a file for storage.

3.3.2 Results of case 1 : Double transmission line

The results in this section are obtained from the double transmission line simulation. The waveforms of current and voltage are collected for both non-fault and fault conditions as described in Section 2.5. The waveforms are collected from both terminals of the transmission line.

The following are examples of these waveforms and the raw data that serves as input to the processing methodology for location estimation and type classification.

3.3.2.1 Case 1. Non-fault situation

By running this system with no faults, the collected waveforms from the sender terminal for a healthy condition are presented in Figure 3.2. Three phase currents and voltages are as shown in Figure 3.2(a) and Figure 3.2(b) respectively, the current and voltage data are also recorded for the receiver terminal but not presented here. Phase A symmetrical components are then calculated using their described equations in Appendix D. The symmetrical components of the non-fault system current are as shown in Figure 3.3(a). And the symmetrical components of the non-fault system voltage are as shown in Figure 3.3(b). In both cases, only the positive sequence component appears while the negative and zero components are at almost zero or negligible value.

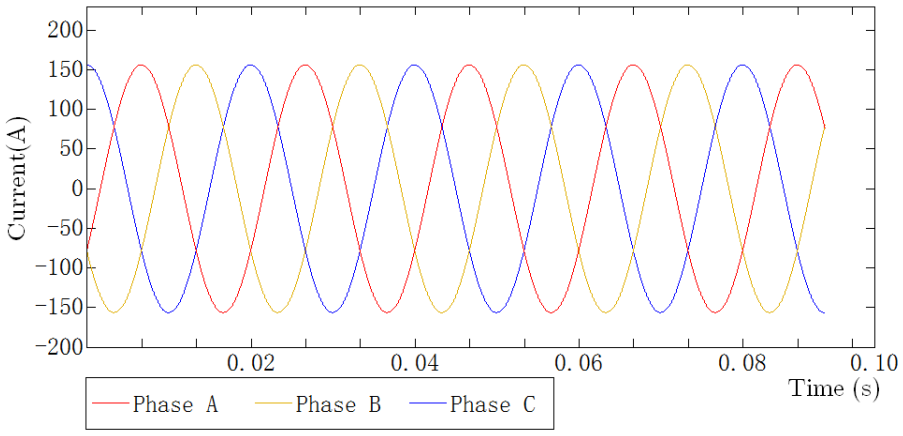

(a) Three phase currents

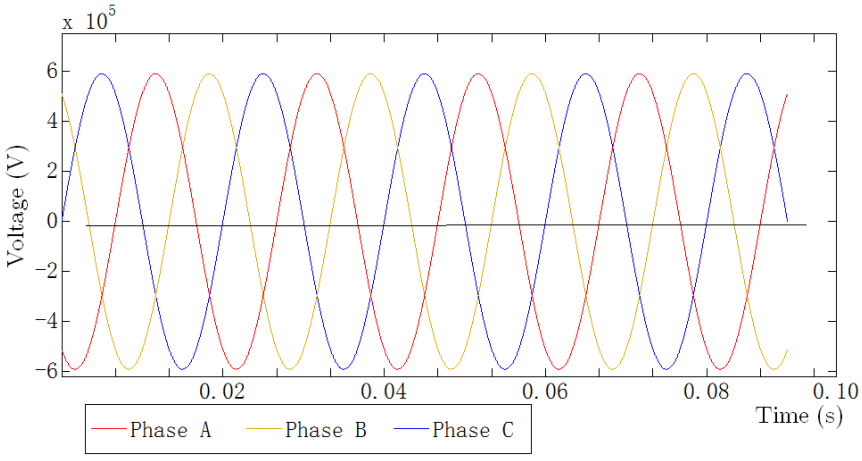

(b) Three phase voltage

Figure 3.2: Healthy system. Waveforms recorded at the sender terminal

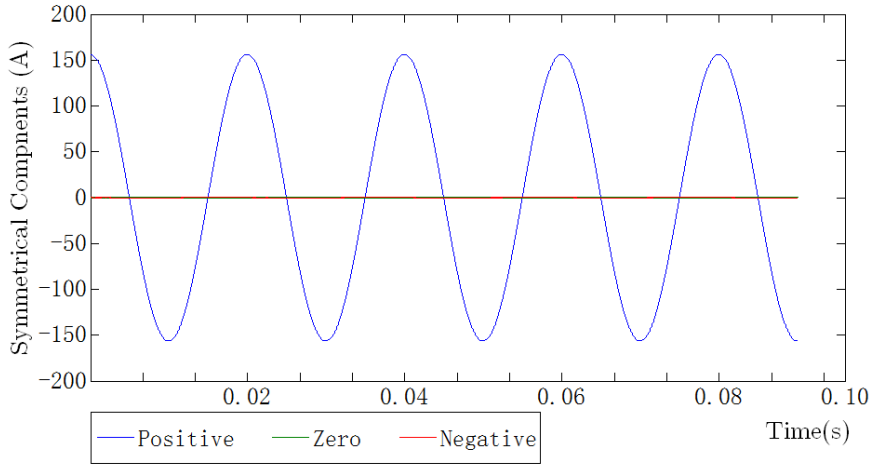

(a) Phase A, current symmetrical components

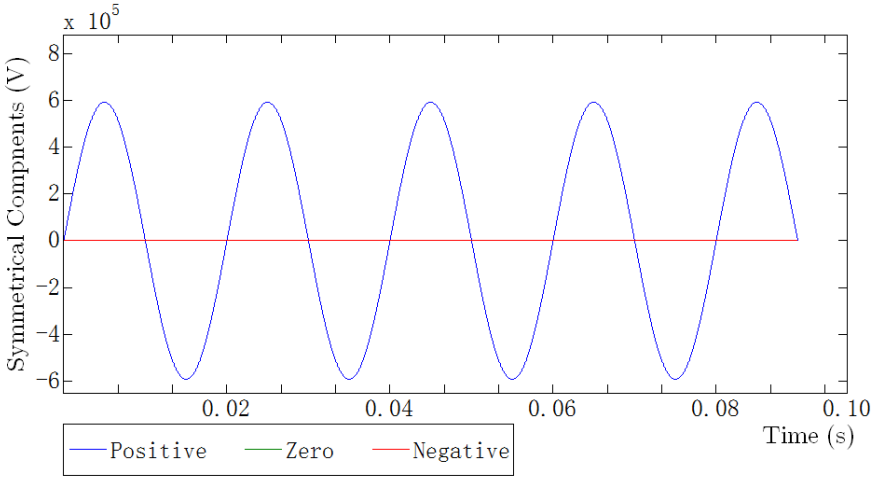

(b) Phase A, voltage symmetrical components

Figure 3.3: Healthy system. Symmetrical components at the sender terminal.

3.3.2.2 Case 1. Single line to ground (SLG) fault

The most common type of faults is the single line to ground fault (SLG). This is a short circuit between one of the three phases A, B or phase C with the ground. This is characterised by a sudden current increase in the appropriate phase. The increase depends on several factors including the system voltage, fault resistance and fault location. The remaining two phases with no faults usually experience disturbances, and their currents are normally affected but to a lesser degree.

3.3.2.2.1 Case 1. SLG fault, at different locations

As an example of SLG fault, the BG fault is induced in the simulation and the results are shown in Figure 3.4, by changing the location of the fault and keeping all other parameters the same, the results from the simulated fault at three different locations 10%, 50% and at 90% of the line length are shown in Figures 3.4(a), (b) and (c) respectively.

High-frequency currents start to propagate immediately following the occurrence of the fault as seen on the figure prominent on the first cycles. These high-frequency oscillations are produced by travelling waves that propagate in the line between the source terminal and the fault point. When the fault is close to the source, Figure 3.4(a) shows an example of a fault current at 10% of the line; the high frequency component and oscillations are greater than for other fault locations far from the source. Figure 3.4(b) shows the currents of the fault in the centre of the line, high-frequency oscillations are recorded, but to a lesser degree and is reduced further when the fault is far from the measurement point (Figure 3.4(c)) due to reflections being attenuated from their detection point.

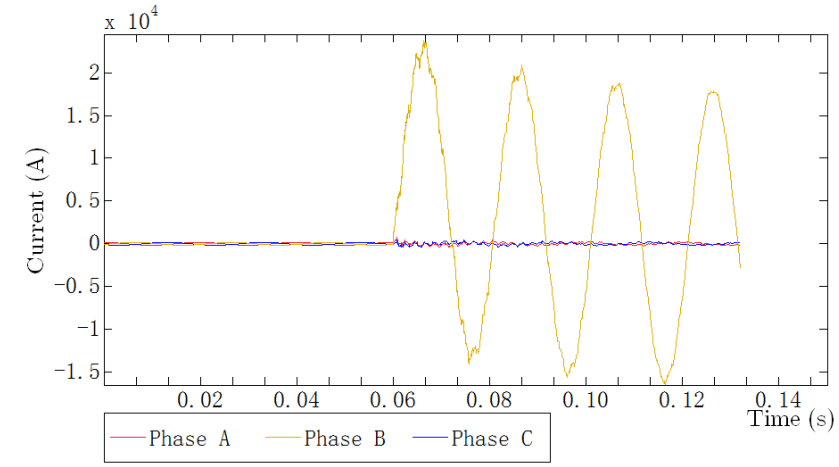

(a) At 10% of the line

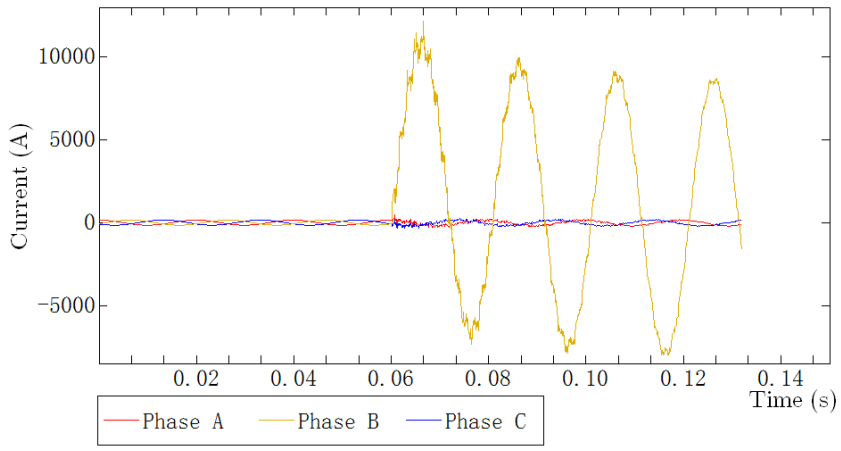

(b) At 50% of the line

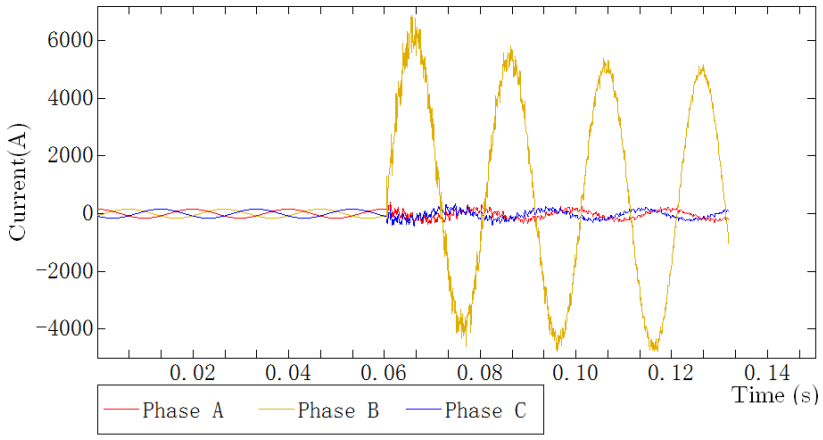

(c) At 90% of the line

Figure 3.4: SLG fault:- BG fault three phase currents waveform at three different locations

Fault locating approaches using wavelet technique utilise the high-frequency component in these signals as they contain a lot of information depends on the location of the fault. The waveforms are processed by a wavelet transform to extract the required signals for analysis [93] [94].

A short circuit in one of the phases represents a sudden change in the network configuration, the power that was generated to supply a specific load is suddenly going through very low resistive fault into the ground. A high current transient is therefore expected; this current will be higher in magnitude when the fault is close to the supply terminal.

A change is also expected in the line current with the fault as the phase changes after fault occurrence. The magnitude, high-frequency component and phase shift change are detected in the remaining two phases as well but to a lesser extent. This occurs due to the mutual inductance between the three phases.

The symmetrical components of the three current waveforms are calculated for phase A using the symmetrical components theory. Figures 3.5(a), (b) and (c) show the symmetrical components of the current at the same three different locations as the fault currents recorded in Figure 3.4.

Before the fault occurrence, due to system symmetry, both the negative and the zero component do not exist. The positive component is the only component that appears. Immediately after the fault occurs, all of the three different components show a change in their characteristics. The faulty phase will experience various changes in the magnitude, phase shift and high-frequency components, and those changes are contributing to changes seen in the symmetrical components.

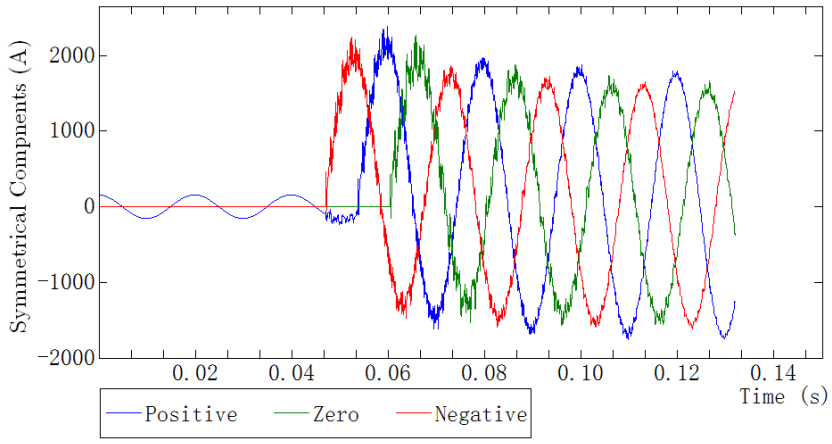

(a) At 10% of the line

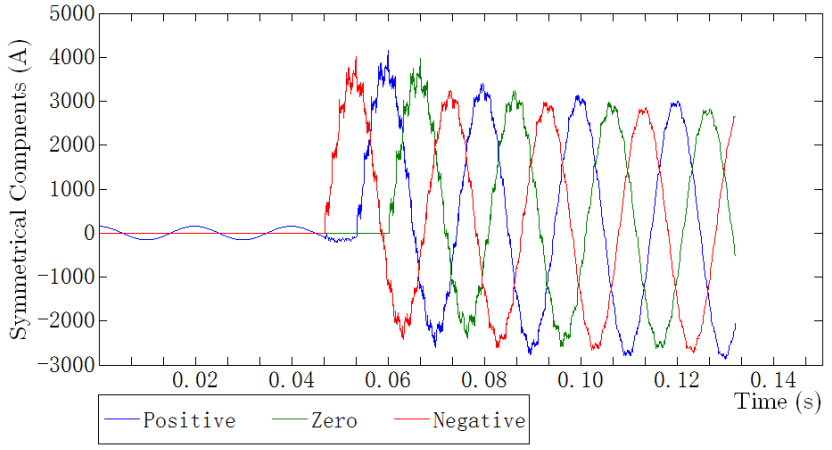

(b) At 50% of the line

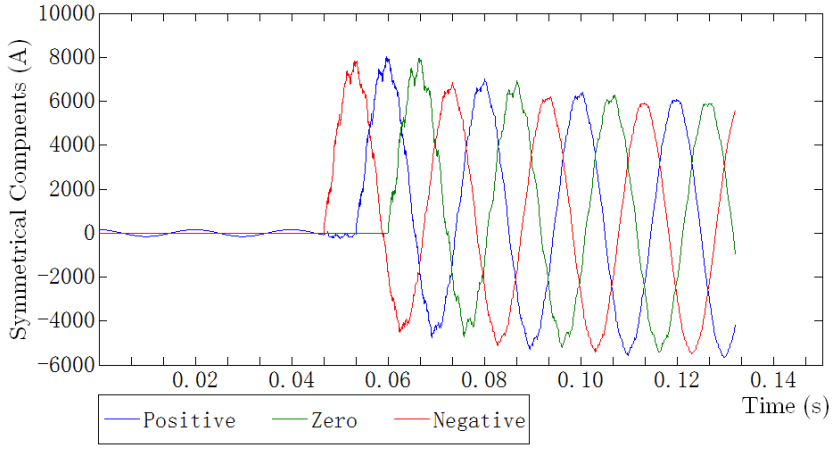

(c) At 90% of the line

Figure 3.5: SLG fault:- BG fault symmetrical components of three phase currents at three different locations

The positive component increases in amplitude, as the phase changes and oscillations occur at the moment of the fault; the negative component increases from a negligible to a high value, and this is a result of the asymmetry in the system caused by the fault. The zero component also increases due to the ground element involvement in this fault condition. The closer the fault to the sending end, the greater the change.

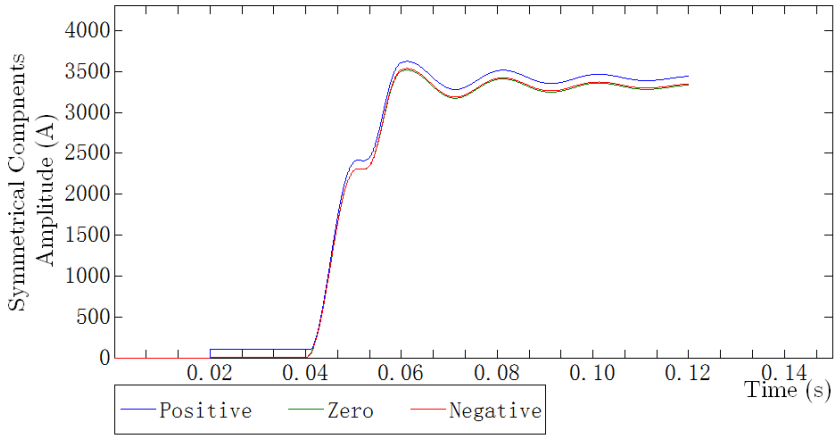

Figure 3.6: SLG fault:- magnitude of current symmetrical components for a BG fault at 50% of the line

Figure 3.6 shows changes in the magnitude of the symmetrical components for the current. And Figure 3.7 shows the changes in the phase shift. The figures relate to the case where the fault is located at 50% of line position.

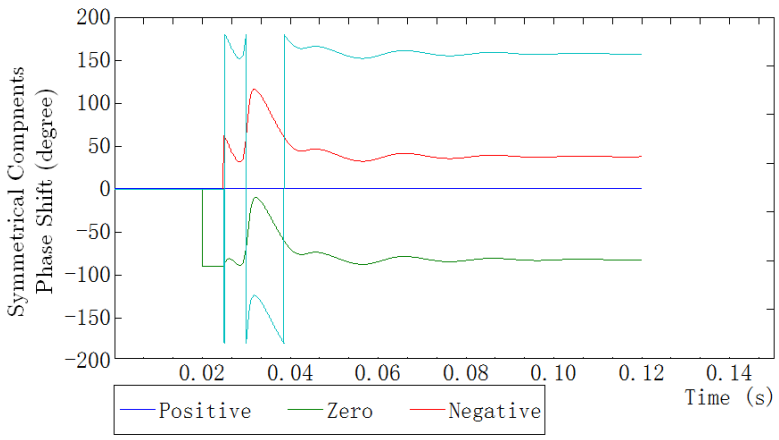

Figure 3.7: SLG fault:- phase shift of current symmetrical components for a BG fault at 50% of the line

3.3.2.2.2 Case 1. SLG fault, voltage waveforms at different locations

The voltage waveforms for the BG fault are shown in Figure 3.8. By changing the location of the fault and keeping the same simulation parameters not associated with distance or length, the results are at the same fault locations as before and are shown in Figure 3.8(a), (b) and (c) respectively.

Various changes are detected in three phases voltage waveforms. Due to the high current flowing through the fault, the voltage level in the faulty phase decreases. This reduction increases as the fault is closer to the receiving end. A slight decrease in voltage is noted in the remaining two phases magnitudes. A change in the phase is also noticed together with a high-frequency component which appears immediately after the fault occurrence.

The symmetrical components of the three voltage waveforms are calculated using the symmetrical components theory. Figures 3.9(a), (b) and (c) shows the symmetrical components for voltage at the three different locations same presented in Figure 3.8.

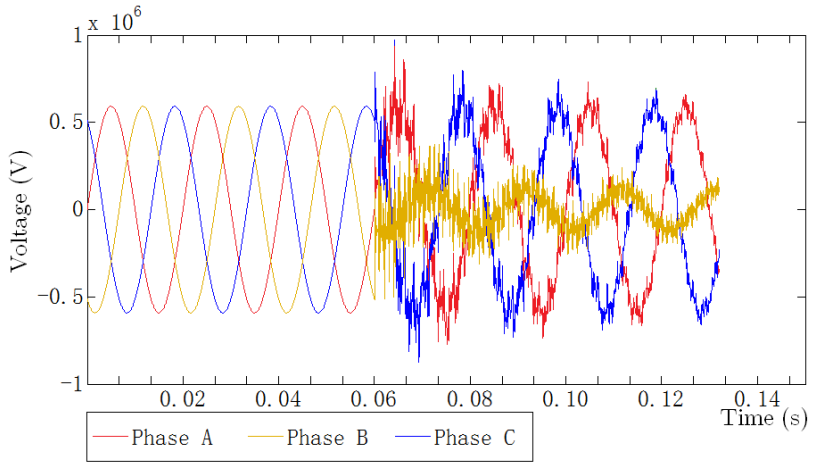

(a) At 10% of the line

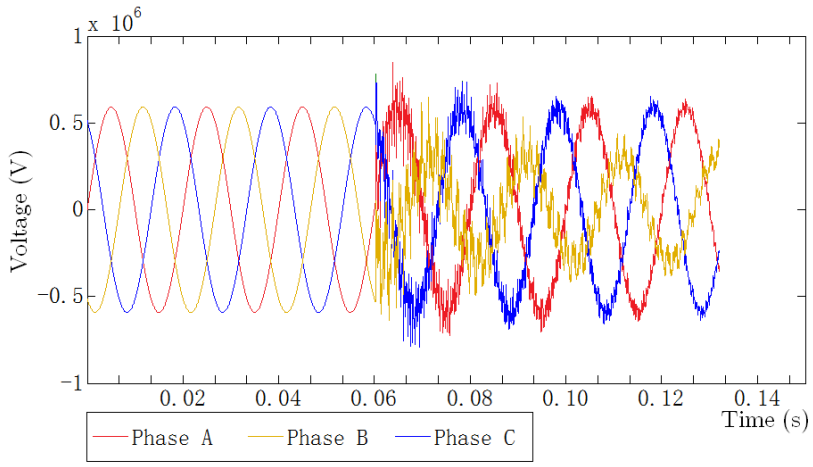

(b) At 50% of the line

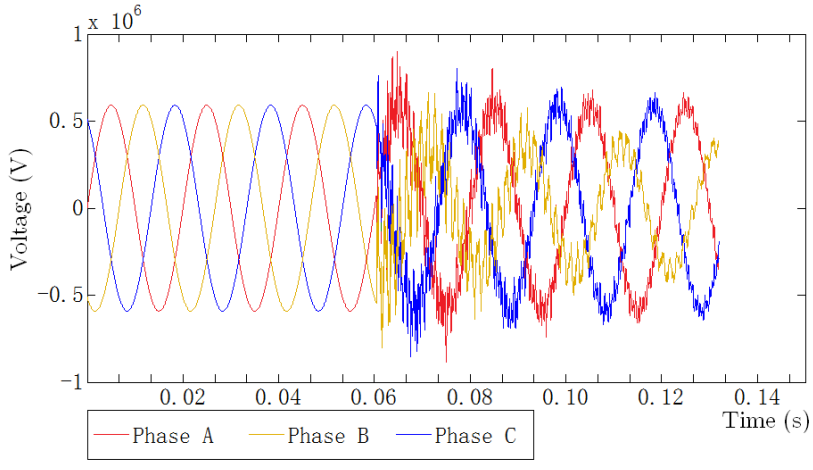

(c) At 90% of the line

Figure 3.8: SLG fault:- BG fault three phase voltages waveform at three different locations

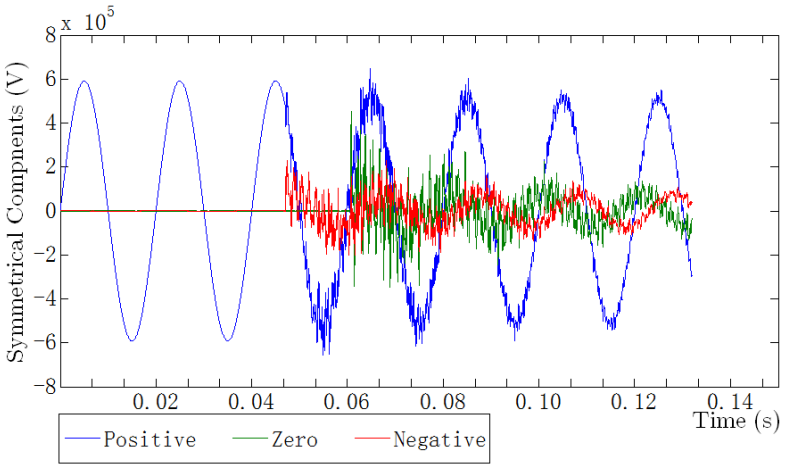

(a) At 10% of the line

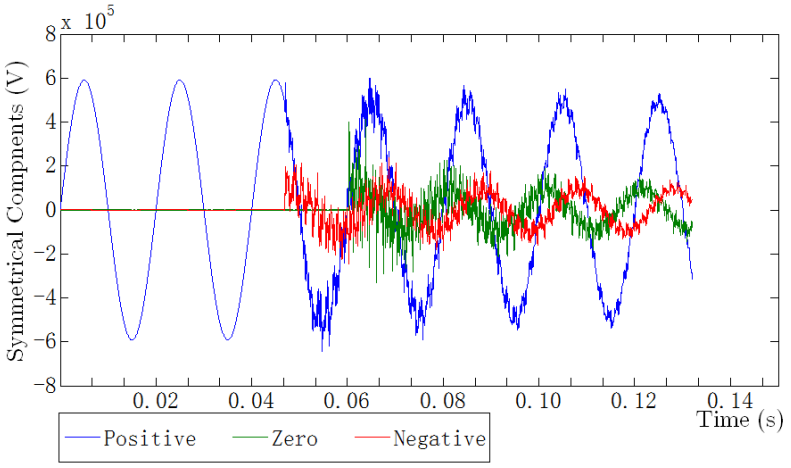

(b) At 50% of the line

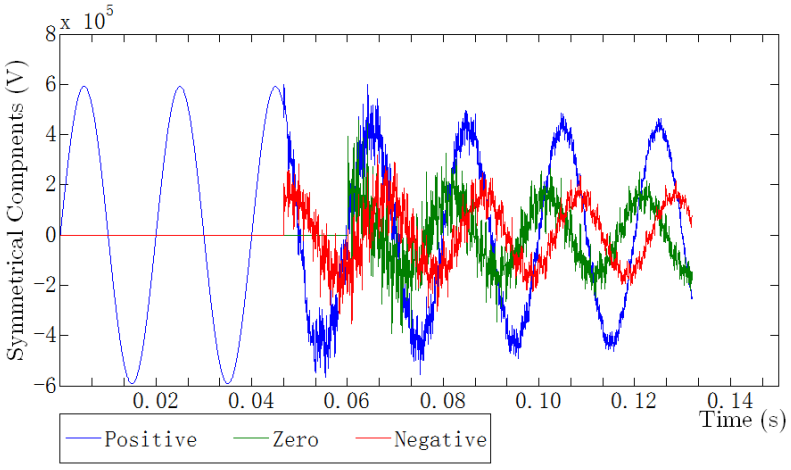

(c) At 90% of the line

Figure 3.9: SLG fault:- BG fault symmetrical components of three phase voltages at three different locations

As previously indicated, before the fault, and owing to system symmetry, both the negative and the zero component do not exist. The positive component is the only component that appears in the figure. Immediately after the fault occurs, all of the three components change.

Again, the positive sequence has a high-frequency component superimposed on the main waveform, and the negative sequence component increases due to asymmetry in the phases. As the position of the fault moves away from the sending end the positive symmetrical component reduces slightly, the negative and zero symmetrical components increases as the position of the fault moves away from the sending end.

Figure 3.10 shows the changes in the magnitude of the voltages symmetrical components. And Figure 3.11 shows the changes in the phase shift. The figures relate to the case of fault located at 50% of the line.

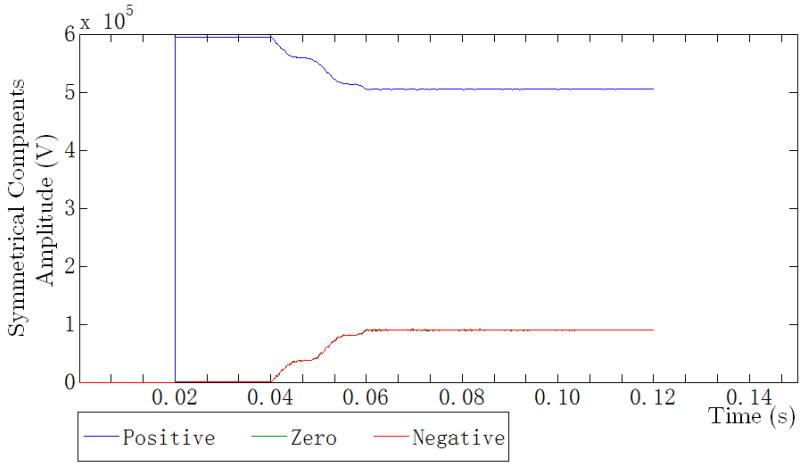

Figure 3.10: SLG fault:- magnitudes of voltage symmetrical components for a BG fault at 50% of the line

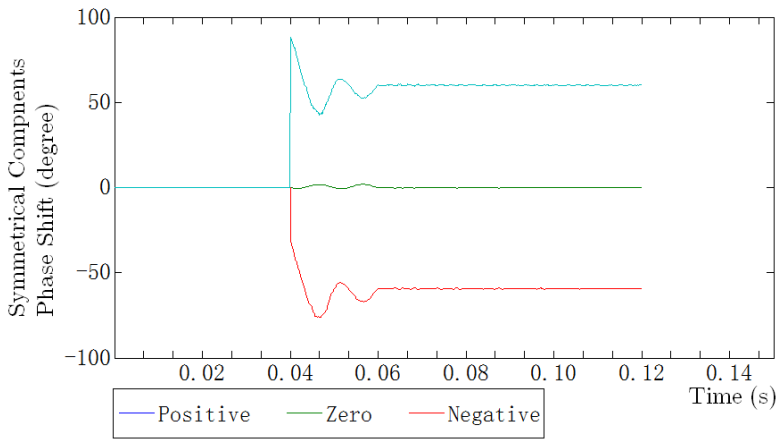

Figure 3.11: SLG fault:- phase shift of voltage symmetrical components for a BG fault at 50% of the line

3.3.2.3 Case 1. DLG fault

The double line to ground fault (DLG) is less common than a single line to ground fault (SLG), a short circuit takes place between two of the three phases A, B or phase C with the ground; in this case, the current in the phase with the fault experiences an increase to a level that depend on various factors. A slight disturbance is noticed in the third phase waveforms.

3.3.2.3.1 Case 1. DLG fault, current waveforms

As an example of DLG fault, the ACG fault is initiated by the simulation software and the simulated current waveforms are shown in Figure 3.12. These are for the current waveforms with the fault location at 50% of the line length.

The short circuit in two of the phases with the ground represents a sudden change in the network power flow. The power that is generated to supply a specific load is suddenly going through very low resistance fault to ground, causing a sharp rise in the current in both lines and changes in the phase. The high-frequency transients on the current waveform are produced by travelling waves in the line.

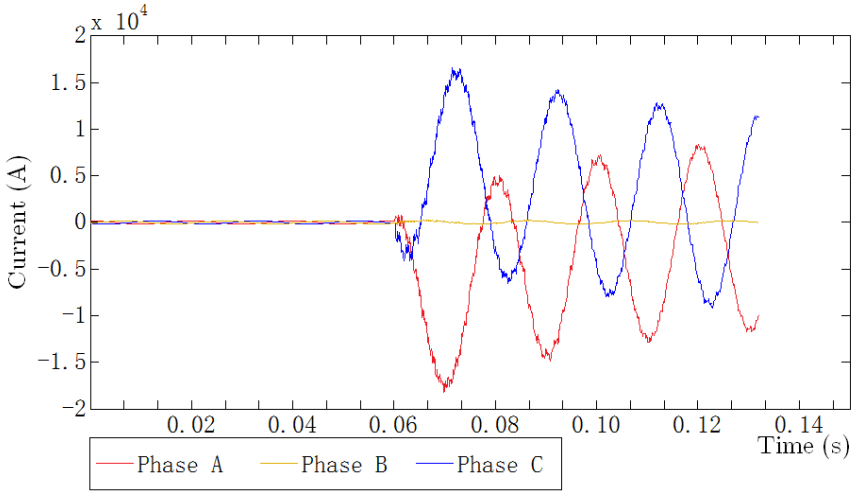

Figure 3.12: DLG fault:- ACG fault, three phase currents

The remaining phase current is affected but to a lesser degree, and this effect is due to the mutual inductance between the three phases. Figure 3.13 shows the calculated symmetrical components. Figure 3.14 indicates the changes in the magnitude of symmetrical components for the current while Figure 3.15 shows the changes in the phase. Both figures are related to the case of fault located at 50% of the line.

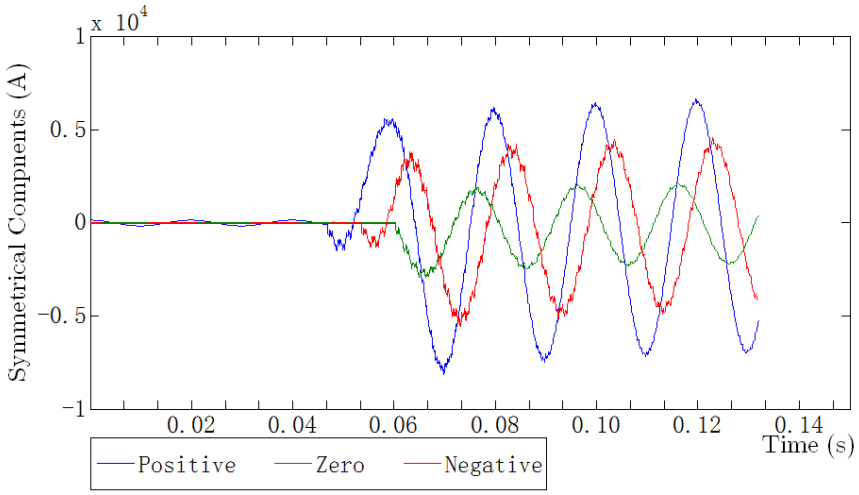

Figure 3.13: DLG fault:- ACG fault, current symmetrical components

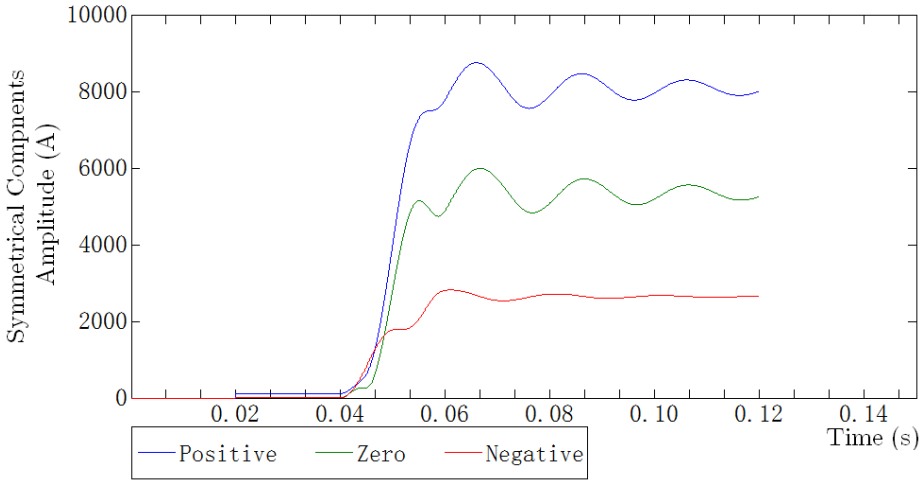

Figure 3.14: DLG fault:- magnitude of current symmetrical components for a ACG fault at 50% of the line

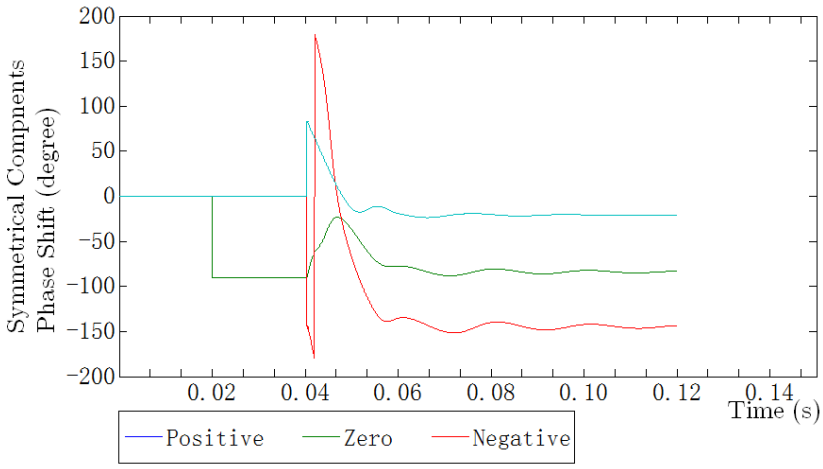

Figure 3.15: DLG fault:- phase shift of current symmetrical components for a ACG fault at 50% of the line

As expected and immediately after the fault occurs, all of the three different components show a change in their characteristics. The change in the positive component is due to the increase in the phase currents. The negative component is an indication of the asymmetry in the system caused by the fault, and the zero component change is reflecting the ground involvement in condition.

3.3.2.3.2 Case 1. DLG fault, voltage waveforms

The voltage for the ACG fault example is shown in Figure 3.16. The fault is simulated at 50% of the line length. Figure 3.16(a) shows the voltage waveforms.

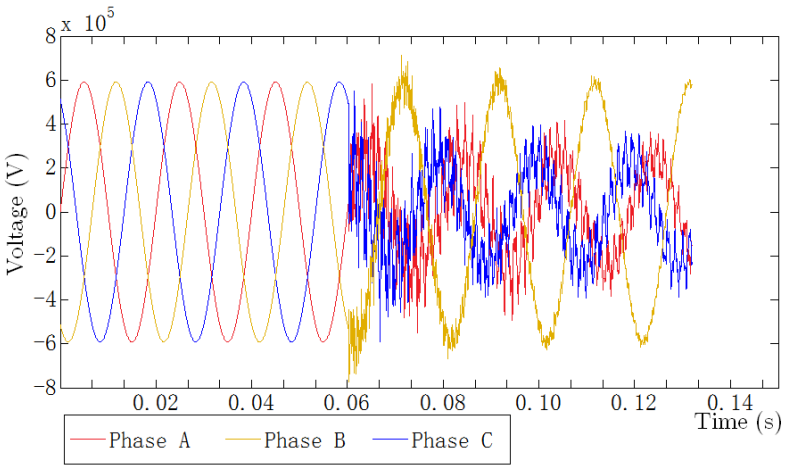

(a) Three phase voltage

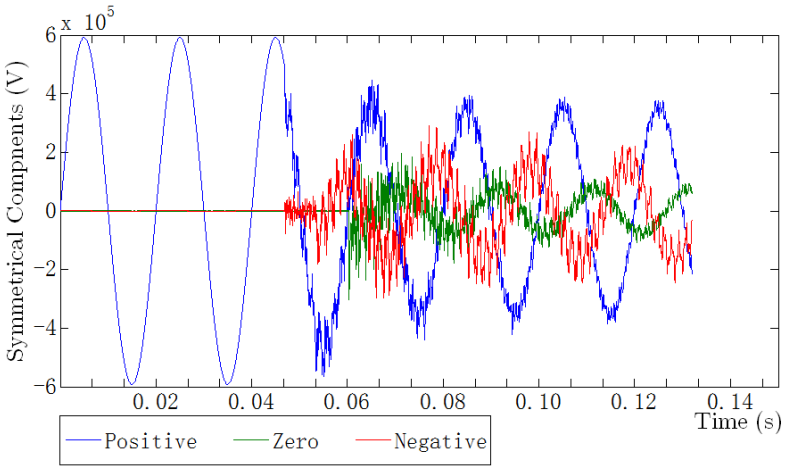

(b) Symmetrical components

Figure 3.16: DLG fault:- ACG fault

As expected, the voltages in the phases with the fault show a reduction with a slight change in the remaining phase. A change in the phase is also noticed together with the high-frequency transient appears immediately as the fault is introduced.

The symmetrical components values from the voltage are shown in Figure 3.16(b). Before the fault, both the negative and the zero components are zero. After the fault initiation, the three symmetrical components change as shown.

Figure 3.17 shows the changes in the magnitude of the voltages symmetrical components over time with Figure 3.18 showing the changes in the phase.

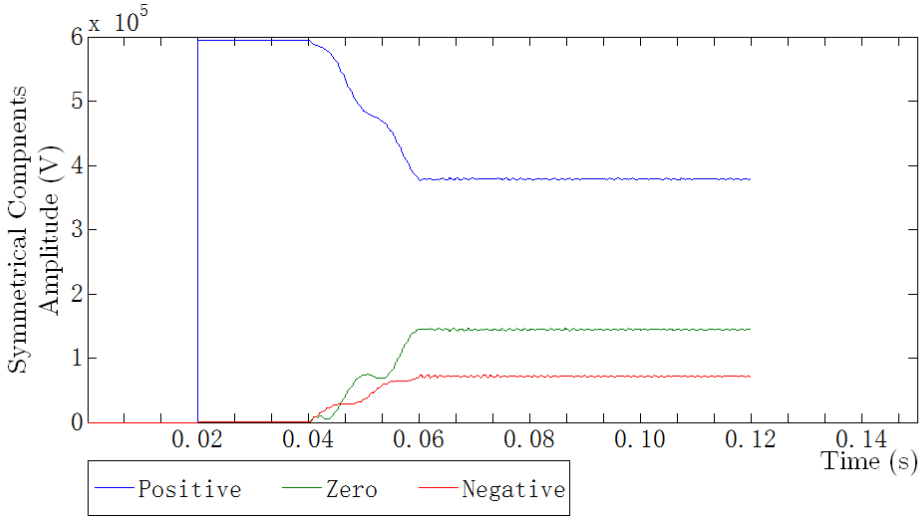

Figure 3.17: DLG fault:- magnitude of voltage symmetrical components for a ACG fault at 50% of the line

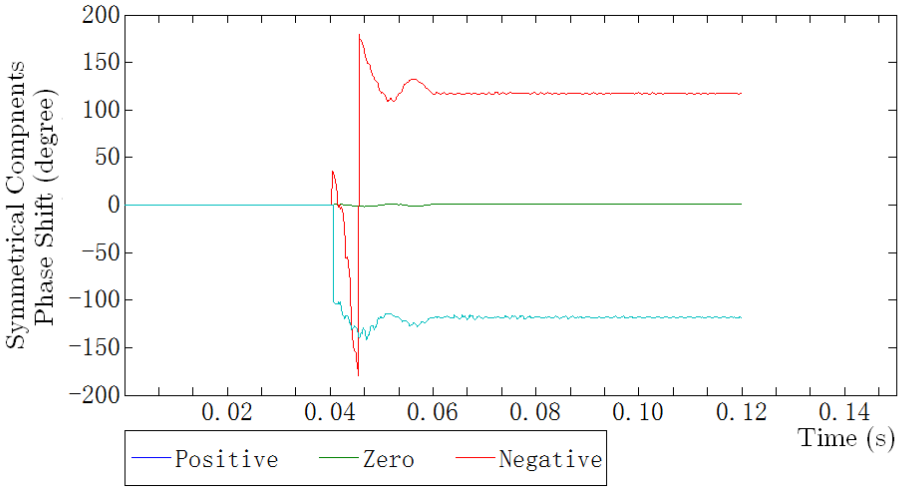

Figure 3.18: DLG fault:- phase shift of voltage symmetrical components for a ACG fault at 50% of the line

Immediately after a fault is initiated, currents and voltages in the phase with the fault show the most changes with the symmetrical components defining those changes are previously outlined. All the changes, in general, are affected by the fault location. The closer to the fault, the greater is the change.

3.3.2.4 Case 1. LL fault

The line to line fault (LL), is a short circuit that take place between two of the three phases A, B or phase C. In this case, the currents in the phases experiencing the fault show an increase to a level that depend on various factors. The third phase with no fault usually experiences a slight disturbance, so its current amplitude is usually affected to some degree but not to the extent of the other phases.

3.3.2.4.1 Case 1. LL fault, current waveforms

As an example of LL fault, a fault between phase A and phase C is initiated. The simulated results are shown in Figure 3.19(a). The fault in this example is located at 50% of the line length.

The short circuit in two of the phases represents a sudden change in the load of the network. A large current flows in both lines due to voltage difference between the two phases; this is accompanied by phase changes and high-frequency transients.

Due to the mutual inductance between the three phases, the current in the remaining phase is affected to a lesser degree. Figure 3.19b shows the calculated symmetrical components values. Figure 3.20 shows the changes in the magnitude of symmetrical components for the currents and Figure 3.21 are the changes in the phase.

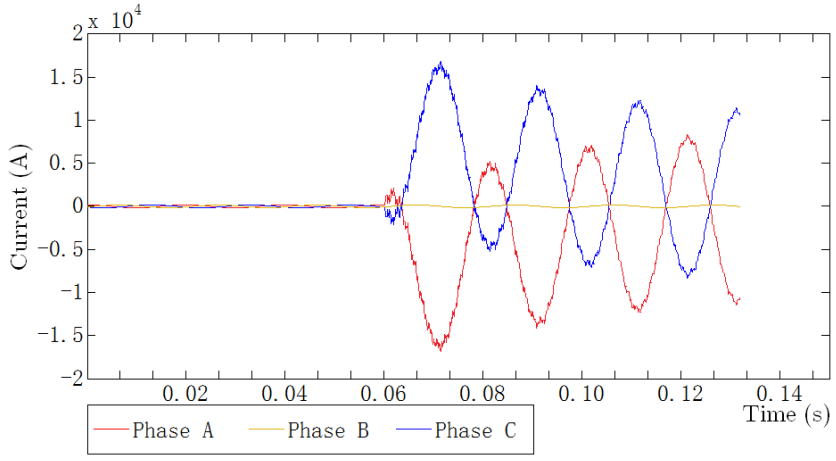

(a) Three phase currents

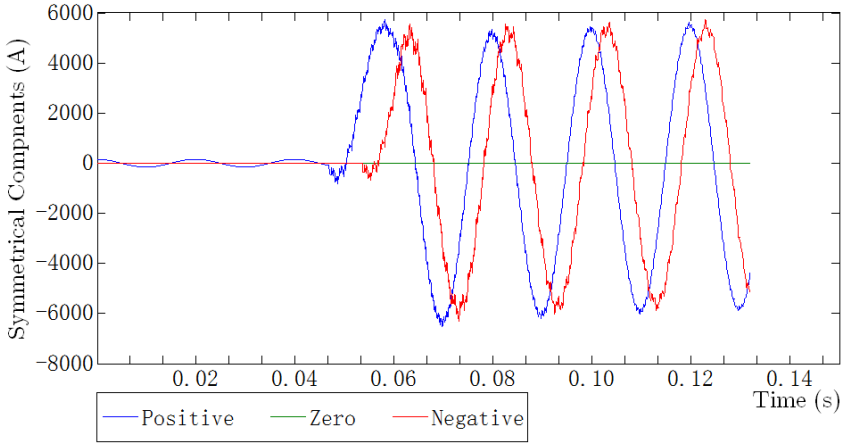

(b) Symmetrical components

Figure 3.19: LL fault:- AC fault

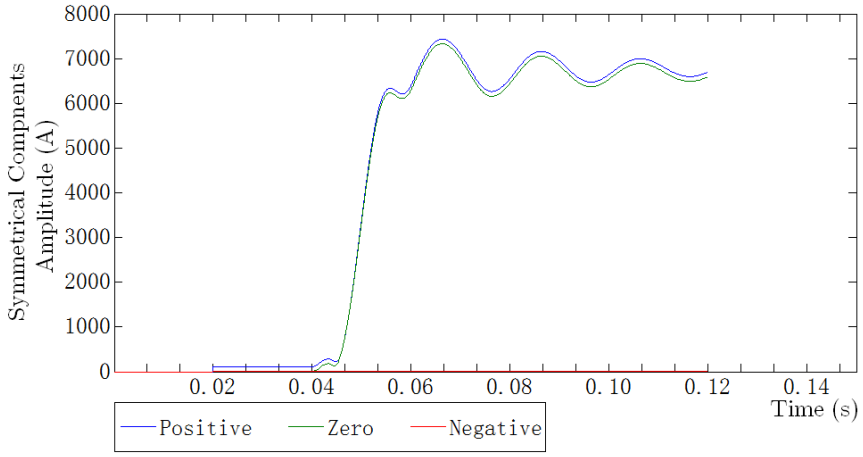

Figure 3.20: LL fault:- magnitude of current symmetrical components for a AC fault at 50% of the line

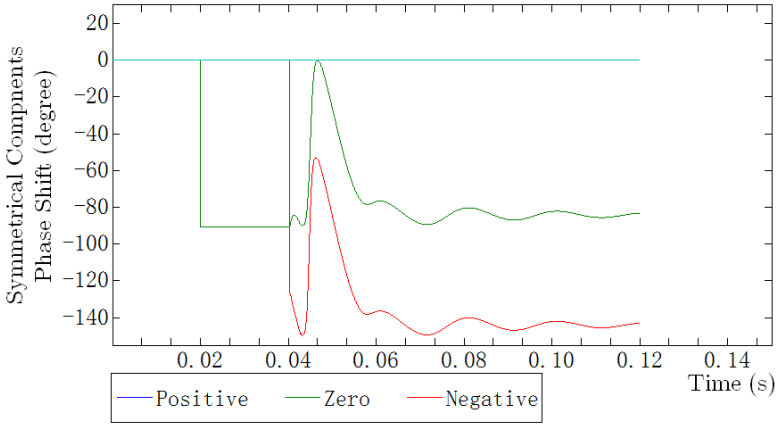

Figure 3.21: LL fault:- phase shift of current symmetrical components for a AC fault at 50% of the line

As expected, immediately after the fault occurred, the three components start to show a change in their values. As previously seen, the positive components experience increase in amplitude at the moment of the fault, and this is due to the increase in the phase currents due to the fault. The negative component increase is due to the asymmetry in the system caused by the fault and, in general, this is influenced by the fault location. On the other hand, no change was observed in the zero component due to the absence of the ground element in this fault scenario.

3.3.2.4.2 Case 1. LL fault, voltage waveforms

The voltage waveforms for the AC fault example are shown in Figure 3.22. The fault is simulated at different locations, but the voltage waveforms in the figure belong to a fault located at 50% of the line length.

The voltage of these two phase shows a reduction in value, and this is affected by the fault location. A slight disturbance in amplitude is noted in the third phase. A change in the phase is also noted and an increase in the high-frequency transient which appears immediately after the fault occurrence.

The symmetrical components are shown on Figure 3.22(b). This shows that the positive component of the voltage decreases in amplitude while the negative component increase from negligible value. The zero component value is not affected by the fault occurrence.

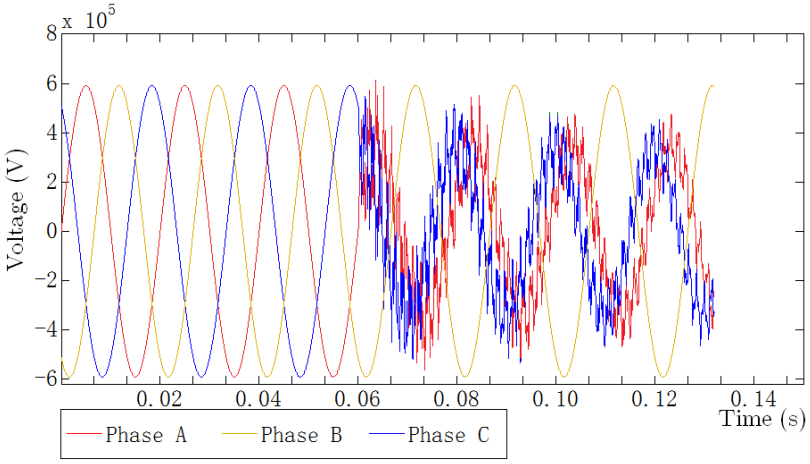

(a) Three phase voltage

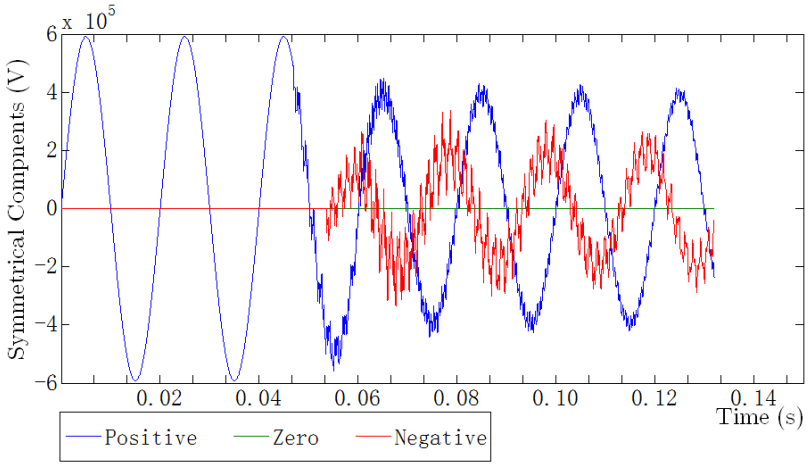

(b) Symmetrical components

Figure 3.22: LL fault:- AC fault

Figure 3.23 shows the changes in the amplitude of the symmetrical components for the voltage with time. And Figure 3.24 shows the changes in the phase.

As before, immediately after the fault occurs, the affected phases show large changes in current and voltages amplitude, phase and the introduction of high-frequency transients and those changes are reflected in the calculated symmetrical components. The positive component of the voltage shows a decrease in ampli-

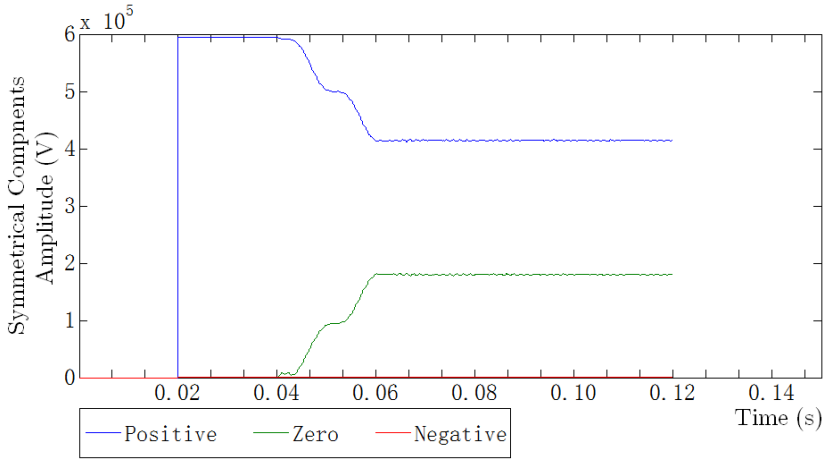

Figure 3.23: LL fault:- magnitude of voltage symmetrical components for a AC fault at 50% of the line

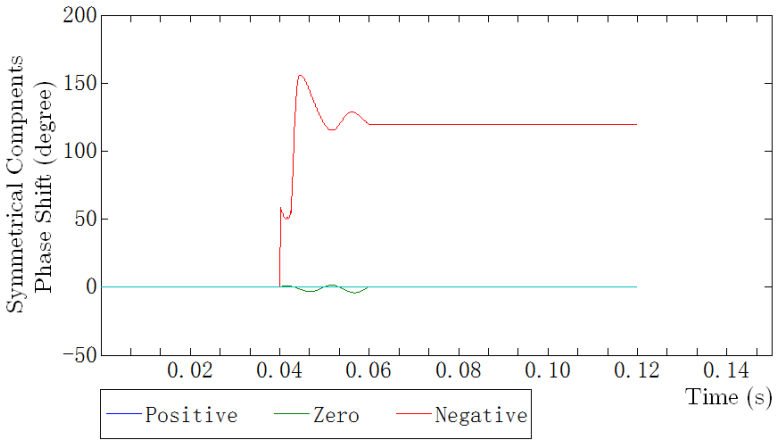

Figure 3.24: LL fault:- Phase shift of voltage symmetrical components for a AC fault at 50% of the line

tude and the phase exhibits some oscillations for a period after the fault occurs. While the negative component shows a notable increase from a negligible value. The zero component on the other hand is not affected due to there being no ground element.

3.3.2.5 Case 1. Symmetrical fault:- LLL/LLLG

In the symmetrical fault (LLL)/(LLLG), the short circuit takes place between all of the three phases A, B and phase C and this includes the case of with/without the ground involvement. Here all of the currents in the phases increase to a level that is a function of numerous factors such as the system voltage, the fault resistance and the location of the fault.

3.3.2.5.1 Case 1. Symmetrical fault, current waveforms

The ABC fault is initiated in the simulation package, and the results are as shown in Figure 3.25(a). These results are for the fault at 50% of the line length.

As expected, the short circuit between the three phases causes a large disturbance. There is a sharp rise in current magnitude in all lines with phase changes and generation of high-frequency transients.

Figure 3.25(b) shows the symmetrical components for this fault. Figure 3.26 indicates the changes in the magnitude of the symmetrical components for the currents while Figure 3.27 shows the changes in the phase.

Due to the high fault currents the positive components increases in amplitude when the fault occurs, but due to the symmetry, both the zero and negative components remain with low or negligible value. The zero component in this type of fault remains at a low value even if the ground is involved in the fault; this is also due to the symmetry in the fault.

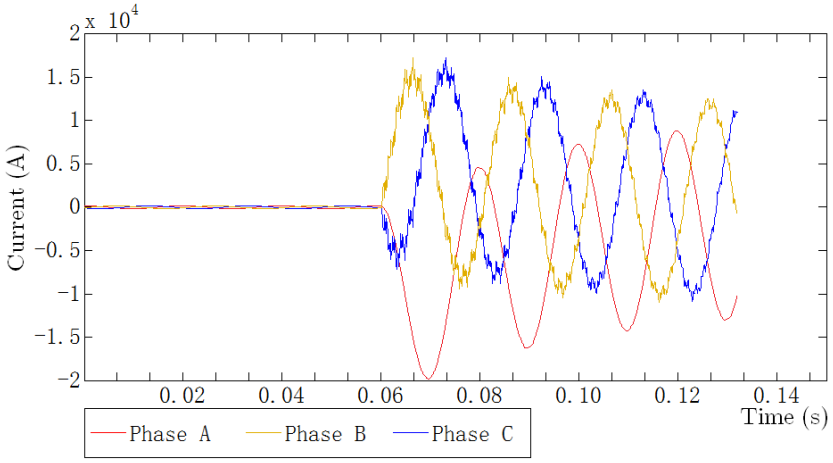

(a) Three phase currents

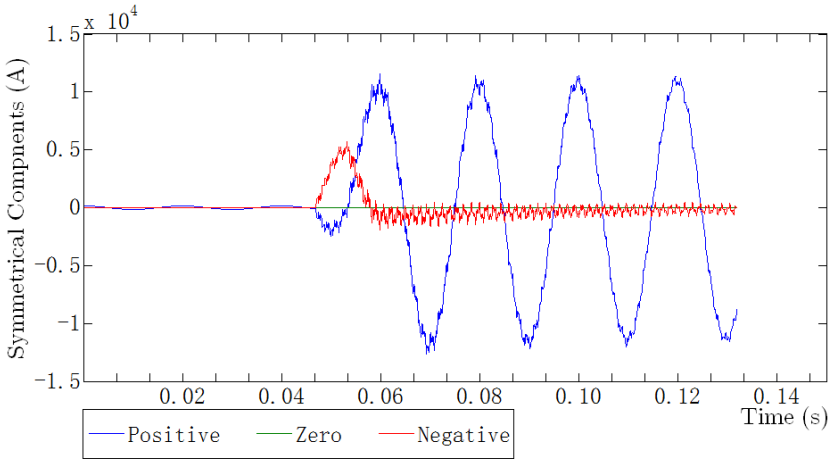

(b) Symmetrical components

Figure 3.25: LLL fault:- ABC fault

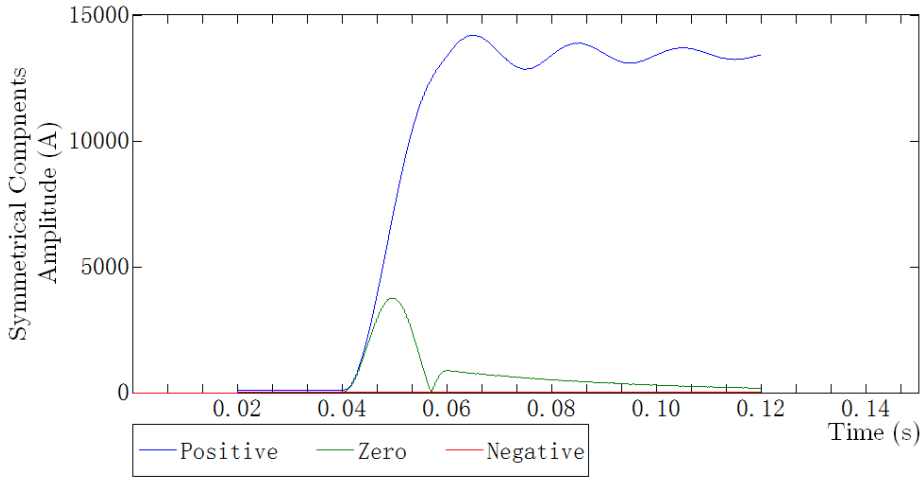

Figure 3.26: LLL/LLLG fault:- current magnitude of symmetrical components for a ABC/ABCG fault at 50% of the line

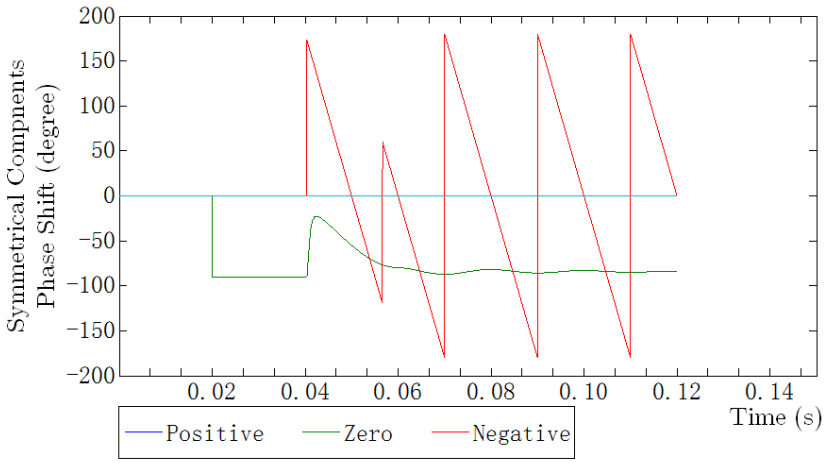

Figure 3.27: LLL/LLLG fault:- current phase shift of symmetrical components for a ABC/ABCG fault at 50% of the line

3.3.2.5.2 Case 1. Symmetrical fault, voltage waveforms

The voltage waveforms for the same example are shown in Figure 3.28. Figure 3.28(a) provides the voltage waveform for a fault located at 50% of the line length.

The fault induces a number of changes in three phase voltages. Due to the high current flowing through the fault point, the voltage amplitude decreased, the phase changes occur with the addition of high-frequency component oscillations.

The symmetrical components for the voltages are shown in Figure 3.28(b), the positive components of the voltage experience a decrease in amplitude while the negative component increases from a negligible value. Owing to symmetry, the zero component value is not affected by the fault.

Figure 3.29 shows the changes in the magnitude of the voltages symmetrical components, and Figure 3.30 shows the changes in the phase shift.

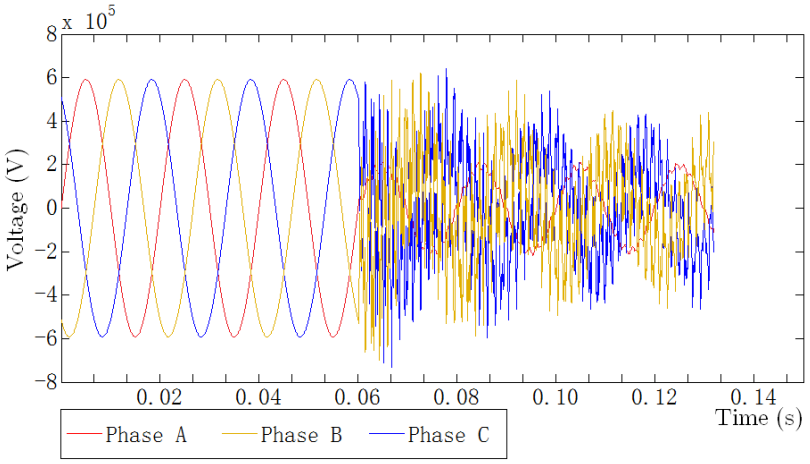

(a) Three phase voltage

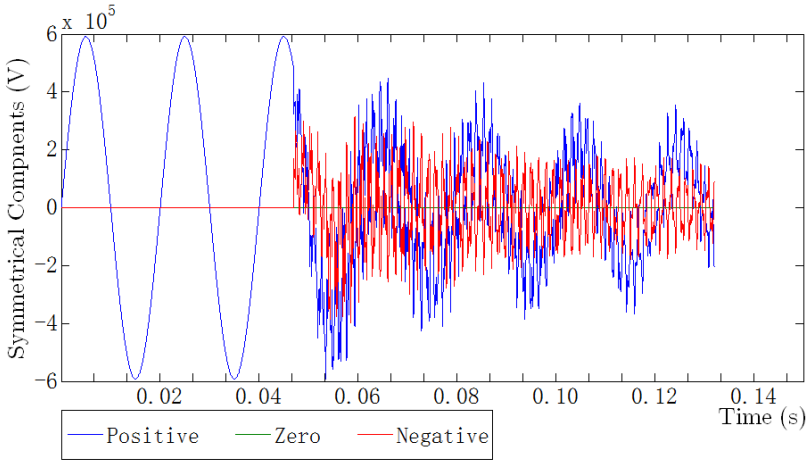

(b) Symmetrical components

Figure 3.28: LLL/LLLG fault:- ABC/ABCG fault

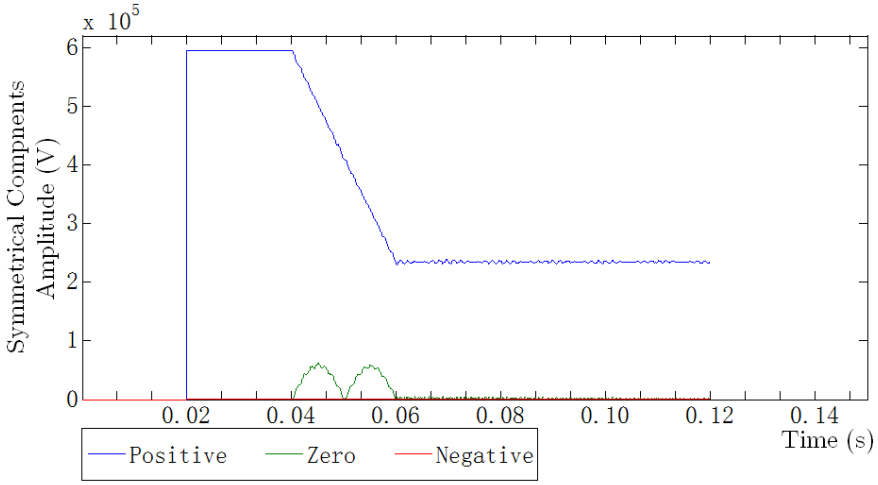

Figure 3.29: LLL/LLLG fault:- voltage magnitude of symmetrical components for a ABC/ABCG fault at 50% of the line

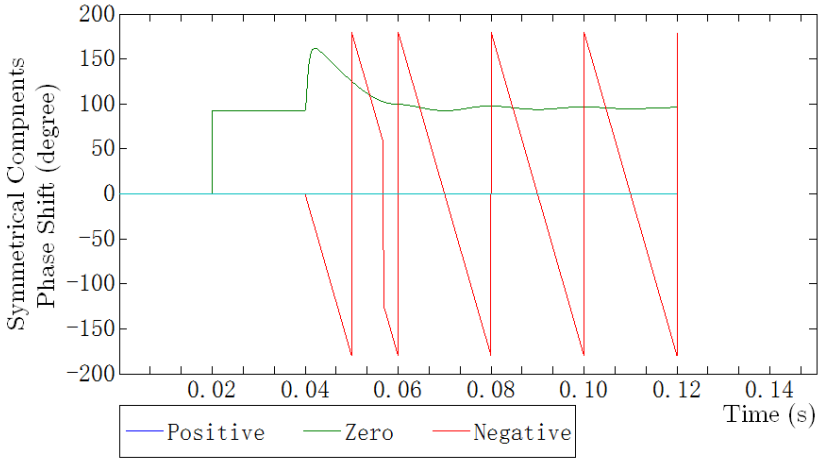

Figure 3.30: LLL/LLLG fault:- voltage phase shift of symmetrical components for a ABC/ABCG fault at 50% of the line

3.4 Case study 2 : Single transmission line

A simple power system model was developed and built in the laboratory. The model represents a simple power system network with a power being supplied to a basic resistive load through a single circuit short transmission line. Different faults can be induced on this simple experimental system. The following sections include a description of the system and the test conditions.

3.4.1 Case 2. System description

Figure 3.31(a) shows a schematic diagram of the hardware. It represents a distribution network of the power system, consisting of a three phase supply and a transmission line model supplying power to a three phase symmetrical load. Figure 3.31(b) shows the assembled experimental system.

The system voltage did not exceed a maximum of 90 Volts for safety reasons and also not to exceed the rating of the loading part of the system. Two transmission line models are used with a designed fault inducing unit between them.

3.4.1.1 Case 2. Used equipment

A three phase step down autotransformer shown in Figure 3.32(a) was used as the supply of the system. The EMT 180 Resistor/Capacitor Figure 3.32(b) board unit is used as the load part of the power system. These resistors are three phase star connected of 66 Ohms each.

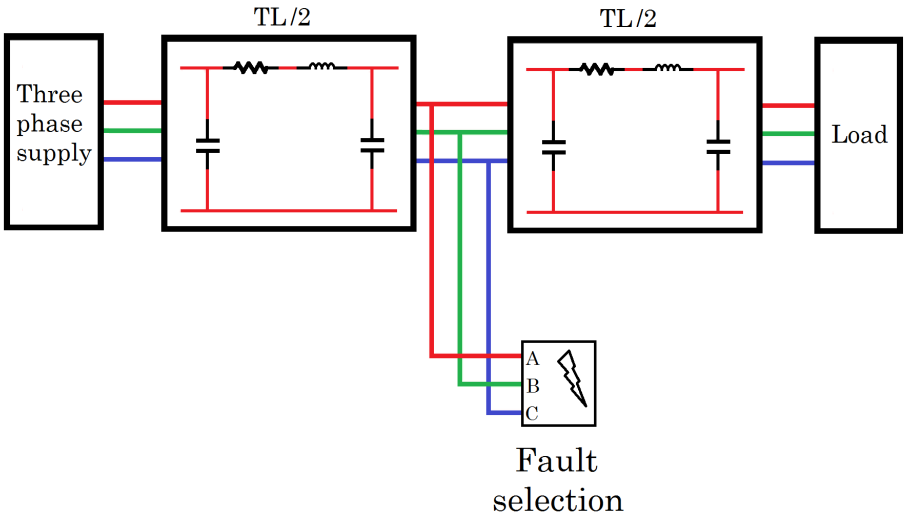

(a) The hardware implementation schematic diagram

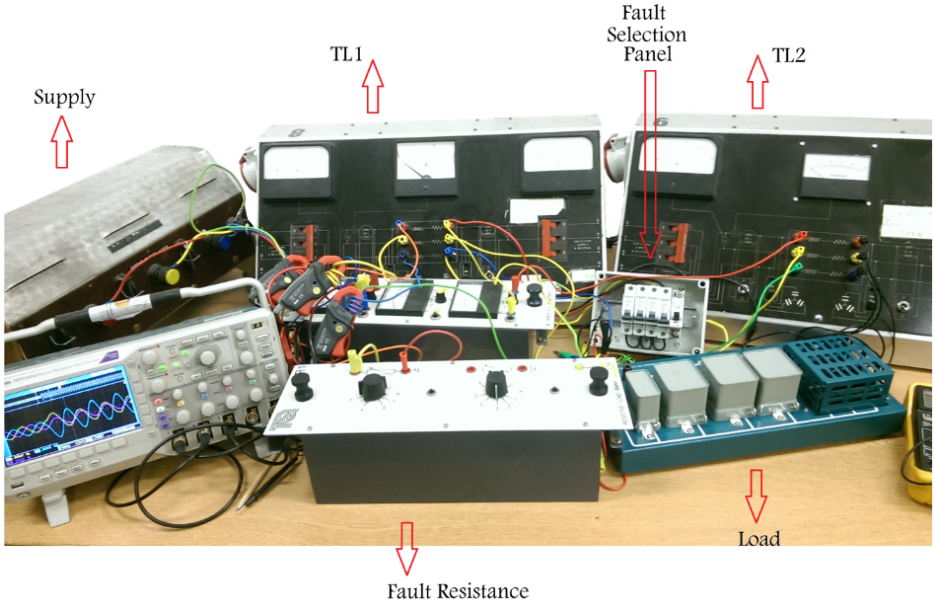

(b) The assembled system during the experiment

Figure 3.31: The hardware implementation

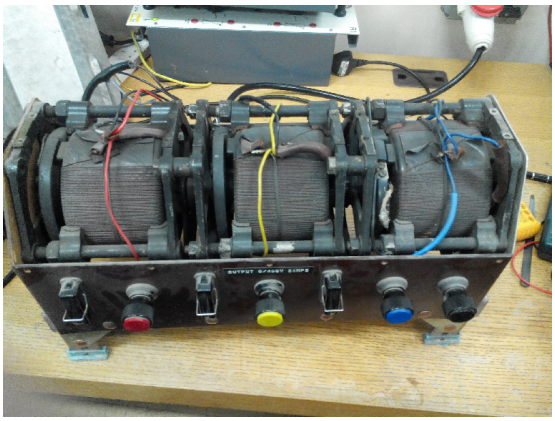

(a) Autotransformer

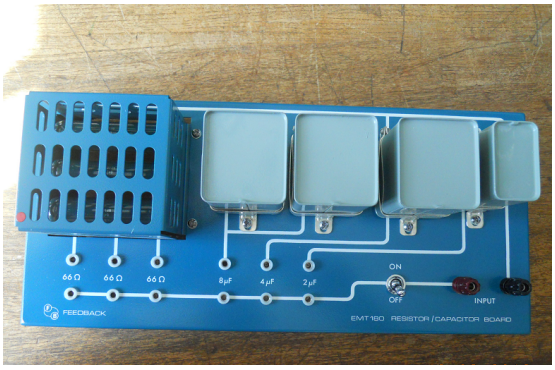

(b) The load unit

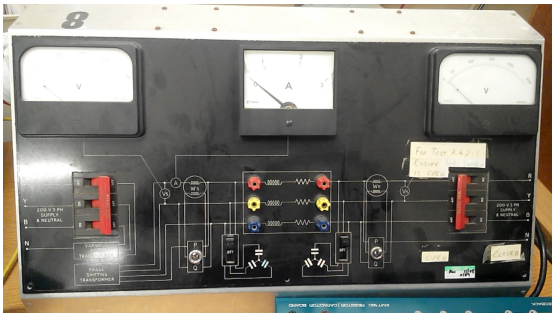

(c) Transmission lines unit

Figure 3.32: The hardware implementation used equipment

Two transmission line units Figure 3.32(c) are connected between the supply and the load unit. The transmission line is based on the π model lumped elements (Figure 3.33(a)). A three phase inductor of 0.15 H with 1.2 Ω resistance per phase and 8 micro Farad capacitors are used to model the line as shown in Figures 3.33(b) and 3.33(c) respectively.

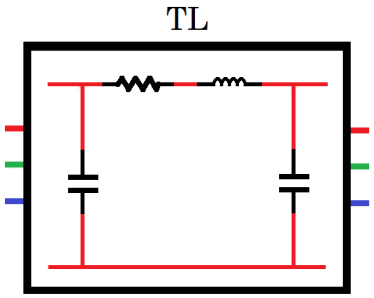

(a) The Pi model lumped elements

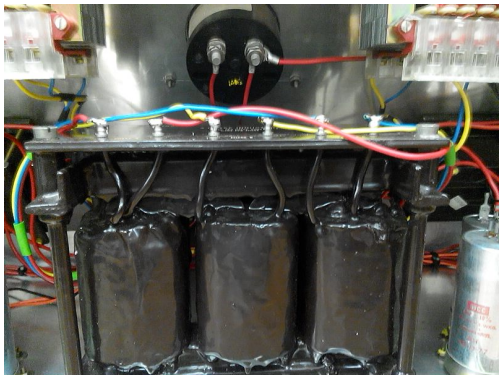

(b) Three phase inductor

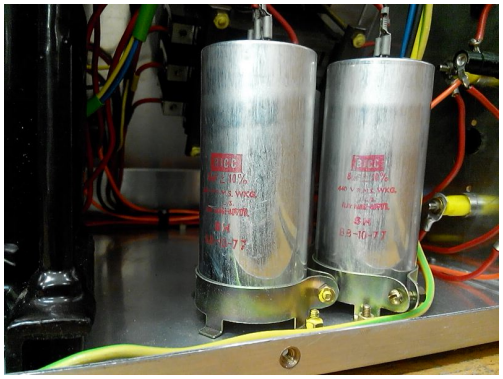

(c) Capacitor

Figure 3.33: Internal construction of transmission line unit

3.4.1.2 Case 2. Fault panel

Several fault conditions are initiated in the middle of the transmission line. The fault selection panel is shown on Figure 3.34 and is simply constructed from four switches, connecting the three lines together with or without ground connection depending on the fault condition to be simulated. Various combinations of switches cover possible faults in the range of the study.

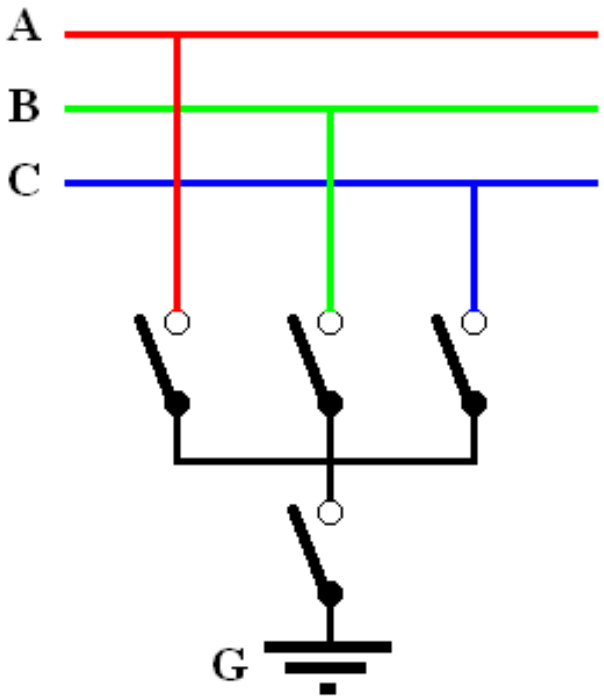

Figure 3.34: The fault selection panel

The fault resistance was controlled by the insertion of a selected value into the panel. The implementation of multiple fault scenario was carried out manually within predefined monitored period through the correct switch sequence.

3.4.1.3 Case 2. Data collection

The three phase current are monitored using CP09 current clamp (Figure 3.35(a)) connect to a digital oscilloscope via a normal probe. Three current clamps are installed after the power source at the start of the transmission line (Figure 3.35(b)) monitoring the currents variation in each of the three phases.

(a) CP09 current clamp

(b) Three current clamps installed

Figure 3.35: Data collection

The maximum range of the selected current clamp is 200 A, and the output sensitivity is 1mV/A. To supply a suitable value for showing on the scope, several turns (4 turns) of the wire were placed through the clamp. This provides a clear amplified signal, and the number of turns is taken into account in the calculation and analysis steps.

Three 1:1 normal voltage probes are used to transfer the three phase collected signals from the current clamp to the digital DPO3034 oscilloscope. The current measurement taken during the monitored duration is accurately recorded on the oscilloscope in a file format specified by the user. All of the three phase signals are recorded and stored in the form of sampled data for further analysis. USB ports on both front and back panels made for quick and easy data copying. The selected format is the CSV which is easily dealt within a GUI application was implemented later in a LabView environment.

The same set of faults illustrated in Section 2.5 was used. The fault location was at 50% of the line length and alteration of it was not applicable due to the nature of the experimental setup. Different fault resistance values were inserted into the selection panel to test for the effect of changing fault resistance.

3.4.2 Results of case 2 : Single transmission line

Similar to the testing procedure carried out in the double transmission line simulation study, by running it with no faults, the collected current waveforms of the healthy system are presented in Figure 3.36(a). Voltage data are also recorded, but not presented here. Symmetrical components are then calculated using their described equations in Appendix D. The symmetrical components are illustrated in Figure 3.36(b).

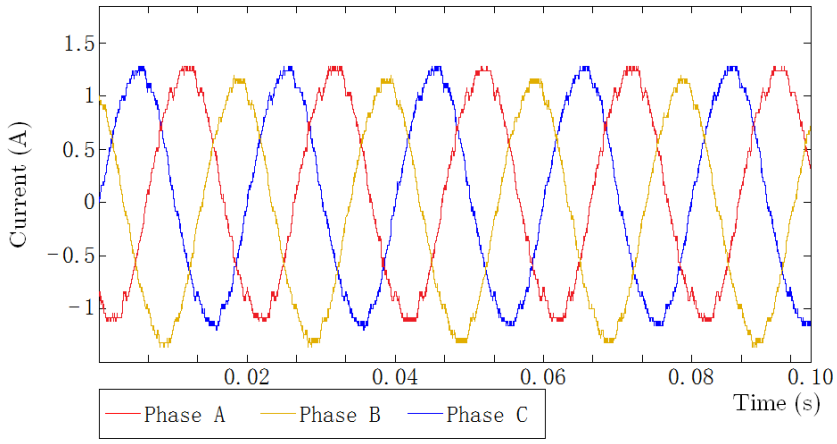

(a) Three phase currents

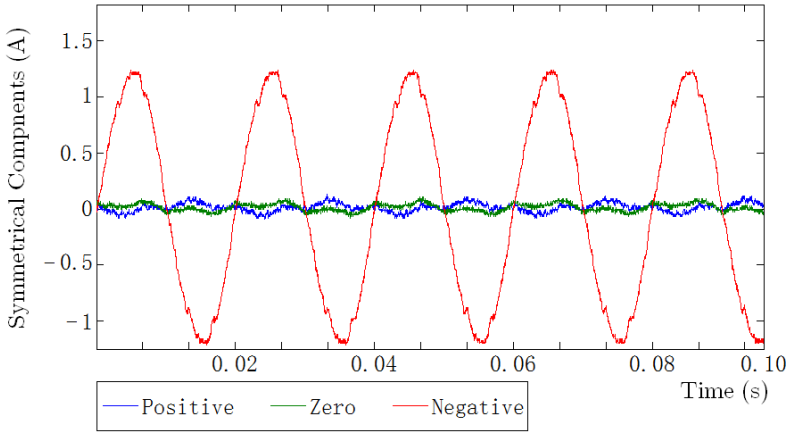

(b) Symmetrical components

Figure 3.36: Hardware setup: healthy system

The symmetry is absent in the supply current waveforms. Despite this and the expected asymmetry in other physical components of the system such as the transmission line module and the loads, but as predicted in theory of symmetrical components calculations for this condition, the healthy waveforms give pure positive components, the negative and zero components are at almost zero or negligible value.

3.4.2.1 Case 2. SLG fault

The BG fault is implemented on the hardware setup, as an example of SLG fault. The collected results are as shown in Figure 3.37(a). A sharp rise in the fault phase current magnitude is noticed. The current increase to a level that depends on several factors which include the system voltage, fault resistance, fault location and the loading of the system. The phases with no faults usually experience slight disturbance, but their magnitudes are usually affected, but to a lesser extent to the faulted phase.

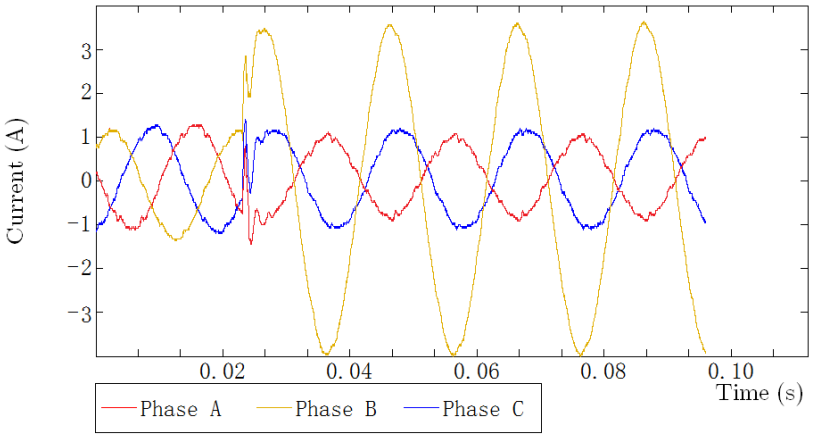

(a) Three phase currents waveform

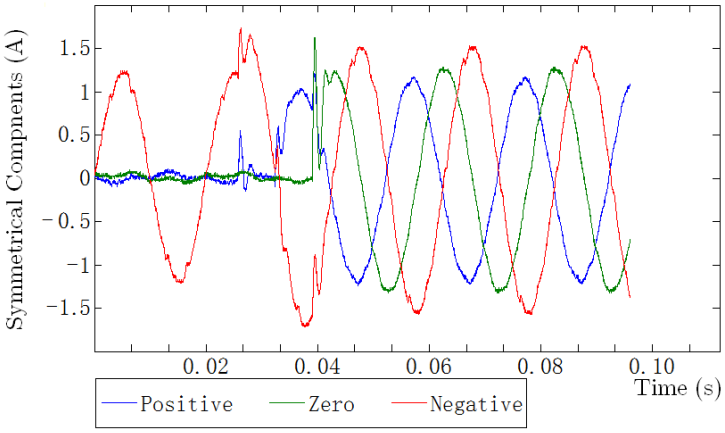

(b) Symmetrical components

Figure 3.37: SLG fault:- BG fault

3.4.2.2 Case 2. DLG fault

The ACG fault is implemented in the hardware setup case as an example of DLG fault, the collected results are as shown in Figure 3.38(a), the current in the fault phases show an increase to a level that depends on various factors in the system, the third phase with no faults usually shows slight disturbance in its current amplitude but to a lesser extent than the fault phases.

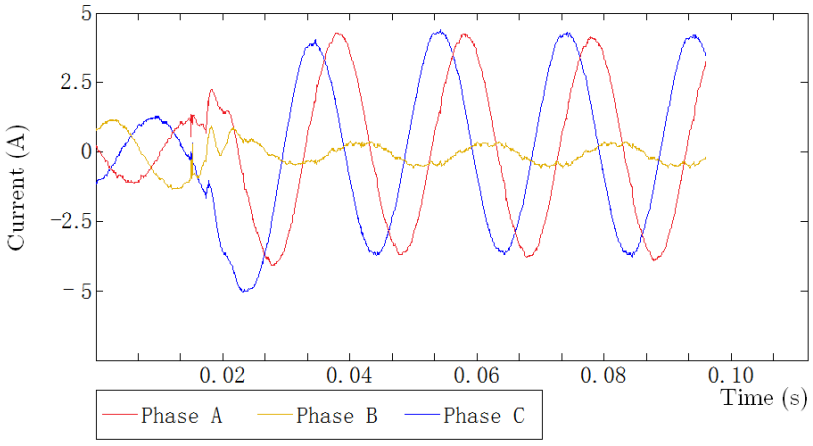

(a) Three phase currents waveform

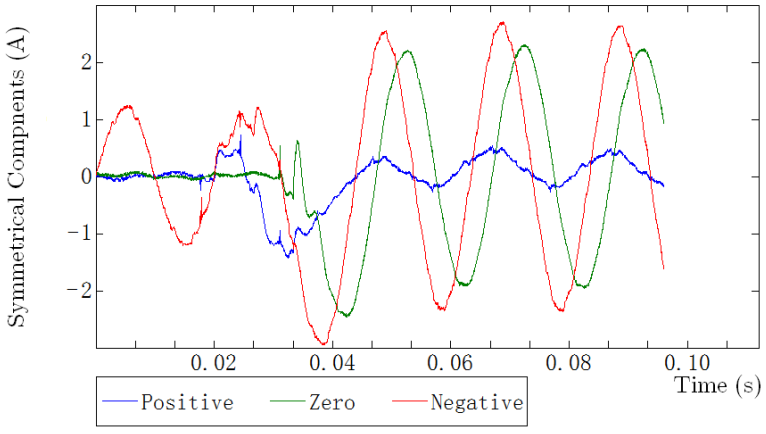

(b) Symmetrical components

Figure 3.38: DLG fault:- ACG fault

The symmetrical components of the three current waveforms are as shown in Figure 3.38(b), the positive component shows increases in amplitude at the moment of the fault occurrence, and this is due to the increase in the phase currents. The negative component shows an increase from negligible value, and this is a result of the asymmetry in the system caused by the fault. The zero component also experiences similar behaviour, and this is justified by the existence of the ground element in this faulty condition.

3.4.2.3 Case 2. LL fault

The AC fault is implemented in the hardware setup case as an example of LL fault, and the results are as shown in Figure 3.39(a), the symmetrical components of the three current waveforms are as shown in Figure 3.39(b), the positive components experience increase in amplitude when the fault occurs and this is due to the increase in the currents. The negative component shows an increase from a negligible value and this is a result of the asymmetry in the system caused by the fault. The zero component in this type of faults stays at a low value, in magnitude and this is because of the ground element absence.

The current in faulty phases experiences an increase to a level that depends on various factors, the third phase with no faults usually experiences a slight disturbance, its current magnitude usually affected but not similar to what happened in the faulty lines.

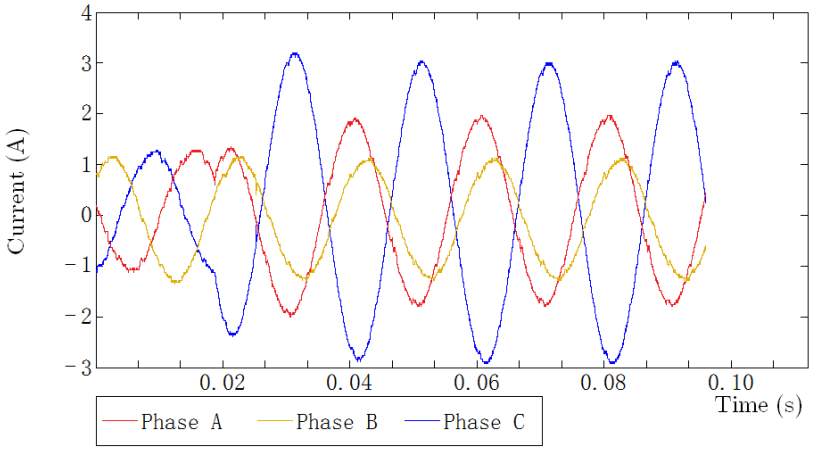

(a) Three phase currents waveform

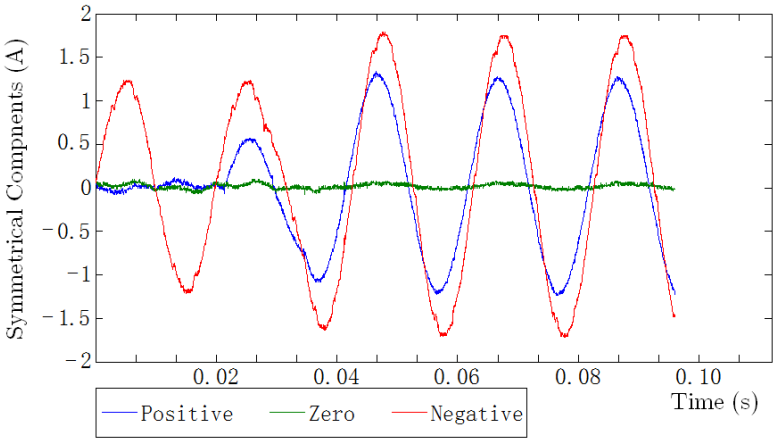

(b) Symmetrical components

Figure 3.39: LL fault:- AC fault

3.5 Summary

This chapter describes two case studies which have been investigated. In the first case, a double circuit transmission lines system is simulated by Simulink® software, selected set of faults arrangement has been implemented. The same set of faults has been also used experimentally in a second case representing a simple model of a power system with single circuit transmission lines.

In the first case (Double circuit transmission line), the fault implementation is repeated at several locations throughout the line length. The fault set is repeated with different fault resistance values. Voltage and current waveforms are collected from both terminals.

In the second case (Single circuit transmission line), due to the nature of the experimental setup the fault location alteration was not applicable. The fault implementation is arranged at the middle of the line with variations of fault resistance values. The waveforms are collected from one terminal.

The symmetrical components theory (Appendix D) was used for evaluating the positive, negative and zero symmetrical component waveforms for the different cases with their various conditions. These waveforms will form the input data for processing by chromatic monitoring methodology.

In both cases, by comparing the waveforms generated when the system has no faults to waveforms from systems exposed to faults, a few observations can be noted. The changes include amplitudes, phase changes, DC transients and frequency component appearance and can be summarised in following paragraphs.

Starting with the positive component for current, the main observation is an immediate increase on the amplitude immediately at fault occurrence moment for all of the faults types. The increase in the amplitude shows a variation with the fault type and its location. Considering the fault type, the maximum increase

was for faults involving all of the phases, and then faults with two phases and the least increase was recorded for faults involving single phase. Regarding the fault location of the fault, the increase in the amplitude was observed to be more if the fault is closer to the measurement point and less if the fault is far. In addition to the amplitude change, DC transient and high frequency component were also pointed out.

Unlike the current, a decrement in the amplitude of the positive component for voltage was remarked. This occurs immediately at fault occurrence moment for all of the faults types. The change in the amplitude also shows a variation with the fault type and its location. The maximum decrement was recorded for faults involving all of the phases, and then faults with two phases and the least decrement was observed for faults involving single phase. Regarding the fault location of the fault, the amplitude decrease more if the fault is closer to the measurement point and less decrement was noticed if the fault is far. High frequency component was also observed in the voltage waveforms.

Although a remarkable immediate increase from a negligible value in the negative component amplitude for both current and voltage was noticed as a reaction to faults occurrence, this was observed only for the asymmetrical group of faults. The phase shift also shows variation with different asymmetrical faults types, but no stability behaviour was observed for symmetrical faults. A variation in the amplitude was noticed with the fault location change, and a high frequency component was also found in both waveforms.

The immediate observations on the zero component was its immediate increase in the amplitude but only for asymmetrical faults and particularly for faults that involved a ground. A variation in the amplitude was noticed with the fault location change, and the high-frequency component was also observed.

The methods discussed in Sections 2.6 and 2.7 shows that high-frequency component resulting from faults was proven to hold useful information about the fault type and the location. The requirement for analysing such feature by chromaticity is the fault waveforms frequency spectrum. For the sake of simplicity, monitoring the frequency domain will be left as a suggestion for future work which will be discussed later in Chapter 6.

The next chapter will include analyses of the waveforms in time domain, with the aim of establishing a connection between changes in amplitudes and phase shifts resulting from fault occurrence to changes in chromatic parameters which could lead eventually to design for accurate and reliable fault diagnostic tools.

Chapter 4

Chromatic monitoring and analysis

4.1 Introduction

When a power system is subjected to abnormal conditions, the normal 50 Hz power frequency waveforms for current and voltage are affected. Sections 3.3 and 3.4 present three phase voltages and currents waveforms and their symmetrical components for different faults conditions described in Section 2.5. Preliminary observations include but not limited to the appearance of a DC component, changes in the fundamental frequency components amplitude and phase shifts in addition to high-frequency oscillations.

A review of fault diagnostic tools presented in Sections 2.6 and 2.7 shows that changes in the fundamental frequency component and changes in the high-frequency oscillations have been used successfully in various diagnostic tools, as changes have enough and useful information for classifying the fault and estimating its location.

In this chapter, a proposed chromatic monitoring analysis approach is presented which is performed in the time domain of the waveforms. An outline of the proposed chromatic processing procedure is given in a form of a simplified flowchart shown in Figure 4.1. The process is divided into steps from (A) to (F).

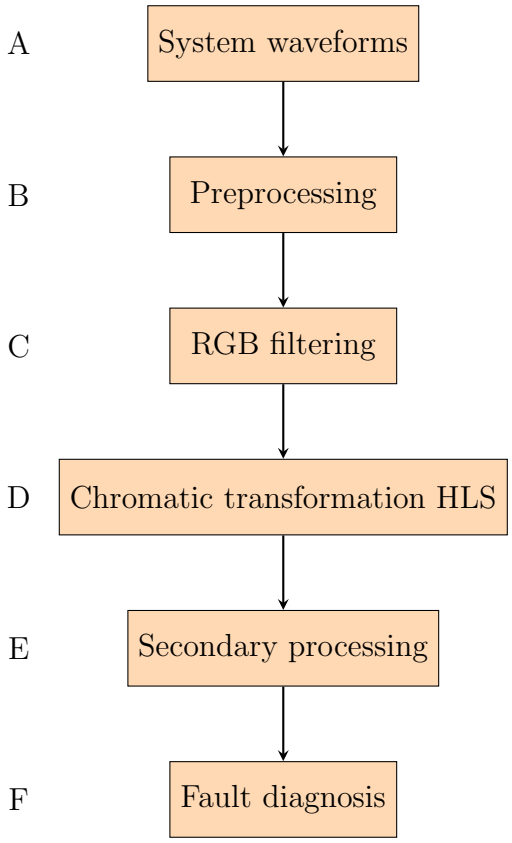

Figure 4.1: General flowchart for proposed chromatic monitoring procedure

The "system waveforms" in (step A) include both three phase voltages and currents collected from the monitored transmission line terminals, samples of waveforms from two case studies are included in Chapter 3.

Preprocessing (step B), is introduced in Section 4.2.1. This step includes symmetrical component calculation step which is applied to all signals. Samples of these calculations are also included in Chapter 3. Further preprocessing may have to be performed for selected waveforms.

Steps (C) and (D) are described in Sections 4.2.2 and 4.3 respectively, and represent the two main steps of the chromatic analyses process. The method starts by applying chromatic filters (presented in Section 2.9.2) to the three phase voltages and currents waveforms on a cycle by cycle basis. The resultant R, G and B values are then transformed chromatically using HLS transformation algorithms detailed in Section 2.9.3.1.

The objective is to investigate a relationship between the fault information, type and its location and these chromatic parameters affected by changes in system's condition.

In Section 4.4, in order to recognise the full implications of the changes in the current and voltage waveforms amplitude, phase and high-frequency component and their effect on chromatic parameters, a study and analyses of chromatically processed pure sine waves is compared to sine waves with the above variations.

While Section 4.5 focuses on the analysis and study of a selection of chromatic parameters, namely: H and L of the negative symmetrical component, L of zero symmetrical component and L of the positive symmetrical component, the aim is to employ them in the faults diagnosis process.

Step (E) of the flow chart in Figure 4.1 represents further processing performed on some chromatic parameters. And the final step (F) represents the integration of the outputs of steps (A) through (E) into achieving the target of this study by providing useful information for accurate diagnosis of different faults. Further analysis and discussion will be presented later (Chapter 5) with the main aim

of developing a fault symptom detector tool which will help the power system operator to narrow the possible diagnosed options.

4.2 Raw data preprocessing

The data collected as described in Sections 3.3 and 3.4 are voltage and current waveforms of which are captured from sender and receiver terminals of the transmission line. The waveform duration is usually selected to include a few cycles before the event occurrence in addition to the event itself with few cycles after it. Before chromatically analysing these raw waveforms, some preprocessing steps are applied.

4.2.1 The symmetrical components calculation

By studying the observations of faults encountered in a three phase transmission line, it was noticed that the variation in the waveform characteristics is only in the affected phase and slight change in the rest of the phases. So, in order to achieve the purpose of this work which is a comprehensive diagnostic system that covers the targeted faults range, it is necessary to monitor all the available signals.

The symmetrical components method (Appendix D) is utilised to transform the three phase waveforms of both current and voltage into new different sets of waveforms in the symmetrical components domain. These calculated components are plotted in Sections 3.3 and 3.4 for the different cases. Rather than monitoring each individual phase, monitoring any one of the three symmetrical components is actually monitoring a collective quantity. Thus, the main benefit that is gained when monitoring symmetrical components is a reduction in the calculation burden.

4.2.2 RGB filtering

Applying chromatic monitoring on the power system currents and voltages waveforms involve applying three non-orthogonal receptors R, G and B (Section 2.9.2) on the measured waveforms. The selected form for the processor profile in this research is the Triangular processors half height overlaps as shown in Figure 4.2.

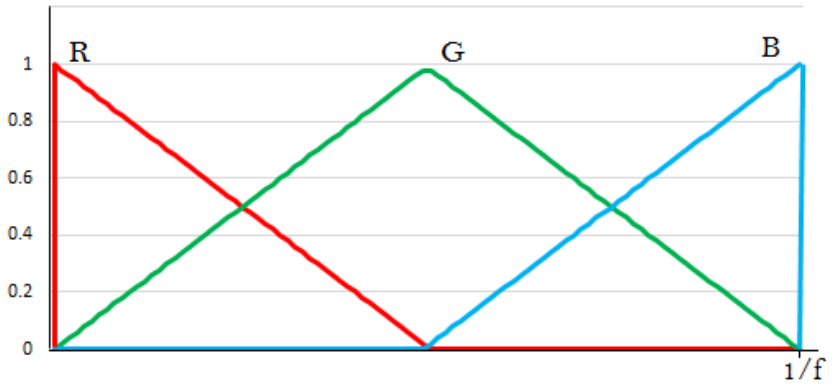

Figure 4.2: Three non-orthogonal receptors

The time window covered by the filters is set to one oscillation period of the voltage/current waveform, where 'f' is the system frequency, and this enables any changes in the wave cycles characteristics to be addressed continually.

Figure 4.3 is an example of the RGB processors superimposed upon complete cycles of the current negative sequence component together with the application of the chromatic transformation step. The first four cycles are those before the occurrence of the fault. The remaining three cycles show the change in the magnitude and phase shift caused by the fault. The figure shows the deployment procedure for the three filters on a waveform for this particular case of a single line to ground fault.

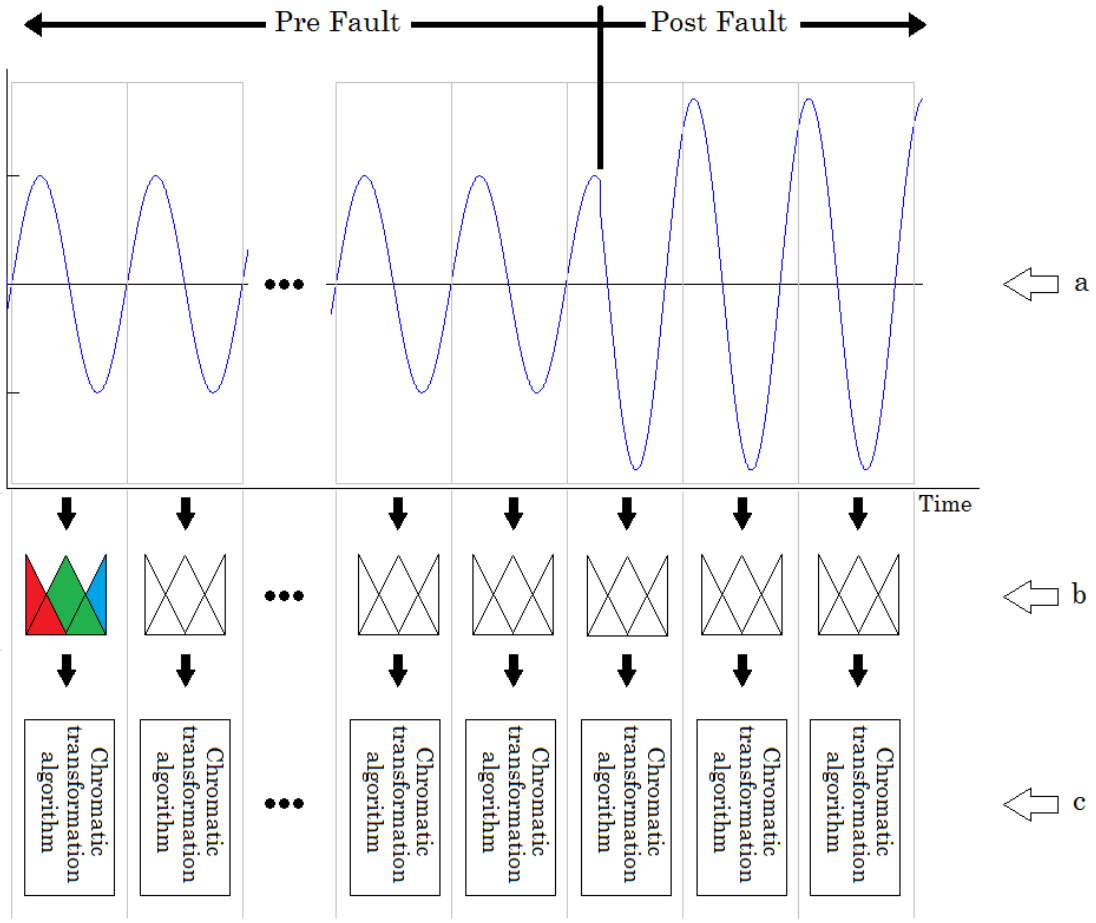

Figure 4.3: Application of RGB processors on pre and post fault of an example waveform

Part (a) of Figure 4.3 shows an illustration example of a monitored symmetrical component. RGB filters illustrated in Figure 4.2 are applied sequentially on a cycle by cycle basis as illustrated on part (b) of the figure. For each cycle of the processed waveforms three parameters R, G and B are generated, they represent filters profile response to cycle variation, calculated by the Formulas 4.1a, 4.1b and 4.1c.

$$R = \int R(t)P(t)dt \tag{4.1a}$$

$$G = \int G(t)P(t)dt \tag{4.1b}$$

$$B = \int B(t)P(t)dt \tag{4.1c}$$

The R(t), G(t) and B(t) are the profiles of the three non-orthogonal filters shown in Figure 4.2, P(t) is a cycle duration of the monitored waveform. R(t) profile is covering the first half of P(t), the B(t) filter is covering the remaining, and the G(t) filter is covering both halves. The three profiles are covering P(t) and overlapping with each other.

4.3 Chromatic transformation HLS

Part (c) of Figure 4.3 describes the RGB filters outputs transformation by chromatic monitoring step, Section 2.9.3 give descriptions of HLS model, its algorithms and equations are used in most of the transformation performed in this work.

The overall procedure in Figure 4.3 is repeated for all of the available waveforms. For each available waveform, three parameters are calculated using HLS algorithms. Figure 4.4 shows the data flow procedure and the groups of new parameters created.

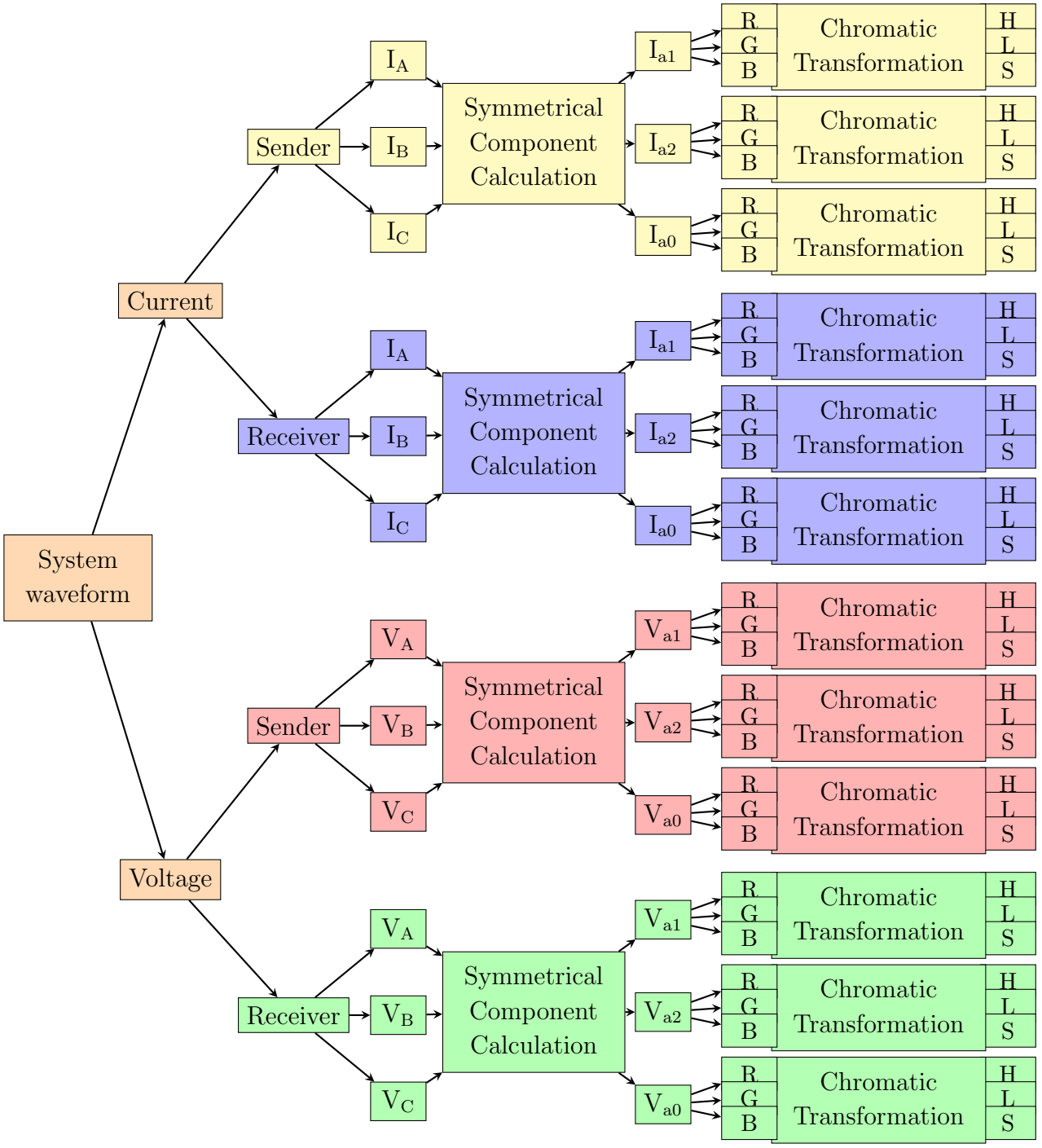

Figure 4.4: Chromatic monitoring: Data flow and outcomes

4.4 Chromatic monitoring of AC waveform cycles

In colour science, the chromatic identifying parameters (H, L and S) resulting from transforming the filtering stage outputs (R, G and B) highlight specific features in colour. Any change in the signal distribution over the monitored spectrum is reflected in these chromatic parameters.

The method presented in this work is based on continuous monitoring of power system waveforms (i.e., current and voltage). The process is performed on a series of time windows. Each window is a single cycle width duration. Any change in the cycle amplitude, phase and frequency component is expected to produce a change in the resulting chromatic parameters. In this section, the study aims to identify the relationship between changes in power cycle and the associated change in the chromatic parameters.

For comparison purposes, a group of sine waves with different characteristics are chromatically processed. Figures 4.5(a)-(e) represent Matlab generated waves under study. Figure 4.5(a) shows pure AC wave of ten cycles. Starting at the third cycle, an increase and decrease in wave amplitude are shown in Figures 4.5(b) and (c) respectively. Figure 4.5(d) shows an 11° shifted cycles waveform, and the last waveform is shown distorted by the addition of high-frequency component. Both the phase shift and the high-frequency addition are also imposed starting at third cycle.

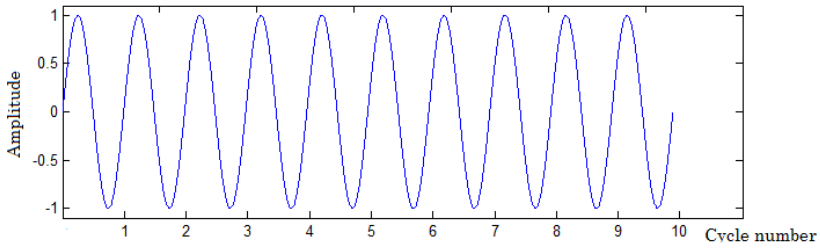

(a) Pure sine wave

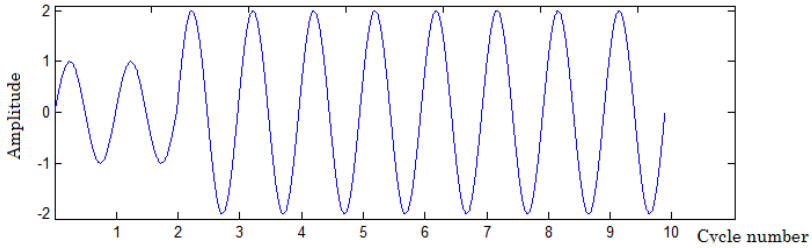

(b) Amplitude increase

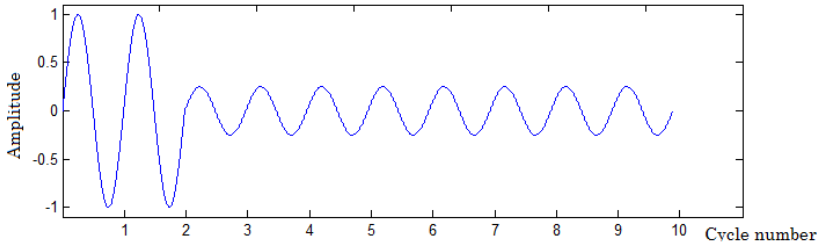

(c) Amplitude decrease

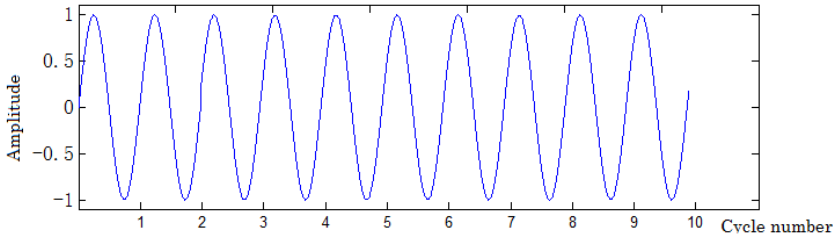

(d) Phase shift

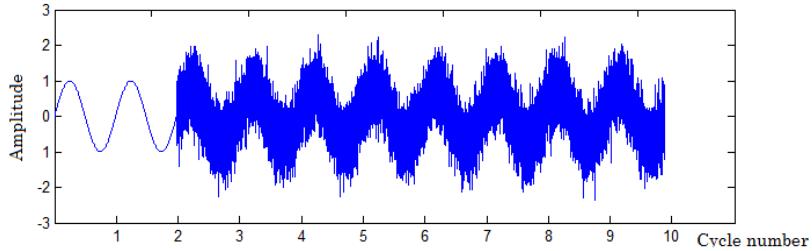

(e) High frequency

Figure 4.5: AC waveforms under study

After applying the chromatic monitoring procedure on the described waveforms, Figure 4.6 shows the H parameter vs. the cycle number for all the cases. Except for the phase shifted waveform case, the H parameter of the different waveforms has the same value. Although The H parameter of the high-frequency distorted waveform shows a slight fluctuation, it is found located around the same H value as the pure waveform.

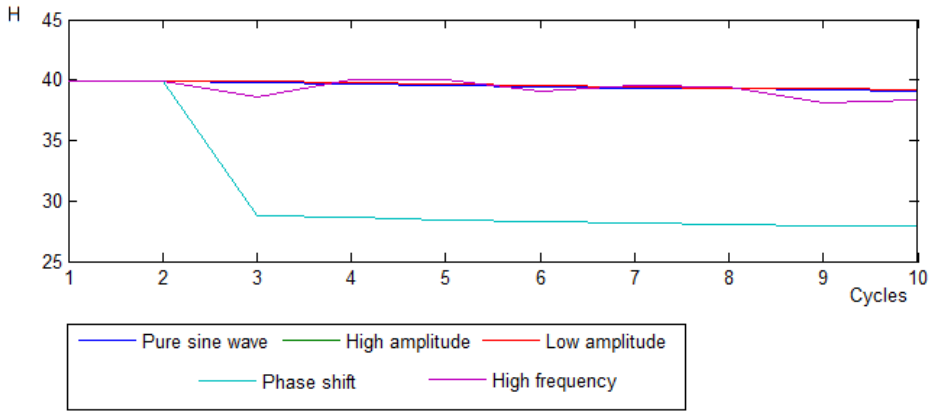

Figure 4.6: H parameter vs. Cycles

To continue testing the phase of the waveform relation with the H parameter, the phase shift of the single cycle window shown in Figure 4.7 is varied from 0° to 360° in steps of 1°. Figure 4.8 shows how the variation in H is clearly affected by the phase shift of the cycles.

On the other hand, the L parameter defined basically as the average of the three filter outputs and calculating this parameter for AC cycles is expected to yield a zero or a negligible value. Figure 4.9 is showing the expected results for all of the tested waveforms except a slight but negligible and random fluctuation in the parameter value for the waveform with high-frequency component.

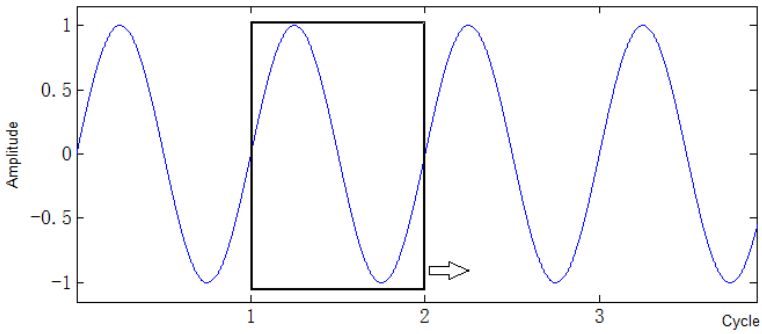

Figure 4.7: Single cycle window

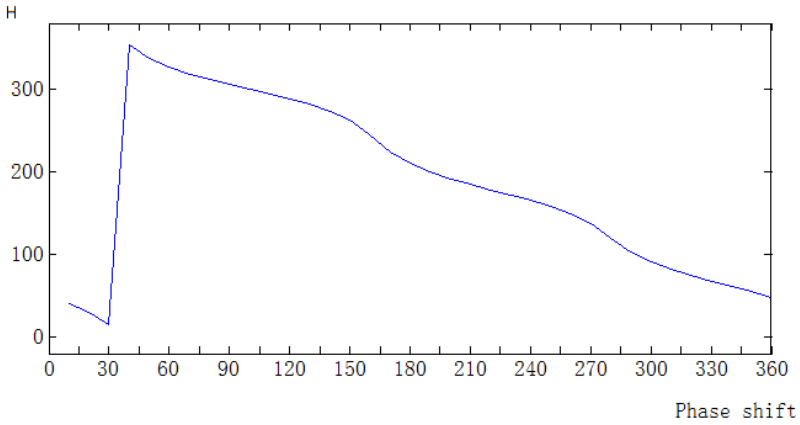

Figure 4.8: H parameters vs. phase shift for a pure AC cycle

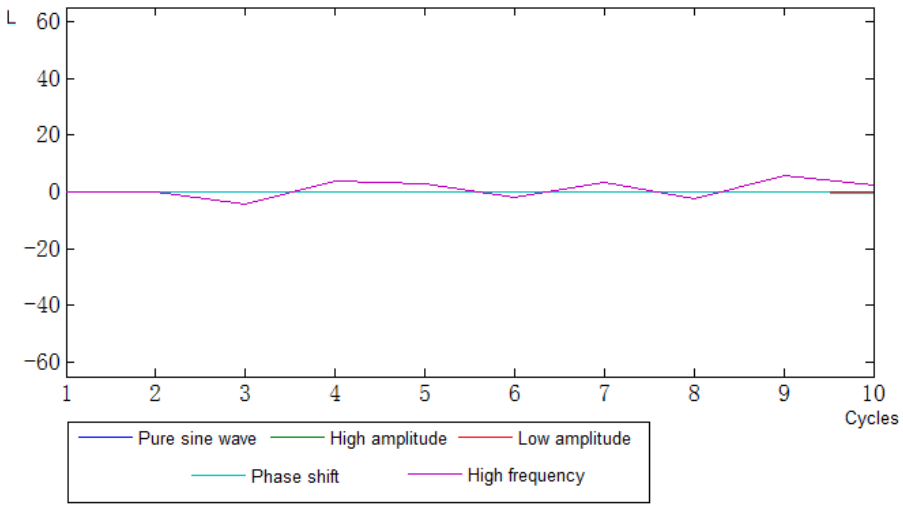

Figure 4.9: L parameter vs. Cycles for non rectified waveforms

When waveforms are rectified before the chromatic processing, Figure 4.10 shows the L parameter to achieve a specified level and remain the same for all of the waveforms cycles. An increase in the parameter value was observed for the high amplitude cycles, and a decrease was observed for the low amplitude cycles. The L parameter value was found immune to the shift in the cycles phase, and a negligible change was noticed with the high-frequency component.

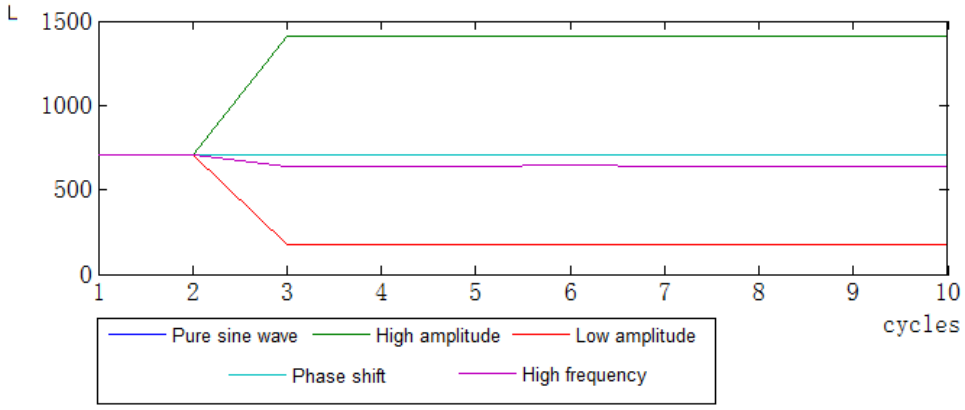

Figure 4.10: L parameter vs. Cycles for rectified waveforms

As a summary, the changes in the waveforms phase change can be examined by studying the waveform H parameter variation. The amplitude change will be reflected in L parameter value if the waveform it rectified.

The high-frequency component effect on the L and H parameters was found to be slight. The effect might be considered if frequency domain monitoring is carried out, which is left as a suggested future work (Chapter 6).

4.5 Fault diagnosis

The flowchart in Figure 4.4 shows how many parameters are produced from the chromatic processing of the system waveforms. Analysis, further processing and discussion in this thesis will focus mainly on parameters which are directly affected by the fault conditions, as these may hold information about the fault. The analysis may also include some parameters that are in addition to the primary algorithms and may need secondary processing that could connect the changes in them with the fault condition.

Considering the outcomes of Section 4.4 as well as the preliminary observations of results presented in Chapter 3 (i.e. the change in the amplitudes of the current and the voltage positive symmetrical components and the changes of the negative sequence components phase shifts); Section 4.5.1 will focus on connecting the value change of the H parameter of both the current and the voltage negative sequence component with the monitored fault type. It will also consider how using such characteristics can lead to the implementation of a fault type classification algorithm.

A further improvement on the proposed classifier is achieved by utilising the L parameter of the zero sequence component in distinguishing between faults with and without ground involvement. Benefits gained from this analysis are explained in details in Section 4.5.2.

Following the fault type classifier, an attempt to estimate its location (Section 4.5.3) is carried out by analysing the L parameter of the current positive sequence component. The analyses will involve current of both terminals from the transmission line and secondary processing of the information.

4.5.1 Fault classifier

To achieve the purpose of correctly classifying fault type, an extensive search is carried out through the various chromatic parameters focusing on those which possess behaviour changes with respect to different faults. The behaviour under study needs to be unique and distinguishable for each fault.

Beside the fault type, the required parameters have to be immune to any other factors as the location of the fault and/or the fault resistance. Analysis of two candidate parameters are presented in the next subsections. The H parameter of the current negative sequence component is analysed in Subsection 4.5.1.1 and the H parameter of the voltage negative sequence component in Subsection 4.5.1.2.

4.5.1.1 H parameter of the current negative sequence component

The fault types considered are the asymmetrical faults which include single line fault to ground (AG, BG, CG), double line faults (AB, AC, BC) and double line faults to ground (ABG, ACG, BCG).

4.5.1.1.1 Different faults, at 50% of the line

Chromatic H parameter values of the current negative sequence component have been calculated for the various faults at the same location but for several fault resistances.

Examples of the H values as a function of the wave cycle just prior and post fault inception are given in Figure 4.11. Figure 4.11(a) shows H vs. cycle number for various types of faults with 0.001 Ω faults occurring at 50% the power line length. Figure 4.11(b) shows the same types of faults at the same location, but with a resistance of 10 Ω.

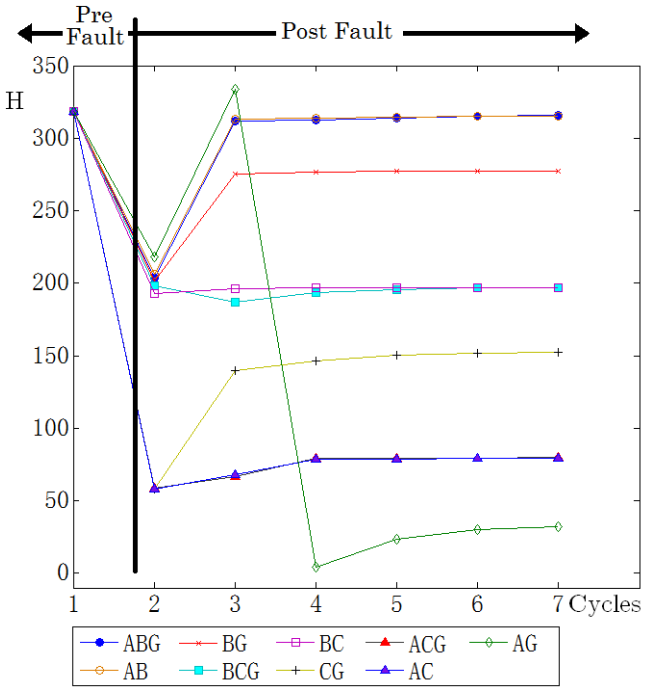

(a) 0.001 Ω fault resistance

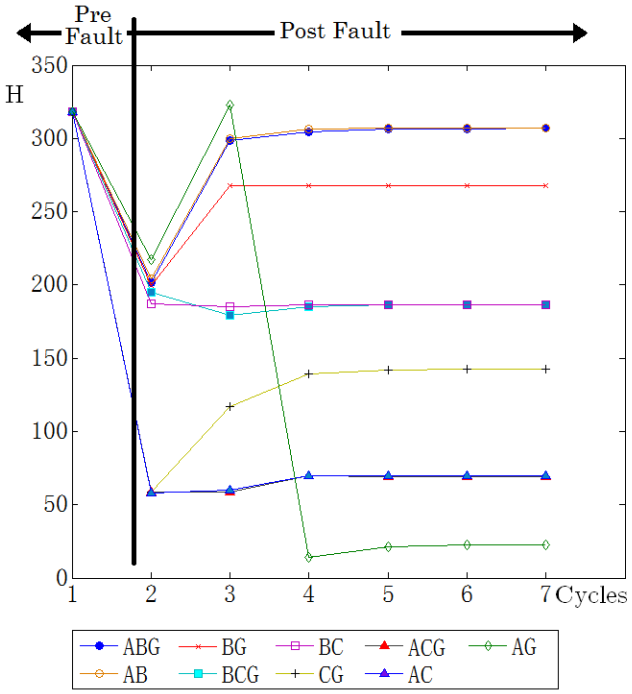

(b) 10 Ω fault resistance

Figure 4.11: H values of the current negative sequence component for various faults located at 50% of the line length with fault resistances of (a) 0.001 Ω (b) 10 Ω

These results show changes in the H value post fault inception which are :-

a) During the first fault cycle (cycle 2), the H fault values reduce substantially from the healthy value ($\sim 318°$) by d(H) $\sim 100°$ – $250°$ for both 0.001 Ω and 10 Ω fault resistances.

b) During subsequent cycles, the H values have, in general, different levels which depend on the type of fault.

c) During these subsequent cycles, the H value for each fault is similar, but not identical, for the two fault resistances, 0.001 Ω (Figure 4.11(a)) and 10 Ω (Figure 4.11(b)).

4.5.1.1.2 Same fault, but at different locations

To illustrate the effect of the fault location on the chromatic H values, the same faults with fixed fault resistance are simulated but at different locations.

Figure 4.12(a) shows results for H: cycle for a 0.001 Ω BG fault occurring at three different locations (10, 50, 90% line length). Figure 4.12(b) shows H: cycle number results for an AC fault of the same resistance (0.001 Ω) and the same three line length locations (10, 50, 90%).

These results show that for the BG faults, the post fault cycles have H values for each location which have similar, but not identical values. Likewise for the AC fault, the H values only weakly depend upon the fault location.

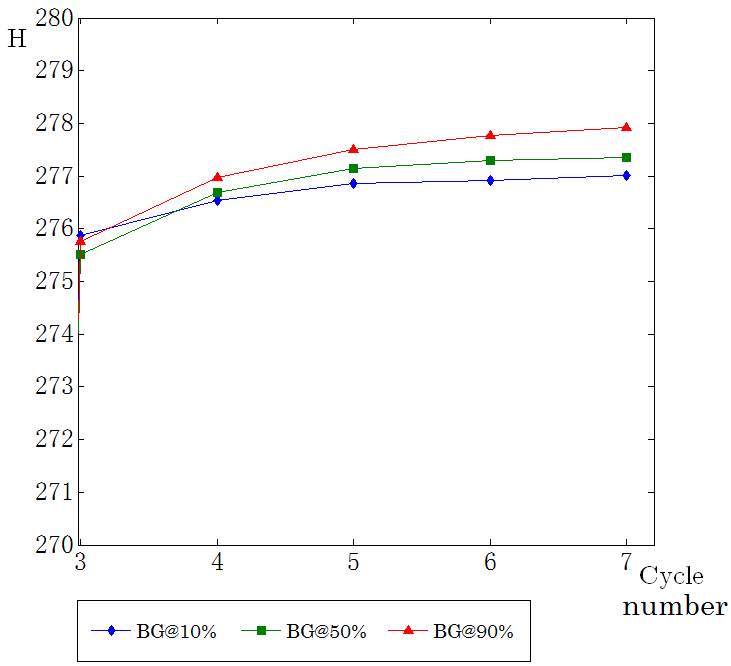

(a) BG fault

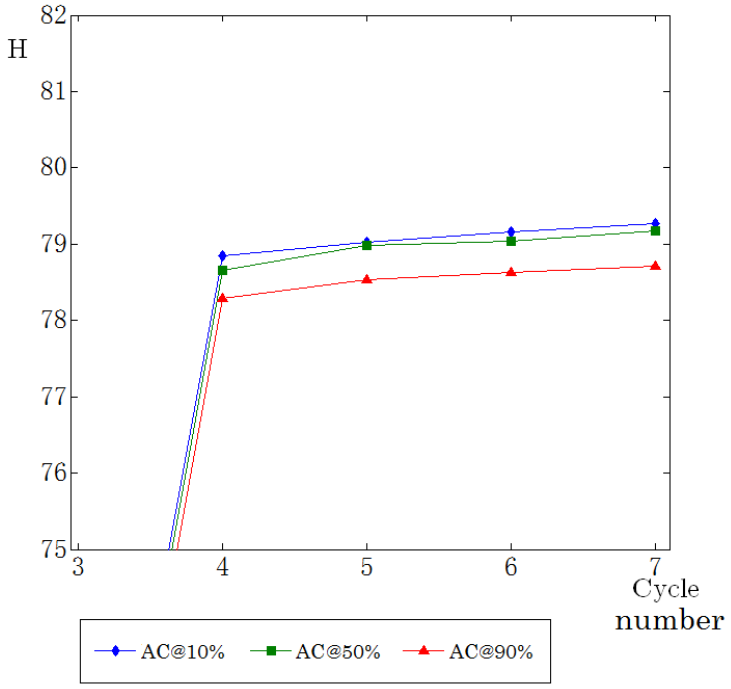

(b) AC fault

Figure 4.12: H : post fault cycle for a 0.001 Ω fault at each of three different line locations (10, 50, 90%) (a) BG fault (b) AC fault

4.5.1.2 H parameter of the voltage negative sequence component

Similar to Section 4.5.1.1, this section considers the H parameter, but for the voltage negative sequence component. The considered fault types are the same set of the asymmetrical faults which include single line fault to ground (AG, BG, CG), double line faults (AB, AC, BC) and double line faults to ground (ABG, ACG, BCG).

4.5.1.2.1 Different faults, at 50% of the line

Chromatic H parameter values of the voltage negative sequence component have been calculated for the various faults at the same location but for several fault resistances.

Figure 4.13 give examples of the H values as a function of the wave cycle just prior and post fault inception. Figure 4.13(a) shows H vs. cycle number for various 0.001Ω faults occurring at 50% the power line length. Figure 4.13(b) shows the same types of faults at the same location but with a resistance of 10Ω.

Results of H value post fault cycles show similar behaviour but different values of current H value in Section 4.5.1.1

4.5.1.2.2 Same fault, but at different locations

To illustrate the effect of the fault location, the same faults with fixed fault resistance are simulated but at different locations.

Figure 4.14(a) shows results for H : cycle for a 0.001 Ω CG fault occurring at three different locations (10, 50, 90% line length). Figure 4.14(b) shows H: cycle number results for a BC fault of the same resistance (0.001 Ω) and the same three line length locations (10, 50, 90%).

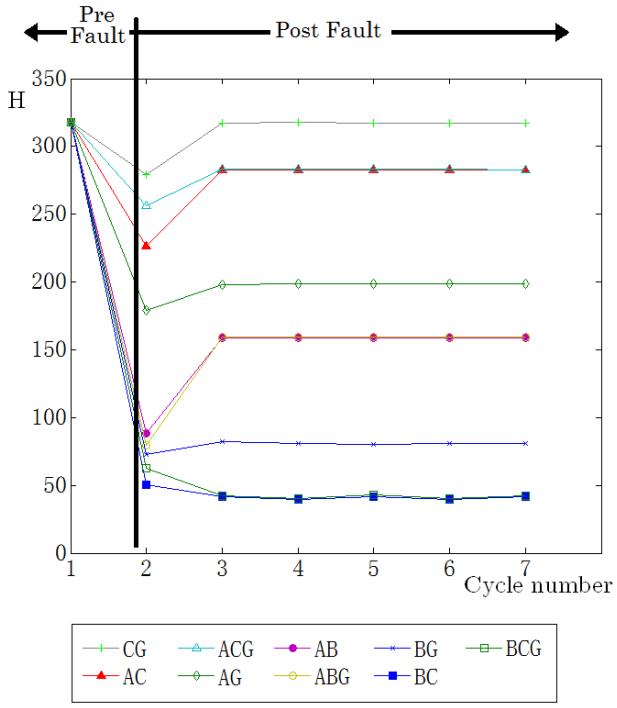

(a) 0.001 Ω fault resistance

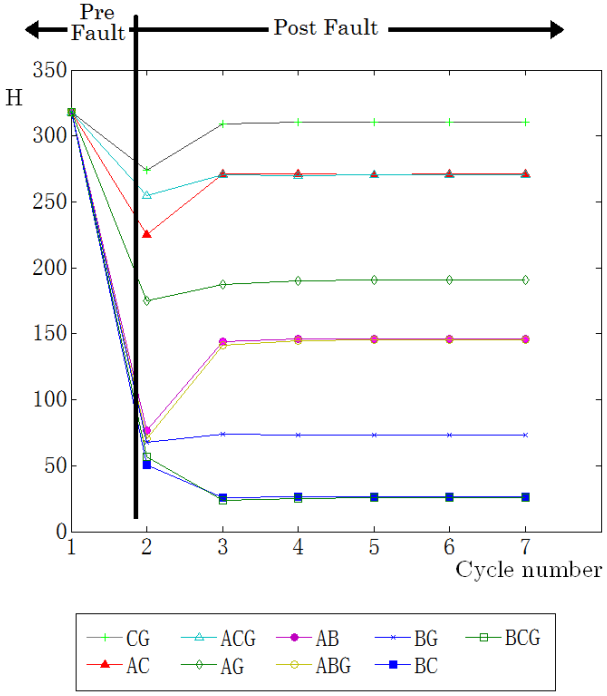

(b) 10 Ω fault resistance

Figure 4.13: H values of the voltage negative sequence component for various faults located at 50% of the line length with fault resistances of (a) 0.001 Ω (b) 10 Ω

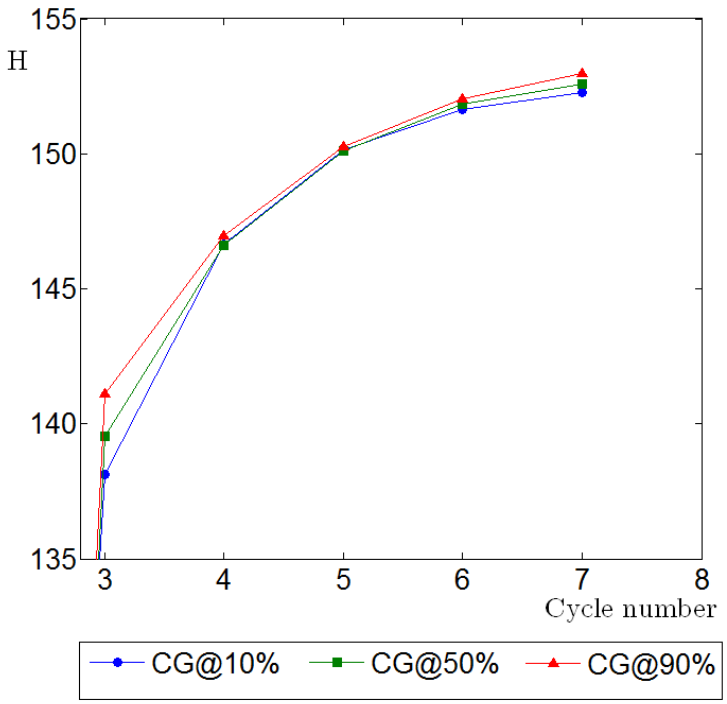

(a) CG fault

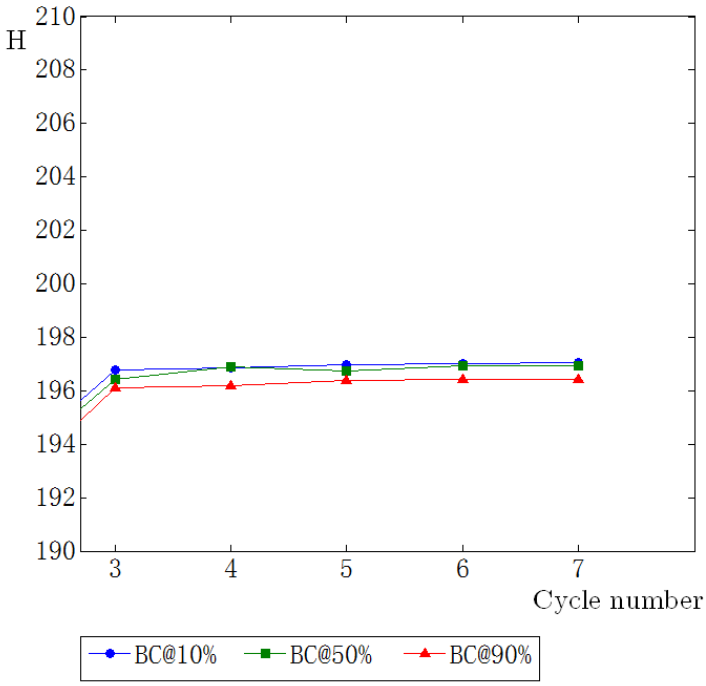

(b) BC fault

Figure 4.14: H : post fault cycle for a 0.001 Ω fault at each of three different line locations (10, 50, 90%) (a) CG fault (b) BC fault

For both examples, H values only weakly depend upon the fault location. Post fault cycles H values for the three locations have similar, but not identical values.

4.5.2 Ground detection

To support the classifier decision, there is a need to find a parameter that is affected by the ground element presence or absence in other fault scenarios. The preliminary inspection of the result in Chapter 3 shows a clear impact of the ground presence on the zero sequence component waveforms.

Next subsection includes analysis of the L parameter of the current zero sequence component which could be a potential candidate for distinguishing between faults with or without ground involvement.

4.5.2.1 L parameter of the current zero sequence component

Figure 4.15 shows results for chromatic L of the zero sequence component for the different types vs. cycle of faults with a fault resistance of 0.001 Ω and location at 50% of the line. This shows the nine different faults plus healthy condition form three clusters of points.

For the first healthy cycle and before the fault occurrence, the L value is almost negligible. The L value post fault inception immediately and following the first fault cycle (cycle 2) reach L $\sim 10^2$ for the double line faults (AB, AC, BC). The double line to ground faults (AG, BG, CG, ABG, ACG, BCG) have L $\sim 10^6$ with the none fault condition continue at a negligible value.

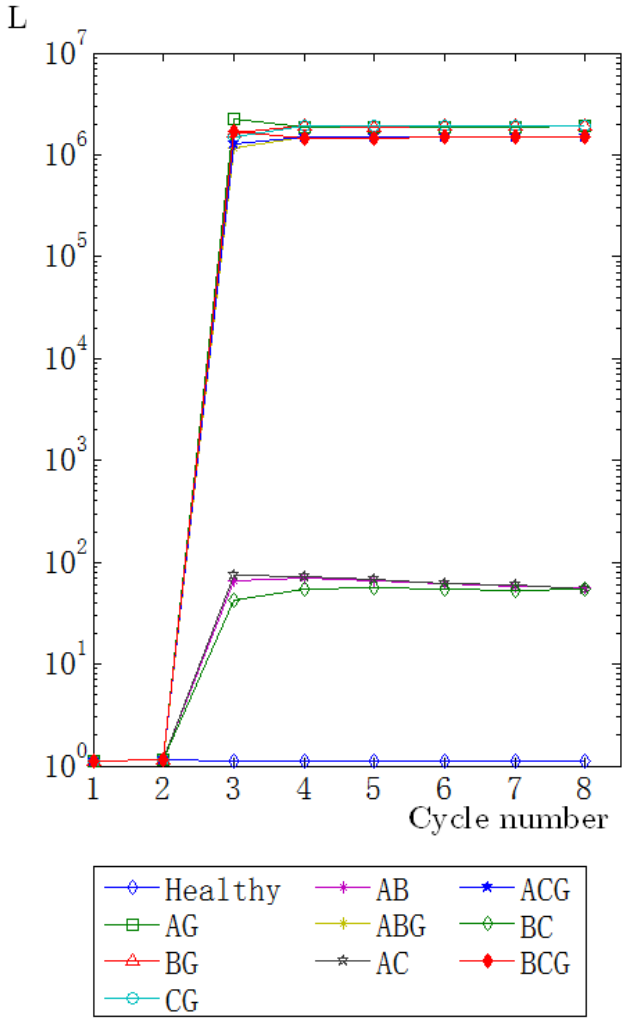

Figure 4.15: L of zero sequence component: cycle for various faults (fault resistance = 0.001 Ω, fault location = 50%)

4.5.3 Fault locator

To function properly, a fault locator will need to provide an accurate estimation of the fault location and this estimation should not be affected by other factors like the type of the fault, the fault resistance, multiple fault condition or any other possible disturbance conditions that are usually accompanied the faults occurrence.

For estimating the location of the fault, the different chromatic parameters are analysed for various faults which are simulated at different locations along the transmission line.

Some of the chromatic parameters are found to be impervious to the change in the fault location. For instance, the H parameter of the negative sequence parameters analyses (Sections 4.5.1.1 and 4.5.1.2) shows immunity to fault location and such parameters with such characteristics, although it was useful in achieving the fault classification purpose, but they are not helpful in designing the required, accurate, reliable locator.

On the other hand, the preliminary results of the system current waveform (Chapter 3) show that the current positive sequence component magnitude change in general is greatly affected by the fault location.

Next subsections will focus mainly on analysing L parameter for the current positive symmetrical component which provide information about the magnitude of the monitored waveform. The analysis will include current waveforms collected from both terminals of the transmission line.

4.5.3.1 L of the current positive symmetrical component

The RGB results of the positive sequence component have been converted to HLS chromatic parameters. A chromatic representation of the rectified positive sequence component data may be made in term of H, S and L. The L parameter calculation is based on averaging the three RGB parameters, and as we have an interest in the change of the wave magnitudes, a rectification step is introduced in the procedure to precede the chromatic processing.

Figure 4.16 shows a basic example illustrating RGB filtering implementations on a fully rectified positive sequence cycles. The filtering procedure presented in Section 4.2.2 is applied to the waveform. A cycle which occurs after a fault occurrence is shown under processing.

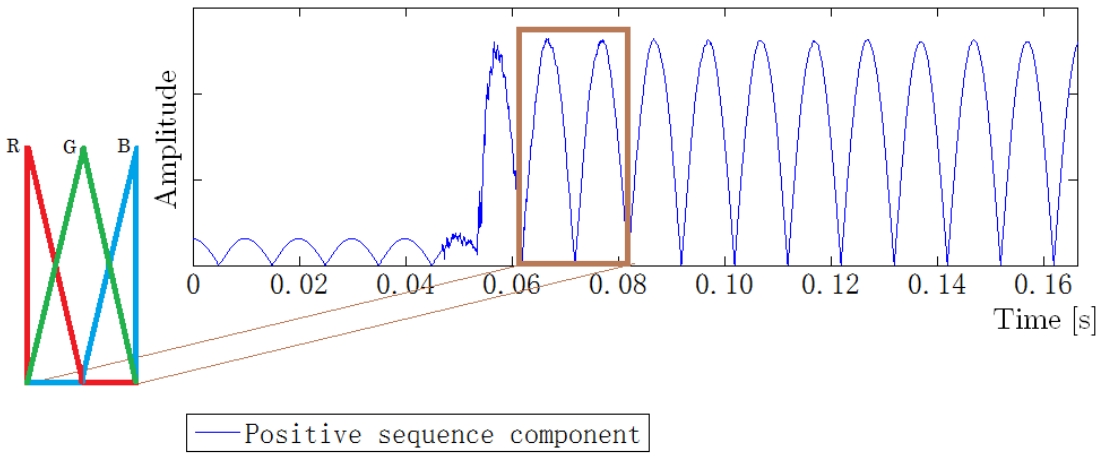

Figure 4.16: Application of RGB processors on a rectified positive sequence component of the current.

The analyses of the L parameter for the current positive symmetrical component considers all of the fault types including both the asymmetrical and the symmetrical faults.

Figure 4.17 shows a sample of L parameter for the current positive symmetrical component changes at receiver terminal plotted vs. cycles, the monitored fault in this case is SLG fault (BG fault), the plotted result is for a simulated fault at three different locations (10%, 50% and 90% of the line length), the fault is a direct line to ground with negligible resistance.

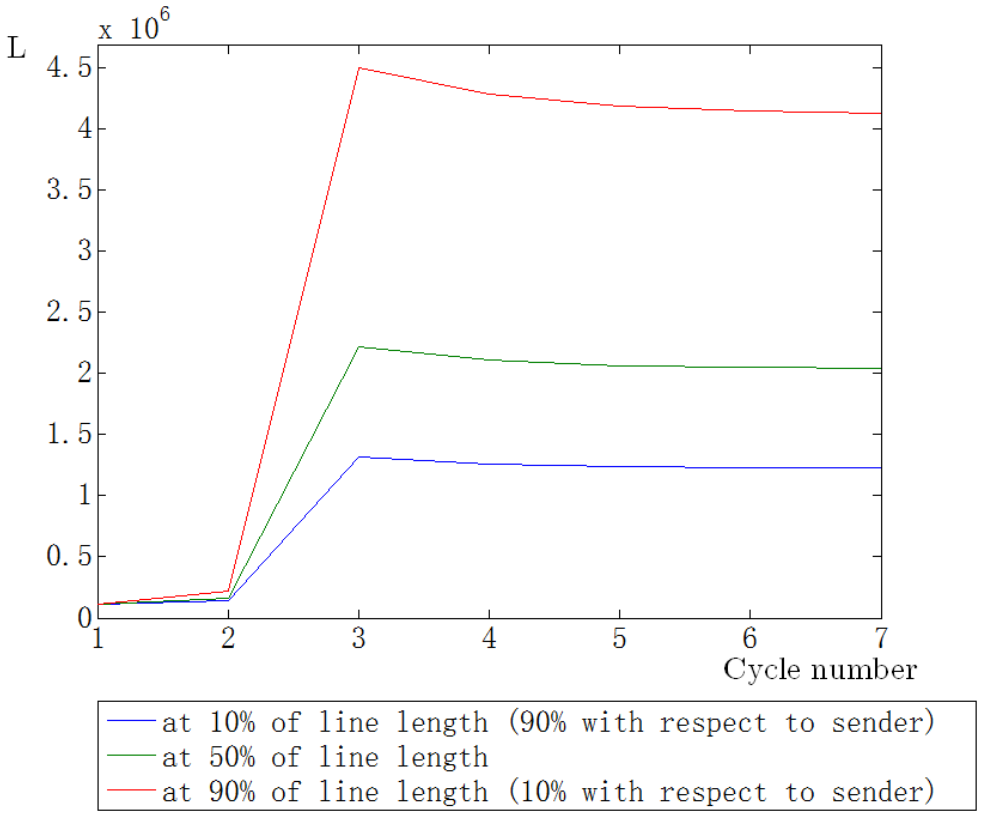

Figure 4.17: L parameter for the current positive symmetrical component from receiver end vs. cycles for a SLG fault (BG fault) with 0.001 Ohms fault resistance. The fault located at 10%, 50% and 90% of the line length with respect to the receiver.

These results show changes in the L value post fault inception for this type of fault which are:-

a) During the first fault cycle (cycle 2), the L values increase sharply from the no fault value ($\sim 1 \times 10^5$) to much higher values depending on the fault location. It reaches ($\sim 4.5 \times 10^6$) for faults at 90%, and for faults at 50% it reaches ($\sim 2.2 \times 10^6$) while its value reaches ($\sim 1.3 \times 10^6$) for faults at 10%.

b) During subsequent cycles, after the decay of the transients, the magnitudes settle down to levels which are related to the location of the fault. The relation is proportional but not linear.

In Figure 4.18, L parameter for the current positive symmetrical component changes at sender terminal are plotted vs. cycles number for the same fault (BG fault), the fault is simulated at three different locations (10%, 50% and 90% of the line length), the fault is direct line to ground with negligible resistance.

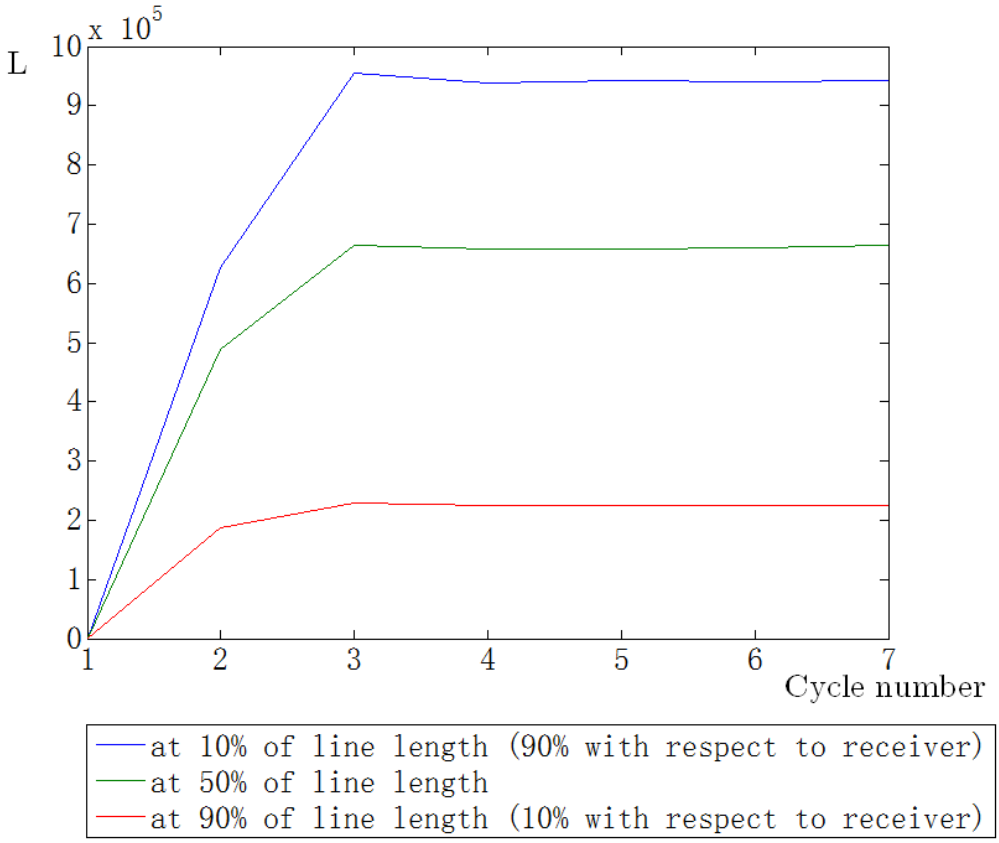

Figure 4.18: L parameter for the current positive symmetrical component from sender end vs. cycles for a SLG fault (BG fault) with 0.001 Ohms fault resistance. The fault located at 10%, 50% and 90% of the line length with respect to the sender

The L magnitudes at the sender terminals have different levels from those found in the receiver terminal. A similar behaviour, in general, is found in the change with respect to the fault location, a proportional relation is but not linear is noticed.

The L value is assessed with respect to the possibility of different fault resistance. Figure 4.19 shows a sample of L parameter for the current positive symmetrical component changes at receiver terminal plotted vs. cycles number, the monitored fault in this case is located at one location (50% of the line length), the plotted result is for a simulated fault with three different fault resistance (0.001 Ohm, 10 Ohm and 200 Ohm).

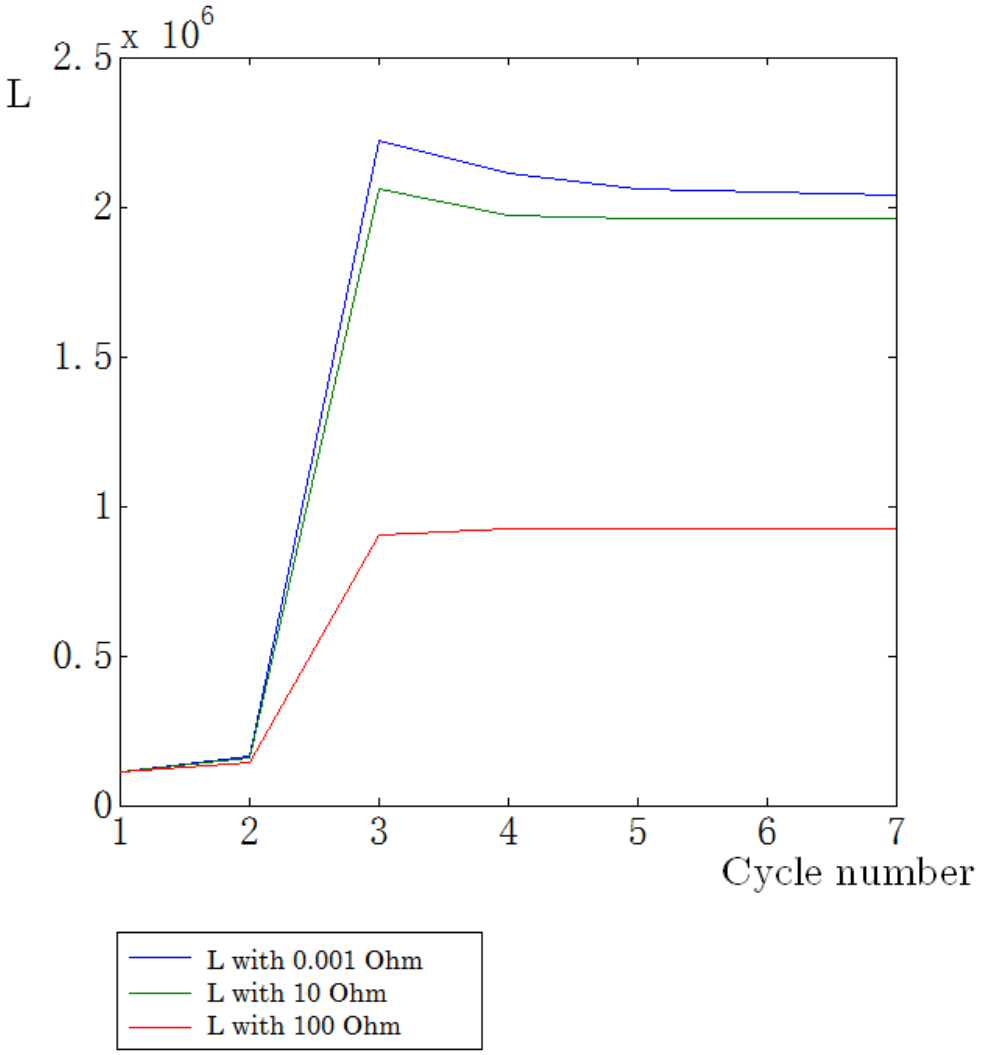

Figure 4.19: L parameter for the current positive symmetrical component vs. cycles for a SLG fault (BG fault) located at 50% of the line length, the fault occur with different fault resistance.

4.5.3.2 Secondary transformation

With the aim of eliminating of the fault resistance effect on the L parameter, a secondary processing procedure is proposed. The idea is based on combining the information collected from both terminals (the source S and receiving ends R) into a new parameter L_{RS} defined by:

$$L_{RS} = (L_R - L_S)/(L_R + L_S) \tag{4.2}$$

The described secondary chromatic procedure is applied to the main chromatic parameter that result from both terminals and this lead to a new parameter, it represents a differential strength parameter (L_R - L_S) normalized with respect to the sum of the sending and receiving strengths (L_R + L_S) for a single cycle. As such, it may be regarded as a secondary, distimulus saturation parameter S. It can be evaluated for sequential cycles to provide indications of the time evolution of the fault induced chromatic signal strength.

To show the results, Figure 4.20 illustrates a sample case of a Line-Ground (BG) fault, variation of L_{RS} with the number of waveform cycles for a fault at three different locations (10%, 50%, 90%) of the line length. The value of this parameter reduces from unity at fault inception (Cycle 1) to (0.1, 0.5 and 0.9) respectively in cycle 3 at which value it remains thereafter. This latter value is indicative of the fractional location of the fault along the line length.

Figure 4.21 shows the result of the simulation when repeated with 0.001,100 and 200 Ohms fault resistance (Rf). Figure 4.22 shows the L_{RS} parameter of the current due to a Line-line-Ground (ABG) fault at 75% of line length. The corresponding L_{RS} variation with waveform cycles is shown for three different values of fault resistance (0.001, 100, 200 Ohms). This shows a reduction in L_{RS}

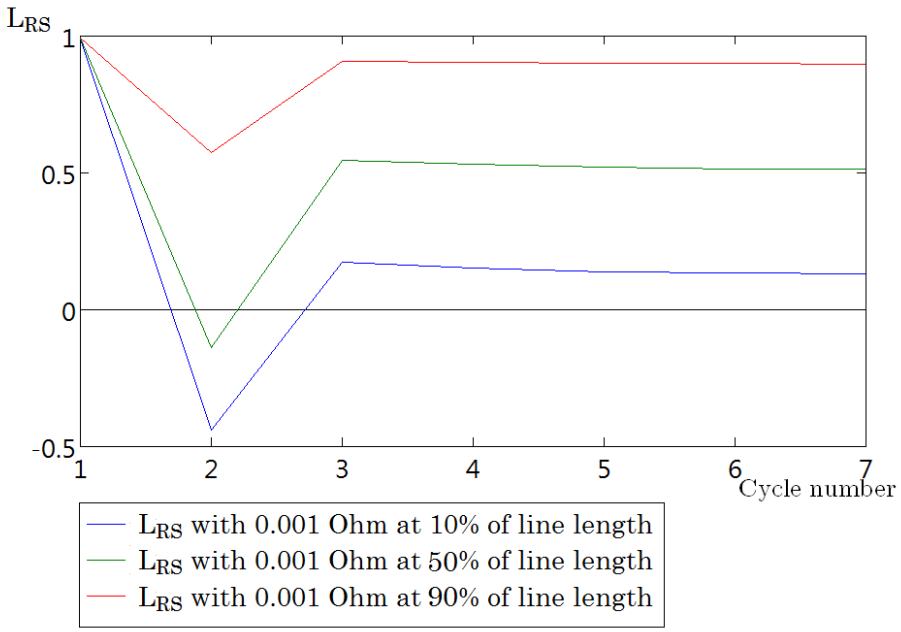

Figure 4.20: L_{RS} vs. cycles for a SLG fault (BG fault) located at different locations (10%, 50%, 90%) of the line length, the fault occurs with 0.001 Ohms fault resistance.

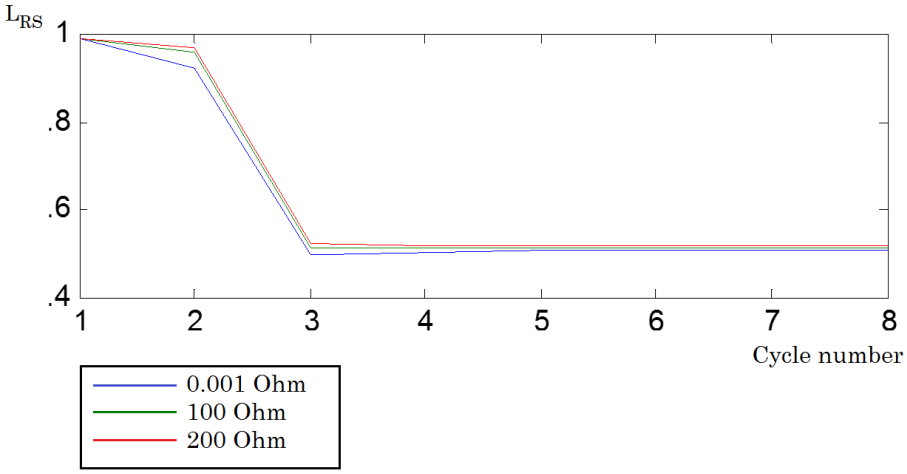

Figure 4.21: LG (BG) fault current: The estimated location of a fault at L_{RS} = 0.5. i.e. 50% of the line length

to 0.75 during cycle 3 indicating a fault at 75 of the line length. Figure 4.23 shows the results for the same fault Line-Line (AB), at the same location (75) but with no ground involved. The reduction in the value of L_{RS} at cycle 3 is again 0.75.

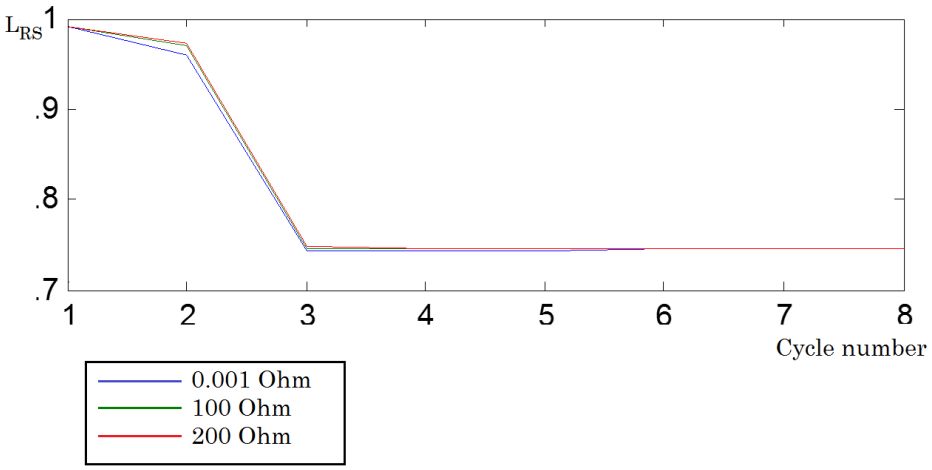

Figure 4.22: DLG (ABG) fault: The estimated location of a fault at $L_{RS} = 0.75$. i.e. 75% of the line length

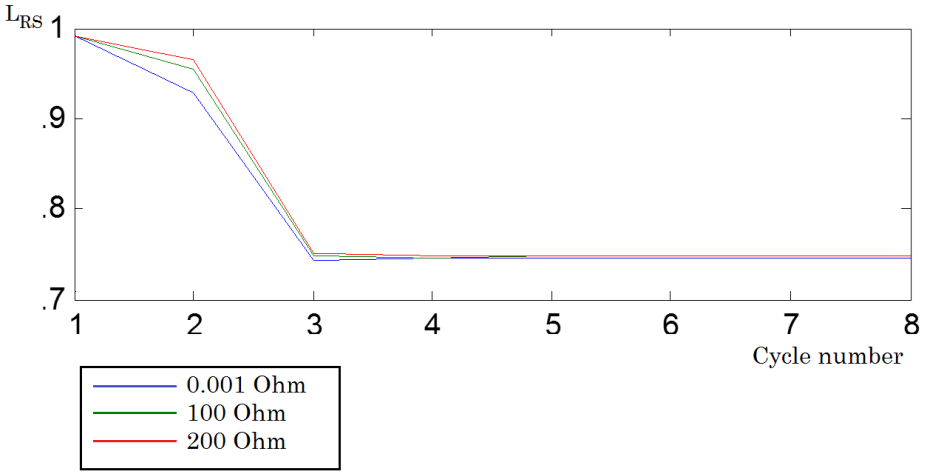

Figure 4.23: LL (AB) fault: The estimated location of a fault at $L_{RS} = 0.75$. i.e. 75% of the line length

For a Line-line-Line-Ground (ABCG) fault at 35 of line length. Figure 4.24 shows the variation of L_{RS} with waveform cycles for this condition and with three different values of fault resistance (0.001, 100, 200 Ohms). L_{RS} value reduces to 0.35 by cycle 3 consistent with the fault location at 35% of the line length.

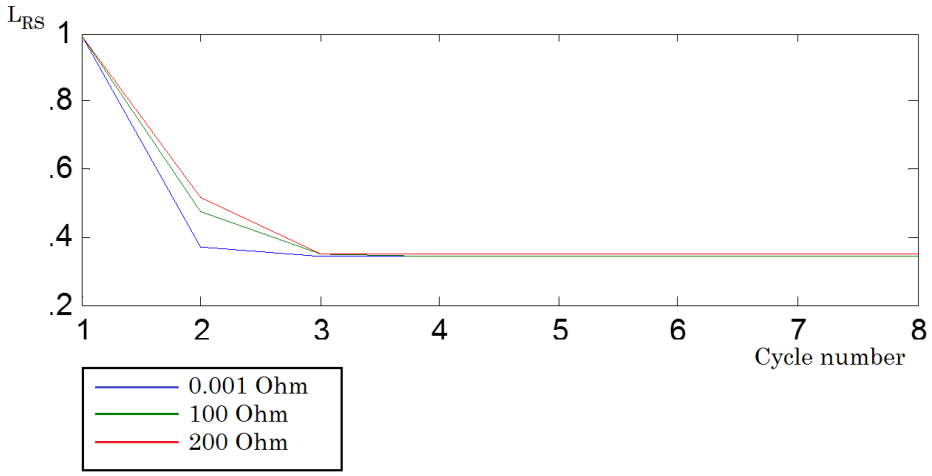

Figure 4.24: LLLG (ABCG) fault: The estimated location of a fault at L_{RS} = 0.35. i.e. 35% of the line length

4.6 Summary

This chapter describes the chromatic monitoring process and the analysis procedure performed on the available waveforms. A preprocessing steps are applied which include calculating the symmetrical components that is followed by applying the of three Triangular receptors on the time domain of the waveforms with a cycle by cycle basis.

Applying the chromatic processing on the filtering stage output yields notably large data set of chromatic parameters. A study is carried out to find a connection between possible changes in the waveforms characteristics and the affected parameters. The study reaches a conclusion of a clear relationship between changes in phase shifts of a waveform and variation in its associated H parameter. On the other hand, the L parameter found to be affected by changes in monitored waveform amplitude only if a rectification preprocessing was applied.

Observations of change in the H parameter for the negative component waveforms of both current and voltage are studied for different asymmetrical faults under operating conditions. Also, changes in L parameter for the rectified pos-

itive component waveforms of current collected from two terminals are studied and fed to a secondary processing stage. The analyses result lay out the basics for diagnostic tool design strategy. These observations are organised and discussed in Chapter 5.

Chapter 5

Discussion

5.1 Introduction

Voltage and current waveforms are obtained from transmission lines simulated in a computer package and an experimental hardware system. These transmission lines represent the types as described in Chapter 3. Samples of these results taken from the terminal ends of a transmission line under different operating conditions are included. These results are analysed using chromatic processing for extracting information that may help in achieving fault condition diagnosis.

Chromatic transformation procedures are applied to the symmetrical sequence components, for the negative component (Section 4.5.1), with changes in the H parameter, used to provide information on the type of the fault. More information can be extracted from the zero component for distinguishing the ground element involvement (Section 4.5.2).

Changes in the magnitude of the positive component after a fault occurrence are used to provide an estimation of fault location, by a secondary chromatic transformation of the result for data from both terminals (Section 4.5.3).

This chapter presents additional analyses and discussion of the involved parameters in addition to proposed improvement and flowcharts for the various diagnostic tools. Also the proposed classifier and locator tools are implemented in a specially designed GUI software using LabView (Appendix C).

5.2 Fault classifier

Analyses included in Section 4.5.1 focuses on H parameters representing current (I_a, I_b and I_c) and voltage (V_a, V_b and V_c) waveforms collected from one terminal. The flowchart in Figure 5.1 represents basic steps which are required for a proposed fault classifier tool procedure.

Samples presented are part of a comprehensive set of computations which have been made covering a wider range of values for the fault resistance and locations. The inspection of these comprehensive results enables ranges of the H value to be determined within which each fault type resides.

Table 5.1: H ranges covered by different types of faults

Fault type	H range	
	>	<
AC/ACG	35	80
CG	80	150
BC/BCG	150	198
BG	198	275
AB/ABG	275	315
AG	315	35

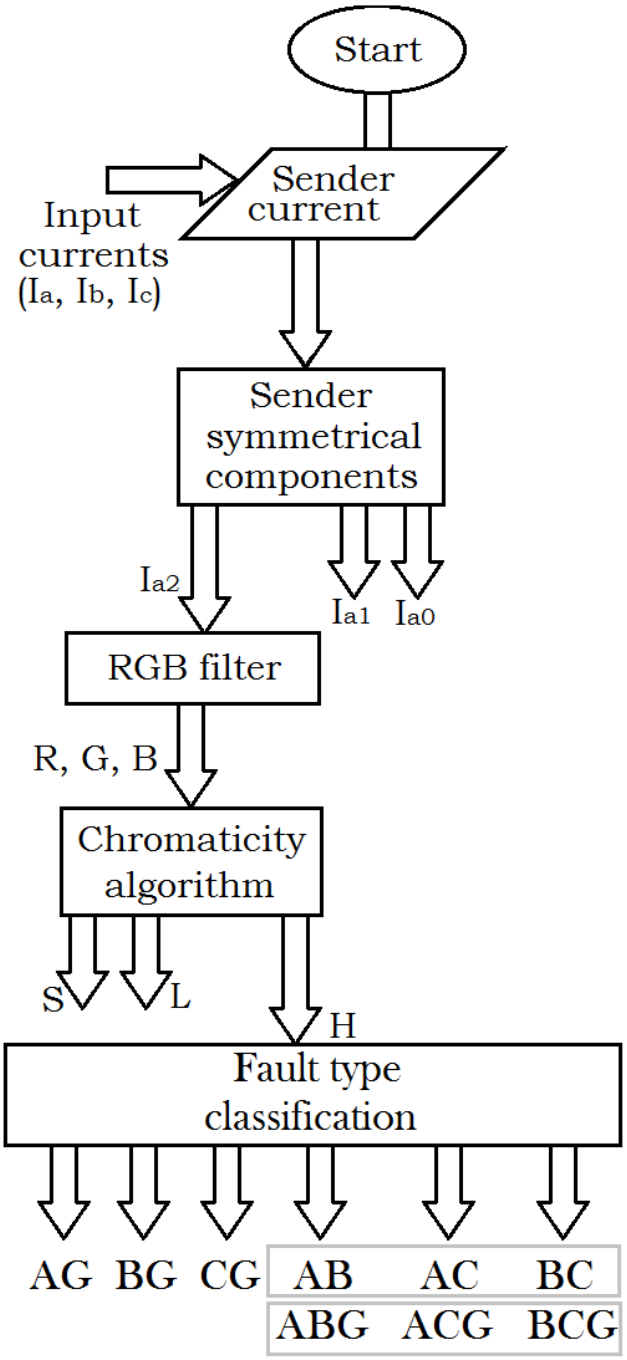

Figure 5.1: Basic classifier flowchart

H ranges for various fault types are listed in Table 5.1, and this shows that:-

a) Various faults may be grouped according to different ranges of H to which they belong.

b) The single line to ground faults (AG, BG, CG) are in general distinguishable from each other and from the other types of faults.

c) Faults involving two lines (AB/ABG, AC/ACG, BC/BCG) are distinguishable from each other, and the single line faults, but the two line-ground faults are not distinguishable from the two line faults.

d) Ambiguities can occur at the boundaries between each of the six ranges whereby there is no distinction between the two faults on either side of the boundary (e.g. H = 80 is a common boundary between faults CG and AC/ACG).

5.2.1 Ground detector

Results presented in Figure 4.15 show that the non-ground and line to ground signals are distinguishable by their different values of the chromatic parameter (L). Thus, by combining the L and H fault groupings, a higher level of fault discrimination is possible.

Figure 5.2 shows a Cartesian chromatic map of L versus H, which provides such a higher level of discrimination. This illustrates how the ambiguities at the range boundaries of the H discriminator are removed using the L parameter.

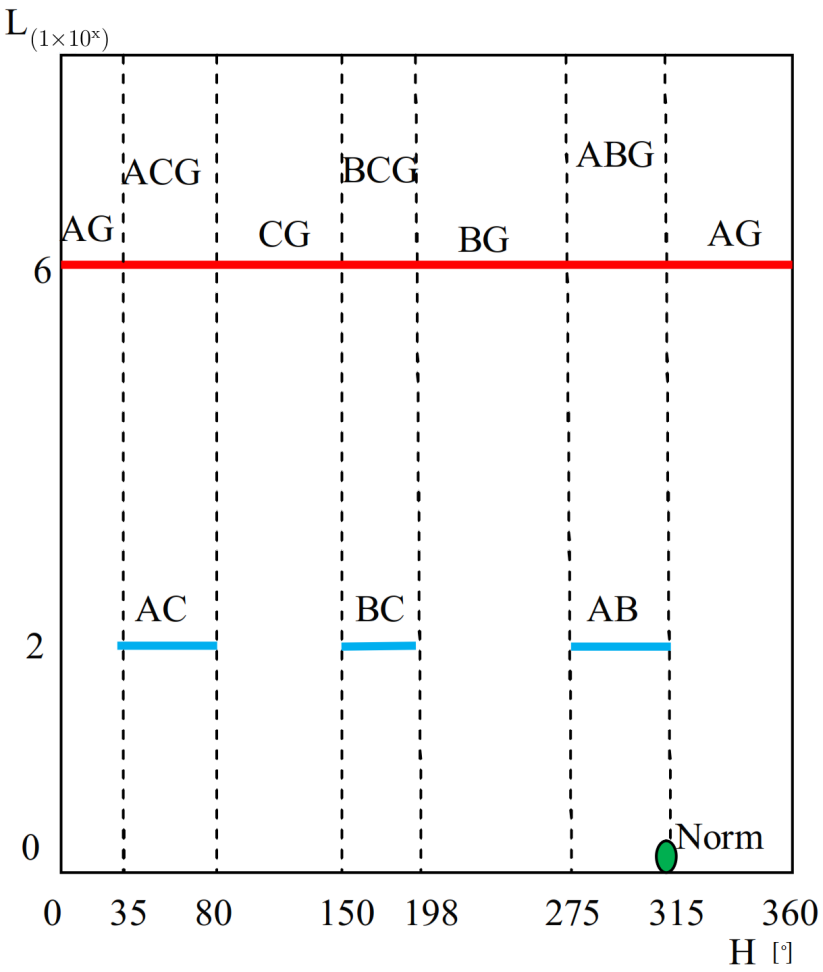

Figure 5.2: Chromatic Map of L versus H with clusters of different faults (AG, BG, CG and AC/ACG, BC/BCG, AB/ABG) plus normal condition (Norm)

5.2.2 Effect of fault resistance

The boundaries ambiguities arise from the overlap of low and very high resistance faults. An example of this is given by the results shown in Figure 5.3 for chromatic H : post fault cycles. This figure compares the H values for a CG fault of resistance values 0.001, 10, 100 Ω with the H values for an ACG fault of resistance 0.001 Ω. The results show that at the fourth cycle H(CG, 100 Ω) = H(AGC, 0.001 Ω). Such comparisons also show that the boundary ambiguities occur due to the overlap of the non-ground and line to ground signals.

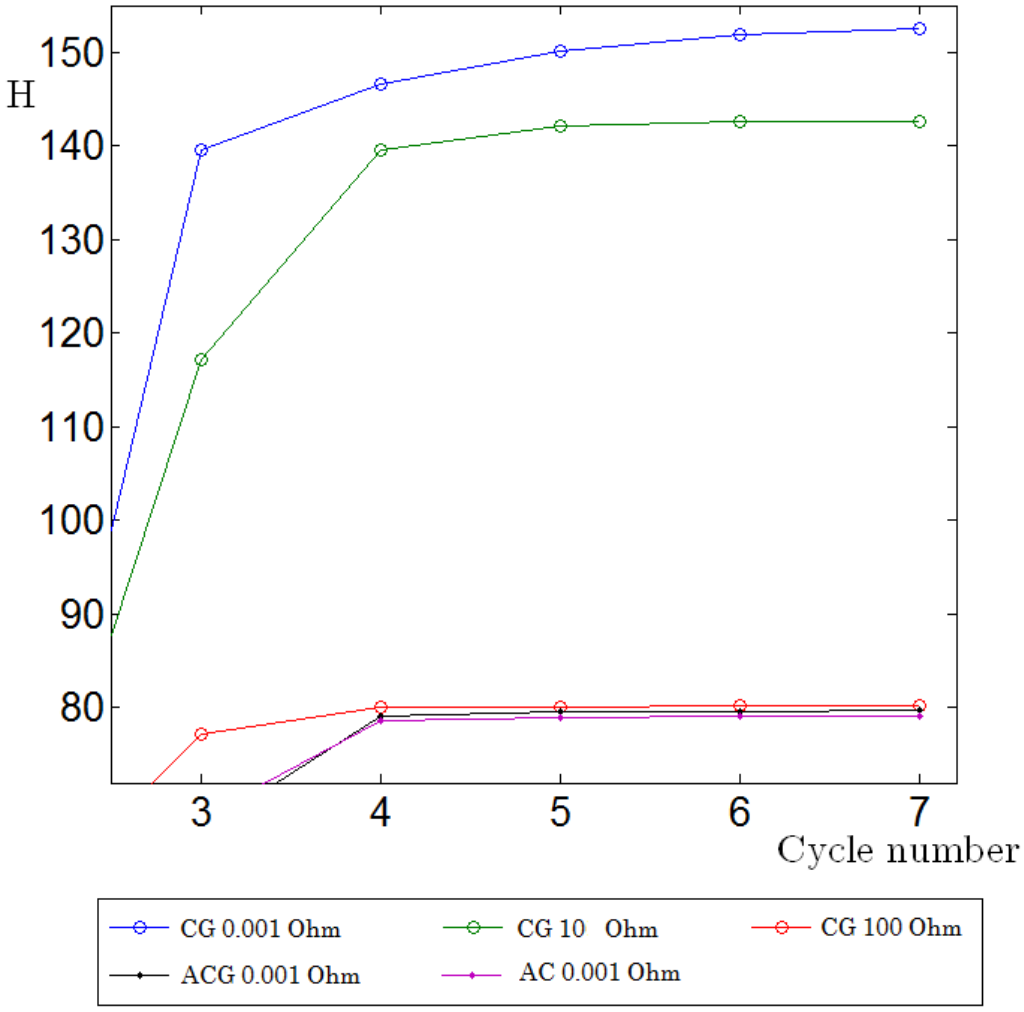

Figure 5.3: Chromatic H: versus post fault cycles for a single line to ground fault (CG) with different fault resistances and for a two line with/without ground fault (ACG/AC) with a low fault resistance.

Further enhancement of the discrimination ability could be obtained through the use of other chromatic parameters combined with the H parameter. For instance, Figure 5.4 shows a polar plot of the L parameter for the rectified negative component waveform vs. the H values for different faults.

In Figure 5.4, each fault type is repeated with three different fault resistance values (0.001, 10, 100 Ω). For the low values of Rf, the H values for the different faults are distinguishable from each other and fall in the ranges shown in Table 5.1.

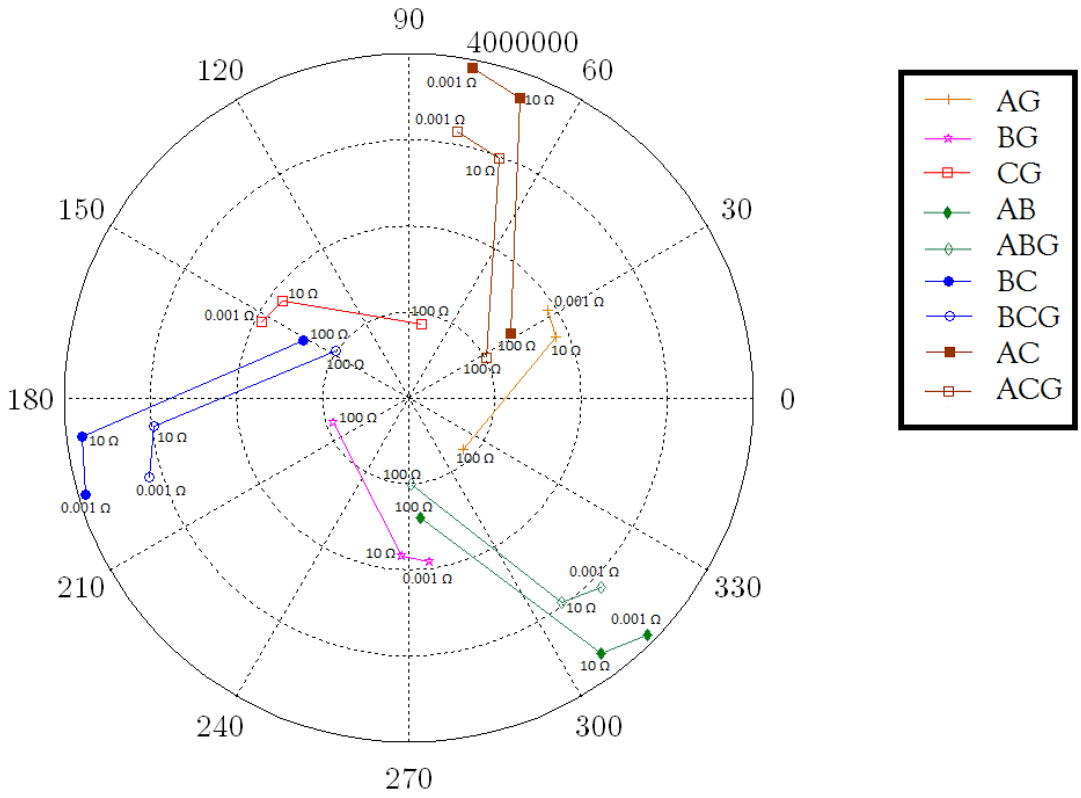

Figure 5.4: Polar plot of L rectified negative vs. H negative

With higher Rf, the overlap between ranges limits the discrimination ability, and the results show a reduced L value moving to the centre of the polar plot. This is due to the low magnitude of the negative waveforms resulting from the high fault resistance.

For illustration purpose, with the aid of grey highlighting, Figure 5.5 provide two examples of highlighted sectors. Figure 5.5(a) shows the H-L values related to the both AC and ACG faults, the discrimination between them has already been shown with the aid of the ground element detector presented in Section 4.5.2. Figure 5.5(b) highlighted sector belongs to the CG fault. Highlighting separate sectors for different faults categories result in six distinct zones shown in Figure 5.6.

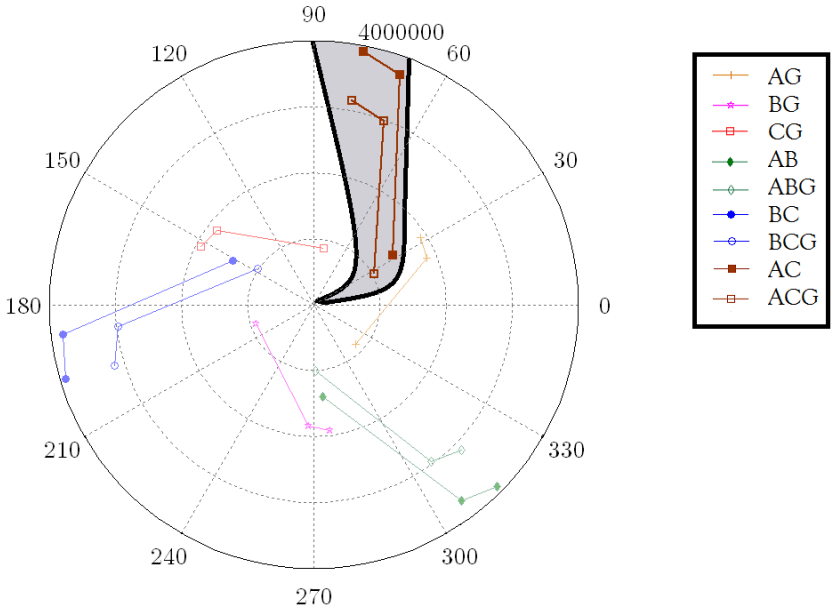

(a) Polar plot of L rectified negative vs. H negative
(Shaded region: AC/ACG fault)

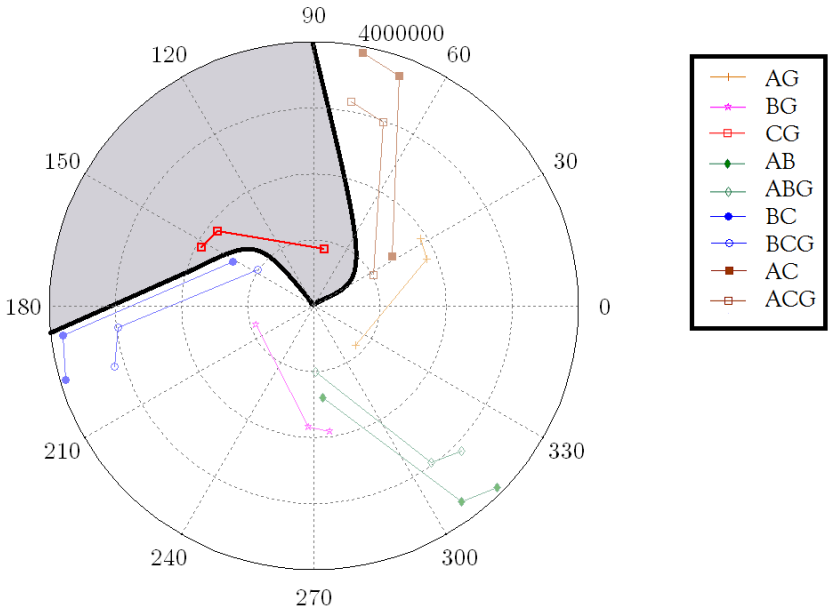

(b) Polar plot of L rectified negative vs. H negative
(Shaded region: CG fault)

Figure 5.5: Polar plot of L rectified negative vs. H negative

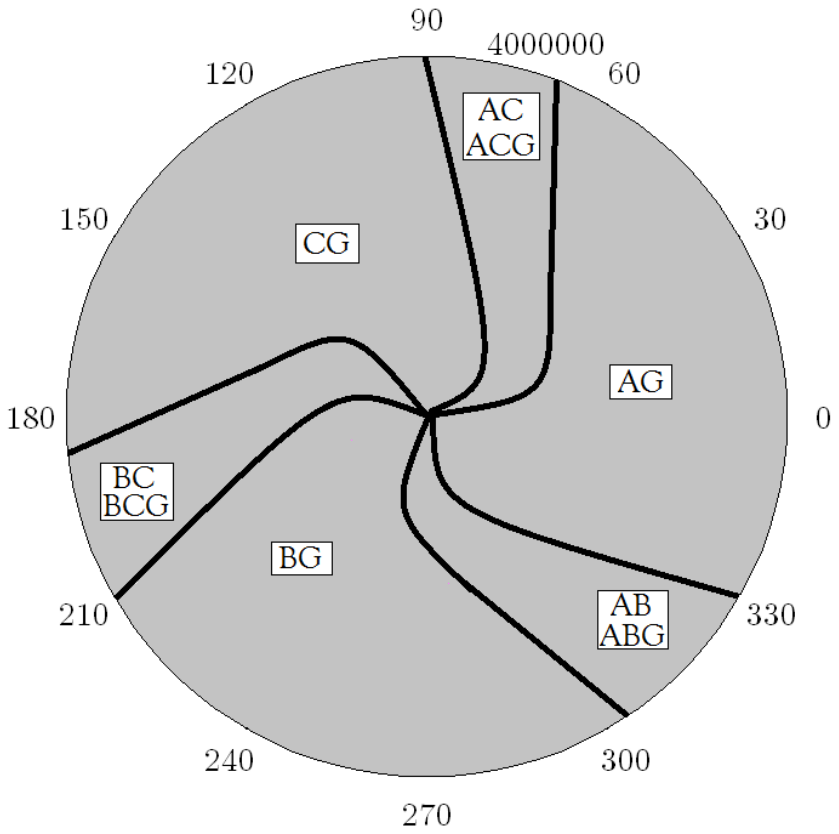

Figure 5.6: Polar plot of L rectified negative vs. H negative

Considering the H values alone, there are overlaps between points from adjacent sectors. However, with the aid of the L value, the trends for the HL values for different faults form clearly distinguishable regions.

Figure 5.7 shows a modified flow chart for the classifier algorithm presented in Figure 5.1. The newly added grey box on the right part of the figure shows the ground detection element presented in Section 5.2.1 based on analysing L of zero sequence component.

The newly added grey box on the left of the flow chart, shows the addition of the L parameter of the rectified negative sequence component to the algorithm, aiming to enhance the discrimination ability by removing ambiguities due to high fault resistance.

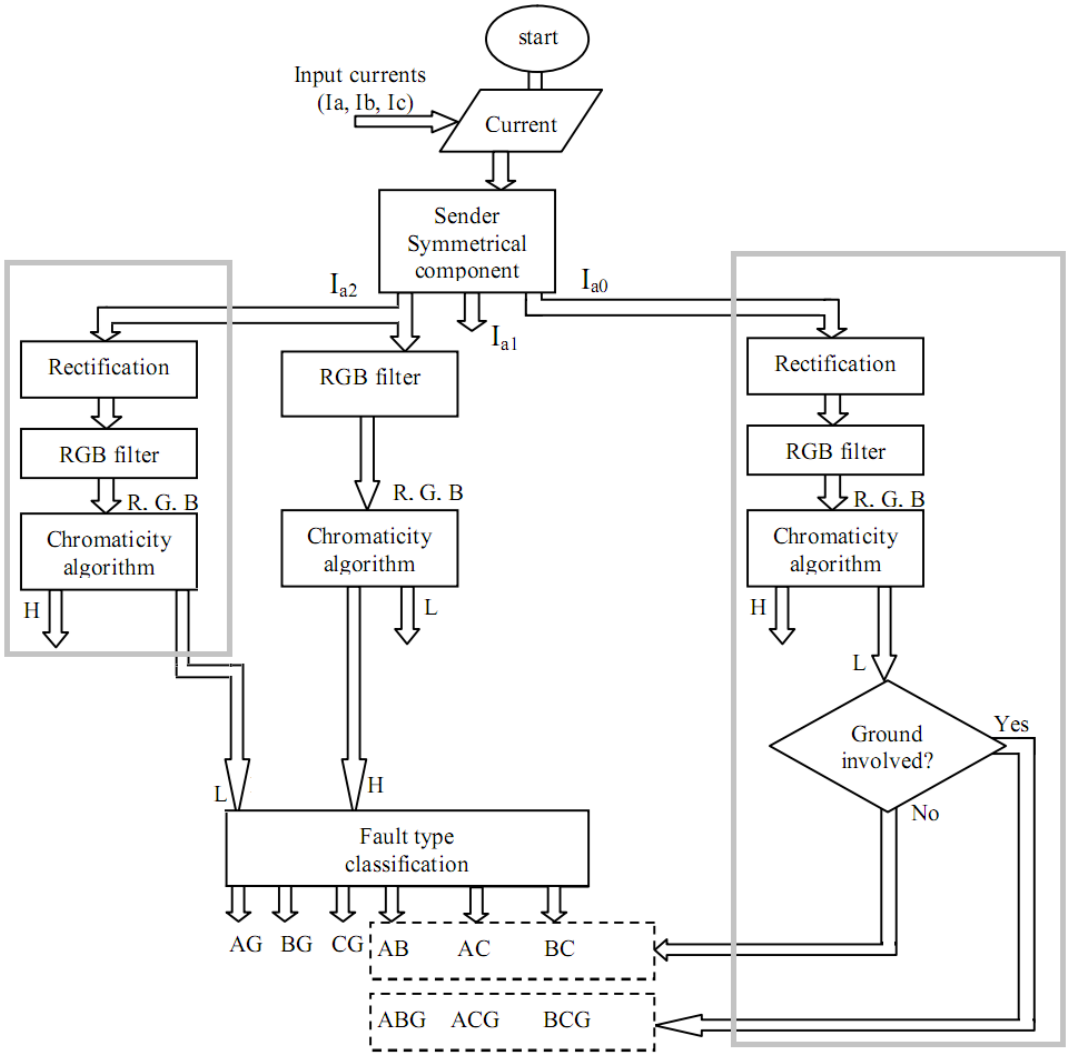

Figure 5.7: Modified classifier flowchart

5.2.3 Effect of inception angle

The effect of the fault inception angle in the fault classification has been investigated. The fault classifier tool is tested considering variations in fault inception angle, of 0, 45, 90, 180 and 270 degrees. Changing the fault inception angles for the same fault type can be achieved easily using simulations, so the following analysed data have been collected from the simulated case study.

Figure 5.8 shows an example of the negative sequence component waveform with five different inception angles for a SLG(AG) fault. The effect of this angle variation in the classifier algorithm outcome is shown in Figure 5.9. The result shows the inception angle slight effect during the first two cycles. Convergence to the same H parameter is achieved over the next few cycles.

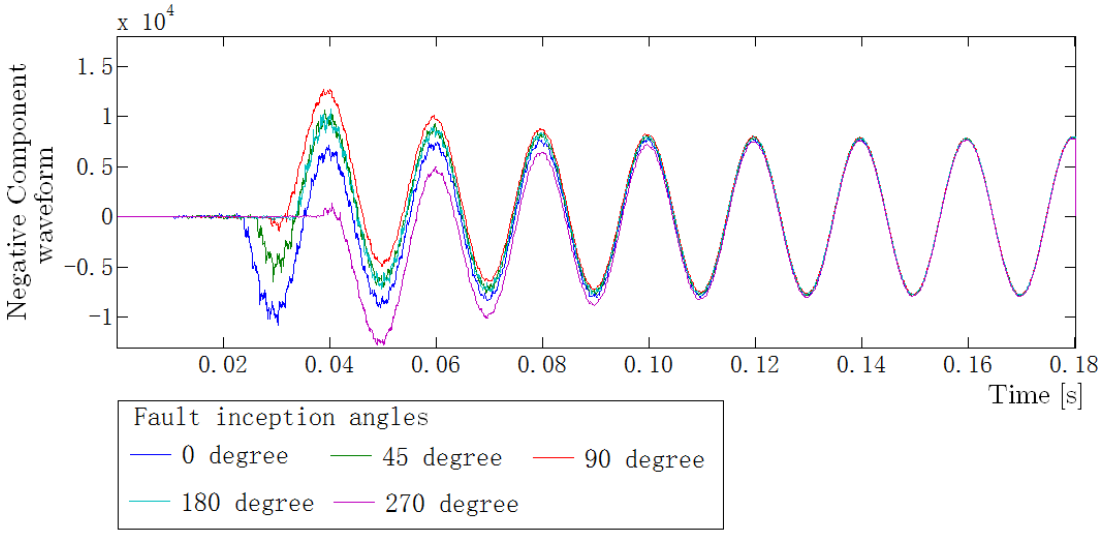

Figure 5.8: Negative sequence component with different inception angles

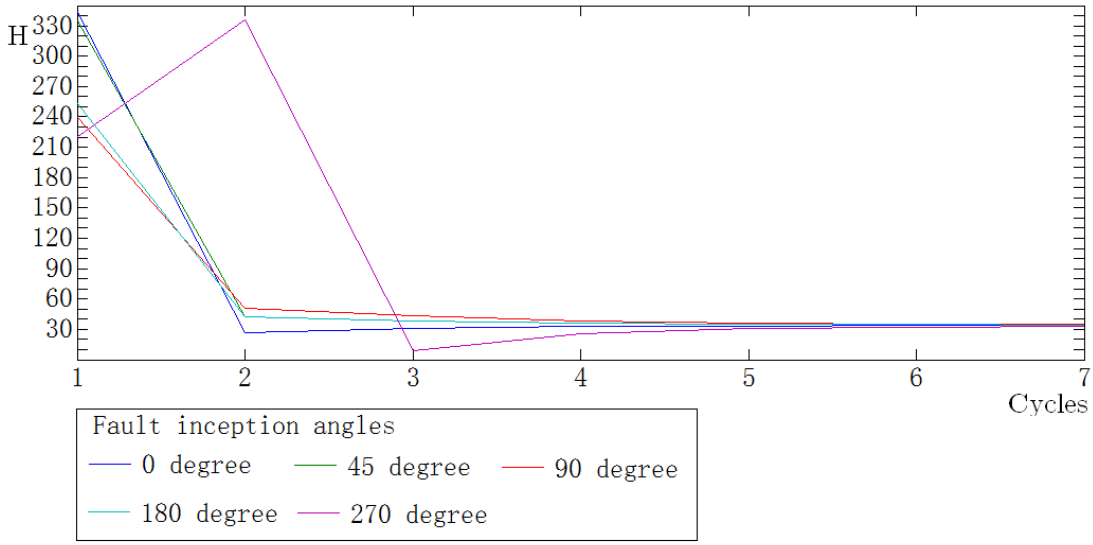

Figure 5.9: Effect of Inception angle on the classifier

5.2.4 Sequential fault scenarios

In power system, complicated fault involving arbitrary faults sequence scenario is probable. Algorithm of good fault classifier should have the ability of correctly classifying the faults events type regardless its previous status i.e. correctly classifying the first detected fault or any following faults as well.

To test the proposed classifier algorithm's ability to deal with sequential fault scenarios, two examples of arbitrary fault scenarios involving two different faults are simulated. The analysed data belongs to faults produced experimentally using the single line case study.

Results for the first example are shown in Figure 5.10 which belong to a SLG(AG) fault followed by DLG(ABG) fault. The fault starts at 11 cycles after simulation start. Line A is shorted for 25 cycles; this is developed into ABG fault, starting at cycle 36.

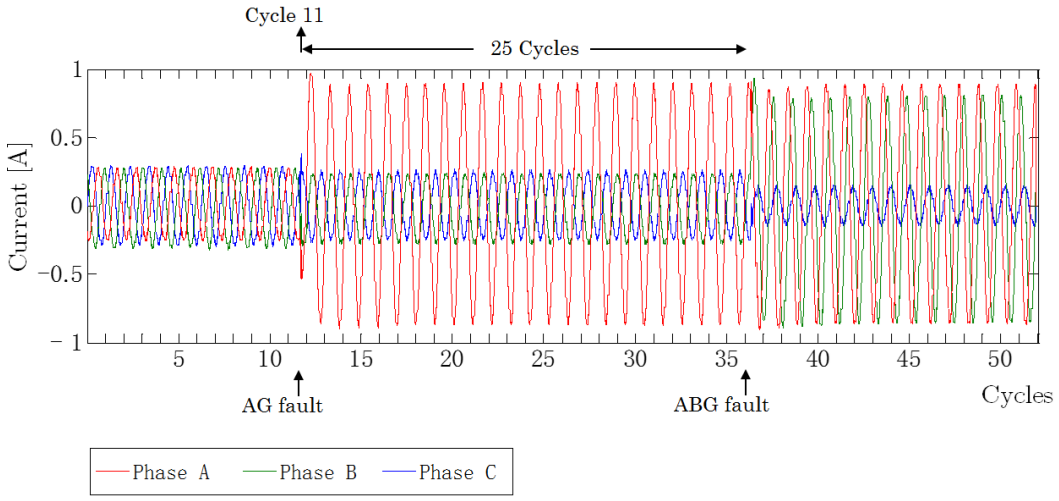

Figure 5.10: Multiple fault scenarios: AG followed by ABG

Figure 5.11 shows the H values from the analysis. For the first fault(AG fault), the H range starts at 357 for the first cycle of the fault (cycle 13) and then start decreasing slightly to reach the value 346 for the last cycle (cycle 34). For the second fault(ABG fault) the H maintains a value between 299 to 301 for all cycles of the fault. All these values show an agreement with ranges reported in Table 5.1, whether it is the first fault in a multiple scenario fault series or the second, the change in H value found to be indicating the occurring faults, regardless the previous status.

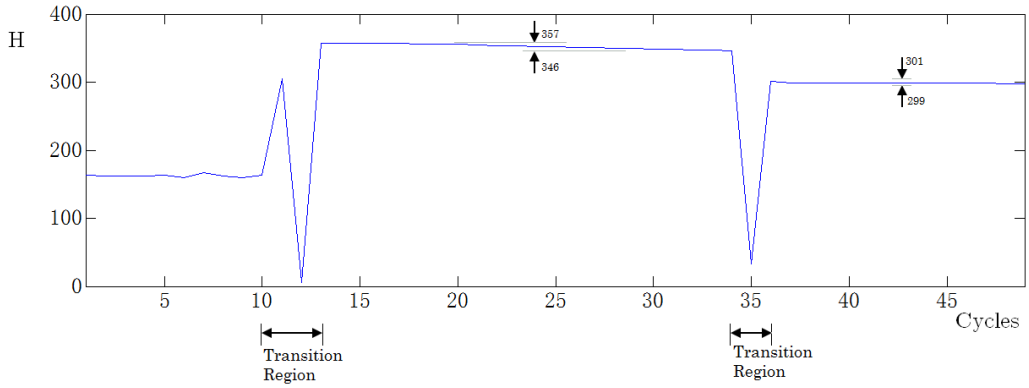

Figure 5.11: H parameter for multiple fault scenarios: AG followed by ABG

For a similar scenario but with different phases, line C is shorted for 27 cycles (Figure 5.12). The fault begins at cycle 9 of the simulation start. This is developed into BCG fault, starting at cycle 36. The fault is implemented on hardware.

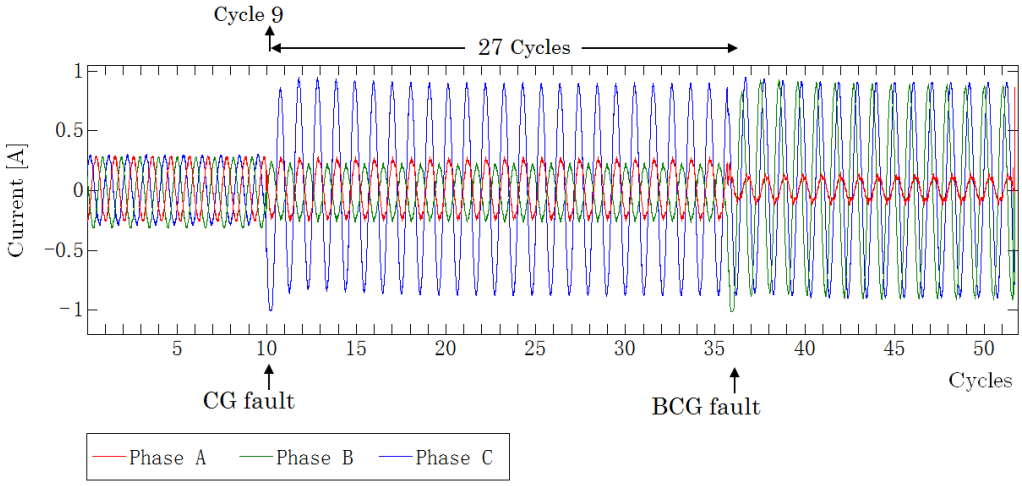

Figure 5.12: Multiple fault scenarios: CG followed by BCG

Figure 5.13 shows the values of the H parameter. For the first fault (CG fault), the H value for cycles of 12 to 33 was found to be between 91 to 136, for the second fault (BCG fault), the H maintains a value between 158 to 162 for all cycles of the fault. In both cases (the AG/ABG and the CG/BCG fault), there is a transient disturbance in H as the type of fault is changed. This disturbance lasts for approximately two cycles after the initiation of the new fault before settling to H value that indicate the occurring fault.

In both examples, the change in H value is found to be indicating the occurring faults, regardless the previous status, and the values shows an agreement with ranges reported in Table 5.1 and the proposed classifier algorithm was found able to deal with Sequential fault scenarios efficiently.

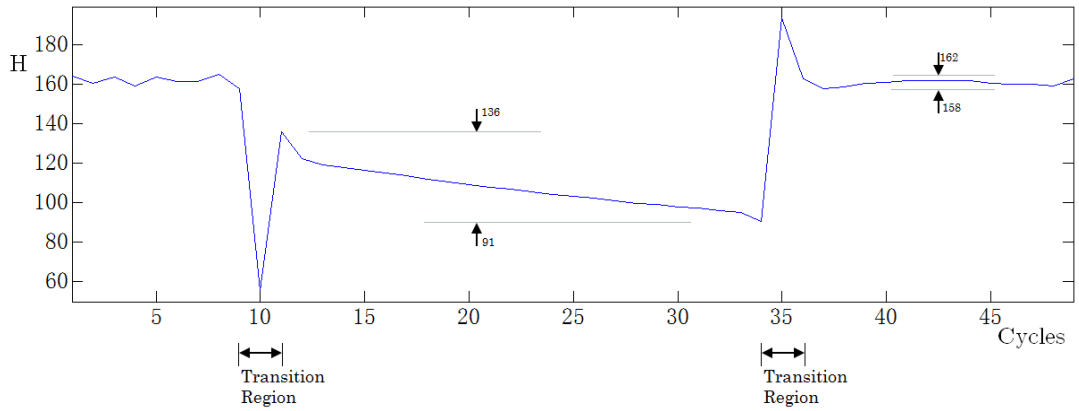

Figure 5.13: H parameter for multiple fault scenarios: CG followed by BCG

5.2.5 Different configurations

Classifier algorithms in both the basic form in Figure 5.1 and its modified version shown in Figure 5.7 are based on data included in Table 5.1 which is produced from analysing data generated by the two systems configurations already described in Sections 3.3 and 3.4.

As illustrated in Section 2.3, transmission line parameter values depend on environmental factors such as the surrounding temperature, etc. but the main factors are the line length, conductor material, line construction and the tower geometry. Most of these factors are fixed; thus the line parameters are not subject to frequent variation unless a planned reconfiguration is carried out on the line for example, when there is a need for increasing its power handling capacity or in case of replacing the line at the end of its life cycle which usually inferred from the increase in its failure rates.

For the purpose of testing the robustness of the classifier algorithm with different system characteristics, results are collected again from the Case (1) configuration but with different transmission line parameters this time.

The values of the power line parameters already used in the Case (1) simulation given in Table 3.1 are based on tower dimensions serving in a 735 kV network. New line parameters are generated if the tower geometry is changed. (L6) design is the largest tower design in normal use for 400 kV in UK grid [95]. Its dimensions are included in Appendix E [96]. The design dimensions are used to calculate new parameters which are shown in Table 5.2. In addition to the tower geometry, a new line length of 50 km is chosen instead of 100 km. The system voltage is also changed to 400 kV.

Table 5.2: New Line Parameters
For standard (L6) power tower design

Positive sequence resistance R1	0.00892 Ω/km
Zero sequence resistance R0	0.19161 Ω/km
Positive sequence inductance L1	4.1 $\times 10^{-4}$ H/km
Zero sequence inductance L0	2.852$\times 10^{-3}$ H/km
Positive sequence capacitance C1	2.783 $\times 10^{-8}$ F/km
Zero sequence capacitance C0	1.3$\times 10^{-8}$ F/km

The chromatic monitoring processing is applied to a new set of data generated by the modified parameter system for fault types under study. The H parameter values for selected fault examples are shown in Table 5.3. For comparison purpose, H parameter values calculated for the same fault set for original Case (1) are included as well. The examples shown are for faults located at 50% of the line length. Examining the values shows a high degree of robustness for the proposed classifier regardless system voltage, transmission line length or change in line parameters. The difference between H values for the same fault and two cases did not exceed 0.35 degree in its worst cases.

Table 5.3: H parameter value for different configurations/line parameters

Fault example	H value	
	Case 1 735 kV line	Modified Case 1 400 kV line (L6)
AG	31.87	33.88
BG	278	278
AB	315.29	315.39
BC	196.93	196.86
ABG	315.52	315.85
ACG	79.56	79.67

5.2.6 Sampling

The effect of sampling rate on the fault classifier results is also investigated. The fault classifier parameter values are recalculated using different sampling ratio of 3333, 555, 67 samples per cycle. The change in the H parameter value with different sampling rates is shown in Figures 5.14 and 5.15 for cases of a SLG(CG) fault and DLG(ABG) fault respectively.

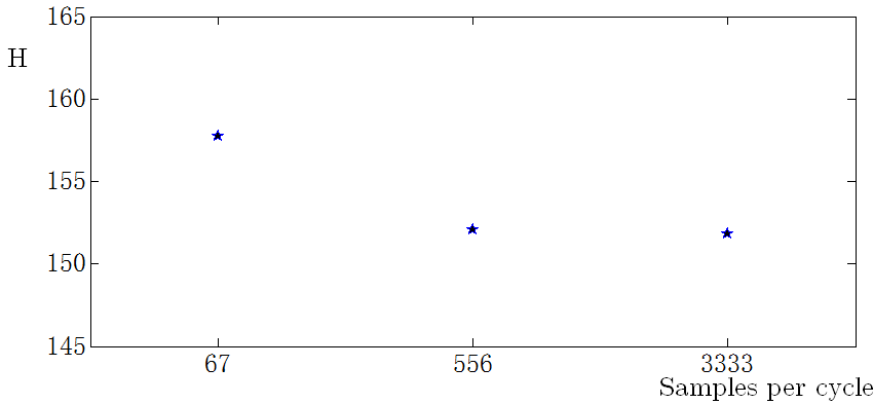

Figure 5.14: Change in the H parameter value with different sampling rates for a SLG(CG) fault

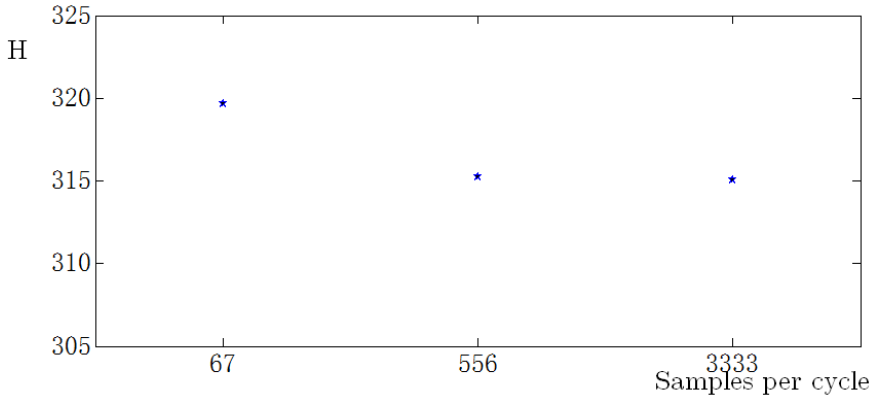

Figure 5.15: Change in the H parameter value with different sampling rates for a DLG(ABG) fault

The results show a small change in the H parameter value from the lowest sample rate compared to the other two. However, for the higher sample rate there is a negligible change in the H value. If an error of ±4 is acceptable, then the lower sample rate provides an adequate value for H.

5.3 Fault Locator procedure

The purpose of the locator algorithm is to enable a diagnostic tool that will give a reasonable estimation of the fault location regardless the surrounding parameter and conditions variation.

The process of the proposed locator procedure is summarized by the flowchart shown in Figure 5.16. This flowchart involves data preprocessing, primary processing and secondary chromatic processing stages.

The parameter L_{RS} represent the outcome of the secondary transformation process, the calculation of this parameter is already described and analysed in Chapter 4. Firstly, the proposed parameter eliminates the effect of fault resistance variation. Secondly, and most important, its value is linearly proportional to the location of the fault.

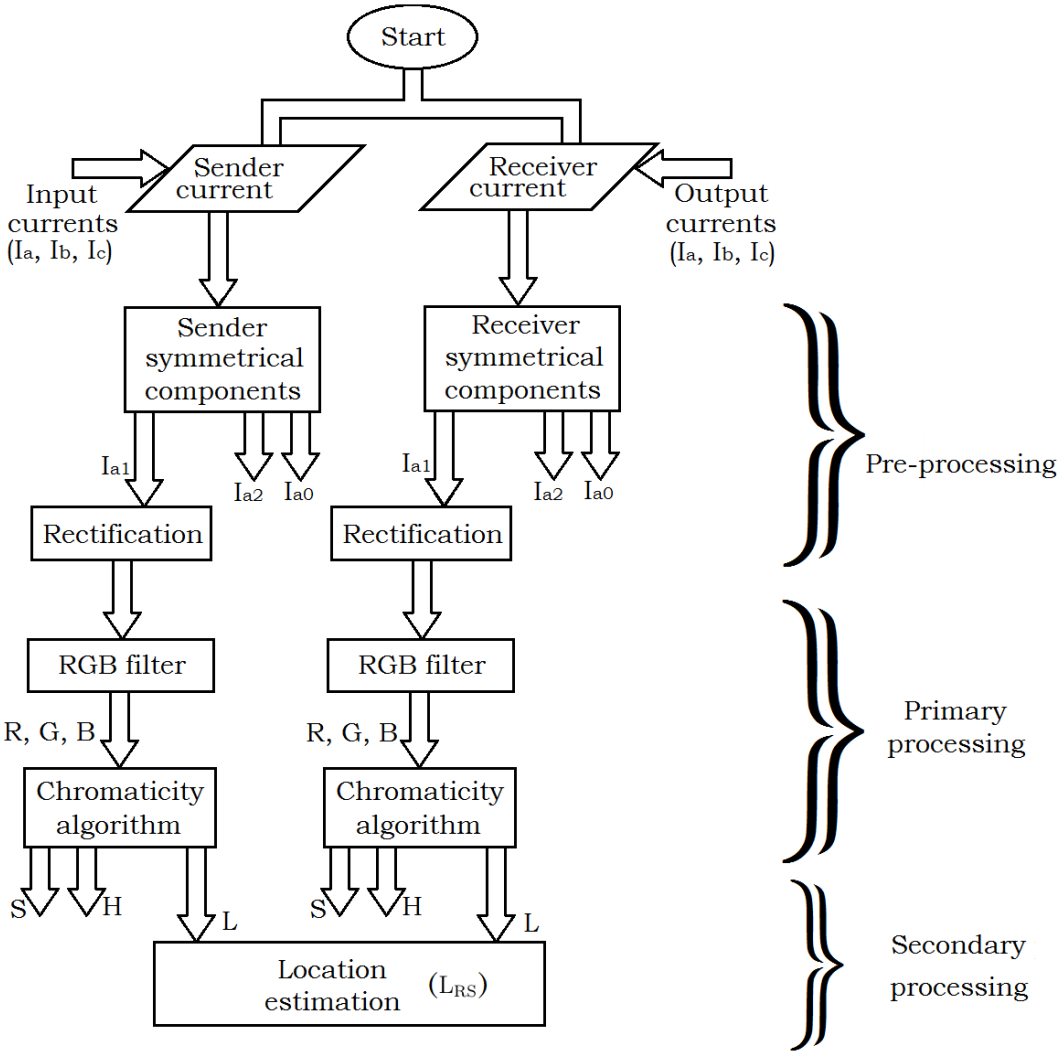

Figure 5.16: Locator flowchart

If we consider the outcome parameter L_{RS} to represent the calculated location, the accuracy of the estimates can be evaluated using the following expression:-

$$Estimated\,error\,percentage = \frac{Actual\,location - Estimated\,location}{line\,length} \times 100\% \tag{5.1}$$

Table 5.4 show the estimated error for the simulated faults at the start of the line (at 10% of the line length), in the middle (at 50% of the line length) and at the end of the line (at 90% of the line length). The faults are simulated with 0.001 Ohms. The error in the majority of cases is less than 1%, and the effect of fault location change is negligible.

Table 5.4: Estimated error percentage

Fault	Estimated error percentage (for faults occurred at 10% of line length)	Estimated error percentage (for faults occurred at 50% of line length)	Estimated error percentage (for faults occurred at 90% of line length)
AG	1.45	0.54	0.91
BG	3.35	1.23	0.26
CG	3.42	1.39	0.24
AB	0.36	0.31	0.55
ABG	0.06	0.62	0.67
BC	0.07	0.55	0.56
BCG	0.36	0.33	0.43
AC	0.21	0.32	0.59
ACG	0.10	0.54	0.67
ABC/ABCG	0.84	0.80	0.62

For most of the faults (LL, DLG, LLL/LLLG), a small error was produced. The average error value is 0.48% which did not exceed 0.84% in its worst cases. While a slightly higher error but acceptable are noted in cases of SLG faults. The average value of the error for this fault type is 1.42% with no greater than 3.4% in its worst case.

Among different fault types, the SLG faults usually receive special treatment in an attempt to estimate their location. It was noticed that unlike most fault types (LL, DLG, LLL/LLLG) which share same locator algorithms, approaches usually specify special algorithms to be assigned to this particular fault. For instance, in the impedance based methods [12], special calculation procedure are followed in their locator algorithms. In other approaches, the uniqueness of such fault are illustrated by using dedicated algorithms in the studies which focus only on this type of faults [97] [98] [99].

The reason for choosing a unique locator algorithm when dealing with SLG faults is due to its low fault current compared to other faults. And this causes a difficulty in achieving accurate estimations which appears clearly with high fault resistance where the fault current appear as a case of heavy loading on the system. A small increase in error values is also noticed when the fault is closer to the measuring point; this is due to higher transient component presence that affects the symmetrical components calculations [100].

In this research work, although a slightly higher error was found for SLG faults, the fault location estimation formula was applied equally to all cases regardless the fault type. This will help in minimising the locator algorithm requirements by avoiding the need for fault type information availability before the implementation of the locator algorithm.

If calculated for all of the types, the average value of the error with the described chromatic approach found to be (∼0.76%). This value is better than some conventional impedance calculations (∼2.6%) [98] [99], and some recent fuzzy logic based methods (> 4%) [73] [61], but more than travelling wave, wavelet and some artificial intelligence methods (0.16% –0.32%) [33] [53] [51] [62].

5.3.1 Effect of fault resistance

In Section 4.5.3.2, the effect of the different fault resistance on the L_{RS} is presented, Figures 4.21, 4.22, 4.23 and 4.24 present examples of four different types of faults that have been simulated at the same location but with different fault resistance. Table 5.5 show a summary of those results and percentage error.

Table 5.5: Summary of the locator results

Fault type	Fault resistance Ω	Actual location km	Calculated location km	Estimated error %
LG (BG)	0.001	50.00	50.56	0.56
	10	50.00	51.27	1.27
	200	50.00	51.89	1.89
DLG (ABG)	0.001	75.00	74.43	0.57
	10	75.00	74.61	0.39
	200	75.00	74.71	0.29
LL (AB)	0.001	75.00	74.51	0.49
	10	75.00	74.73	0.27
	200	75.00	74.87	0.13
LLLG (ABCG)	0.001	35.00	34.39	0.61
	10	35.00	34.57	0.43
	200	35.00	34.70	0.30

The simulations are repeated with 0.001, 100 and 200 Ohms fault resistance (Rf). The L_{RS} value reduces from unity at fault inception to a value that is indicative of the fractional location of the fault along the line length, and it remains at that value thereafter. This is the value used in Table 5.5.

The results summarised in Table 5.5, shows that the L_{RS} results for a SLG (BG) fault with different fault resistances indicate a percentage error of less than 2% in the worst case. In both the cases for DLG(ABG) and LL(AB), the estimated location results are in good agreement and independent of the fault resistance to within less than 1% error. The results of LLLG(ABCG) also yield an estimated error of less than 1%. Thus, overall the fault location results are accurate to within 1.9%.

Published literature indicates that some accurate algorithms will lose location estimation accuracy for some special conditions such as high resistance faults [18]. While results in Table 5.5 show the proposed chromatic based method immunity to high resistance faults for all types of faults. For the SLG fault case and as expected, a slight increase in the estimation error was noticed, and this value is not exceeding 1.9% in its worst case.

5.3.2 Effect of inception angle

The effect of changing the inception angle for the fault on the fault locator output has been investigated. The fault locator tool is tested considering variations in fault inception angle (0, 45, 90, 180 and 270 degrees). Changing the fault inception angle for the same fault can be achieved easily through simulation, so the following analysed data are from the simulation.

Figure 5.17 shows an example of a SLG(AG) fault at 50% of the line length and occurring with five different inception angle. The figure shows the effect of

this angle variation on the outcome of the locator algorithm. The result illustrates that the inception angle affects slightly the value during the first two cycles, but converges by cycle 6 to the same value. This means that the location of the fault can be estimated to a similar degree of accuracy as before and this gives the proposed method an advantage over some other methods such as the travelling wave where fault inception angle variation have an effect on the estimations [101].

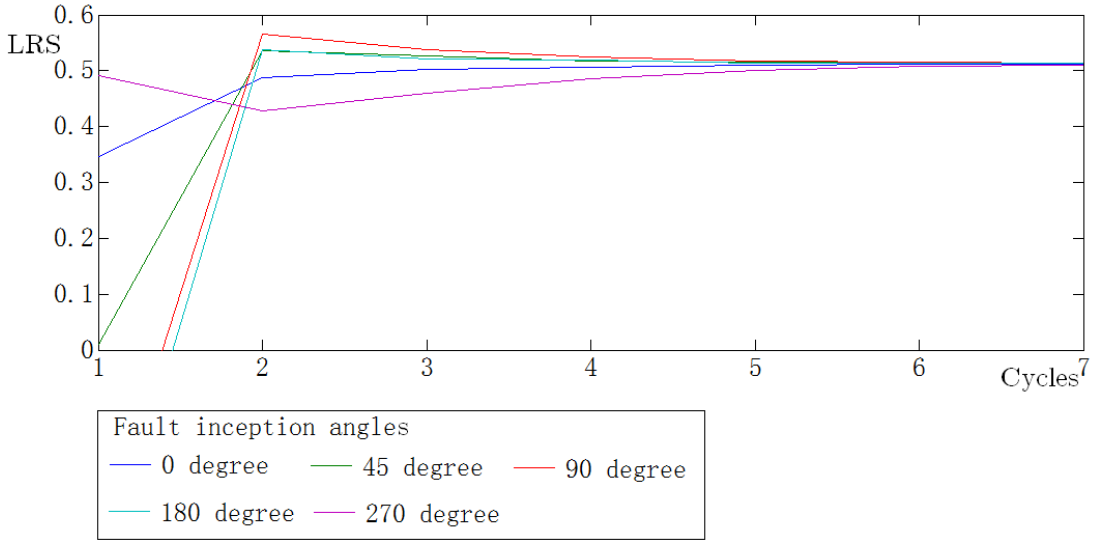

Figure 5.17: Effect of Inception angle on locator results of a SLG(AG) fault at 50% of the line length

5.3.3 Sequential fault scenarios

The complicated fault involving arbitrary faults sequence scenario is probable to occur in power systems. The efficient fault locator algorithm should be able to give an excellent estimation of the fault location, and this should not be affected by the sequential occurrence of further faults.

To test the locator algorithm's ability in dealing with sequential fault scenarios, two examples of arbitrary fault scenarios involving three different faults

are simulated. The locator algorithm is then implemented. The same scenario is repeated at two different locations. The following data are collected from the simulation of double transmission line case study.

The first scenario is shown in Figure 5.18. There are three cycles of non fault waveforms before a SLG(AG) fault is introduced for eight cycles and then a double line to ground fault(ABG) is initiated for another eight cycles followed by a three line to ground fault. The fault scenario is simulated halfway along the line.

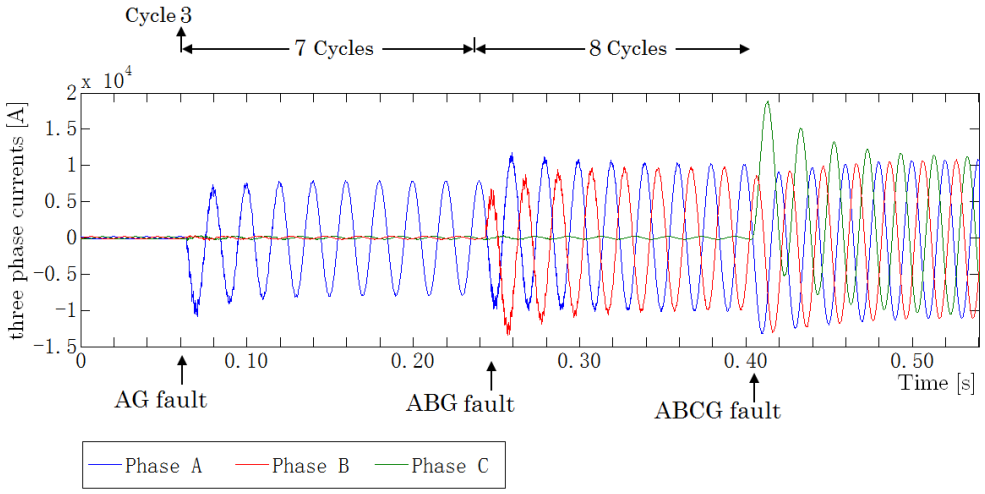

Figure 5.18: Multiple fault scenarios: AG, ABG, ABCG at 50%

Figure 5.19 shows the result of the L_{RS} parameter; the estimated location is calculated by the same equation as used before. Different types of the faults will produce a negligible effect on the estimated location. The error for the first fault was in the range of 1.2% which drops to a value of 0.2% for the second fault and 0.4% for the last one. These error values are similar to fault cases coming directly after healthy condition. This indicates that the location estimation error is not dependent on the previous status of the fault whether healthy condition or series of multiple faults.

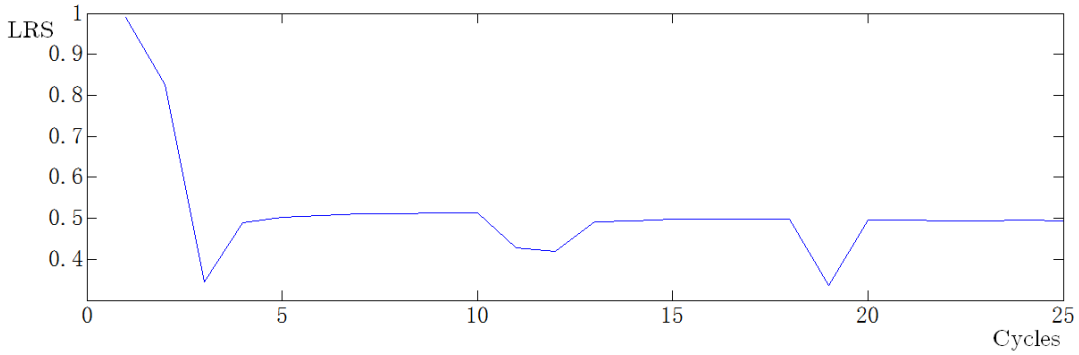

Figure 5.19: Multiple fault scenarios: AG, ABG, ABCG at 50%

Figure 5.20 shows the same faults, but at 30% of the line length. Figure 5.21 shows the result of the L_{RS} parameter. The error for the first fault, in this case, was in the range of 2.4% which drops to the value of 0.1% for the second fault and 0.5% for the last fault. There is no effect of the previous fault condition on the present fault location estimation. This is consistent with previous results.

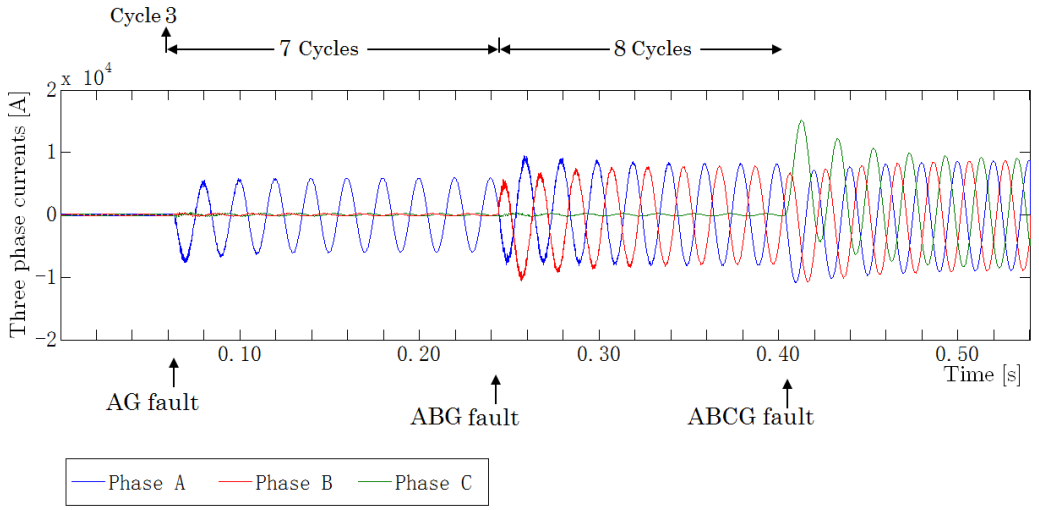

Figure 5.20: Multiple fault scenarios: AG, ABG, ABCG at 30%

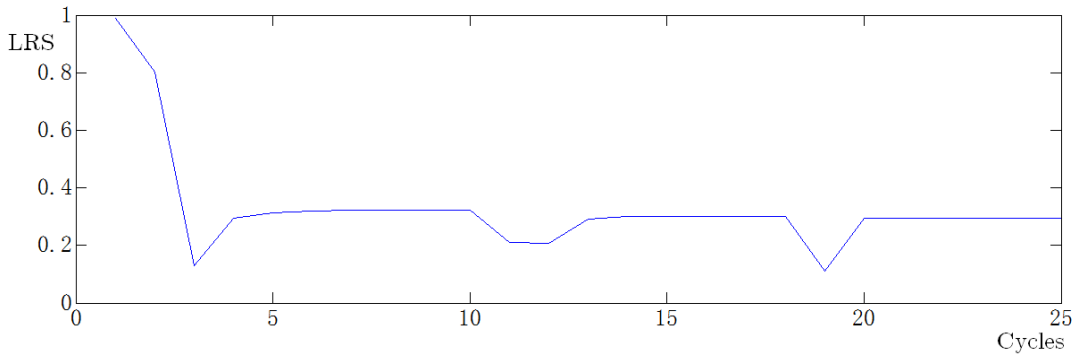

Figure 5.21: Multiple fault scenarios: AG, ABG, ABCG at 30%

In both cases, the estimated L_{RS} experience slight disturbance through the transition between two consecutive faults. The disturbance is damped within two cycles of the new fault occurrence and the L_{RS} value quickly settle down to the same accurate estimation.

In both examples, the proposed locator algorithm was found able to deal with Sequential fault scenarios efficiently. The fault location was estimated accurately regardless the fault type and/or its previous status i.e., if it is the first occurring fault or any fault among the simulated arbitrary sequential faults scenario.

5.3.4 Effect of different line parameter

Locator algorithm shown in Figure 5.16 are based on processing the L parameters for current waveforms from two terminals of Double circuit transmission line described in Section 3.3.

For the purpose of testing the locator algorithm robustness, results are collected again from Case (1) configuration, but with two new set of transmission line parameters. The new parameters are generated by changing the tower geometry and choosing a new length for the line as described in Section 5.2.5. Two standard UK tower designs are adopted in this section. Namely (L6) and (L12)

designs [95]. The two designs dimensions included in Appendix E [96] are used for calculations of new parameters.

Line parameters resulting from (L6) design are included Table 5.2. The (L12) design size is smaller than (L6) design which is reflected as a slight change in the calculated parameters as shown in Table 5.6. In addition to the tower geometry changes, a new line length of 50 km is chosen instead of 100 km. The system voltage is changed to 400 kV.

Table 5.6: New Line Parameters
For standard (L12) power tower design

Positive sequence resistance R1	0.00893 Ω/km
Zero sequence resistance R0	0.19349 Ω/km
Positive sequence inductance L1	4.067 $\times 10^{-4}$ H/km
Zero sequence inductance L0	2.889$\times 10^{-3}$ H/km
Positive sequence capacitance C1	2.830 $\times 10^{-8}$ F/km
Zero sequence capacitance C0	1.322$\times 10^{-8}$ F/km

The chromatic processing is applied to new sets of data generated by the modified parameter system for fault types under study. Table 5.7 shows the error percentage in location estimation for the double transmission line three different parameters sets.

Examples shown are for faults at different locations of the line length. Examining the values shows a high degree of robustness for the proposed locator regardless of variation in the transmission line parameters. In all cases, the error is acceptable regardless of the change in the system voltage, fault location or different line parameters.

Table 5.7: Error percentage in location estimation for different line parameters

Fault example	Fault location (% of the line length)	Estimation error percentage		
		Case 1	Modified Case 1 (L6 tower design)	Modified Case 1 (L12 tower design)
AG	90%	0.68 %	0.30 %	0.30 %
BG	90%	0.32 %	0.22 %	0.22 %
AB	50%	0.33 %	0.28 %	0.28 %
BC	50%	0.43 %	0.24 %	0.25 %
ABG	10%	0.06 %	0.28 %	0.31 %
ACG	10%	0.56 %	0.32 %	0.32 %

5.3.5 Sampling

The effect of different sampling rates on the Fault locator results is investigated. The fault locator error values are calculated using different sampling 3333, 555, 67 samples per cycle. Figure 5.22 shows the L_{RS} for cases of a SLG(CG) fault, DLG(ABG) fault and three phase to ground fault(ABCG) fault plotted for the three different sampling rates.

The simulated cases are for faults in the middle (at 50% of the line length). The results show a negligible change in the estimation error. For all cases, the effect due to using different sampling rates did not exceed a change of + 0.5% on the final estimation with the lowest sample rate. Being independent of the sampling rate within the range used, gives the proposed method an extra advantage over other methods such as the travelling wave where the high sampling rate form one of its major requirement [10] [102].

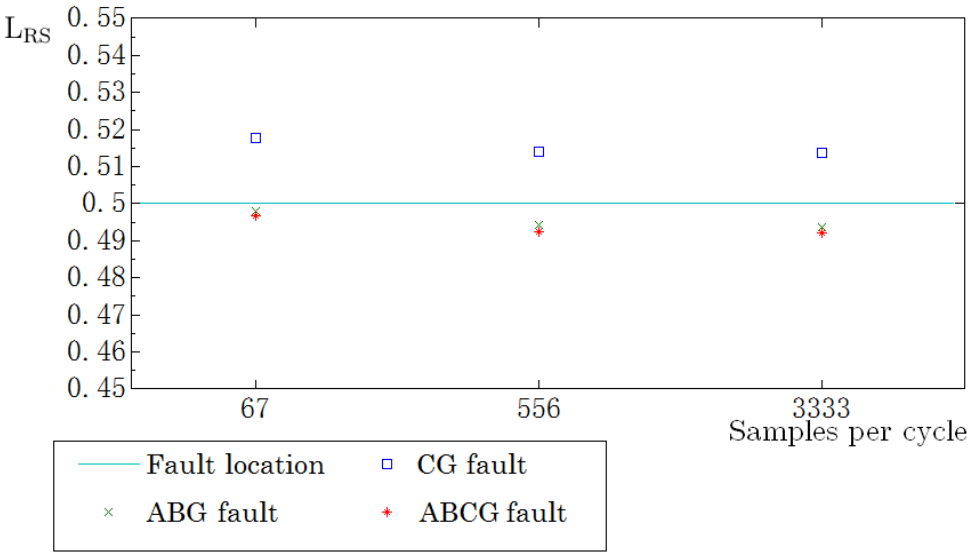

Figure 5.22: Change in the L_{RS} parameter value with different sampling rates for SLG(CG), DLG(ABG) and LLLG(ABCG) faults

5.4 Summary

In this chapter, further analyses, testing and discussions of the results are presented. The basic fault classifier idea is based on monitoring H parameter of the negative components. Preliminary testing results indicate misclassification due to high fault resistance values in addition to limitations in distinguishing ground faults from those ground free. In analyses chapter, the ground detection limitations were solved using information from the L parameter for the zero sequence component. In this chapter, a solution is suggested for the misclassification due to high fault resistance values. The solution was achieved using information from the L parameter for negative sequence component.

The classifier performance was also evaluated under different operating conditions such as variations of the fault inception angle, the possibility of multiple fault scenarios, different system configurations and low sampling of the waveforms.

The basic fault locator idea is based on monitoring L parameter of the positive components for waveforms collected from double circuit transmission line both terminals. Preliminary testing results indicate acceptable accuracy in estimating the fault location with immunity to high fault resistance or changes in the fault location.

The locator performance was also evaluated under different operating conditions such as variations of the fault inception angle, the possibility of multiple fault scenarios, different line parameters and low sampling of the waveforms.

Chapter 6

Conclusions and future work

The work presented in this thesis represents the first attempt in exploring the possibility of using the chromatic methodology to provide transmission line fault diagnostic. The outcome of this research can be involved in designing a standalone diagnostic tools or adding supporting functions to the existing relaying systems.

The successful diagnosis of the fault requires identifying its characteristics such as its type and estimating its location. The need for such information develops with the progress and expansion in the modern complex power system network sizes and services. A literature review was provided with the aim of categorising the current different diagnostic approaches and summarising their advantages, requirements and limitations encountered.

The high error in fault locations estimations and misclassification of their types in some methods leads researchers to propose new approaches; while the expensive requirement and complexity of other methods algorithms impacts their commercial implementations.

In this work, new diagnostic tool's algorithms based on the chromatic monitoring approach are proposed for transmission line fault location estimation and its type classification. The overall design theme considers combining the simplicity with acceptable accuracy and avoiding design complexity and the high implementation cost at the same time.

The locator method for locating various faults on a double transmission line is based on monitoring the positive sequence component of the current at both sender and receiver ends. The capability of the new method has been demonstrated by simulating numerous cases on a parallel transmission line. The results show that the method has high accuracy in determining the fault locations which are not affected by the value of the fault resistance nor the actual fault location.

The classifier method to distinguish between particular faults on different transmission line configurations is based basically on monitoring the negative sequence component of the current at a single end. The capability of the new method has also been demonstrated by simulating various cases.

The combination of processing signals with two chromatic parameters (L for rectified zero component and H for negative component) provides a high level of fault discrimination. This enables single line to ground faults to be distinguished from line to line faults and for different single line to ground faults to be distinguished from each other.

A limitation in the classifier ability was encountered with the high fault resistance and this was solved by another modification on the algorithm implemented by a combination of processing signals with two chromatic parameters (L for rectified negative component and H for negative component). The results of the modified classifier show that the method has high accuracy in determining the fault type and the discrimination is independent of fault resistance and location

along the line length.

Based on work presented in this thesis, further research and investigation is necessary and should be commenced in future and the following recommendations may help the further contributions in this area.

Starting with the chromatic parameters, few are used in the design of this work algorithms such as the H of the negative components and the L parameters of different components. The study and analyses of extra parameters such as the rest H and L parameters of the different components in addition to the S parameter might hold potential information regarding, for example, the nature of the fault and this could aid the diagnostic tools integrity.

Further investigation may also help in enhancing the tool's efficiency or providing design simplifications. Change could also be proposed to include analytical methods such as monitoring the frequency domain of the signals or selecting different filtering profiles, etc.

Studying the different diagnostic approaches developmental stages show that combining artificial intelligence methods with the conventional methods gives an enhancement to the overall accuracy which could also be suggested as a future work. Artificial intelligence methods are a potential candidate to be included in the system of chromatic monitoring, especially with the final modified version of the classifier algorithm.

Current proposed locator algorithm retains its applicability for the double line transmission line system; as a suggested future work, the algorithm needs modifications to include different network configurations. For instance, in underground cables, it is more difficult to classify the fault type and to find its location than those of overhead lines [103], so the implementation could include a chromatic based diagnostic tool for underground cables or lines contain sections of under-

ground cable. Tools might be suggested for aiding the protection of additional power system vital equipment such as transformers. Fault classifier might also be suggested for monitoring the fault signature in current and/or voltage waveforms for faulted induction machines.

Bibliography

[1] P. M. Anderson. *Analysis of faulted power systems [electronic book].* IEEE Press series on power engineering. Piscataway, NJ, 1995.

[2] A. Yadav and A. Swetapadma. Enhancing the performance of transmission line directional relaying, fault classification and fault location schemes using fuzzy inference system. *IET Generation, Transmission & Distribution*, 9(6):580–591, October 2014.

[3] D. M. Welton. *Transmission lines [electronic book] : theory, types and applications.* Electrical engineering developments. Hauppauge, N.Y. : Nova Science Publishers., 2011.

[4] G. R. Jones, A. G. Deakin, and J. W. Spencer. *Chromatic monitoring of complex conditions.* Series in sensors. Boca Raton ; CRC Press., 2008.

[5] *Transmission line reference book: 345kV and above.* Electric Power Research Institute, Palo Alto (Calif.)., 1987.

[6] M. R. Patel. *Introduction to Electrical Power and Power Electronics.* Boca Raton, FL : December 10, 2012 by CRC Press, 2012.

[7] J. J. Grainger and W. D. Stevenson. *Power system analysis.* McGraw-Hill series in electrical and computer engineering: Power and energy. New York: McGraw-Hill., 1994.

[8] R. Ciprian and B. Lehman. Modeling effects of relative humidity, moisture, and extreme environmental conditions on power electronic performance. In *2009 IEEE Energy Conversion Congress and Exposition, ECCE 2009*, pages 1052–1059, Diversified Technologies Inc., 2009.

[9] L. L. Grigsby. *The electric power engineering handbook.* The electrical engineering handbook series. Boca Raton, FL : CRC Press/IEEE Press., 2001.

[10] M. M. Saha, J. Izykowski, and E. Rosolowski. *Fault location on power networks [electronic book].* Power systems. London ; Springer., 2010.

[11] T. W. Stringfield, D. J. Marihart, and R. F. Stevens. Fault location methods for overhead lines. *Transactions of the American Institute of Electrical Engineers, Part III: Power Apparatus & Systems*, 76(3):518, 1957.

[12] IEEE. *IEEE Guide for Determining Fault Location on AC Transmission and Distribution Lines [electronic book].* Online access with subscription: IEEE IET Electronic Library. Standards. Piscataway : Institute of Electrical and Electronics Engineers., 2005.

[13] K. Zimmerman and D. Costello. Impedance based fault location experience. In *Papers Presented at the 50th Annual Conference - Rural Electric Power Conference, College Station, TX, USA*, pages C5–1–C5–16, Schweitzer Engineering Laboratories, Inc. USA, 2006.

[14] E. O. Schweitzer. A review of impedance-based fault locating experience. *Proceedings of the 15th Annual Western Protective Relay Conference*, 1988.

[15] T. Takagi, Y. Yamakoshi, J. Baba, K. Uemura, and T. Sakaguchi. A new alogorithm of an accurate fault location for EHV/UHV transmission lines: Part I - Fourier transformation method. *IEEE Transactions on Power Apparatus & Systems*, PAS-100(3):1316, 1981.

[16] T. Takagi, Y Yamakoshi, M. Yamaura, R. Kondow, and T. Matsushima. Development of a new type fault locator using the one-terminal voltage and current data. *IEEE Transactions on Power Apparatus & Systems*, PAS-101(8):2892, 1982.

[17] D. Novosel, D. G. Hart, E. Udren, and M. M. Saha. Fault location using digital relay data. *IEEE Computer Applications in Power*, (3):45, 1995.

[18] Q. Zhang, Y. Zhang, W. Song, and Y. Yu. Transmission line fault location for phase-to-earth fault using one-terminal data. *Generation, Transmission and Distribution, IEE Proceedings-*, 146(2):121–124, Mar 1999.

[19] A. T. Johns and S. Jamali. Accurate fault location technique for power transmission lines. *IEE Proceedings C: Generation Transmission and Distribution*, 137(6):395–402, 1990.

[20] H. Y. Li, E. P. Southern, P. A. Crossley, S. Potts, S. D. A. Pickering, B. R. J. Caunce, and G. C. Weller. A new type of differential feeder protection relay using the global positioning system for data synchronization. *IEEE Transactions on Power Delivery*, 12(3):1090–1097, 1997.

[21] A. A. Girgis, D. G. Hart, and W. L. Peterson. A new fault location technique for two- and three-terminal lines. *IEEE Transactions on Power Delivery*, 7(1):98–107, 1992.

[22] M. Kezunović, J. Mrkić, and B. Peruničić. An accurate fault location algorithm using synchronized sampling. *Electric Power Systems Research*, 29(3):161–169, 1994.

[23] M. Kezunović and B. Peruničić. Automated transmission line fault analysis using synchronized sampling at two ends. *Proceedings of Power Industry Computer Applications Conference*, page 407, 1995.

[24] D. Novosel, D. G. Hart, E. Udren, and J. Garitty. Unsynchronized two-terminal fault location estimation. *IEEE Transactions on Power Delivery*, 11(1):130–136, 1996.

[25] Y. Liao and S. Elangovan. Unsynchronised two-terminal transmission-line fault-location without using line parameters. *IEE Proceedings – Generation, Transmission & Distribution*, 153(6):639 – 643, 2006.

[26] C-S. Yu. An unsynchronized measurements correction method for two-terminal fault-location problems. *IEEE Transactions on Power Delivery*, 25(3):1325–1333, 2010.

[27] B. Datta and S. Chatterjee. A literature review on use of Bewley's lattice diagram. *2012 1st International Conference on Power & Energy in NERIST (ICPEN)*, page 1, 2012.

[28] E. O. Schweitzer, A. Guzman, M. V. Mynam, V. Skendzic, B. Kasztenny, and S. Marx. Locating faults by the traveling waves they launch. In *Pro-*

tective Relay Engineers, 2014 67th Annual Conference for, pages 95–110, March 2014.

[29] G. Krzysztof, R. Kowalik, D. Rasolomampionona, and S. Anwar. Traveling wave fault location in power transmission systems: An overview. *Journal of Electrical Systems*, 7(3):287 – 296, 2011.

[30] P. F. Gale and P. A. Crossley. Fault location based on travelling waves. *IEE Fifth international conference on Developments in Power System Protection, University of York UK*, pages 54–59, 1993.

[31] F. V. Lopes, D. Fernandes Jr., and W. L. A. Neves. Fault location on transmission lines based on travelling waves. *the International Conference on Power SystemsTransients (IPST2011), Delft, the Netherlands, June 14-17*, 2011.

[32] D. C. Robertson, O. I. Camps, J. S. Mayer, and W. B. Gish. Wavelets and electromagnetic power system transients. *Power Delivery, IEEE Transactions on*, 11(2):1050–1058, April 1996.

[33] A. Elhaffar. *Power Transmission line fault location based on current travelling waves.* Helsinki University of Technology : Thesis Ph.D., 2008.

[34] N. A. Sundaravaradan, D. Rajaraman, P.and Suzith, M. Dilip Kumar, G. Abilash, M. J. B. Reddy, and D. K. Mohanta. Wavelet based transmission line fault analysis: A literature survey. pages 254–259, Department of EEE, National Institute of Technology, 2014. 14th International Conference on Environment and Electrical Engineering, EEEIC 2014 - Conference Proceedings, Poland.

[35] C. H. Kim and R. Aggarwal. Wavelet transforms in power systems. I. general introduction to the wavelet transforms. *Power Engineering Journal*, 14(2):81–87, April 2000.

[36] M. Mirzaei, M. Z. A Ab Kadir, E. Moazami, and H. Hizam. Review of fault location methods for distribution power system. *Australian Journal of Basic & Applied Sciences*, 3(3):2670–2676, 2009.

[37] D. C. Park, O. Mohammed, M. A. El-Sharkawi, and R. J. Marks. An adaptively trainable neural network algorithm and its application to electric load forecasting. *Proceedings of the First International Forum on Applications of Neural Networks to Power Systems*, page 7, 1991.

[38] M. A. El-Sharkawi, S. Oh, R. J. Marks, M. J. Damborg, and C. M. Brace. Short term electric load forecasting using an adaptively trained layered perceptron. *Proceedings of the First International Forum on Applications of Neural Networks to Power Systems, Seattle, WA*, page 3, 1991.

[39] T. Saksornchai, Wei-Jen Lee, K. Methaprayoon, J. R. Liao, and R. J. Ross. Improve the unit commitment scheduling by using the neural-network-based short-term load forecasting. *Industry Applications, IEEE Transactions on*, 41(1):169–179, January 2005.

[40] A. K. Chandel, G. Guleria, and R. Chandel. Classification of power quality problems using wavelet based artificial neural network. In *Transmission and Distribution Conference and Exposition. IEEE/PES*, pages 1–5, April 2008.

[41] P. L. Mao and R. K. Aggarwal. A novel approach to the classification of the transient phenomena in power transformers using combined wavelet

transform and neural network. *Power Delivery, IEEE Transactions on*, 16(4):654–660, October 2001.

[42] O. A. S. Youssef. Discrimination between faults and magnetising inrush currents in transformers based on wavelet transforms. *Electric Power Systems Research*, 63:87 – 94, 2002.

[43] M. T. Haque and A. M. Kashtiban. Application of neural networks in power systems; a review. *World Academy of Science, Engineering and Technology, International Journal of Electrical, Computer, Electronics and Communication Engineering.*, 1(6):885–889, 2007.

[44] M. Krawczak. *Multilayer neural networks [electronic book] : a generalized net perspective.* Studies in computational intelligence: 478. Cham : Springer., 2013.

[45] V. Malathi and N. S. Marimuthu. Wavelet transform and support vector machine approach for fault location in power transmission line. *International Journal of Electrical and Electronics Engineering*, 39:666–671, 2010.

[46] A. J. Ghanizadeh and G. B. Gharehpetian. ANN and cross-correlation based features for discrimination between electrical and mechanical defects and their localization in transformer winding. *Dielectrics and Electrical Insulation, IEEE Transactions on*, 21(5):2374–2382, October 2014.

[47] M. R. Zaman and M. A. Rahman. Experimental testing of the artificial neural network based protection of power transformers. *Power Delivery, IEEE Transactions on*, 13(2):510–517, April 1998.

[48] A. I. Megahed and O. P. Malik. An artificial neural network based digital differential protection scheme for synchronous generator stator winding

protection. *Power Delivery, IEEE Transactions on*, 14(1):86–93, January 1999.

[49] N. Yadaiah and N. Ravi. A new protection algorithm for synchronous generators using artificial neural networks. In *Hybrid Intelligent Systems (HIS), 2011 11th International Conference on*, pages 625–629, December 2011.

[50] E. A. Mohamed and N. D. Rao. Artificial neural network based fault diagnostic system for electric power distribution feeders. *Electric Power Systems Research*, 35(1):1–10, 1995.

[51] T. Bouthiba. Fault location in EHV transmission lines using artificial neural networks. *Int. J. Appl. Math. Comput. Sci.*, 14(1):69–78, 2004.

[52] S. Osowski and R. Salat. Fault location in transmission line using hybrid neural network. *COMPEL - The International Journal for Computation and Mathematics in Electrical and Electronic Engineering*, 21(1):18–30, 2002.

[53] S. Soleymani, M. Bastam, and B. Mozafari. Fault diagnosis of transmission system based on wavelet transform and neural network. *Journal of Intelligent & Fuzzy Systems*, 25(2):271 – 277, 2013.

[54] A. G. Shaik and R. R. V. Pulipaka. A new wavelet based fault detection, classification and location in transmission lines. *International Journal of Electrical Power and Energy Systems*, 64:35–40, 2015.

[55] R. K. Aggarwal, S. L. Blond, P. Beaumont, G. Baber, F. Kawano, and S. Miura. High frequency fault location method for transmission lines based

on artificial neural network and genetic algorithm using current signals only. In *IET Conference Publications*, volume 2012, University of Bath, 2012.

[56] G. K. Purushothama, A. U. Narendranath, D. Thukaram, and K. Parthasarathy. Ann applications in fault locators. *International Journal of Electrical Power and Energy Systems*, 23:491 – 506, 2001.

[57] H. Singh, M. M. Gupta, T. Meitzler, H. Zeng-Guang, G. Kum Kum, A. M. G. Solo, and L. A. Zadeh. Real-life applications of fuzzy logic. *Advances in Fuzzy Systems*, pages 1 – 3, 2013.

[58] K. Michels. *Fuzzy control [electronic book] : fundamentals, stability and design of fuzzy controllers.* Studies in fuzziness and soft computing: 200. Berlin : Springer., 2006.

[59] R. A. Aliev. *Fundamentals of the fuzzy logic-based generalized theory of decisions [electronic book].* Studies in fuzziness and soft computing: 293. Berlin ; Springer., 2013.

[60] C. Pothisarn and A. Ngaopitakkul. Wavelet transform and fuzzy logic algorithm for fault location on double circuit transmission line. *16th International Conference on Electrical Engineering (ICEE), Busan, Korea, July 11-14,*, 2010.

[61] M. J. Reddy and D.K. Mohanta. A wavelet-fuzzy combined approach for classification and location of transmission line faults. *International Journal of Electrical Power and Energy Systems*, 29:669 – 678, 2007.

[62] M. G. Davoudi, J. Sadeh, and E. Kamyab. Time domain fault location on transmission lines using genetic algorithm. In *Environment and Electrical*

Engineering (EEEIC), 2012 11th International Conference on, pages 1087–1092, May 2012.

[63] M. J. Reddy and D. K. Mohanta. Adaptive-neuro-fuzzy inference system approach for transmission line fault classification and location incorporating effects of power swings. *IET Generation, Transmission & Distribution*, 2(2):235 – 244, 2008.

[64] S. Chakraborty, S. Singh, A. Bhalla, P. Saxena, and R. Padarla. Wavelet transform based fault detection and classification in transmission line. *International Journal of Research in Engineering & Applied Sciences*, 2:67–74, 2012.

[65] O. A. S. Youssef. Fault classification based on wavelet transforms. In *Transmission and Distribution Conference and Exposition, 2001 IEEE/PES*, volume 1, pages 531–536 vol.1, 2001.

[66] W. M. Lin, C. D. Yang, J. H. Lin, and M. T. Tsay. A fault classification method by RBF neural network with OLS learning procedure. *IEEE Transactions on Power Delivery*, 16(4):473–477, 2001.

[67] K. Gayathri and N. Kumarappan. Comparative study of fault identification and classification on EHV lines using discrete wavelet transform and fourier transform based ANN. *World Academy of Science, Engineering and Technology, International Science Index, International Scholarly and Scientific Research & Innovation*, 2(5):529–538, 2008.

[68] D. M. Jwad and P. W. Lefley. Evaluation studies of combined wavelet and neural network applications in high voltage transmission line protection. In

Developments in Power System Protection (DPSP 2014), 12th IET International Conference on, pages 1–5, March 2014.

[69] A. Ferrero, S. Sangiovanni, and E. Zappitelli. A fuzzy-set approach to fault-type identification in digital relaying. In *Transmission and Distribution Conference, 1994., Proceedings of the 1994 IEEE Power Engineering Society*, pages 269–275, April 1994.

[70] O. A. S. Youssef. Combined fuzzy-logic wavelet-based fault classification technique for power system relaying. *Power Delivery, IEEE Transactions on*, 19(2):582–589, April 2004.

[71] A. K. Pradhan, A. Routray, S. Pati, and D. K. Pradhan. Wavelet fuzzy combined approach for fault classification of a series-compensated transmission line. *Power Delivery, IEEE Transactions on*, 19(4):1612–1618, October 2004.

[72] F. Chunju, K.K. Li, W.L. Chan, Y. Weiyong, and Z. Zhaoning. Application of wavelet fuzzy neural network in locating single line to ground fault (SLG) in distribution lines. *Electrical Power and Energy Systems*, 29:497–503, 2007.

[73] P. K. Dash, A. K. Pradhan, and G. Panda. A novel fuzzy neural network based distance relaying scheme. *Power Delivery, IEEE Transactions on*, 15(3):902–907, July 2000.

[74] S. Vasilic and M. Kezunovic. Fuzzy ART neural network algorithm for classifying the power system faults. *Power Delivery, IEEE Transactions on*, 20(2):1306–1314, April 2005.

[75] N. Zhang and M. Kexunovic. Coordinating fuzzy ART neural networks to improve transmission line fault detection and classification. In *Power Engineering Society General Meeting, 2005. IEEE*, pages 734–740 Vol. 1, June 2005.

[76] P. Kumar, M. Jamil, M. S. Thomas, and Moinuddin. Fuzzy approach to fault classification for transmission line protection. In *TENCON 99. Proceedings of the IEEE Region 10 Conference*, volume 2, pages 1046–1050 vol.2, December 1999.

[77] Z. He, S. Lin, Y. J. Deng, X. P. Li, and Q. Q. Qian. A rough membership neural network approach for fault classification in transmission lines. *International Journal of Electrical Power and Energy Systems*, 61:429 – 439, 2014.

[78] J. W. Spencer, A. Deakin, and G. R. Jones. Monitoring of complex systems. *2008 17th International Conference on Gas Discharges & Their Applications, Cardiff, UK*, page 41, 2008.

[79] F. Ankel-Simons. *Primate anatomy [electronic book] : an introduction.* Online access with subscription: Ebrary. San Diego, CA : Elsevier Academic Press., 2007.

[80] G. R. Jones, J. W. Spencer, L. M. Shpanin, and A. G. Deakin. A chromatic analysis of current interrupters. In *Gas Discharges and Their Applications, 2008. GD 2008. 17th International Conference on*, pages 153–156, September 2008.

[81] M. K. Agoston. *Computer Graphics and Geometric Modeling : Implementation and Algorithms.* London : Springer-Verlag., 2005.

[82] H. R. Kang. *Computational color technology. [electronic book].* SPIE Press monograph: PM159. Bellingham : SPIE., 2006.

[83] P. C. Russell, I. Khandaker, E. Glavas, D. Alston, R. V. Smith, and G. R. Jones. Chromatic monitoring for the processing of materials with plasmas. *Science, Measurement and Technology, IEE Proceedings* -, 141(2):99–104, March 1994.

[84] A. G. Deakin, G. R. Jones, J. W. Spencer, E. J. Bongard, M. Gal, A. T. Sufian, and C. C. Butler. A portable system for identifying urinary tract infection in primary care using a PC-based chromatic technique. *Physiological Measurement*, 35(5):793 – 805, 2014.

[85] E. Elzagzoug, G. R. Jones, A. G. Deakin, and J. W. Spencer. Condition monitoring of high voltage transformer oils using optical chromaticity. *Measurement Science & Technology*, 25(6):1, 2014.

[86] A. G. Deakin, D. H. Smith, J. W. Spencer, D. Jones, and N. Johnson. Chromatic acoustic condition monitoring of transformers. *Sensor Review*, 34(3):291 – 296, 2014.

[87] Mohamed Ragaa. *Monitoring partial discharge signals using a chromatic approach.* Liverpool : Thesis Ph.D.., 2012.

[88] J. Zhang, G. R. Jones, J. W. Spencer, P. Jarman, I. J. Kemp, Z. Wang, P. L. Lewin, and R. K. Aggarwal. Chromatic classification of RF signals produced by electrical discharges in HV transformers. *Generation, Transmission and Distribution, IEE Proceedings*-, 152(5):629–634, September 2005.

[89] A. G. Deakin, J. W. Spencer, D. H. Smith, D. Jones, N. Johnson, and G. R. Jones. Chromatic optoacoustic monitoring of transformers and their

onload tap changers. *IEEE Transactions on Power Delivery*, 29(1):207 – 214, 2014.

[90] M. M. Yaacob and M. Abdulrazzaq Alsaedi. Review of partial discharge signal monitoring in power transformer using chromatic approach. *Jurnal Teknologi (Sciences and Engineering)*, 64(4):9–11, 2013.

[91] R. J. Marceau, A-R. Sana, and D. T. McGillis. *Asymmetric Operation of AC Power Transmission Systems: The Key to Optimizing Power System Reliability and Economics.* Presses inter Polytechnique, 2006.

[92] J. Beiza, S. H. Hosseinian, and B. Vahidi. Fault type estimation in power systems. *Iranian Journal of Electrical & Electronic Engineering*, 5(3):185–195, 2009.

[93] A. A. Hajjar and M. M. Mansour. Fault location for six-phase transmission lines based on the wavelet transform of the fault induced high frequency transients. In *Universities Power Engineering Conference, 2007. UPEC 2007. 42nd International*, pages 252–256, September 2007.

[94] D. Jalali and N. Moslemi. Fault location for radial distribution systems using fault generated high-frequency transients and wavelet analysis. In *Electricity Distribution, 2005. CIRED 2005. 18th International Conference and Exhibition on*, pages 1–4, June 2005.

[95] Nationalgrid.com. Development near overhead lines. Electronic Booklet. http://www2.nationalgrid.com/uk/services/land-and-development/planning-authority/development-near-ohl/. National Grid. Utility company., 2008.

[96] EMFs.info. National Grid, utility company. Geometries of power lines, http://www.emfs.info/sources/overhead/ohl-calculating/geometries/, accessed 13 february 2015,.

[97] S. Hong-chun and X. Bai. A novel fault line selection algorithm of single-phase ground faults in ungrounded neutral system using wavelets transform. In *Power System Technology, 2002. Proceedings. PowerCon 2002. International Conference on*, volume 4, pages 2532–2536 vol.4, 2002.

[98] W.-H. Zhang, U. Rosadi, M.-S. Choi, S.-J. Lee, and I. Lim. A robust fault location algorithm for single line-to-ground fault in double-circuit transmission systems vol. 6, no. 1,. In *Journal of Electrical Engineering & Technology*, volume 6, pages 1–7, 2011.

[99] M.H. Idris, M.W. Mustafa, and Y. Yatim. Effective two-terminal single line to ground fault location algorithm. In *Power Engineering and Optimization Conference (PEDCO) Melaka, Malaysia, 2012 Ieee International*, pages 246–251, June 2012.

[100] A. G. Phadke, M. Ibrahim, and T. Hlibka. Fundamental basis for distance relaying with symmetrical components. *Power Apparatus and Systems, IEEE Transactions on*, 96(2):635–646, Mar 1977.

[101] M. AbdelSalam, A. Ahmed, and W. Ahmed. Wavelet based analysis for transmission line fault location. *Innovative Systems Design and Engineering*, 4(14):145–156, 2013.

[102] P. Warlyani, A. Jain, A.S. Thoke, and R.N. Patel. Fault classification and faulty section identification in teed transmission circuits using ANN.

International Journal of Computer and Electrical Engineering, 3(6):807–811, December 2011.

[103] M. Pirouti. Neural-network-based fault location estimator for short medium voltage underground cable. *International Journal of Electrical and Power Engineering*, 2(5):340–344, 2008.

[104] C.L. Fortescue. Method of symmetrical co-ordinates applied to the solution of polyphase networks. *American Institute of Electrical Engineers, Proceedings of the*, 37(6):629–716, June 1918.

Appendix A

List of conference papers

Two conference papers are based on work presented in this thesis:-

- Conference paper(1). Page 197.

  Fault Locator for a Parallel Transmission Line Using Chromatic Processing. Z. S. D. Almajali, J.W. Spencer, and G.R. Jones

  The 8th Jordanian International Electrical and Electronics Engineering Conference, (JIEEEC 2013). Amman, Jordan. 16-18 April 2013.

- Conference paper(2). Page 203.

  Asymmetrical Fault Classifier for a Parallel Transmission Line Using Chromatic Processing. Z. S. D. Almajali, J.W. Spencer, and G.R. Jones

  The 7th IET international conference on power electronics, machines and drives (PEMD 2014). Manchester, UK. 8 - 10 April 2014.

Fault Locator for a Parallel Transmission Line Using Chromatic Processing

Ziyad S. D. Almajali
Department of Electrical Engineering
University of Liverpool
Liverpool, UK
almajali@liv.ac.uk

Joseph W. Spencer
Department of Electrical Engineering
University of Liverpool
Liverpool, UK
joe@liv.ac.uk

Gordon R. Jones
Department of Electrical Engineering
University of Liverpool
Liverpool, UK
grjones@liv.ac.uk

***Abstract*—A novel approach for fault location estimation on a double transmission line is described in this paper. A two terminal method is based on applying the chromatic monitoring methodology on the positive sequence component of the three phase currents of both sender and receiver ends. Fault scenarios at different locations, with various fault resistance are simulated using MATLAB software and its associated Simulink and Simpowersystem toolboxes. Three non-orthogonal detectors outputs are transformed into chromatic parameters Hue, Lightness and Saturation and the Lightness is utilized for providing a fault location estimation tool.**

***Keywords*— symmetrical component; double transmission line; fault locater; chromatic monitoring; double terminal method**

I. INTRODUCTION

Enhancing the overall power system performance and the quality of supply plus reducing outage times are all essential features to be incorporated in a protection system. An accurate fault locator can assist in the control of the system and enable faulty parts of the system to be efficiently located and isolated for correcting the system and restoring it to its previous healthy condition.

Various faults can occur in the process of power transmission, and the complex conditions that accompany the fault can increase the difficulty of correct detection, classification and accurately locating the fault.

The fault conditions could threaten the stability and the reliability of the power system, therefore there is a need for a scheme of protection that can analyze the available complex waveforms and extract the useful information from them.

Various kinds of relaying schemes exist, some using fuzzy systems, or neural networks approaches. Others employ the wavelet transform [14], use time-frequency analysis [13] or a combination of the several methods [8][1]. Many techniques have been used and good results achieved. Although there is active research in this subject, a literature review has shown no known approach that is based upon the methodology of chromatic monitoring.

This paper explores the possibility of using an approach based upon Chromatic monitoring techniques, which is derived from color science and the photic fields concepts [11]. It has already been applied for monitoring systems with complex conditions, and useful results have been obtained [7].

The modern Power system and its faults with their accompanying system interactions is an example of complex system conditions. Extending the application of chromaticity to the domain of power system waveforms monitoring, might provide tools which could aid in the design process of a reliable and high speed protection scheme, or further improvement of existing protection functions. To preserve clarity, this paper considers only one specific chromatic parameter for a fault locator, namely Lightness, Other parameters (saturation, dominant factor) and their benefits will be reported in subsequent papers.

II. SIMULATION STUDY

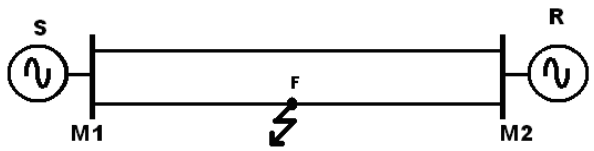

Fig. 1. Transmission Line Model

A 735 kV, 60 Hz parallel 200 Km transmission line is considered using simulation with MATLAB® software and its associated Simulink® and Simpowersystem® toolboxes. A schematic diagram is given of such a line on Fig. 1 which shows a fault (F) located between the sending (S) and receiving (R) ends of such a line with data collecting points at M1 and M2.

The line models used are distributed parameter lines, and simulations of various types of short circuit faults have been performed. Various cases have been considered by varying the fault resistance and with faults occurring at different positions along the transmission line. Fault signals are collected for an Alternating Current cycle of 60 Hz. These signals are captured in discrete form and data obtained for all three phases of the power transmission with different types of faults. The values of

the power line parameters used in the simulation are given on Table I.

TABLE I. LINE PARAMETER

Positive sequence resistance R1, Ω/KM	0.01165
Zero sequence resistance R0, Ω/KM	0.2676
Positive sequence inductance L1, H/KM	0.8679e-3
Zero sequence inductance L0, H/KM	3.008e-3
Positive sequence capacitance C1, F/KM	13.41e-9
Zero sequence capacitance C0, F/KM	8.57e-9

For the purpose of the algorithm testing, various types of faults were simulated which included the following conditions.

- Fault location: 5%, 10%, 15%, …, 90%, 95% of the distance.
- Fault types: AG, BG, CG, AB, BC, AC, ABG, BCG, ACG, ABC, ABCG.
- Fault resistance: 0.001, 100 and 200 ohm.

III. METHOD DESCRIPTION

A. Overall Procedure

The procedures used in the simulation are summarized on the flow chart of Fig. 2. The currents from the three phases (I_a, I_b, and I_c) at the power source (S) and the power receiving (R) ends are obtained and treated identically. Two pre-conditioning steps are taken, the first of which is the calculation of the symmetrical component of the current waveforms [2]. This is to reduce computational demands if current waveforms from each of the three phases were used. Instead the monitoring is performed on the positive symmetrical component only of one of the three phases. The second preconditioning step is to rectify this signal. The output waveform from these two steps is then processed cycle–by–cycle using three chromatic processors (R, G, B) to yield waveform identifying chromatic parameters (H, L, S). The chromatic parameter L from the power source end (L_{M1}) and the power receiving end (L_{M2}) are then used to form a secondary chromatic parameter L_{RS} which provides the required fault location indicator. Details of these various steps are given below.

B. Symmetrical Components

The symmetrical components concept leads to the set of the three-phase currents (I_a, I_b, I_c) being expressed as the positive, negative and zero sequence components denoted by I_{a_1}, I_{a_2} and I_{a_0} respectively according to equations (1).[10]

$$I_{a_1} = \frac{1}{3}[I_a + \alpha I_b + \alpha^2 I_c]$$
$$I_{a_2} = \frac{1}{3}[I_a + \alpha^2 I_b + \alpha I_c]$$
$$I_{a_0} = \frac{1}{3}[I_a + I_b + I_c] \quad (1)$$

Where α is a unit vector at an angle of 120 degrees. $\alpha = 1\angle 120^o$ and $\alpha^2 = 1\angle 240^o$.

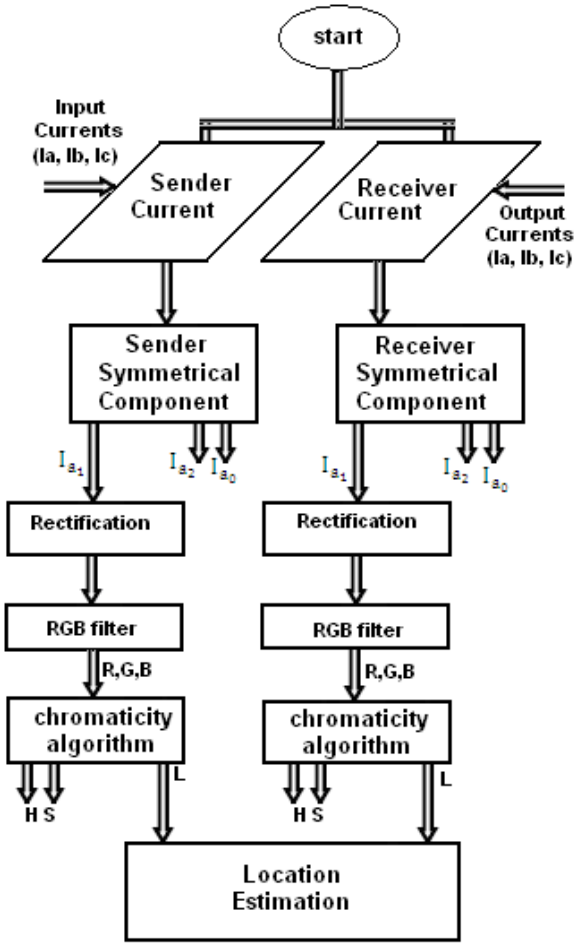

Fig. 2. Flow chart for the proposed method

C. Chromatic Processing

Chromatic processing of the rectified current waveforms is performed by applying three non-orthogonal processors R, G and B [7] to each full cycle of the waveforms in the time domain. The selected form for the RGB processors profiles for this purpose was Triangular with overlaps at half heights. Fig. 3 shows an example of the RGB processors superimposed upon

one complete cycle of the rectified positive sequence component of the current.

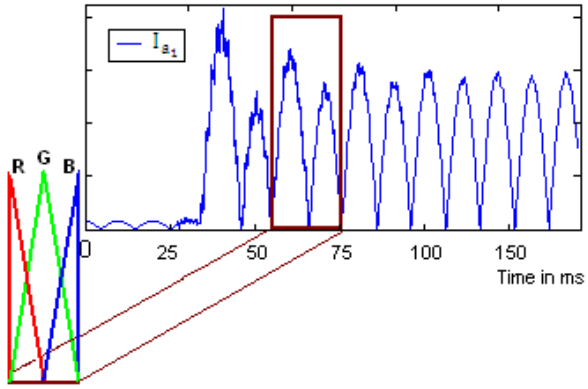

Fig. 3. Application of RGB processors on a the rectified positive sequence component of the current

The outputs from the three R, G, and B processors were then transformed into H, L, S chromatic parameters with the algorithms given in equations (2) [7]

$$\begin{aligned} H &= 240 - 120.\ g/(g+b) && r = 0 \\ &= 360 - 120.\ b/(b+r) && g = 0 \\ &= 120 - 120.\ r/(r+g) && b = 0 \end{aligned}$$

Where

$$\begin{aligned} r &= R - MIN(R, G, B) \\ g &= G - MIN(R, G, B) \\ b &= B - MIN(R, G, B) \end{aligned}$$

$$L = (R + G + B)/3$$

$$S = \frac{[\,MAX(R, G, B) - MIN(R, G, B)\,]}{[\,MAX(R, G, B) + MIN(R, G, B)\,]} \qquad (2)$$

The process is performed for waveforms at both ends, S and R (Fig. 1.), of the transmission line. To estimate the location of a fault, the L chromatic parameters for the source and receiving ends (L_{M1}, L_{M2}) are used to yield a parameter L_{RS} defined by

$$L_{RS} = (L_{M2} - L_{M1}) / (L_{M2} + L_{M1}) \qquad (3)$$

This represents a differential strength parameter ($L_{M2} - L_{M1}$) normalized with respect to the sum of the sending and receiving strengths ($L_{M2} + L_{M1}$) for a single waveform cycle. As such it may be regarded as a secondary, distimulus saturation parameter S (3). It can be evaluated for sequential cycles to provide indications of the time evolution of the fault induced chromatic signal strength. The accuracy of the estimates can be evaluated using the following expression.

$$\text{Estimated error percentage} = \left[\frac{\text{Actual location} - \text{Calculated location}}{\text{line length}}\right] X\ 100 \qquad (4)$$

IV. RESULTS

Figures 4, 5, 6, 7 present results for examples of different fault conditions with various operating modes, and TABLE II show a summary of those results and percentage error according to (4).

Fig. 4(a) shows the waveforms for the receiver end, three phase currents due to a Line-Ground (BG) fault at 50% of the line length. Fig. 4(b) is a plot of the calculated positive sequence component, the simulation is repeated with 0.001,100 and 200 ohms fault resistance (Rf), Fig. 4(c) shows the variation of L_{RS} with the number of waveform cycles. The value of this parameter reduces from unity at fault inception (cycle 1) to 0.5 in cycle 3 at which value it remains thereafter. This latter value is indicative of the fractional location of the fault along the line length.

Fig. 5(a) shows the waveforms of the receiver end current due to a Line-line-Ground (ABG) fault at 75% of line length. Fig. 5(b) shows the corresponding L_{RS} variation with waveform cycles for three different values of fault resistance (0.001, 100, 200 ohms). This shows a reduction ion in L_{RS} to 0.75 during cycle 3 indicting a fault at 75% of the line length. Figures 6(a) and (b) show the results for the same fault Line-Line (AB), at the same location (75%) as Fig. 5, but with no ground involved. The reduction in the value of L_{RS} at cycle 3 is again 0.75.

Fig. 7(a) shows the waveforms of the receiver end current due to Line-line-Line-Ground (ABCG) fault at 35% of line length. Fig. 7(b) shows the variation of L_{RS} with waveform cycles for this condition and with three different values of fault resistance (0.001, 100, 200 ohms). The L_{RS} value reduces to 0.35 by cycle 3 consistent with the fault location at 35% of the line length.

The fault location results given on figures 4(c), 5(b), 6(b), 7(b) for different fault resistances allows the errors in estimating the fault location associated with different resistance values to be estimated. These are summarised on Table II which shows that the L_{RS} results of Fig. 4(c) for the different fault resistances indicate a percentage error of less than 2% in the worst case. In both the cases of Fig. 5(b) and 6(b) the estimated location results are in good agreement and independent of fault resistance to within less than 1% error. The results of Fig. 7(b) also yield an estimated error of less than 1%. Thus overall the fault location results are accurate to within 1.9%.

The accuracy with which a fault may be located with the described chromatic approach (~1.9 %) is relatively high compared with other available techniques. It is better than conventional impedance calculations (~ 2.6 %) [15] [16], similar to travelling wave, wavelet, time-frequency analysis (0.6% – 1.41%) [17][13] but less than artificial intelligence methods (~0.006%) [12]. Published literature also indicates that some accurate algorithms will lose location accuracy for some special conditions such as high resistance faults [18] and it is difficult to achieve the robustness with other algorithms (e.g. neural network systems) [19] which could not maintain the claimed accuracy with any change in the monitored system component characteristics. It has been shown that the chromatic system described here has immunity to fault resistance variation, the type of fault and its performance is not affected by changes in the system parameters.

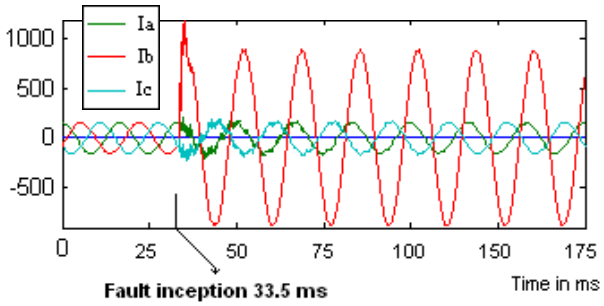

(a)

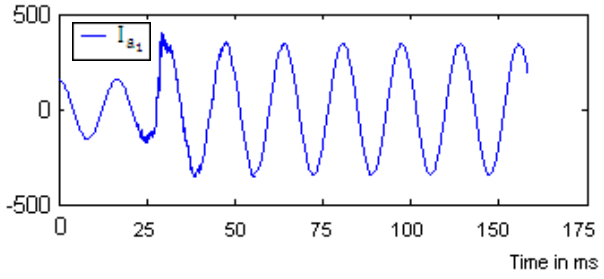

(b)

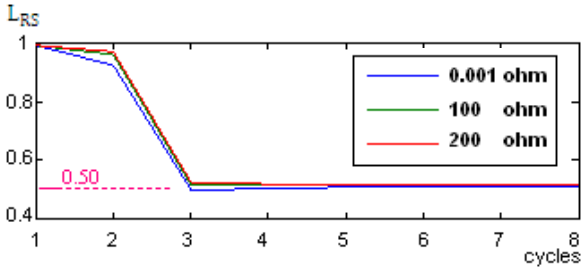

(c)

Fig. 4. LG (BG) fault current

(a) Three phase current waveforms

(b) Positive symmetrical component

(c) The estimated location of a fault at LRS = 0.5 i.e 50% of the line length

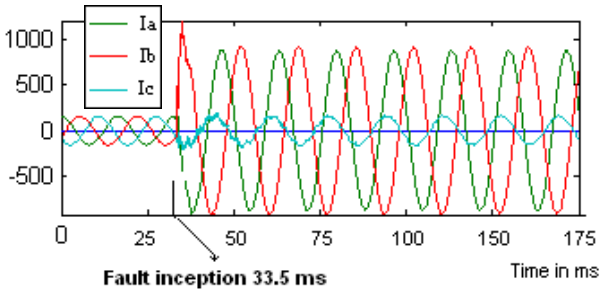

(a)

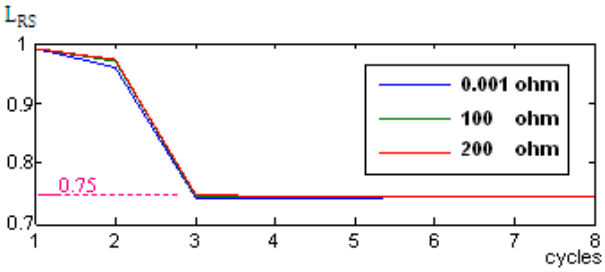

(b)

Fig. 5. LLG (ABG) fault

(a) Three phase current waveforms

(b) The estimated location of a fault at L_{RS} = 0.75 i.e 75% of the line length

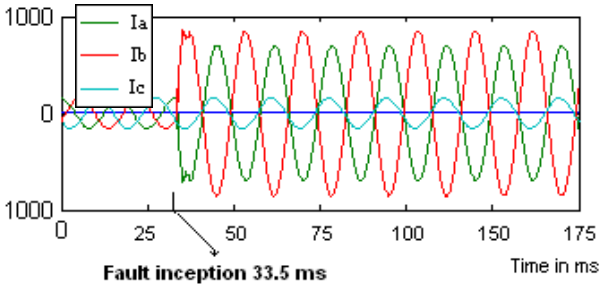

(a)

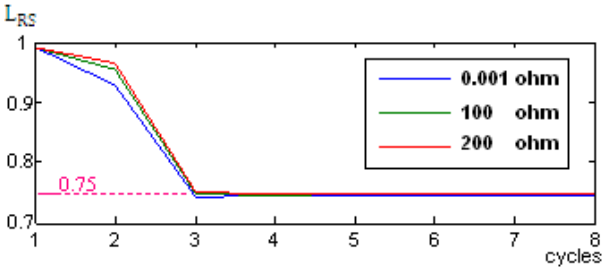

(b)

Fig. 6. LL (AB) fault

(a) Three phase current waveforms

(b) The estimated location of a fault at LRS = 0.75 i.e 75% of the line length

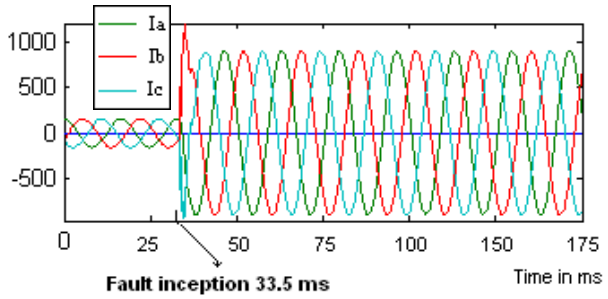

(a)

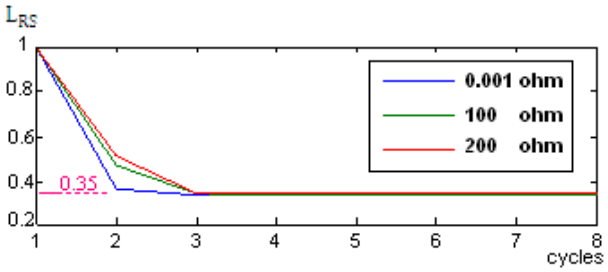

(b)

Fig. 7. LLLG (ABCG) fault

(a) Three phase current waveforms

(b) The estimated location of a fault at LRS = 0.35 i.e 35% of the line length

TABLE II. ERRORS IN DETERMININGTHE FAULT LOCATION FOR DIFFERENT TYPES OF FAULTS AND FAULT RESISTANCE

Fault type	Fault resistance Ω	Actual location Km	Calculated location Km	Estimated error %
LG (BG)	0.001	50.00	50.56	-0.56
	100	50.00	51.27	-1.27
	200	50.00	51.89	-1.89
LLG (ABG)	0.001	75.00	74.43	0.57
	100	75.00	74.61	0.39
	200	75.00	74.71	0.29
LL (AB)	0.001	75.00	74.51	0.49
	100	75.00	74.73	0.27
	200	75.00	74.87	0.13
LLLG (ABCG)	0.001	35.00	34.39	0.61
	100	35.00	34.57	0.43
	200	35.00	34.70	0.30

V. CONCLUSIONS

A method for locating various faults on a double transmission line has been described, which is based on monitoring the positive sequence component of the current at both sender and receiver ends and analyzing this using chromatic techniques.

The capability of the new method has been demonstrated by simulating various cases on a parallel transmission line. The results show that the method has high accuracy in determining the fault location and is suitable for incorporation in the design of a protective scheme for transmission lines. The accuracy of the location result is not affected by the value of the fault resistance nor the actual fault location.

Further information regarding for example the nature of the fault may be identified through the use of additional chromatic parameters, but this aspect requires further investigation.

VI. REFERENCES

[1] A. Hosny, M. Safiuddin. (2009). ANN-Based protection system for controllable series-compensated transmission lines. Power Systems Conference and Exposition, PSCE '09.

[2] A. M. AI-Kandari, S. A. Soliman and M.E. El-Hawaly. (2004). Fuzzy measurements of power system symmetrical components. Large Engineering systems Conference on Power Engineering.

[3] Crossley, P., & McLaren, P. (September 1983). Distance protection based on travelling waves. IEEE Transactions on Power Apparatus and Systems,Vol. -PAS-102, No. 9, , 2971-2983.

[4] Crossley, P., Gale, P., Bingyin, X., Yaozhong, G., Cory, B., & Barker, J. (1993). Fault location based on travelling waves. Fifth International Conference on Developments in Power System Protection (pp. 54-59). Conference Publication No. 368.

[5] Dong, X., Kong, W., & Cui, T. (April 2009). Fault Classification and Faulted-phase selection based on the initial current traveling wave. Power Delivery, IEEE Transactions on , 552 - 559.

[6] Eriksson, L., Saha, M., & Rockefeller, G. (Feb. 1985). An accurate fault locator with compensation for apparent reactance in the fault resistance resulting from remote-end feed. Power Apparatus and Systems, IEEE Transactions on , 423 - 436 .

[7] G.R. Jones, A.G. Deakin and J.W. Spencer. (2008). Chromatic monitoring of complex conditions. CRC Press.

[8] Jain, A. , Thoke, A.S. , Koley, E. , Patel, R.N. (2009). Fault classification and fault distance location of double circuit transmission lines for phase to phase faults using only one terminal data. Kharagpur, INDIA: Third International Conference on Power Systems.

[9] Kajoijilertsakul, P., Asawasripongtom, S., Sanposh, P., Suwatthikul, J., & Fujita, H. (17-19 May 2011). Wavelet based fault detection, classification and location in existing 500 kV transmission line. Electrical Engineering/Electronics, Computer, Telecommunications and Information Technology (ECTI-CON), 2011 8th International Conference on (pp. 873 - 876). IEEE.

[10] Kolla, S. R. (1988). Block pulse functions based algorithm for symmetrical components calculation. IEE Proceedings, Vol.135, pt. C, No.6 , 487-488.

[11] Moon, P. and Spencer, D. E. (1981). The photic field. Cambridge: MIT Press.

[12] Pranav.D.Raval. (2008). ANN based classification and location of faults in EHV transmission line. the International MultiConference of Engineers and Computer Scientists .

[13] S.R. Samantaray , P.K. Dash, G. Panda,. (2006). Fault classification and location using HS-transform and radial basis function neural network. 76 (897–905).

[14] Simi P. Valsan, K.S. Swarup,. (2009). Wavelet transform based digital protection for transmission lines. 31 (379–388).

[15] W.Zhang, U Rosadi, M Choi, S Lee, I Lim. 'A Robust Fault Location Algorithm for Single Line-to-ground Fault in Double-circuit Transmission Systems'. Journal of Electrical Engineering & Technology , Vol. 6, No. 1, pp. 1~7, 2011

[16] T. Takagi,Y. Yamakoshi, M.Yamaura, R. Kondow, T. Matsushima, 'Development of a New Type Fault Locator Using the One-Terminal Voltage and Current Data' IEEE Transactions on Power Apparatus and Systems, 1982 Volume:101 , Issue: 8 , Page(s): 2892 – 2898

[17] A. Tabatabaei, M. Mosavi, A. Rahmati. Fault Location Techniques in Power System based on Traveling Wave using Wavelet Analysis and GPS Timing. Przeglad Elektrotechniczny (Electrical Review), ISSN 0033-2097, R. 88 NR 6/2012

[18] A. Sauhats, M. DanilovaFault Location Algorithms for Super High Voltage Power Transmission Lines, Power Tech Conference Proceedings, 2003 IEEE Bologna, 23-26 June 2003

[19] M. M. Saha,J. Izykowski, E. Rosolowski. (2010). Fault Location on Power Networks. Springer

Asymmetrical Fault Classifier for a Parallel Transmission Line Using Chromatic Processing

Z. S. Almajali, J. W. Spencer and G. R. Jones

Department of Electrical Engineering, University of Liverpool, Liverpool, UK
almajali@liv.ac.uk, joe@liv.ac.uk, grjones@liv.ac.uk

Keywords: symmetrical component; double transmission line; fault classifier; fault diagnosis; chromatic monitoring; one terminal method;

Abstract

A novel approach for asymmetrical fault type classification on a parallel transmission line is described in this paper. The method is based on applying chromatic monitoring methodology on the negative and zero sequence components of the three phase currents of either sender or receiver end of a transmission line. Different asymmetrical Faults scenarios at different locations, with various fault resistance are simulated using MATLAB software and its associated Simulink and Simpowersystem toolboxes. The simulated outputs are transformed chromatically into effective magnitude and dominant phase shift parameters. In this paper a new concept of fault classification for asymmetrical faults is presented based upon chromatic maps of dominant phase shift and relative magnitude parameters.

1 Introduction

To achieve helpful diagnoses of a transmission line fault, it is necessary to have fast fault detection with accurate location estimation, and an indication of the fault type. Such information can improve fault correct ion efficiency, enhance overall power system performance and supply and power supply plus reduce outage times.

Various faults can occur during the process of power transmission, the majority of which are asymmetrical faults (97%), 80% of which are single line to ground and 17% are double line to ground faults [1, 2]. The complex conditions that accompany the faults can increase the difficulty of correct detection, classification and accurate fault location.

There is therefore a need to analyse the available complex waveforms rapidly and accurately to extract useful and pertinent information from them.

Various kinds of relaying schemes exist, and the fault type classification has been covered by different research approaches. Some involve conventional calculation approaches, while new methods such as fuzzy logic [3-5], or neural networks are used [6-9]. Others employ wavelet transforms [10, 11], travelling wave [12] or a combination of several methods [13-18]. Many techniques have been used and good results have been obtained. Although there is active research on this subject, a literature review has shown that no approach based upon chromatic principles has been attempted.

This paper explores the possibility of introducing a fault type classification approach based upon Chromatic monitoring techniques, which is derived from colour science and the photic fields concepts [19]. The method has already been applied successfully for monitoring systems with complex conditions [20].

The Lightness chromatic parameter algorithm has been used recently in deriving an effective magnitude parameter which is used in determining the fault location [21]. In this paper the Hue chromatic algorithm (representing a dominant phase shift) will be discussed and its use for a fault type classification will be presented.

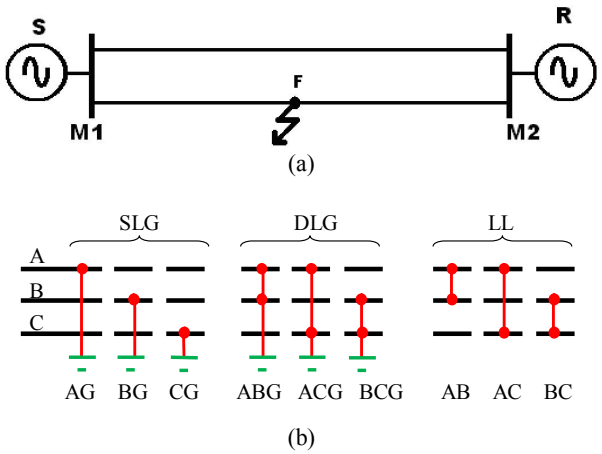

Figure 1: Transmission Line Model (a) simulated double transmission line (S–Source, R–Receiver) (b) Asymmetrical faults

2 Simulation study

A 735 kV, 60 Hz parallel 200 Km transmission line is considered using simulation with MATLAB® software and its associated Simulink® and Simpowersystem® toolboxes. A schematic diagram is given of such a line on Fig. 1(a) which shows a fault (F) located between the sending (S) and receiving (R) ends of such a line with data collecting points at M1 and M2.

The selected case study represent part of a typical power system, the power is delivered through a parallel transmission line between two complex networks, the receiver network could be a residential area or an industrial facility and thus represents a final stage in the delivery of power to end users.

The line models used are distributed parameter lines, and simulations of various types of short circuit faults have been performed. Various cases have been considered by varying the fault resistance and with faults occurring at different positions along the transmission line. Fault signals are collected for an alternating current cycle of 60 Hz. These signals are captured in discrete form and data obtained for all three phases (A, B, C) of the power transmission with different types of asymmetrical faults. The values of the power line parameters used in the simulation are given on Table I

Positive sequence resistance R1, Ω/KM	0.01165
Zero sequence resistance R0, Ω/KM	0.2676
Positive sequence inductance L1, H/KM	0.8679e-3
Zero sequence inductance L0, H/KM	3.008e-3
Positive sequence capacitance C1, F/KM	13.41e-9
Zero sequence capacitance C0, F/KM	8.57e-9

Table I: Line parameter

For the purpose of the algorithm testing, various types of faults were simulated which included the following conditions.

- Fault location: 10%, 50%, and 90% of the distance.
- Fault types : figure1(b)
  1. Single line to ground (SLG) faults :- AG, BG and CG
  2. Double line to ground faults(DLG) faults:- ABG, BCG, and ACG
  3. Double line to line faults(LL) faults:-AB, BC and AC.
- Fault resistance: 0.001, 10 and 100 Ω.

3 Method description

A. Overall Procedure

The procedures used in the simulation are summarised on flow chart of Fig. 2. The currents from the three phases (Ia, Ib, and Ic) at one end of the transmission line (either the sender source (S) or the power receiving (R) end), are obtained and the symmetrical component of the current waveforms is calculated. This is to reduce computational demands if the current waveforms from each of the three phases were used. Instead the monitoring is performed on the negative symmetrical component (I_{a2} equation (1b) below) only of one of the three phases. The output waveform from these two steps is then processed cycle–by –cycle using three chromatic processors (R, G, B) to yield waveform identifying chromatic parameters (H, L).

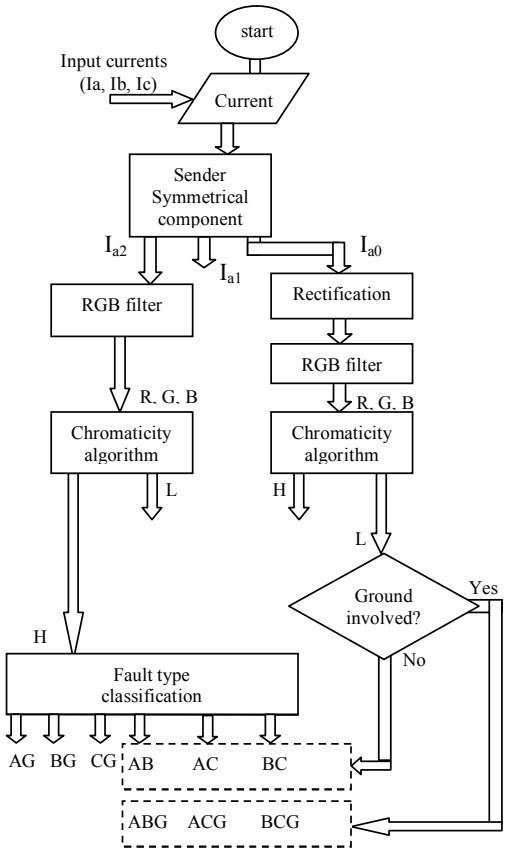

Figure 2: Flow chart for the proposed chromatic method

The algorithm defining the Hue chromatic parameter will be used in deriving the dominant phase shift parameter (H) which provides the required fault type classifier. Details of these various steps are given in sections B and C below.

B. Symmetrical Components

The symmetrical components concept leads to the set of the three-phase currents (Ia, Ib, Ic) being expressed as the positive, negative and zero sequence components denoted by I_{a1}, I_{a2} and I_{a0} respectively according to Equations (1)[22].

$$I_{a1} = 1/3[I_a + \alpha I_b + \alpha^2 I_c] \quad (1a)$$

$$I_{a2} = 1/3[I_a + \alpha^2 I_b + \alpha I_c] \quad (1b)$$

$$I_{a0} = 1/3[I_a + I_b + I_c] \quad (1c)$$

Where α is a unit vector at an angle of 120 degrees.
$\alpha = 1\angle 120^o$ and $\alpha^2 = 1\angle 240^o$

C. Chromatic Processing

Chromatic processing of the current waveforms is performed by applying three non-orthogonal processors R, G and B [20] to each full cycle of the waveforms in the time domain. The

selected form for the RGB processors profiles for this purpose is triangular with overlaps at half heights. Fig. 3 shows an example of the RGB processors superimposed upon complete cycles of the negative sequence component of the current (I_{a2} equation (1b)) together with the application of the chromatic transformation step. The first four cycles are those before the occurrence of the fault, the last three cycles show the change in the magnitude and phase shift caused by the fault. This selected case is for a single line to ground fault (AG).

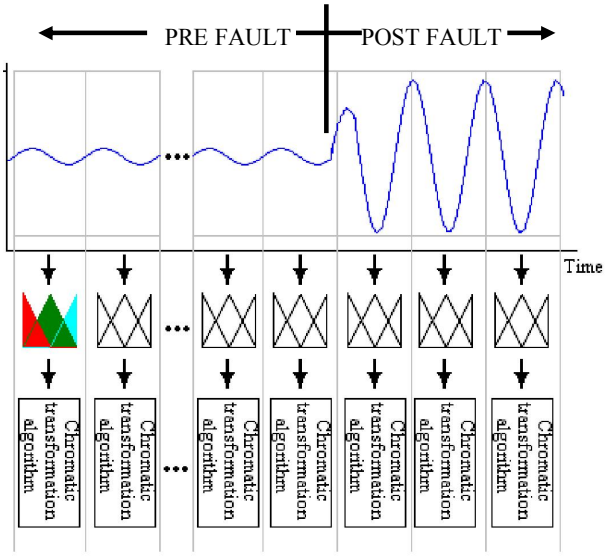

Figure 3: Application of RGB processors pre and post fault to a negative sequence component of the current (single line to ground fault).

The outputs from the three R, G, and B processors were then transformed into the dominant phase shift parameter (H) and the effective magnitude parameter (L) using the chromatic transformation algorithms Equations (2) below [20]

$$H = 240 - 120.\ g / (g + b) \quad r = 0 \qquad (2a)$$
$$= 360 - 120.\ b/ (b + r) \quad g = 0 \qquad (2b)$$
$$= 120 - 120.\ r/(r + g) \quad b = 0 \qquad (2c)$$

Where

$$r = R - MIN(R, G, B)$$
$$g = G - MIN(R, G, B)$$
$$b = B - MIN(R, G, B)$$

$$L = (R + G + B)/ 3 \qquad (2d)$$

The process is performed for waveforms at one end, M1or M2 (figure 1(a)), of the transmission line.

4 Results

4.1Chromatic H values for different faults at same location

Values of the H chromatic parameter have been calculated for various faults at the same location and for several fault resistances. The fault types considered are single line fault to ground (AG, BG, CG), double line faults (AB, AC, BC) and double line faults to ground (ABG, ACG, BCG), (figure 1(b)).

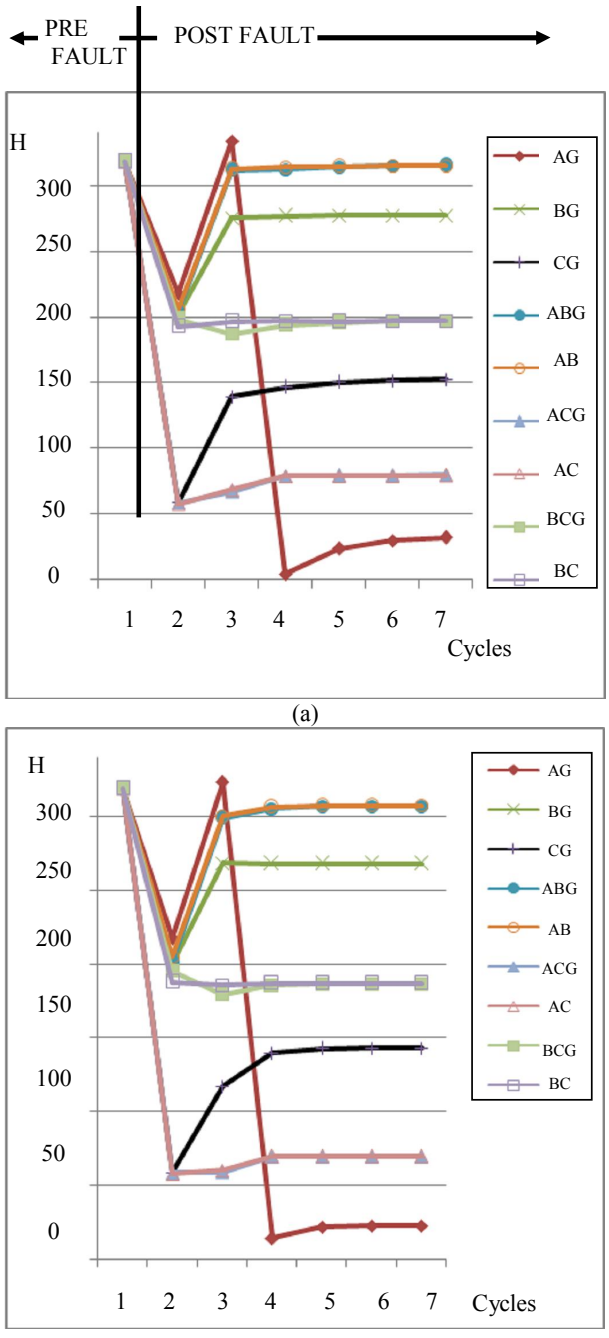

(a)

(b)

Figure 4: H values for various faults located at 50% of the line length with fault resistances of (a) 0.001 Ω (b) 10 Ω

Examples of the H values as a function of the wave cycle just prior and post fault inception are given on figure 4. Figure 4 (a) shows H ; cycle for various 0.001 Ω faults occurring at 50% the power line length. Figure 4 (b) shows the same types of faults at the same location but with a resistance of 10 Ω.

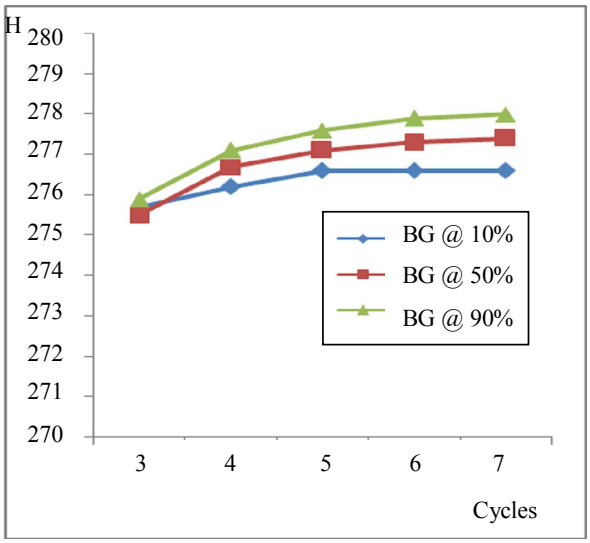

(a)

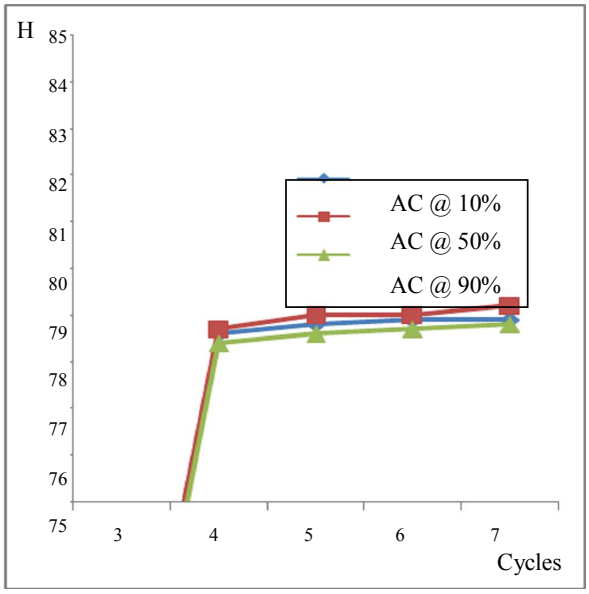

(b)

Figure 5: H : post fault cycle for a 0.001 Ω fault at each of three different line locations (10, 50, 90%) (a) BG fault (b) AC fault

4.2 Chromatic H values for different fault locations

These results show changes in the H value post fault inception which are

a) During the first fault cycle (cycle 2), the H fault values reduce substantially from the healthy value (~ 360) by d(H) ~ 100 – 250 for both 0.001 Ω and 10 Ω fault resistances.
b) During subsequent cycles the H values have in general different levels which depend upon the type of fault
c) During these subsequent cycles the H value for each fault is similar, but not identical, for the two fault resistances, 0.001 Ω (figure 4(a)) and 10 Ω (figure 4(b)).

Figure 5 (a) shows results for H : cycle for a 0.001 Ω BG fault occurring at three different locations (10, 50, 90% line length). Figure 5 (b) shows H: cycle results for an AC fault of the same resistance (0.001 Ω) and the same three line length locations (10, 50, 90%). These results show that for the BG faults, the post fault cycles have H values for each location which have similar, but not identical values. Likewise for the AC fault, the H values only weakly depend upon the fault location

4.3 Chromatic L values for different types of faults

Figure 6 shows results for chromatic L: cycle of the zero sequence component (I_{ac} equation (1c)) for the different types of faults with a fault resistance of 0.001 Ω and location line location 50 % This shows that the nine different faults plus healthy condition form three clusters of points. The line – line faults (AB, AC, BC) have L ~ 1.E+02, the lines to ground faults (AG, BG, CG, ABG, ACG, BCG) have L ~ 1.E+06 and the healthy line has L ~ 1.E+00.

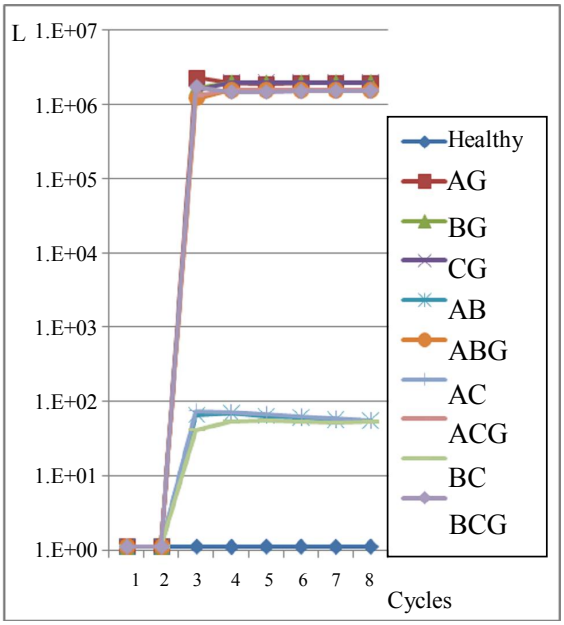

Figure 6: L of zero sequence component: cycle for various faults (fault resistance = 0.001 Ω, fault location = 50 %)

5 Discussion of Results

The H : cycle results for various types of faults, different locations and fault resistances presented on figures 4 and 5 are typical of more comprehensive computations which have been made covering a wider range of values for the fault resistance and locations. Inspection of these comprehensive results enables ranges of H values to be determined within which each fault type resides. These ranges for each fault are listed on Table II.

Fault type	H range	
	>	<
AC/ACG	35	80
CG	80	150
BC/BCG	150	198
BG	198	275
AB/ABG	275	315
AG	315	35

Table II: H ranges covered by different types of faults (Normal lines H = 0/360)

This shows that
a)Various faults may be grouped according to different ranges of H to which they belong.
b)The single line to ground faults (AG, BG, CG) are in general distinguishable from each other and from the other types of faults
c)Faults involving two lines (AB/ABG, AC/ACG, BC/BCG) are distinguishable from each other and the single line faults but the two line-ground faults are not distinguishable from the two line only faults..
d)Ambiguities can occur at the boundaries between each of the six ranges whereby there is no distinction between the two faults on either side of the boundary (e.g H = 80 is a common boundary between faults CG and AC/ACG).

The boundaries ambiguities arise from the overlap of low and very high resistance faults. An example of this is given by the results shown on figure 7 for chromatic H : post fault cycles. This figure compares the H values for a CG fault of resistance values 0.001, 10, 100 Ω with the H values for an ACG fault of resistance 0.001 Ω. The results show that H(CG, 100 Ω) = H(AGC, 0.001 Ω). Such comparisons also show that the boundary ambiguities occur due to the overlap of the non-ground and line to ground signals.

However the results of figure 6 shows that the non-ground and lines to ground signals are distinguishable by their different values of the chromatic L parameter. Thus by combining the L and H fault groupings, a higher level of fault discrimination is possible. Figure 8 shows a Cartesian Chromatic Map of L(1.E+0x) versus H which provides such a higher level of discrimination. This shows how the ambiguities at the range boundaries of the H discriminator are removed using the L parameter.

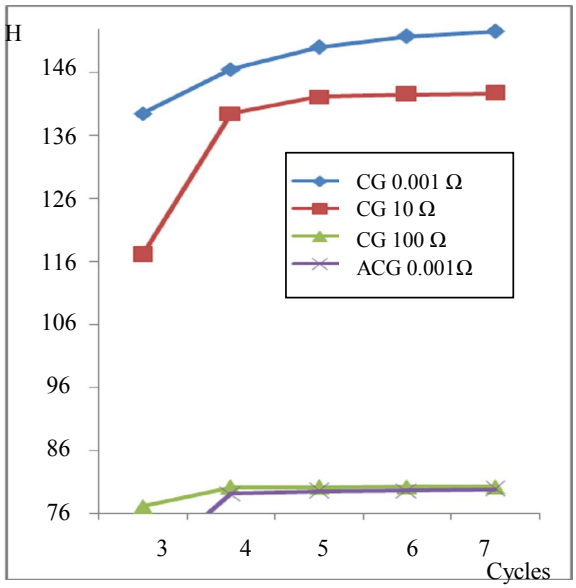

Figure 7: Chromatic H: versus post fault cycles for a single line to ground fault (CG) with different fault resistances and for a two line to ground fault (ACG) with a low fault resistance.

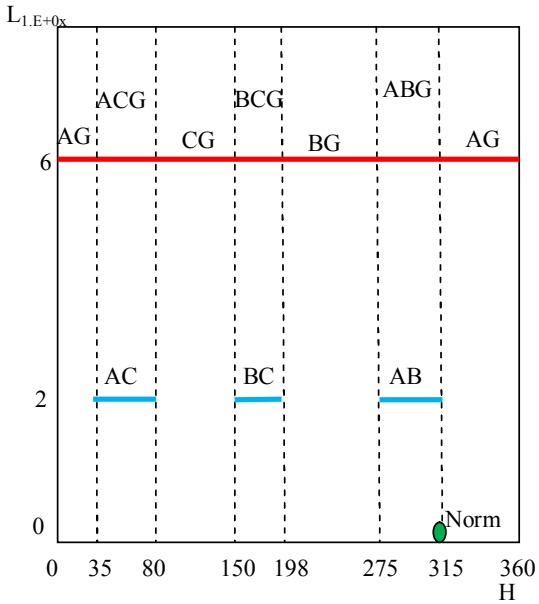

Figure 8 Chromatic Map of L versus H with clusters of different faults (AG, BG, CG and AC/ACG, BC/BCG, AB/ABG) plus normal condition (Norm)

5 Conclusions

It has been shown how the application of chromatic techniques for power line monitoring can distinguish between particular transmission line faults. The combination of processing signals with two chromatic parameters (L and H) provides a high level of fault discrimination enabling single line to ground faults to be distinguished from line to line faults and for different single line to ground faults to be distinguished from each other.

The discrimination is independent of fault resistance and location along the line length. (The effect of line length has already been distinguished with chromatic techniques in a previous paper [21]).

Unlike other fault discriminating methods (e.g. neural networks etc) the chromatic approach provides a high level of transparency and traceability in the distinction between different faults.

Further discrimination may be possible through the extension of the chromatic approach.

References

[1] Saha, Murari Mohan, Jan Izykowski, and Eugeniusz Rosolowski. "Fault Location on Power Networks", London: Springer, (2010).

[2] Beiza, J., S. H. Hosseinian, and B. Vahidi. "Fault Type Estimation in Power Systems", Iranian Journal of Electrical & Electronic Engineering, pp. 185-195. (2009).

[3] Mahanty, R.N., and P.B. Dutta Gupta. "A fuzzy logic based fault classification approach using current samples only", Electric Power Systems Research, **77**, pp. 501–507. (2007).

[4] Youssef, Omar A.S. "a novel fuzzy-logic-based phase selection technique for power system relaying", Electric Power Systems Research, **68**, pp. 175–184. (2004).

[5] Youssef, Omar A.S. "Applications of Fuzzy Inference Mechanisms to Power System Relaying", Power Systems Conference and Exposition. New York: IEEE, pp. 560 - 567. (2004).

[6] Mahanty, R.N., and P.B.D. Gupta. "Application of rbf neural network to fault classification and location in transmission lines", IEE Proceedings Generation, Transmission & Distribution, pp. 201 - 212. (2004).

[7] Jain, Anamika, A. S. Thoke, and R. N. Patel. "Fault classification of double circuit transmission line using artificial neural network", International Journal of Electrical and Computer Engineering, pp. 1029-1034. (2008).

[8] Sanaye-Pasand, M., and H. Khorashadi-Zadeh. "Transmission line fault detection & phase selection using ANN", International Conference on Power Systems Transients. New Orleans, (2003).

[9] Jain, Anamika, A.S.Thoke, Ebha Koley, and R. N. Patel. "fault classification and fault distance location of double circuit transmission lines for phase to phase faults using only one terminal data", Third International Conference on Power Systems. Kharagpur: IEEE, Paper No: 41. (2009).

[10] S.A.Shaaban and Takashi Hiyama. "Transmission line faults classification using wavelet transform", 14th International Middle East Power Systems Conference. Cairo, pp. 532-537. (2010).

[11] Kajoijilertsakul, Pairoj, Santi Asawasripongtorn, Peerayot Sanposh, Jittiwut Suwatthikul, and Hideaki Fujita. "Wavelet based fault detection, classification and location in existing 500 KV transmission line", The 8th Electrical Engineering, Electronics, Computer, Telecommunications and Information Technology (ECTI). Thailand, pp. 873-876. (2011).

[12] Dong, Xinzhou, Wei Kong, and Tao Cui. "Fault classification and faulted-phase selection based on the initial current travelling wave", IEEE Transactions on power delivery, **24**, pp. 552-559. (2009).

[13] Wang, Huisheng, and W. W. L. Keerthipala. "fuzzy-neuro approach to fault classification for transmission line protection", IEEE Transactions on Power Delivery, pp. 1093 - 1104. (1998).

[14] Patel, Mamta, and R. N. Patel. "Fault detection and classification on a transmission line using wavelet multi resolution analysis and neural network", International Journal of Computer Applications, pp. 27-33. (2012).

[15] Ekici, Sami. "Support vector machines for classification and locating faults on transmission lines", Applied Soft Computing, pp. 1650–1658. (2012).

[16] Thukaram, D., H. P. Khincha, and H. P. Vijaynarasimha. "Artificial neural network and support vector machine approach for locating faults in radial distribution systems", IEEE Transactions on power delivery, **20**, NO. 2, (2005).

[17] Upendar, J., C. P. Gupta, and G. K. Singh. "Discrete wavelet transform and genetic algorithm based fault classification of transmission systems", Fifteenth National Power Systems Conference (NPSC). Bombay, pp. 323-328. (2008).

[18] Samantaray, S.R., P.K. Dash, and G. Panda. "Fault classification and location using HS-transform and radial basis function neural network", Electric Power Systems Research, pp. 897–905. (2006).

[19] Moon, P., and D. E. Spencer. "The Photic Field", Cambridge: MIT Press, (1981).

[20] G.R. Jones, A.G. Deakin and J.W. Spencer. "Chromatic Monitoring of Complex Condition", CRC Press, (2008).

[21] Z. S. D. Almajali, J.W. Spencer and G.R. Jones "Fault Locator for a Parallel Transmission Line Using Chromatic Processing", the 8th Jordanian International Electrical and Electronics Engineering Conference, (JIEEEC 2013) Amman, (2013).

[22] Kolla, S. R. "Block pulse functions based algorithm for symmetrical components calculation", IEE Proceedings, **135**, pt. C, No.6, pp. 487-488. (1988).

Appendix B

Matlab code

This appendix contains sample of Matlab code used for application of HLS chromatic model transformation procedure. Figure B.1 shows a flowchart of the code steps.

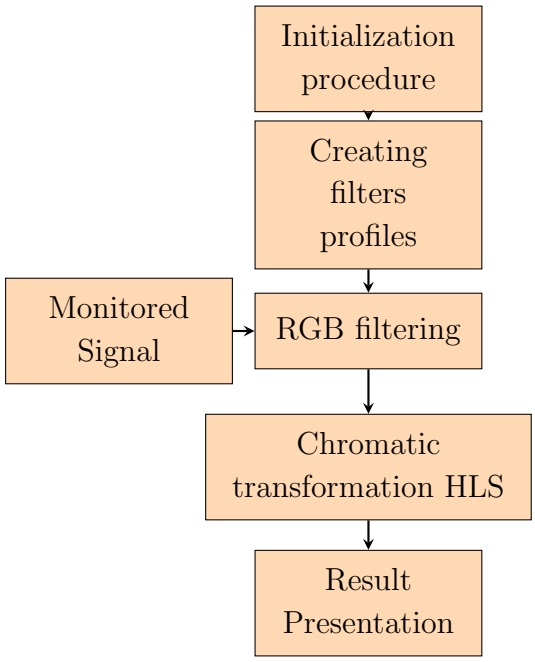

Figure B.1: Matlab code for chromatic processing procedure

```
% Matlab code for chromatic transformation for one of the
% symmetrical sequence component of the current waveform
% cycles from the sender terminal of the transmission line.
%-------------------------------------------------------------
%The Procedure is repeated for the three symmetrical sequence
% component for both current and voltage waveforms collected
% from both terminals of the transmission line.
%-------------------------------------------------------------
% Initialization procedure
%-------------------------------------------------------------
NOofCYCLES=size(cyclesAIS)-1;
h=[];
s=[];
L=[];
g=[];
%-------------------------------------------------------------
% Sample count in cycles
%-------------------------------------------------------------
ff=size(cyclesAIS);
ff=ff(1);
max_of_size=0;
while ff>1
gg=cyclesAVS(ff)-cyclesAVS(ff-1);
max_of_size=max(max_of_size,gg);
ff=ff-1;
end
```

```
x1=max_of_size;                    % read the size
if mod(x1,2) == 0                  % make it even
                %The number is even
else
                %The number is odd
x1=x1+1;
max_of_size=max_of_size+1;
end


%-------------------------------------------------------------------
% Creating the R,G and B filters profiles
%-------------------------------------------------------------------
b11=1:-2/(x1-2):0;          %create the last part of B
b12=zeros(1,(x1/2));        %create the first part of B
B1=horzcat(b11,b12);        %create B
B1 = rot90(B1,2);
r11=0:2/(x1-2):1;           %create the first part of R
r12=zeros(1,(x1/2));        %create the last part of R
R1=horzcat(r12,r11);        %create R
R1 = rot90(R1,2);
G1=abs(1+(-1*R1+-1*B1));    %create G
```

```
%-------------------------------------------------------------------------
% Evaluating the filtering stage outcomes
%-------------------------------------------------------------------------
Rcycle1=abs(currentcycle.*R1);
Gcycle1=abs(currentcycle.*G1);
Bcycle1=abs(currentcycle.*B1);
Rtotal1=sum(Rcycle1);
Btotal1=sum(Bcycle1);
Gtotal1=sum(Gcycle1);
rr1=Rtotal1-min(min(Rtotal1,Gtotal1),Btotal1);
gg1=Gtotal1-min(min(Rtotal1,Gtotal1),Btotal1);
bb1=Btotal1-min(min(Rtotal1,Gtotal1),Btotal1);


%-------------------------------------------------------------------------
% Chromatic transformation
%-------------------------------------------------------------------------
if rr1 == 0
H1=240-120*(gg1/(gg1+bb1));
end
if gg1 == 0
H1=360-120*(bb1/(rr1+bb1));
end
if bb1 == 0
H1=120-120*(rr1/(gg1+rr1));
end
```

```
L1=((Rtotal1+Btotal1+Gtotal1)/3);
S1=(max(max(Rtotal1,Gtotal1),Btotal1) ...
        -min(min(Rtotal1,Gtotal1),Btotal1))/ ...
             (max(max(Rtotal1,Gtotal1),Btotal1) ...
                  +min(min(Rtotal1,Gtotal1),Btotal1));

%-------------------------------------------------------------------

h =[h H1];
s= [s S1];
L= [L L1];
NOofCYCLES(1)=NOofCYCLES(1)-1;
end


%-------------------------------------------------------------------
% Plotting results in form of polar plot as (H vs. L)
%  or (H vs. S)
%-------------------------------------------------------------------
reply = input('H-L -->1, H-S -->2   ?    ', 's');
if isempty(reply)
reply = '1';
end

h=h.*((2*pi)/360);
H_A_I_S=[H_A_I_S ;h];
```

```
S_A_I_S=[S_A_I_S ;s];
L_A_I_S=[L_A_I_S ;L];
h =[h 0];
s= [s 1];
L= [L 1];

if reply=='1'
myplot= polar(h, L, '.');
set(myplot,'Color','red','LineWidth',1,'MarkerSize',5)

end
if reply=='2'
myplot= polar(h, s, '.');
set(myplot,'Color','red','LineWidth',1,'MarkerSize',5)
end

%-------------------------------------------------------------------
%-------------------------------------------------------------------
```

Appendix C

LabView GUI

The LabVIEW graphical programming feature-rich package is utilised for applying the (HLS) chromatic transformation procedures and the implementation of algorithms proposed in this work.

C.1 Chromatic transformation

The Hue(H), Lightness(L), and Saturation(S) parameters of the (HLS) colour model are evaluated by Equations 2.37a-c, 2.39 and 2.40 respectively. The LabVIEW block implementations of the three parameters are as illustrated in Figures C.1, C.2 and C.3 respectively.

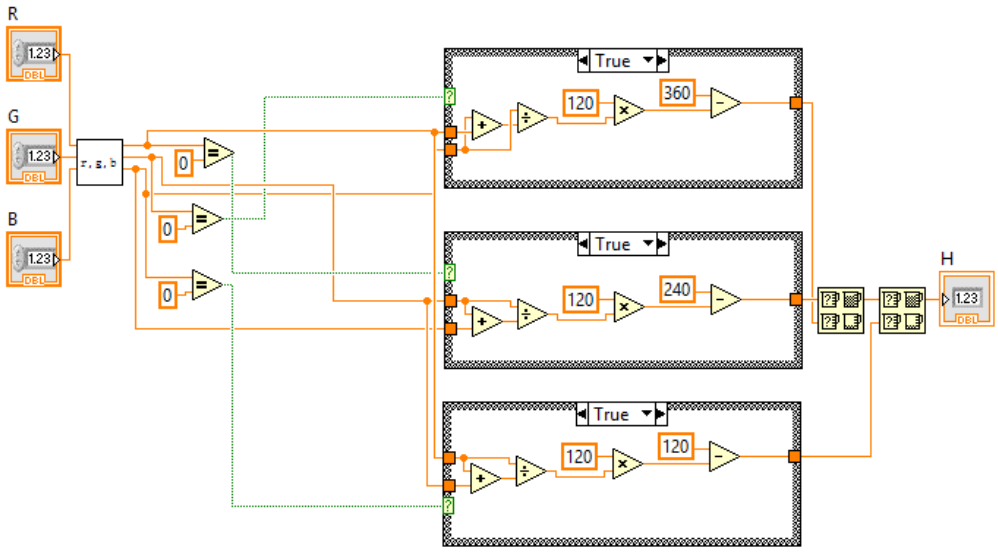

Figure C.1: H parameter calculation

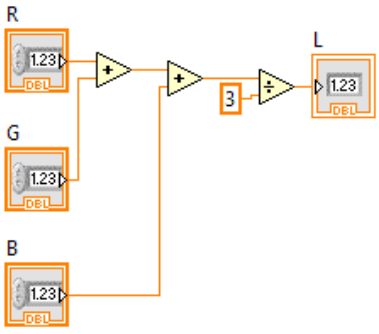

Figure C.2: L parameter calculation

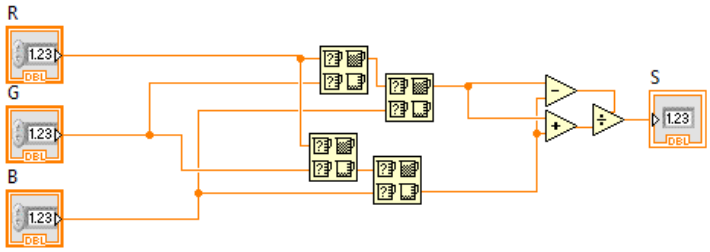

Figure C.3: S parameter calculation

C.2 Proposed algorithms

- Figure C.4 illustrate the rectified waveforms of the current positive sequence component utilisation in implementation of the proposed locator algorithm.

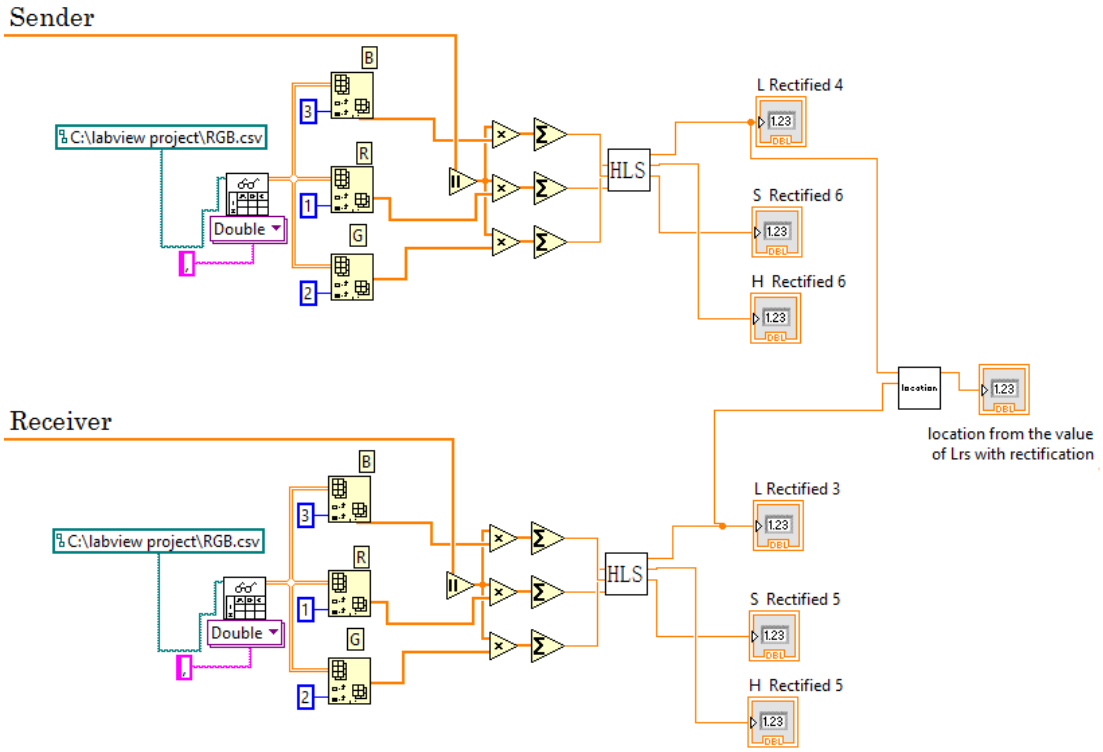

Figure C.4: Locator algorithm using rectified positive sequence component

- The voltage negative sequence component is used in the implementation of the proposed classifier algorithm, Figure C.5 shows its LabVIEW block diagram.

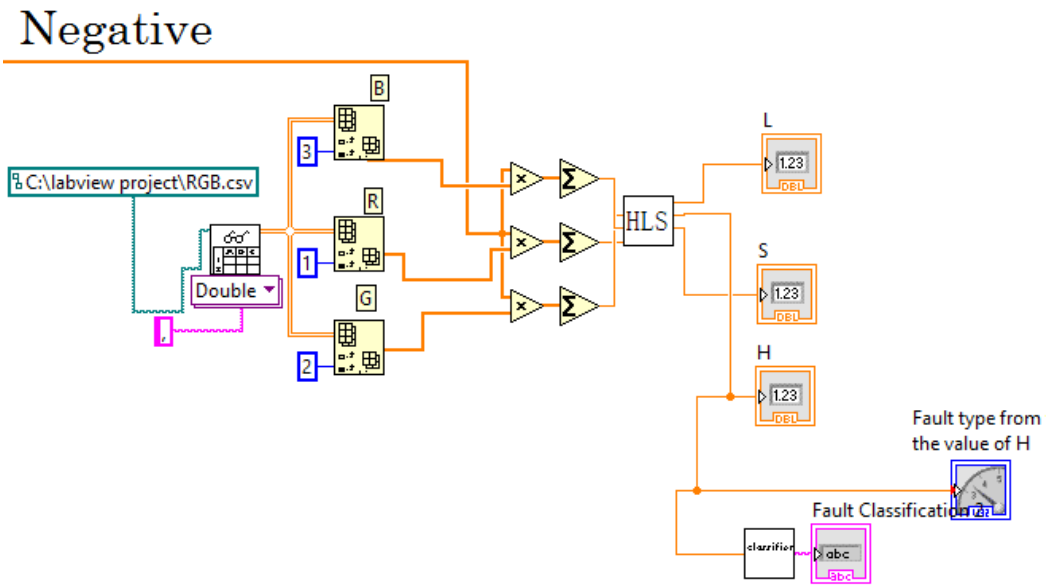

Figure C.5: Classifier algorithm using negative sequence component

- The rectified current zero sequence component is used in the implementation of the proposed ground detector algorithm, Figure C.6 shows its LabVIEW block diagram.

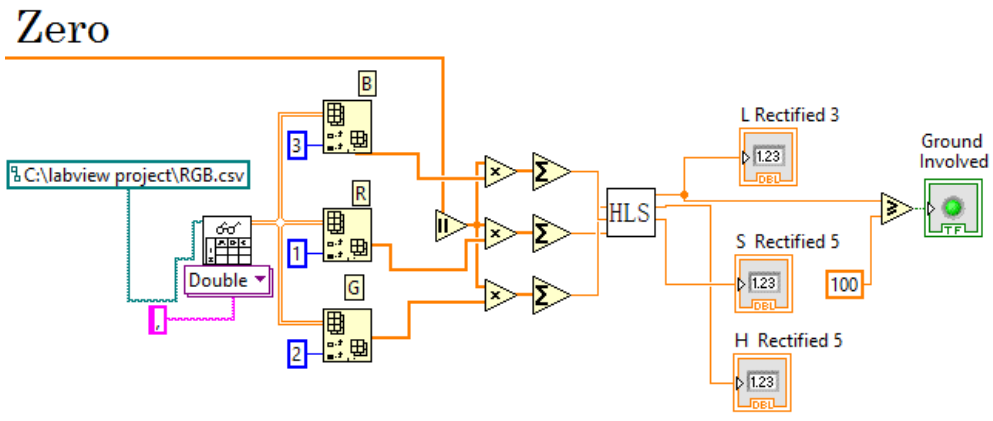

Figure C.6: Ground detector algorithm using the zero sequence component

C.3 LabView GUI

Figure C.7 shows the final version of the LabVIEW GUI and its components. The different algorithms implementations are compound in one application package for chromatic processing of power system waveforms.

The GUI components are:-

1. Case selection: To specify case files storage locations, and the fault condition under study.
2. Fault resistance selection: Different values are available.
3. Fault Location selection: To change the location throughout the line length.
4. Signal selection: To toggle between the voltage and current signal.
5. Transmission line end selection: To toggle between the sender and receiver ends of the transmission line.
6. Waveforms: To show the three phase and the symmetrical components waveforms.
7. Cycle selection: To select the waveform cycle under study.
8. Cycle waveforms: To show the symmetrical component waveforms for the selected cycle.
9. HLS parameters: Provide the chromatic parameter calculation results.
10. Classifier: The fault classification results.
11. Locator: The fault locator estimation results.
12. Ground detector: The ground detection result.

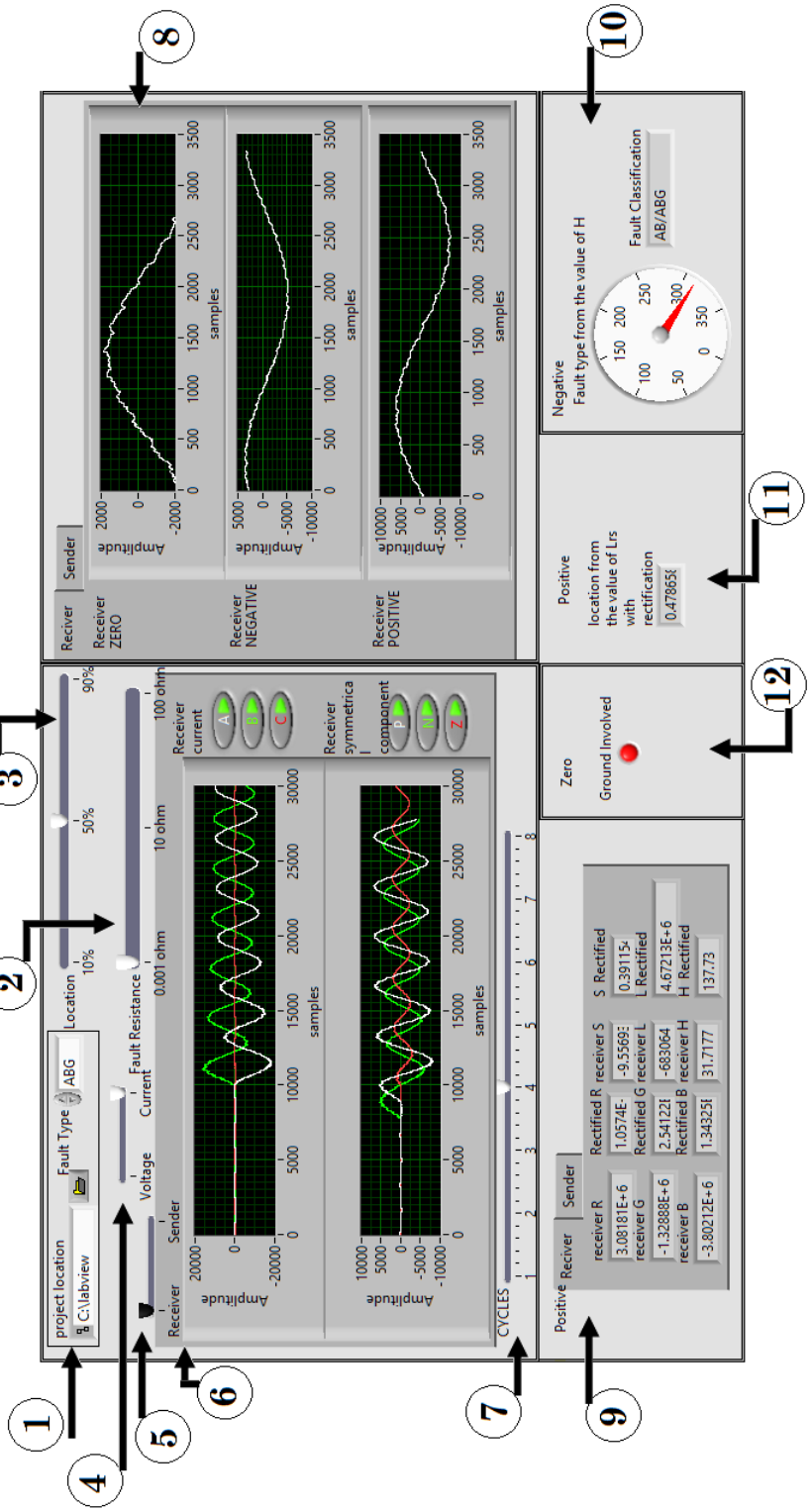

Figure C.7: LabView GUI and its components

Appendix D

Symmetrical component

In his well-known work [104], C. L. Fortescue shows that any set of N unbalanced phasors could be transformed into N sets of balanced phasors called the symmetrical components.

Targeting power systems, the considered calculations will belong to cases of three phases, and this is applicable to current and voltage phasors.

The symmetrical components for the three-phase currents ($\mathrm{I_a}$, $\mathrm{I_b}$, $\mathrm{I_c}$) can be expressed as the positive, negative and zero sequence components denoted by $\mathrm{I_{a_1}}$, $\mathrm{I_{a_2}}$ and $\mathrm{I_{a_0}}$ respectively according to equations:-

$$I_{\mathrm{a_1}} = \frac{1}{3}[I_{\mathrm{a}} + \alpha I_{\mathrm{b}} + \alpha^2 I_{\mathrm{c}}] \tag{D.1}$$

$$I_{\mathrm{a_2}} = \frac{1}{3}[I_{\mathrm{a}} + \alpha^2 I_{\mathrm{b}} + \alpha I_{\mathrm{c}}] \tag{D.2}$$

$$I_{\mathrm{a_0}} = \frac{1}{3}[I_{\mathrm{a}} + I_{\mathrm{b}} + I_{\mathrm{c}}] \tag{D.3}$$

Where α is a unit vector at an angle of 120 degrees.

α=1$\angle$120° and α^2 =1$\angle$240°.

And similarly, the symmetrical components for the three-phase voltages (V_a, V_b, V_c) can be expressed as the positive, negative and zero sequence components denoted by V_{a_1}, V_{a_2} and V_{a_0} respectively according to equations:-

$$V_{a_1} = \frac{1}{3}[V_a + \alpha V_b + \alpha^2 V_c] \tag{D.4}$$

$$V_{a_2} = \frac{1}{3}[V_a + \alpha^2 V_b + \alpha V_c] \tag{D.5}$$

$$V_{a_0} = \frac{1}{3}[V_a + V_b + V_c] \tag{D.6}$$

Appendix E

Overhead transmission line tower geometry

Table E.1 [96]include standard geometries for two typical tower examples used in UK power network. The tower configuration is as shown in Figure E.1 [96].

Table E.1: Geometries of overhead transmission line towers

Code on Figure E.1	Tower type	
	L6	L12
EY:- Earth wire	29.51 m	27.67 m
TX:- Top phase	6.98 m	6.30 m
TY:- Top phase	19.54 m	18.00 m
MX:- Middle phase	10.45 m	9.12 m
MY:- Middle phase	9.00 m	8.70 m
BX:- Bottom phase	8.44 m	7.12 m
Ground clearance	12 m	12 m

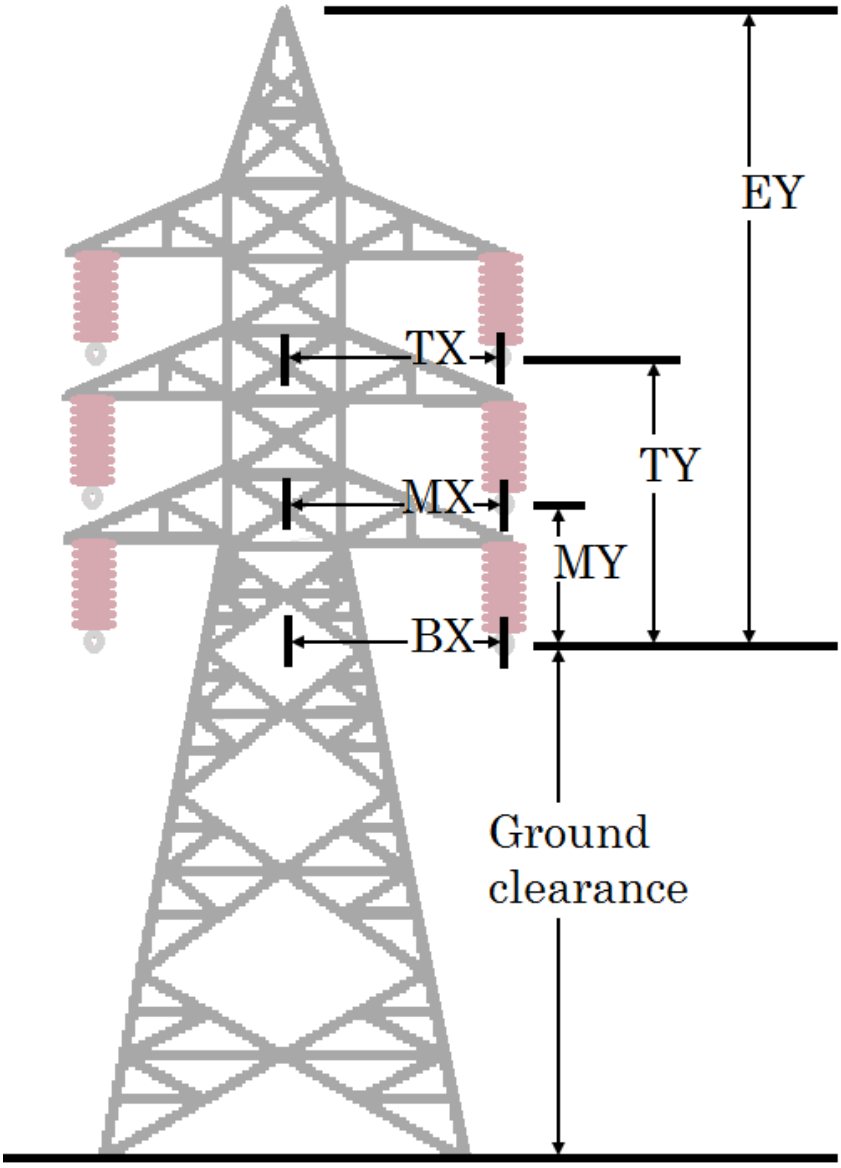

Figure E.1: Power Tower Dimension